The Effects of Sample Disturbance on Preconsolidation Pressure for Normally Consolidated and Overconsolidated Clays

by

Nikolaos S. Kontopoulos

Diploma in Civil Engineering (2005)
National Technical University of Athens, Department of Civil Engineering

Submitted to the Department of Civil and Environmental Engineering
in Partial Fulfillment of the Requirements for the Degree of

Doctor of Philosophy in the Field of Civil and Environmental Engineering

at the

MASSACHUSETTS INSTITUTE OF TECHNOLOGY

June, 2012

Signature of Author .....
Department of Civil and Environmental Engineering
February 21, 2012

Certified by .....
John T. Germaine
Senior Research Associate of Civil and Environmental Engineering
Thesis Supervisor

Accepted by .....
Heidi M. Nepf,
Chair, Departmental Committee for Graduate Students

The Effects of Sample Disturbance on Preconsolidation Pressure for Normally Consolidated and Overconsolidated Clays

By

Nikolaos S. Kontopoulos

Submitted to the Department of Civil and Environmental Engineering
on February 21st, 2012 in Partial Fulfillment of the
Requirements for the Degree of Doctor of Philosophy in the Field of
Civil and Environmental Engineering

ABSTRACT

Sample disturbance has always been a particularly challenging topic in Geotechnical Engineering exercise. The effect and importance of disturbance on stress-strain history and undrained shear strength of soft clays are well stated in the literature over the past decades. However, in practice, few qualitative methods are used even in the most complex engineering projects. Furthermore, there is not a widely accepted, quantitative method in order to assess sample disturbance and treat the lab engineering values to match the "in-situ" properties of the soil.

This research consists of a systematic review of the methods available to estimate preconsolidation pressure and sample quality. It focuses on multiple disturbance-simulation triaxial tests on resedimented San Francisco Bay Mud (RSFBM) specimens. The effect of different ISA disturbance amplitudes (Baligh et al. 1987) on the compression curve and the preconsolidation pressure is quantified. After every disturbance simulation circle, the specimens are reconsolidated using SHANSEP technique, well into the Virgin Compression Line (VCL), to erase all the previous effects of disturbance. Then, every recompression curve is treated as an initial compression phase but, of known disturbance. A series of tests are performed in Normally Consolidated (NC) and Overconsolidated (OC) specimens over a wide range of stresses. The effect of disturbance on an element outside the centerline of the sampling tube is simulated. A

new method to quantify disturbance based on a modified recompression and compression indices ratio is proposed.

Results indicate that for medium sensitivity soils, disturbance does not have a significant effect on preconsolidation pressure. However, increasing disturbance decreases significantly the researcher's capability to define with accuracy the preconsolidation pressure value. The calculated value can be overestimated as well as underestimated. Santagata and Germaine's (1994) conceptual model is verified experimentally. The model characterizes the loss of effective stresses and the change of VCL slope as the two most important outputs of disturbance that play a key role in the value of preconsolidation pressure. Results also indicate that the effects of disturbance are much less apparent when the OCR increases and that accounting for swelling leads to an overestimation of the preconsolidation pressure.

Thesis Supervisor: John T. Germaine
Title: Senior Research Associate of Civil and Environmental Engineering

ACKNOWLEDGMENT

I would like to express my gratitude to the following people that contributed a great deal to the completion of this research:

My committee members:

My supervisor, Dr. Jack Germaine for this constant guidance and support. His deep knowledge on laboratory procedures and soil mechanics, advices and suggestions had a tremendous effect on and made possible the completion of this research. He is a mentor with a unique humor and patience.

Professor H. Einstein for the very useful remarks and meticulous comments even in a topic different than that of his area of studies.

Professor Don De Groot that took the time to be a member of this committee and commute for every meeting from University of Amherst. His different perspective on the topic of Sample Disturbance and his comments deeply affected this research and my understanding of soil behavior.

Dr. Lucy Jen, for her guidance, support and useful advices. An example of mother, instructor, and professional engineer.

Our head of the Department, Professor Andrew Whittle as well as Prof. Eric Adams for providing me the opportunity to serve as a Computer Administrator for building 1.

Stephen Rudolph, for his help on the design and customization of the modified suction cap.

The MIT staff:

This research would never be possible without the support from the MIT CEE Staff. I feel blessed that I had the opportunity to work with each one of them.

Pat Dixon for being always there to back up my any concern. She helped me to a great extent financially and mentally to keep the balance between research and working as the Computer Administrator for building 1.

Jeanette Marchocki for the great laughs we had, facing every possible computer problem. Kris Kipp for all her administrative assistance and advice. Patty Glidden for her help and politeness. Carolyn Jundzilo – Comer, Sheila Fay, Lauren McLean, Donna Hudson, Deborah Levey, Denise Brehm, Bori Stoyanova, Mira Parsons and all the MIT staff family.

Family and friends:

Lagousis Andreas, for being a good friend and a mentor. Vasilis Gkortsas and Nikos Andrikogiannopoulos, two good friends for our walks of sanity in Boston. Kleio Palaska for all her companion and support through the ups and downs. Korchaipruk Attasit and Sangyoon Min for their early on guidance and mentorship.
My classmates and friends: Antonios Vytiniotis, Sherif Alk, Naeem Abdulhadi, Brendan Casey, Amy Adams, Zhan Orazalin, Gianni Zervantonaki, Apostolo Ferti, Despoina Zymnis, Maria Nikolinakou, and Gonzalo Corral. All the MIT Geotech team (labrats) and the large Greek Community of MIT.

Most importantly, I would like to thank my parents, Stefanos and Maria. Their love, support and understanding helped me overcome any obstacle that came on the way. They had always set the example on my life and made me the person I am today. I will never regret anything from my MIT experience other than the moments I spend away from them.
Finally, I would always be grateful to my brother, George Kontopoulos. He is the one that showed me the way, and guided me through whenever needed.

To my family

TABLE OF C O N T E N T S

LIST of FIGURES

LIST of TABLES

LIST of SYMBOLS

A (A_f)	Skempton's pore pressure parameter (at failure)
A/D	analog to digital converter
AC	alternating current
AR	Area ratio
A_u	A parameter for the undrained release of the shear stresses
B	sampler's diameter
B	Skempton's pore pressure saturation parameter
BBC	Boston Blue Clay
C_a	Secondary compression index
C_c	Compression index
Ci	i consolidation phase
CK_0UC	K_0 consolidated undrained compression test
CK_0UE	K_0 consolidated undrained extension test
CR	Compression ratio
C_r	Recompression index
C_s	Swelling index
C_v	coefficient of consolidation
D	particle diameter
D	specimen/sampler diameter
D/A	digital to analog
DC	direct current
E	secant Young's modulus

e_0	initial void ratio
e_f	final void ratio
E_u	undrained secant Young's modulus
G_s	Specific Gravity
H_0	initial sample height
H_s	sample height at σ'_{v0}
ICR	inside clearance ratio
I_L	Liquidity index
I_p	Plasticity Index
$K_{0\,NC}$	lateral stress ratio for NC specimens
$K_{0\,OC}$	lateral stress ration for OC specimens
K_0	lateral stress ratio
k_v	hydraulic conductivity
L	Length
LL	Liquid Limit
LVDT	Linear variable differential transformer
m	OCR exponent in SHANSEP equation for undrained strength ratio
m	the slope of the regression line in SHANSEP equation
M_B	Mass of the volumetric
M_s	Mass of dry soil
m_v	coefficient of volume change
NC	Normally consolidated
OC	Overconsolidated
OCR	Overconsolidation ratio
p, p'	average effective stress, $(\sigma'_1+\sigma'_3)/2$
PI	Activity
PVA	pressure-volume actuator
PVC	pressure-volume controller
q	shear stress, $(\sigma'_1-\sigma'_3)/2$
q_u	unconfined shear strength
r^2	coefficient of determination

RBBC	Resedimented Boston Blue Clay
RR	Recompression ratio
RSFBM	Resedimented San Francisco Bay Mud
S	Degree of Saturation
S	the undrained strength ratio for NC clays
SD	Specimen Quality
SFBM	San Francisco Bay Mud
SHANSHEP	Stress History and Normalized Soil Engineering Properties
Si	i disturbance phase
SR	Swelling ratio
s_u	undrained shear stress
t	sampler's wall thickness
t	time
t	time to the end of primary
T_c	Temperature
TX	triaxial
u_e	excess pore pressure
v	Poisson's ratio
V_B	Volume of the volumetric
VCL	Virgin Compression Line
V_{SCPTU}	shear wave velocity from seismic piezocone in-situ test
V_{uh}	shear wave velocity
Wc	water content
W_L	Liquid Limit
γ_w	unit weight of water
Δe	the change in void ratio
Δu	the pore pressure change
ε_a	vertical axial strain
ε_{max}	the maximum vertical axial strain
ε_{vol}	volumetric strain
ρ_w	unit weight of water

σ'_{h0}	horizontal effective stress
σ'_{p}	preconsolidation pressure
σ'_{ps}	perfect sampling effective stress
σ'_{s}	sampling effective stress
σ'_{v}	vertical effective stress
σ'_{v0}	in situ vertical effective stress
σ'_{vc}	the maximum vertical effective stress at the end of primary consolidation
σ'_{vc}	the maximum vertical effective stress corresponding to the interpolated VCL value (for the same void ratio at the end of secondary compression, e_{min})
σ'_{y}	yield stress or preconsolidation pressure
$\sigma_1, \sigma_2, \sigma_3$	principal stresses
φ	the angle of compression or recompression slope

Chapter 1 INTRODUCTION

1.1 Problem Statement

Over the past fifty years significant progress has been made towards the understanding of soft clay behavior. Laboratory testing techniques, such as Constant rate of strain (CRS) or triaxial tests (TX) are now often employed in order to quantity the engineering properties of clays. Soft clay properties and behavior are best described through the stress-strain-strength behavior and undrained shear strength derived from these tests. Knowing the stress-strain history, one can define the preconsolidation pressure (σ'_p), the compressibility indices and the overconsolidation ratio (OCR), which are the most important factors in order to understand soil behavior and calculate soil deformation.

Laboratory investigation on soft soil samples has already successfully addressed many issues such as soil anisotropy, rate effects, and sample disturbance. Across all these issues, sample disturbance still remains the most unclear and the most difficult to deal with in practice. Sample disturbance influences, to a great extent, all engineering properties of the soil, from stress history and preconsolidation pressure to undrained shear strength. Although sample disturbance importance when assessing the stress-strain-strength behavior of soft soils is well established over the literature, there is still not a correct and generally accepted quantitative method to evaluate sample quality. So far, the only method to assess sample quality used in common practice, if any, is the Specimen Quality Designation (SQD, Tezaghi et al. 1996, Lunne et al. 1997). This criterion is a rough indication of sample quality and is only used to characterize samples from A to E or from very good to excellent to very poor categories respectively. The lack of a quantitative method to calculate sample disturbance makes also extremely difficult to try to back-calculate the actual, "in-situ" soil properties from the calculated engineering values in the lab. So, there is still a great debate on how disturbance affects some of the most important engineering properties of the soil such as the preconsolidation pressure; one of the most critical parameter in stress-strain history and deformability of the soil.

Sample disturbance, by definition, is related to all the changes in stress, water content and structure that a soil element undergoes, from the time it rests in the field, to the time it is on the

lab bench, ready to be tested. This includes all the sampling operations, before, during and after the actual sample retrieval; drilling, tube sampling, tube extraction, transportation and storage, sample extrusion and sample preparation (Ladd and Lambe, 1963; Hypothetic Stress Path). So, even at ideal conditions, where appropriate equipment and procedures are followed during sampling, there is going to be some unavoidable disturbance.

In soft, normally consolidated or low overconsolidated clays, the problem of sample disturbance comes across mostly when we try to evaluate the preconsolidation pressure versus depth. Sample quality can significantly alter the preconsolidation pressure calculated from lab tests and can lead to a misinterpretation of the preconsolidation pressure profile. In these cases, it is often observed that disturbance increases with depth. It is also common to exclude many data, as fault, due to low sample quality (SQD). So, great experience and engineering judgment is needed in order to come up with the correct soil profile and properties.

1.2 Research Objectives

This research focuses on the understanding of the effects of sample disturbance on the compression curve and the preconsolidation pressure of soft clays. It is a comprehensive study of the most important available methods to estimate preconsolidation pressure and disturbance. It uses simple element triaxial equipment and employs the SHANSEP approach (Ladd and Foot, 1974) to reconsolidate San Francisco Bay Mud (SFBM) specimens and recover the intact soil behavior after disturbance. Disturbance is simulated in respect with the Ideal Sample Approach (ISA, Baligh et al., 1987).

Effects of ISA disturbance are examined on intact and resedimented normally consolidated (NC) San Francisco Bay Mud (SFBM) specimens. Then, a similar methodology is applied to evaluate the effects of disturbance on overconsolidated (OC) resedimented specimens and on a wide range of stresses. The effects of disturbance on an element outside the centerline of the sampler tube, as it is defined by the ISA, are experimentally investigated. This is done by incorporating a second disturbance phase after the ISA simulation, swelling the specimens to a lower volumetric strain. A new methodology is proposed in order to quantitative evaluate sample quality based on the shape of the compression curves for SFBM specimens. The method is based

on the modified indices ratio (the modified recompression to the modified compression index) that is an indirect way to measure the curvature of compression curves in a void ratio – log stress space. Stress level dependences on the K_0-consolidation and undrained shear behavior of the Resedimented San Francisco Bay Mud (RSFBM) are investigated through the extensive experimental triaxial program.

1.3 Organization of Thesis

Chapter 2 presents the background information on the topic of sample disturbance and preconsolidation pressure. In the first section, the early studies on the topic and Hvorslev work are being discussed. Also, an introduction is made to the Ladd and Lambe (1963) hypothetic stress path during sampling. The two different approaches on disturbance, the Perfect Sample Approach (PSA, Ladd and Lambe, 1963) and the Ideal Sample Approach (ISA, Baligh et al. 1987), which is the one used to simulate the disturbance in this research program, are presented. This is followed by the description of the two reconsolidation procedures available for triaxial testing; the recompression method (Bjerrum, 1973) and the SHANSEP method (Ladd and Foot, 1974). The later is further analyzed as it is the one implemented in this research in order to consolidate the SFBM specimens and erase the previous effects of disturbance. This is followed by a review of the most important techniques to estimate the preconsolidation pressure along with the compression and recompression indices. The chapter continues in describing the different approaches to the problem of quantification of disturbance, including the Specimen Quality Designation, the nondestructive – "in situ" assessments and some theoretical concepts based on the idea of the rigid – plastic boundaries and the intrinsic state line (ISL).

Chapter 3 provides a comprehensive description of the supporting technology and equipment used to complete the research program. The resedimentation procedures are described in detail and the material's geology and index properties are shortened. A brief overview of the MIT automated stress path cells (Sheahan and Germaine, 1992) as well as the low pressure and high pressure apparatus are reviewed. The design and build of the suction cap to incorporate extension capabilities on the high pressure cell are presented in detail. A short review of other instrumentation and essential elements used for the triaxial testing concludes the chapter.

Chapter 2 LITERATURE REVIEW - BACKGROUND

2.1 Introduction

Sample disturbance has always been a challenging topic of research from the time it was introduced, back at 1950's from Hvorslev (1949) and Ladd. From that point onwards disturbance is by far the most important factor in defining with accuracy the stress history and consolidation properties of the soil. This is due to the fact that disturbance has a significant effect to the quality and the reliability of laboratory test data. Anisotropy, stress history and rate effects also influence soil behavior but for practical applications, we can relatively easy take into consideration these factors. However, where sample disturbance is concerned, there is not a correct or generally accepted method to quantify disturbance or a standard way to treat the engineering properties from a lab test to derive the "true", in situ characteristics of the soil.

The most important effects of sample disturbance are the significant reduction of the sample effective stress (σ'_s) and a reduction in σ'_p during one-dimension compression. A hypothetical stress path for a soil element from the time it was sitting at the field (point A) to the time it is ready to be tested at the lab (point F) can be summarized in figure 2.1 (after Ladd and Lambe, 1963). This figure shows how the different procedures; drilling, tube sampling, extrusion, cavitation and water content redistribution within the tube, trimming and mounting in the triaxial cell, can alter in a complicated manner the stress path of the soil, resulting in a significant difference in the potential stress path of the soil during undrained compression shear (starting either from point A or F, dash line). Yet, much geotechnical practice relies in soil properties that are determined from soil specimens starting at the "laboratory" state of stress without accounting for this large state of stress difference, nor disturbance.

Ladd and Lambe (1963) also showed through their research that disturbance can lead to a decrease in the sample effective stress by as much as 80% of the in situ effective stress. They also noted that it is very difficult to define the correct in situ properties of

the soil, even after reconsolidation of the specimen because the disturbed sample will undergo significant volumetric changes and destructuring. This will cause a decrease in strength and stiffness during undrained shearing.

This chapter covers a wide range of what methods have been proposed to deal with disturbance and its effects. Section 2.2 presents Hvorslev's work on sample disturbance and Ladd and Lambe's theoretical stress path for a NC element during sampling and specimen preparation. Sections 2.3 and 2.4 present the Perfect Sample and the Ideal Sample Approach respectively that are the two main theories used to simulate and understand the effects of disturbance. Section 2.5 is about reconsolidation procedures; Recompression and SHANSEP. The advantages and the drawbacks of these methods are also discussed. Section 2.6 is about the compression curves of soft clays and the preconsolidation pressure. A variety of methods to define preconsolidation pressure are presented in chronological order. At last, section 2.7 presents different approaches to the problem of quantification of disturbance. The Terzaghi et al. (1996) and Lunne et al. (1997) criteria - which are the most significant methods so far - will be introduced. Proposals from the literature review on how to correct engineering values based on the degree of disturbance are stated.

2.2 Early studies

The first study on the subject of sample disturbance was introduced by J. Hovrslev (1949) in "Subsurface Exploration and Sampling of Soils for Civil Engineering Purposes". This was the final report of the Committee of Sampling and Testing of the Soil Mechanics and Foundation Engineering Division of ASCE.

This report was a comprehensive review of the, at that time, existing methods and equipment for soil sampling while focusing at the investigation of the effects of sample disturbance and at new improved methods and techniques for good quality samples.

Within this outline Hvorslev classified sample disturbance into five types to which the soil is subjective during sampling:

Chapter 4 presents an introduction to the framework of this research that has its core on work from Santagata and Germaine (1994) is presented. The ambiguity in preconsolidation pressure profiles with increasing depth is discussed. The chapter consists also a comprehensive report of the testing procedures followed in the majority of tests that were carried through for the completion of this research. The CRS and triaxial procedures for the low pressure and high pressure apparatus are described. Each chambers special characteristics are presented.

Chapter 5 presents an overview of the experimental results for the CRS and triaxial tests performed for this research. The phase relation calculation for the intact and the resedimented SFBM specimens used are presented. Results of the K_0-consolidation undrained triaxial testing program for normally consolidated, NC, intact and NC Resedimented SFBM follow. Then the overconsolidation behavior is introduced along with the results from test that account for swelling; volumetric change. The stress path, on a MIT p', q space is review for all the above cases. The modified compression and recompression indices are introduced.

Chapter 6 is complementary to chapter 5 and presents the interpretation of the results. The effects of stress level and lateral stress ratio on the undrained shear strength are discussed. The OCR and the strain at failure are also connected to different strength observations. Interpretation focuses on the effects of ISA on preconsolication pressure for intact and resedimented material, as well as for resedimented material of different OCR. The effect disturbance and swelling on the preconsolication pressure and the compression curve are presented. A method to quantitatively use the shape of the compression curve to estimate disturbance is proposed.

Chapter 7 contains a summary of the most important findings of this research. Future recommendations and research directions on the topic of sample disturbance are given.

i) changes in stress conditions,

ii) changes in water content and void ratio,

iii) disturbance of the soil structure,

iv) chemical changes,

v) mixing and segregation of soil components

The effects of disturbance on the engineering properties of the soil were also criticized. As far as stress changes during boring and sampling are concerned, the soil can undergo different phases of increasing or decreasing stresses but also it was noted that finally the external stresses on the sample will be reduced from those acting in the ground to atmospheric pressure. Hvorslev also observed that in saturated clays the changes in stress conditions will lead to decrease of the shearing resistance observed in unconfined compression tests. However this reduction will be less apparent on the results from tests in which the specimen is subjected to higher stresses than the original stresses in the ground.

Disturbance will also lead to changes in volume and void ratio before, during and after sampling. Changes in volume affect mostly the upper portion of the sample during boring and they are very difficult to estimate. The volume changes during sampling should not represent a major concern for saturated clays unless the boring procedures are slow enough to allow drainage. Finally when the sample is already at the tube there are some local water content changes due to internal mitigation of the water that are also very difficult to determine.

Emphasis was also given to the effect of disturbance on the soil structure which was described as the weakening of the inter-particle bonds and the rearrangement of the soil grains. In addition, results from UU and CU tests where used to observe the effects of disturbance on the compression curves reproduced in the lab. To summarize, it was noticed that highly disturbed samples will produce more rounded compression curves and obscure stress history. Disturbance will also reduce the unconfined strength. However in CU tests, this loss can be balanced or even erased by the increase in strength caused in consolidation when we decrease the void ratio.

Changes in chemistry of soils as a type of disturbance are also analyzed in detail. Generally changes are caused during storing samples for an extended period of time in untreated containers. The most common form of chemical disturbance is oxidation which can be caused by the prolonged exposure of the soil to the air and penetration of salts from the wash water from the drilling mud into the soil at the bottom of the borehole.

Finally, mixing and segregation is a gross form of disturbance that can be caused by improper cleaning of the borehole, by using of an open sampler or by piping or partial liquefaction caused by the creation of a vacuum over the sample. However, it must be said that mixing and segregation can generally be controlled and limited by using the right boring techniques and equipment.

Having defined the different categories of disturbance, Hvorslev tried to identify when a soil sample can be considered as undisturbed. There are three necessary requirements that need to be met. The sample must suffer no alteration of the soil structure, there should be no change in water content or void ratio and no change in constituents or chemical composition.

He also mentions some "practical requirements" and qualitative indications in order to identify disturbance in a sample mostly during testing and shipping of the soil. These requirements are:

- The ratio between the penetration of the sampler below the bottom of the borehole and the length of the recovered sample must be very close to 1.
- No distortions or other signs of disturbance must be visible
- The net length and the weight of the sample should not change during shipment, storage and handling.

Of course, it was noted that all these requirements were considered complimentary in order to get good quality samples.

Some further indications to identify disturbance in soil samples can also be made by:

- observing the shape of the compression curve as well as the stress strain curve during compression tests; more rounded shapes can be translated as more disturbance to the sample
- observing the variation in test results within the sample
- comparing the quality of samples taken by various methods
- comparing test results from samples of different diameter.

Hvorslev pointed out that the magnitude of disturbance and its influence on the engineering properties measured in the lab tests depend on the equipment, the procedures used for sampling and shipping and also on the characteristics of the soil itself. He suggested the most proper techniques existing at the time, in order to obtain good quality samples in different soil types and he indicate methods and practical hinds in order to reduce disturbance in practice. Particular emphasis was placed on the use of fluid to prevent caving of the borehole and on performing the sample operations as quickly as possible in order to minimize swelling caused by the excavation.

Ladd and Lambe (1963) based on the hypothetical stress path during sampling (figure 2.1) proposed many practical solutions that one should bear in mind during the different procedures to eliminate the effects of disturbance.

Borehole drilling (path point 1 to 2) involves mainly a reduction in the total vertical stresses. This stress path passes through a point for which the vertical stress is equal to the horizontal stress (σ_{h0}). This point at the X axis will correspond to the "perfect sampling effective stress" (σ'_{ps}) as it was defined by Ladd and Lambe. In order to avoid this extensive stress relief at the bottom of the borehole a weighted drilling mud must be used (figure 2.2). The weight of the mud must be such that point 2 is being kept as close to the perfect sampling effective stress as possible, and of course avoid extension. Later on, Ladd and DeGroot recommended a typical mud weight to range between 1.2 ρ_w to 1.3 ρ_w. The mud can be developed by using cutting material from the site and/or commercial drilling products such as barite (barium sulfate, specific gravity of 4.2).

Tube sampling (path points 2, 3, 4 and 5) involves the cycle straining that a soil element at the centerline of the tube undergoes during the process of the tube entering the soil mass (after Baligh et al. 1987, figure 2.3, 2.4). To decrease the advert effect of extensive shearing one should use modified tube geometries for the samplers (table 2.1; dimensions of typical samplers). For soft clays large diameter samplers should be used ($\geq$ 76 mm) with a sharp edged (5° to 10°, depending on stiffness), a small area ratio (AR < 10%, where AR = $(D_2^2 - D_1^2) / D_1^2$) and an approximately zero inside clearance ratio (ICR $\approx$ 0, where ICR = $(D_3 - D_1) / D_1$) (figure 2.5). Tubes should be made from noncorrosive materials and have clean, lubricated inside surface.

Path from point 5 to 6 involves tube extraction. Disturbance during extraction involves debris or disturbed soil that can be entered into the tube and result to a significantly altered sample quality especially at the top and bottom of the tube. To eliminate these effects, fixed piston sampler should be used if high quality samples are a necessity.

Transportation and storage (points 6 to 7), can also contribute to disturbed samples. Excessive vibrations or temperatures changes can radically alter sample quality. Oxidation might occur over time unless proper handling procedures are used. Additionally, during storage the overall effective stress of the sample is expected to slightly decrease because of the positive induced pore pressure of the perimeter zone of the tube that goes through excessive shearing. To avoid further disturbance during this step, the sample tube should be carefully sealed with wax, duct tape and a plastic cap (figure 2.6). Tubes should not be subjected to excessive temperatures or humidity.

Path points from 7 to 8 involve sample extraction. Samples should be extruded from the tube only after breaking in advance the bonding between the inside of the tube and the soil. This can be easily done by using the wire saw. Extrusion of the sample should preferably be done in the same direction the sample was taken; from bottom to top of the tube.

Path from point 8 to 9 involves specimen preparation. When the sample is on the lab bench, trimming and handling may cause a further stress relief. For standard quality samples of soft clays the pre-test effective stress should be $\sigma'_s/\sigma'_{ps} \approx 0.25$. Specimens

should be carefully trimmed in humid environment with sharp cutting tools and a wire saw (figure 2.7).

2.3 The Perfect Sample Approach

In 1963 Ladd and Lambe made the first rational effort to quantify the minimum disturbance effects. From their work, "Perfect Sample Approach" it was suggested that the only disturbance that cannot be avoid during sampling operations is the release of the in situ shear stress. It was also suggested that when all other sources of disturbance have been eliminated, it is possible to predict the effective stress after sampling as:

$$\sigma'_{ps} = \sigma'_{vo} [K_0 + A_u(1-K_0)]$$

where σ'_{ps} is the effective stress at the end of perfect sampling, σ'_{vo} is the in situ vertical effective stress, K_0 is the lateral stress ratio and A_u is the A parameter for the undrained release of the shear stresses. It should be noted that Perfect Sample Approach should only be used in the case of block samples since it ignores the strain path history of the soil sample.

2.4 The Ideal Sample Approach

A few years later, Baligh et al. (1987), based on Strain Path Method and the previous work of Ladd and Lambe will present the Ideal Sample Approach. In their work will point out that tube sampling can also cause other inevitable disturbance besides that produced by the release of the in situ shear stresses. This inevitable tube-sampling disturbance and its effects are primarily due to tube-penetration. So, their work is mainly focusing in trying to analyze and model the motion and its effects that a soil element is subjected to, during the tube penetration into the soil.

More specifically, during the process of tube penetration, the soil is subjected to a complex strain path history, depending on the position of the soil element within the sampler and the tube geometry expressed as the thickness to the diameter ratio. Using the Strain Path Method and by superimposing the effects of a ring source and a uniform flow, Baligh presented the magnitude and the extent of straining due to steady state penetration of an S-sampler. Figure 2.3 presents contours of the different strain components produced by the penetration of an S-sampler with typical dimensions for thin-walled tube samplers (B/t=40). Furthermore they indicated the complexity of the strain field around the tip of the sampler and showed that the shear strain is very large in vicinity of the sampler wall and is sharply reduced after passing the tip. From their work it was also interfered that soil disturbance, as described by the level of shear distortion decreases towards the center of the sample. Also, while in the inner half of the sample the variations in the soil strains are minor (ε_{zz} is dominant, $\varepsilon_{rr}=\varepsilon_{\theta\theta}$ and ε_{rz} is almost zero), at the outer half of the sampler soil disturbance involve significant non-uniformities. At the same presentation of his work, Baligh suggests that a reasonable estimate of the soil disturbance within the sampler can be obtained from results at the centerline of the tube. So, he describes the effects of the tube penetration by presenting the undrained strain paths of a soil element located at the centerline of a simple-sampler. The retrieval and extrusion of the sample are modeled as in PSA, by the undrained shear stress release. Figure 2.4 presents the vertical straining to which an element at the centerline of the tube is subjected. The straining for different sampler diameters is also being stated (B/t=20, 40, 50). For thin wall samplers, B/t >> 1, the maximum axial strain in compression and extension at the centerline of the sampler, $\varepsilon_{zz\,MAX}$, is given from the equation (Baligh et al. 1987):

$$\varepsilon_{zz\,MAX} = 0.385 \cdot t/B$$

As we can see from the figure, there are three main phases of undrained triaxial shearing. The initial phase is when our element is ahead to the sampler, and it is subjected to compression which reaches a peak at 0.35*B bellow the tip of the tube (ε_{max}). The second phase, when the element passes through the tip of the tube and is subjected to extension. This extension makes ε_{zz} equal to zero at exactly the tip of the tube and we

reach again a ε_{min} at distance 0.35*B above the tip of the sampler. At the third phase and when the element is well into the tube (distance greater than 0.35*B) a last phase of compression is taking place. Gradually ε_{zz} approaches zero when the sample is being relaxed into the sampler. Here it should be noted that the thicker the tube's walls the more the straining at our soil element. For example, analysis shown that for a standard Shelby tube with B/t=40, the maximum compressive strain would be approximately 1%. This means that for a NC or low OCR clays the axial strain at peak is exceeded and the soil fails during the initial compression phase and when the soil has not enter the sampler yet. At Baligh et al. work, it was also stated that from some K_0-triaxial test conducted at MIT on NC Recentimented Boston Blue Clay (RBBC), the soil disturbance predicted by the ISA have significant effects on the undrained behavior of clay and predicts a large reduction in the mean effective stresses in comparison with the PSA. It was also shown from UU tests on BBC that the ISA describes in terms of residual effective stresses, undrained strength, strain at peak, stiffness, post peak behavior and stress path, more accurately than the PSA. It was also suggested that for tube sampling, the ratio between σ'_s, the effective stress in the sample and σ'_{is}, the value predicted by ISA, should be used as an indication of the "avoidable" disturbance undergone by the sample and possibly to correct the normalized strength parameters obtained in UU tests.

2.5 Reconsolidation Procedures

There are two main reconsolidation procedures that have been widely recognized and used in triaxial testing of cohesive soils: The Recompression method proposed by Bjerrum in 1973, and the SHANSEP (Stress History and Normalized Soil Engineering Properties) approach proposed by Ladd and Foott in 1974.

The recompression method is based in the logic that the significant effects of swelling caused by disturbance can be limited if prior to shear the specimen is consolidated to the in situ vertical effective stress (σ'_{v0}), figure 2.8, point 3. In these levels of stresses the excess water that is absorbed during sampling will be squeezed out of the soil. However, Bjerrum also suggested that this method is only applicable and can

give safe results when the swelling is so small that is of elastic nature. For that reason, Recompression technique should only be used in the case of highly structured, brittle and sensitive clay, for highly overconsolidated material or cemented soils that retain much of their small strain stiffness (less than 1%). In addition, as many researchers have point out (Jamiolkowski et al. 1985, Ladd 1986) the technique give good results only when high quality sampling is available (block sampling such us the downhole Sherbrooke sampler or large diameter tube samplers).

Recompression should always be accompanied by an evaluation of the in situ stress history in order to estimate K_0, check the reasonableness of the measured s_u/σ'_{v0} values and extrapolate and interpolate the data versus OCR (after Ladd, 1991).

In this research, following the recommendations of previous work at MIT (Santagata and Germaine, 1994) the SHANSEP reconsolidation method is being employed. SHANSEP (Ladd and Foott, 1974) technique is based in the idea that the effects of disturbance can be erased by reconsolidating the soil to the pre-disturbance OCR. This was based in the assumption that natural soils exhibit normalized behavior influenced only by the value of the OCR. For normally consolidated soils (NC) this means that effects of disturbance can be erased simply by reconsolidating soil well into the virgin compression line.

SHANSEP method is applicable to uniform cohesive soils that have been mechanically overconsolidated or are truly normally consolidated and maintain the same basic structure during loading beyond the in situ stresses and therefore exhibit behavior that can be normalized by the preshear consolidation stresses. This means that we can simulate at the laboratory the in situ stress history and by it we can make accurate predictions of the in situ soil behavior in different OCRs even though the actual stresses between the field and the laboratory divert. The new stress history is achieved by 1-D (K_0) consolidation well past the preconsolidation pressure (σ'_p) and into the Virgin Compression Line (VCL), to a new maximum stress (σ'_{vm}), (Points A, B figure 2.5). Ladd (1991) proposed that σ'_{vm} must be greater than 1.5 to 2 times the preconsolidation pressure (σ'_p). For OCRs greater than 1, the soil is mechanically unloaded by K_0 swelling

to the desired OCR. It is assumed that no matter the physical mechanisms causing the in situ overconsolidation, same OCR soils will share identical behavior (points C or D).

The method is not intended to be used in highly structured soils such as sensitive clays, cemented clays or drying crust of soil deposits (highly OCR soils). This is due to the fact that consolidating to normally consolidated state alters significantly whatever structure was intrinsic to the soil. Also, it has been shown (Estabrook 1991, Clayton et al. 1992) that the SHANSEP procedure does not lead to an accurate evaluation of the stiffness of the soil. However this method is the only one to be applied for NC soils or under-consolidated soils, such us recent marine sediments.

The method although it can be used for either drained or undrained conditions, is most commonly used to describe the undrained shear in triaxial compression and extension tests, plane strain compression and extension, and in direct simple shear tests.

Ladd and Foott also performed a series of CK_0U tests on clay and by consolidating to deferent stresses (Figure 2.9, 2.10) they established a relationship to predict the undrained strength for any given OCR from the parameters S and m from the equation:

$$s_u/\sigma'_{vc} = S \cdot (OCR)^m$$

where S is the undrained strength ratio for the normally consolidated clay, and m is the slope of the regression line.

Comparing the two methods, recompression and SHANSEP, (de la Beaumelle, 1991 and Estabrook, 1991) findings show that recompression seems to result in higher S values for triaxial compression, and a higher m value for triaxial extension while it exhibits lower strain to failure, especially in triaxial extension tests.

A summary table of the advantages and disadvantages of the two methods are presented in table 2.2.

2.6 Compression Curve and Preconsolidation Pressure

It is widely acceptable nowadays that disturbance has obvious influence at the shape of the compression curve as well as at the compressibility parameters and the Preconsolidation Pressure. Theoretically, one can assess sample disturbance by these indications. However, there is not yet a standard methodology, or a correct solution to deal with disturbance and handle the results from lab tests so as to derive the "true", in situ properties of the soil. Additionally, there is a disagreement at the effects of disturbance at preconsolidation pressure (σ_p') and how σ_p' is related with sample quality.

Lacasee et al. (1995) and La Rochelle et al. (1981) present their results for quick and sensitive clay, using block and 90mm tube samples, and indicate that even though the values of the preconsolidation pressure estimated from the piston samples are lower than those obtained by testing the block samples, very small differences are observed at the preconsolidation pressure profile. Holtz et al. (1986) came to the same conclusions after a series of oedometer tests performed on block and piston samples. Hight et al. (1992) noted at his work that, even though σ'_p should normally be located on the limit state curve at the intersection with the K_0 line, this path depends on factors such as p'_i (mean effective stress) and disturbance. It is therefore possible that in different quality samples, not only the location of the boundary surface is different, but also the region in which the oedometer path meets the bounding surface varies. So, the effects of disturbance on the preconsolidation pressure will not always be apparent.

In general the effect of sample disturbance for Normally Consolidated clay (NC) can be summarized at figure 2.11. So, increasing disturbance is associated with more rounded compression curve which implies an increase in the slope recompression curve (C_r) and a decrease at the compression ration (C_c), the slope of Virgin Compression Line. Moreover, it was so far commonly implied that disturbance decreases σ'_p (Jamiolkowski et al. 1985, Peters 1988, Don J. DeGroot 2001) which as the results of this research show, is not always the case. Disturbance does further decreasing significantly sampling effective stress σ'_s and increasing reconsolidation strains. This was commonly stated

from different researchers over the past few years but non systematic research was done at this topic leaving the misbelief that σ'_p generally reduces with disturbance.

Lunne et al. 1997 presented how different sampling methods can alter the stress - strain behavior calculated at the lab for Norway clay. At their research they used three different sampling techniques; the NGI 54 mm diameter sampler, a standard 75 mm diameter fixed piston, thin-walled tube sampler, and the Sherbrooke block - high quality sampler. Results from (CAU) triaxial tests clearly shown that disturbance causes more volumetric changes when reconsolidating the samples back to the in situ stresses and will significantly alter the strain - stress behavior as in figure 2.12. Disturbance's effects are also clear at the undrained strength and the failure more of the sample; more disturbance results in more ductile response during shearing, lower strengths and an increase at strain at peak (figure 2.13).

2.6.1 Determination of the Preconsolidation Pressure

Over the past decades, many methods have been employed for the interpretation of the vertical effective yield stress or preconsolidation pressure, σ'_p. The concept of preconsolidation pressure and its importance is well defined in geotechnical engineering for calculating settlements or normalizing other engineering parameters like undrained shear strength. Bearing this in mind many methods have been proposed to define σ'_p with accuracy but all these do depend on good to high quality samples. As Becker et al. (1988) pointed out when he was trying to quantify the different methods on his studies: "it is not a question of which technique is correct; rather the issue is which technique provides the most repeatable result and is least ambiguous".

The need of defying with accuracy the preconsolidation pressure derives primarily from its use on the well known equations to calculate consolidation settlements on soft soils.

- Based on these equations, the consolidation settlement for a normally consolidated (NC) soil with a layer thickness of H and an initial void ratio of e_0, would be:

$$S = \frac{C_c}{1+e_0} \cdot H \log\left(\frac{\sigma'_{v0}+\Delta\sigma'}{\sigma'_{v0}}\right),$$

where S is the total settlement, C_c is the compression index corresponding to the slope of the virgin compression line on a e – logσ' space, $\Delta\sigma$' is the increases in stress and σ'_{v0} is the in situ vertical effective stress.

For overconsolidated soils (OC), the equivalent equation can have two forms;

- When the maximum effective stress is less than the preconsolidation pressure of the soil, $\sigma'_{v0} + \Delta\sigma' < \sigma'_p$, the settlement is dominated by the recompression portion of the compression curve, so:

$$S = \frac{C_r}{1+e_0} \cdot H \log\left(\frac{\sigma'_{v0}+\Delta\sigma'}{\sigma'_{v0}}\right),$$

where C_r is the recompression index corresponding to the slope of the recompression curve on a e – logσ' space.

- When $\sigma'_{v0} + \Delta\sigma' > \sigma'_p$, then the settlement is dominated by both the compression and recompression portion of the compression curves, and:

$$S = \frac{C_r}{1+e_0} \cdot H \log\left(\frac{\sigma'_p}{\sigma'_{v0}}\right) + \frac{C_c}{1+e_0} \cdot H \log\left(\frac{\sigma'_{v0}+\Delta\sigma'}{\sigma'_p}\right)$$

Among others, Casagrande's method (1963) is the oldest and most commonly used technique to estimate the preconsolidation pressure, σ'_p. The advantage of this method is that it is quick and easy to perform. The method gives good results when there is a well defined break point in the e-log σ'_v space. It is based at the assumption that the soil experiences a change in stiffness, from a stiff response (elastic behavior) to a soft response (plastic behavior), close to the yielding stress. From this breaking point which is

also the point of maximum curvature on a e - logσ'_v , one must drawn two lines; one tangent to the curve at this point and a second horizontal line passing from this same point. Bisecting this angle, the point at which this bisector will intersect the virgin compression line (VCL), would represent the preconsolidation stress (point B, figure 2.14). However, this technique is rather subjective and difficult to be applied in stiff clays or in samples where the transition boundary between elastic and plastic state is not well defined, so it can result in a large range of estimated values. The technique can also be influenced significantly from scale effects (Pinto 1992 and Clementino 2005).

Schmertman (1955) proposed a way to correct the compression curve from soil samples due to disturbance in order to better \ match the in-situ stress-strain history of the soil. This correction accounts for disturbance of the soft clay from sampling, transportation and storage, trimming and reloading during reconsolidation. Corrections for compression index Cc were proposed. The method that is mainly applied for overconsolidated soils can be described at the following steps (Holtz and Kovacs, 1981):

- Define Preconsolidation pressure using the Casagrande (1963) Technique.

- From the initial void ratio e_0 draw a horizontal line up to the existing vertical overburden pressure σ'_{v0}. This would establish point 1 at figure 2.15.

- From point 1 draw a line parallel to the unload-reload curve slope and up to the preconsolidation pressure σ'_p. This will define point 2.

- From a point of void ratio $0.42 \times e_0$ draw a horizontal line to the virgin compression line curve. This would be point 3.

- Connection points 1, 2 and 3 by straight lines one can get the corrected stress-strain curve. The slope of line defined from points 2 and 3 would give the corrected, in-situ compression index C_c.

Schmertmann defined the $0.42 \times e_0$ as a reasonable estimate point for most clays where the field virgin compression slope intersects the virgin compression slope of laboratory consolidation tests.

Janbu Method (1969) proposed that the preconsolidation stress could be determined from a plot of constrained modulus, $m = 1/ m_v$, where m_v is the coefficient of volume compressibility) versus the axial stress in a linear scale. The stress where m exhibits a marked drop would reflect the preconsolidation stress (figure 2.16).

Pacheco Silva Method (1970), using e-log σ'_v space is also a widely used in Brazil fast and empirical construction technique. It requires no subjectivity and it is easy to use in soft soils even when changes in compressibility are not that evident. It initially requires to draw a horizontal line at e_0. Where this line intersects the VCL slope (the line tangent to VCL curve), a new vertical line is drawn to define a point at the compression curve. From this point a second horizontal line is drawn to meet VCL. This point would be the preconsolidation pressure (figure 2.17). However, Grozic et al. 2005, demonstrated that this method can produce some ambiguity for highly overconsolidated natural soils that exhibit more rounded compression curves.

The Butterfield method (1979), is based on the plot of variation between effective stress and volume changes. The intersection of linear fit lines of $\ln(1+e)$ and $\ln\sigma'_p$, plotted in linear space can define the preconsolidation stress (figure 2.18).

Tavenas Method (1979) was the first to plot the work ($\Delta H/H$) versus the effective stress and assumed linear relationship for the recompression part of the curve.

Following the path from previous research at MIT, in this project, the strain energy method was employed in order to compute σ'_p. The strain energy method was proposed by Becker et al. (1987) and is a much more consistent, objective method which uses the work per unit volume as a criterion to evaluate preconsolidation pressure. This method is easy to use and produces more rounded compression curves, making definition of σ'_p easier even for stiffer soils (Ladd and DeGroot 1992).

The strain energy is defined as the summation of the product of an increment in strain by the average stress over that increment and the preconsolidation pressure is defined as it can be seen in figure 2.19. In the plot of work versus the vertical effective stress two lines are defined; one tangent to the initial portion of the graph, line a, and one

tangent to the latter straight portion of the curve that corresponds to the VCL, line b. The intersection between the two lines is the calculated preconsolidation value. Regression analysis can be easily employed to make this method easily repeatable. This method however requires some subjectivity in the determination of the "best - fit" line especially of the recompression part of the curve for triaxial testing. For this reason when this method is been applied a minimum, a maximum, and a best fit value of preconsolidation pressure are reported. This allows a determination of preconsolidation pressure value with an error of ± 10% (Santagata and Germaine, 1993). However, because of the high volume of experimental tests compared in this research program, such an exercise would be impractical. So, the focus of this research was to use the method having good repeatability and the least ambiguity when reporting results.

Also at 1987, Oikawa suggested finding preconsolidation pressure from the intersection of fit lines from log (1+e) and stress plotted on a log (10) scale. Using a similar criterion, Onituka et al. 1995 used fit lines at ln (1+e) and log stress space. Burland 1990, used the e_{100}, defined as the void ratio at effective stress of 100 kPa and C_c, to plot void index, $I_v = (e-e_{100})/C_c$ on a linear scale and applied stress on a log scale and define preconsolidation pressure as the intersection of the two fit lines; for the recompression and virgin compression segments of the curve. Other worth mentioning methods are presented in table 2.3.

Pinto (1992), Gronic et al., (2003) and Clementino (2005) concluded in their papers - comparing different methods defining preconsolidation pressure - that the work method of Becker et. al. (1987) can provide the most systematic results and it should be preferred in most cases since it requires the least subjectivity.

Recently, Boone et al. (2010) proposed a new approach to estimate the preconsolidation pressure. This method derives mathematically the preconsolidation pressure based on an estimate of the compression and recompression index (C_c and C_r) and the in situ stress, σ'_{v0}. Figures 2.20 (a), (b) and (c) show interpretations of σ'_p for Wallaceburg and Beaufort Sea silty clay from Becker et al. (1987). An estimate of preconsolidation pressure using the Casagrande (1963) method, the Strain Energy

Approach $\sigma'_{p(B)}$, the Pacheco Silva (1970) method $\sigma'_{p(PS)}$, and the Booner (2010) new method $\sigma'_{p(C, \text{this paper})}$, are also reported for comparison and consistency.

2.6.2 The Compression and Recompression Ratio

When trying to calculate settlements in soft soil, the compression and recompression ratio or index, play a key role. Compression or recompression index refer to a void ratio – log stress space (e-log σ'_v). Respectively, compression or recompression ratios refer to a vertical axial strain – log stress space (ε_a-log σ'_v). Both represent the variation of the void ratio or axial strain as a function of the vertical effective stress and they are calculated as shown in figure 2.21. For the compression ratio (ε_a-log σ'_v):

$$CR = \frac{\Delta \varepsilon_a}{\Delta\{log_{10}(\sigma'_v)\}}$$

For the compression index (e-log σ'_v):

$$C_c = \frac{\Delta e}{\Delta\{log_{10}(\sigma'_v)\}}$$

The two are connected as:

$$CR = \frac{C_c}{1 + e_0}$$

where e_0 is the initial void ratio of the specimen for the relevant compression curve.

A typical range of compression index is from 0.1 to 10. Table 2.7 presents typical values of Cc for different soft clays and silts (Prof. Pestana, Berkeley 2007). The reported values for recent sediments of San Francisco Bay Mud on Pestana's report are from 0.4 to 1.2 and from 0.7 to 0.9 for the Old San Francisco Bay Mud. Table 2.8 presents typical

values of compression index as reported by Kaufmann & Shermann, 1964. On their table they gave a range of consolidation stress for the reported values and they discriminate values of compression index based on the plasticity of clays.

Table 2.9 presents a summary of empirical relationships that have been reported over the years in order to calculate compression index from water content (w_c %), liquid limit (w_L %) or initial void ratio (e_0).

The recompression ratio (RR) or index (C_r) would be calculated as the variation on the axial strain (ε_a) or void ratio (e) versus the change in log vertical effective stress on the initial part of every recompression curve and before reaching the preconsolidation pressure (green line, figure 2.30). This is the part of the compression curve that the soil behavior is, to a great extent, elastic. For normally consolidated soils the recompression index is about $C_r \approx 1/5$ to $1/10$ of C_c. This value increases with increases OCR as the compressibility of overconsolidated soils increases.

The swelling ratio (SR) or swelling index (C_s) would be respectively the variation on the axial strain (ε_a) or void ratio (e) versus the change in log vertical effective stress on the swelling part of the soil stress-strain behavior. An example can be seen on figure 2.22 (grey line); A resedimented San Francisco Bay Mud specimen is loaded up to 12 ksc vertical stress and then allowed to swell to a specific OCR. The swelling ratio (SR) is calculated as the slope of this swelling curve in the vertical stain – log vertical effective stress space.

2.7 Quantification of Disturbance

In many geotechnical projects the need of assessing sample quality can be critical. These are projects where high quality samples are not available due to geotechnical conditions (deep offshore sampling) or cost constrains. Over the past few years, the significance of sample disturbance in soil properties and the projects' infeasibility to provide high quality samples, leaded researchers employ a variety of methods to quantify the degree of sample disturbance.

A simple and visual method that has been used at MIT over the past 30 years is Radiography. It significantly facilitates the planning of the testing program especially in projects where high quality samples are limited. Radiography can be employed to nondestructively select the most representative soil for consolidation or strength tests since it can assess the quality of the sample by looking at the macrofabric features of the sample and the curvature of layering adjacent to the sample edges. Radiography also allows identifying other features in our samples before trimming or breaking the sample apart such as variations in soil type, bedding or shear planes, crucks, varves, presence of intrusions such as stones, shells or drilling mud and voids. However it must be said that especially in uniform deposits, structural damage of the clay may not always be visible by the means of radiography.

As early as in 1949, Hvorslev was the first to consider the specific recovery ratio (SRR) as a measure of overall assessment of sample quality corresponding to any macro-structural feature. Ladd and Lambe (1963) indicate that although the total stress reduces to zero upon extraction of the sample, the internal residual effective stress, σ'_R does not automatically reduce to zero. So, disturbance can be calculated as the difference (σ'_{ps} - σ'_R). Where σ'_{ps} is the isotropic effective stress for a perfect sample and can be calculated as a function of the in situ overburden pressure, σ_{vo} and the pore pressure parameter for undrained loading from the coefficient of earth pressure at rest, K_0.

Later on, Andresen and Kolstad (1979) suggested that, the vertical strain during K_0 consolidation, that is required to consolidate the sample back to its in situ vertical effective stress (σ'_{v0}) should be a relative indicator of sample quality. A good quality

sample is expected to have very little strain upon recompression while large strains would be a good indicator that sample is highly disturbed and results should not be trusted. The Anderson and Kolstad criterion is shown at table 2.4. Sample quality level A is supposed to be very good to excellent, quality B is good, C is fair, while D and E is poor and very poor respectively. The vertical strain at the in-situ vertical effective stress can be calculated as:

$$\varepsilon\ (\%) = \{(H_o - H) / (H_o)\} * 100,$$

where H_o = Initial Sample Height and H_s = Sample height at σ'_{vo}

The most significant so far trials to quantify disturbance are the ones that measure volumetric strains during reconsolidation. Terzaghi et al. (1996) and a year later Lunne et al. (1997) developed two simple and widely used qualitative methods to characterize sample quality. Both of them try to connect volumetric strain (ε_{vol}) during reconsolidation to the previous maximum effective stress with disturbance. Terzaghi et al. (1996), adapting a method of Andresen and Kolstad (1979), proposed the term Specimen Quality Designation (SQD) to rank samples for A (best) to E(worst) quality in regard with the measured volumetric strain. They also suggested that reliable estimates of engineering parameters of soils should require sample with SQD equal to B or A. This means that soil samples with disturbance falling at the last three categories should not be trusted for deriving the engineering properties. More recently, Lunne et al. (1997) tried to connect disturbance with ($\Delta e/e_o$), the change in void ration to the initial void ratio for reconsolidation to σ'_{vo}. This criterion is more complete than the one of Terzaghi since it accounts for the fact that a certain amount of change in pore volume during reconsolidation will be increasingly detrimental to the particle skeleton as the initial pore volume decreases. It is also expressed as a function of over consolidation ratio (OCR) since an equal amount of volumetric strain is more detrimental in higher OCR samples. The two criteria are summarized in table 2.5.

Later studies also by Lunne et al. 2006 on three different soft Norwegian marine clays came to validate the $\Delta e/e_0$ criterion. In a systematic study of parallel laboratory tests, three different sampling techniques were employed; the Sherbrooke block sampler, the NGI 54 mm composite sampler and the 75 mm Japanese piston sampler. Table 2.6 is a summary of the dimensions and features of the three samplers used. Figure 2.23 presents the change in the $\Delta e/e_0$ parameter during reconsolidation back to the in situ vertical effective stress for triaxial tests on the three different clays and for various depths. Specimens of Lierstranda (w(%)= 41, I_p(%)= 20), Daneviksgate (w(%)= 52, I_p(%)= 28), and Onsøy (w(%)= 63, I_p(%)= 38) clay were used. Results clearly indicate that the Sherbrooke block sample provides the best quality sampling method in most cases with all block samples in the "very good" to "excellent" quality category. The 54 mm samples have larger values of $\Delta e/e_0$ and fall in the categories "good to fair" and "poor". The 75 and 76 mm diameter samples were falling somewhere in between. The ratio $\Delta e/e_0$ or the magnitude of disturbance always increases with depth for all samplers.

The undrained stress – strain behavior of the three clays results indicate the following general pattern: The shear strength at peak of block samples is greater than the corresponding values for the tube samples; The peak shear stress for high quality samples (block samples) occur at axial strains less than 1%, and at much higher strains in tube, low quality samples; The shear stress at large strains (>10%) is higher for tube, low quality samples and lower for high quality, block samples, making the strain softening for block samples much more significant. Strain softening for disturbed, low quality samples is much less imminent. The reason for this behavior in soft soils is the following: At small strains, the main effect of sample disturbance is the breakdown of the clay structure and the cementation bonds resulting in distinct peaks and brittle collapses of shear strength. On the other hand, at larger strains where the structure of the specimen is more or less completely disturbed, the increase in shear resistant will be dominated by the reduction in water content. Thus, the peak shear stress will occur gradually and at much larger strains.

Anisotropy, rate effects, different reconsolidation techniques and delayed consolidation effects were also investigated. The effects of delayed consolidation for triaxial tests and undrained strength on Lierstranda clay are presented at figure 2.24.

Results showed that even after 4 to 6 months there is a rapid increase in both the undrained shear stress, s_u, and the preconsolidation pressure, σ'_p, of about 25%. This means that under in situ conditions the soil will almost never behave as pure normally consolidated clay. Cementation bonds developing in the field during and after sedimentation can cause an increase in the small-strain peak and a much more brittle behavior at larger strains.

Based on Lunne et al (2006) previous research, Berre et al (2007) proposed empirical procedures in order to estimate the potential increase in undrained shear strength that may be achieved when obtaining high quality block samples. The study is based on a comparison of high quality block samples and 54 mm tube samples on deposits of soft Norwegian marine clay. These empirical procedures should not be used for design unless they are verified with results from high quality samples. Furthermore, they are only valid for clays similar to the ones studies at this project; marine clays, normally consolidated to slightly overconsolidated, with plasticity index, I_p = 6% - 43%, water content, w_c = 20% - 67%, and depth less than 25m below ground level.

The first correction that Berre proposed is that of small strains (up to 3% shear strain). From the comparison of high quality block samples and low quality 54mm tube sample he conclude that high quality specimens tend to follow an "elastic" stress path with no tendency to dilate or contract much (zero induced pore pressure) up to the peak shear stress. At the MIT p' – q' space this corresponds to an inclination of 3:1 (figure 2.25). Disturbed normally consolidated samples tend to follow a stress path as this represented by curve ABC. So, a good approximation to correct for sample disturbance would be to say that the shear strength would be at point D, the intersection of line OB (the line drawn by the origin and passing through the peak shear stress point) and line AD (the vertical line passing through the starting shearing point). The horizontal line is preferred for NC or low OC clays since they tend to show a small contractive behavior just before failure. However for higher OCR values where their behavior can even be dilative line AF and slope 3:1 should be used to correct shear stress.

The second correction is that of large shear strains, about 15%. Here the behavior of soil depends more on the water content (w_c) and less at the soil structure which has more or less collapse. This correction takes into account the reduction in water content

during the reconsolidation phase by using the VCL from oedometer tests; for reasonable stress range the ratio between the undrained shear strength and vertical consolidation stress is assumed to be constant. The corrected shear strength at higher strains for sample disturbance for CAUC tests will then be (figure 2.26): $(s_u)_{cor.} = s_u \cdot \sigma'_1/\sigma'_2$

Clayton et al. (1992) and later Santagata and Germaine (1994) connected the strain amplitude of cycles in the ISA disturbance simulation with the reconsolidation strains when increasing disturbance in Bothkennar and Boston Blue clay respectively (figure 2.27, after Santagata and Germaine, 1994).

In all specimens used for this research program both criteria (Terzaghi et al. (1996) and Lunne et al.) where applied in order to connect the new observations to the well known and widely applied quantification methods. Varying the strain cycle amplitude from 0.5 to 10% (ε_c %) for different OCRs, resulted in a wide range of specimen quality characterization. Results for San Francisco Bay Mud will be presented at chapter 6.

A third category in trying to quantify disturbance has to do with methods developed to measure the "in situ" sampling effective stress. Ladd and Lambe (1963) were the first to propose a way to measure soil suction using fine ceramic porous stones or a mid height probe. Using soil suction they could then calculate the sampling effective stress and use this value as a first indication of disturbance. However, this criterion has the disadvantage that it completely disregards the amount of destructuring that the sample can undergo during sampling. Also the method cannot be applied in cemented clays where effective stress can be near zero even without any significant destructuring of the soil.

Poirier and Degroot, 2005 developed a non destructive, in situ method to quantify disturbance. Based in previous observations High et al. (1992), Tanaka et al (2001), Kirkpatrick et al. (1986) and Santagata and Germaine (2002) tried to use soil suction or residual porewater pressure as a way to quantify the sample quality immediately after sampling. For the scope of their research they used a portable suction probe, consisting of

a high air-entry porous ceramic stone and a pressure transducer capable of direct suction measurements in soil samples. The research involved the collection of high quality block samples and of conventional split spoon samples. Suction was measured in all the samples immediately after sampling or for the case of block samples few days after storing. Their results were compared with the assessment of sample quality based on consolidation tests that were conducted on all samples and based on the volumetric strain methods (Terzaghi et al. 1996 and Lunne et al. 1997 criteria). Results indicate that the high quality samples had much higher suctions (figure 2.28) and that the suction probe could potentially be a practical tool for making assessments of sample quality in the field and immediately after sampling.

Another very interesting nondestructive method to assess sample quality is that of using bender elements to measure shear wave velocity. The method was presented by Landon and DeGroot back at 2007. It uses a field bender element device to measure soil shear wave velocity, V_{uh}, immediately after collecting samples of BBC of different quality (Sherbrook block, tube, and split spoon samples). V_{uh} values were then compared to in situ values from seismic piezocone tests for the same depth (V_{SCPTU}). Then the ratio of V_{uh} / V_{SCPTU} was used in comparison with the conventional Lunne et al., 1997 criteria for sample quality ratings, as it is determined by $\Delta e/e_0$ during reconsolidation to the in situ vertical effective stress (σ'_{v0}). Results indicated a consistent correlation between the two methods (figure 2.29) and different ratios of V_{uh} / V_{SCPTU} were proposed to assess sample quality for BBC ranging from 0.77 for the block sample to 0.28 for split spoon samples. Landon and DeGroot also pointed out that the reduction in shear wave velocity from the in situ value for block samples was mainly due to stress relief whereas the additional reduction in shear wave velocity for tube and SPT samples was a result of both stress relief and destructuring. Overall the method showed consistency with Lunne et al. criterion and can be used as a rapid, on site test to provide an indication of sample quality. This information can also be used to adjust the sampling procedures as needed.

Nagara et al. (1990) offered a simple way to assess disturbance studying the compression path of monotonic loading of partially disturbed samples. They also noticed

that properties like undrained shear strength, tangent modulus can be corrected if the disturbance is known. They proposed that for different degrees of disturbance the yield stress σ'_y is along a line normal to each of the e - log σ'_v paths at their points of maximum curvature. They also proposed that the degree of disturbance can be calculated as:

$$SD\ (\%) = (\sigma'_{yf} - \sigma'_y) / (\sigma'_{yf}) * 100,$$

where σ'_y is the yield stress (preconsolidation pressure) obtained from the test data and σ'_{yf} is the intersection point where the horizontal line from the initial void ratio meets the perpendicular line to the tangent at the yield point of the compression curve (figure 2.30). Based on SD (%) Nagara et al. also proposed corrections to compression index and the unconfined compression strength obtained from experimental results on partially disturbed samples.

Consequently, plotting consolidation data in a ln(1+e) - log σ'v space as proposed by Butterfield (1979), Onitsuka and Hong (1995) proposed a similar equation to assess disturbance:

$$SD\ (\%) = (p_{yf} - p_{cL}) / (p_{yf}) * 100,$$

where p_{cL} and p_{yf} can be calculated from figure 2.31 and as in Nagaraj et al. (1990) method.

Using the same consolidation space, ln(1+e) - log σ'_v, but different approach, Hong and Onitsuka (1998) observed that the degree of disturbance is directly associated with the magnitude of the compression index in the pre-yield state. So disturbance can be calculate as the ratio of the value of the slope of pre-yield slope for test data, C_{CLB}, to the value of the slope of the compression path for the completely remolded state of the same clay C_{CLR}. This way disturbance ranges from close to zero for undisturbed samples to 100% for the remolded state.

$$SD\ (\%) = (C_{CLB} / C_{CLR}) * 100.$$

Two years earlier, Shogaki (1996) proposed a quantitative index based on the calculated volumetric strain ε_{vo} back to the maximum vertical effective stress and based in oedometer compression tests (figure 2.32). The criterion is close to Terzaghi et al. 1996, and SD can be calculated as:

$$SD\ (\%) = \{(e_0 - e_1) / (1 + e_0)\} * 100,$$

where e_0 is the initial void ratio of the sample and e_1 is the void ratio corresponding to the overburden pressure.

Last but not least, another theoretical method to quantify disturbance is the one based on the concept of Intrinsic State line (ISL) as it was proposed by Burland (1990). The ISL is supposed to be the liquid limit state of clays where most clays have the same order of pore water pressure (5-6 kPa) and exhibit the same order of shear strength (1.7 to 2.5 kPa). In this reference state the fabric of soil is not prone to disturbance (Nagaraj and Miura, 2001). The monotonic compression paths of clays with initial state corresponding to the liquid limit state were also calculated to be (data from Nagaj & Srinivasa Murthy 1986, Burland, 1990):

$\log_{10} (1+ e/e_L) = 0.365 - 0.072* \log_{10} \sigma'_v$, ISL path with an R^2 of 0.978 for 54 samples.

Using the concept of Intrinsic State Line and the concept of rigid - plastic behavior Nagaraj et al. 2003 proposed the following relation for assessing the degree of disturbance. This was based on the idea that for zero disturbance, ideally we expect initially rigid soil behavior and a perfectly non particulate response. This will give small compression up to the yield point. The yield point for a perfect sample would be a point of sudden collapse and a brittle failure where, from then on the sample experience completely plastic behavior:

$$SD\ (\%) = \{(\sigma'_y - \sigma'_{y(a,b,..)}) / (\sigma'_y - \sigma_R)\} * 100,$$

where σ_y is the most probable yield stress for the least disturbed state, $\sigma_{y(a,b,..)}$ is the yield stress of partially disturbed samples, and σ_R is the remolded stress corresponding to completely disturbed state (figure 2.33).

Using the theoretical concept of rigid - plastic behavior material and combining the Nagaraj et al. 2003 method and Hong and Onitsuka (1998) observations, Prasad and Nagaraj, 2007 proposed the following method to quantify disturbance.

$$SD\ (\%) = (C_{c1} / C_{c2}),$$

where C_{c1} is the pre-yield slope of the compression path in a log (1+e) - log σ'v space, and C_{c2} is the post-yield slope of compression path for the same test.

This method agrees with the observations that mechanical disturbance and stress release would result in partial failure of bonding of the soil structure and thus would increase pre-yield compression index. Also the greater the disturbance the flatter would be the slope of the post-yield portion of compression. For the ideal non particulate response, C_{c1} tends to approach zero while C_{c2} value tends to infinity for plastic flow. This would result to an ideal case zero sample disturbance. On the opposite side, for the completely remolded case, C_{c1} tends to be equal to C_{c2} and no difference in soil structure pre and post-yield stress can be noticed. This would give an SD close to 100%, and corresponded to a completely disturbed sample. Prasad and Nagaraj also mentioned that the two compression indexes are complimentary to each other in inverse proportion. The following corrections for compression index, yield stress and unconfined strength were proposed.

$$C_{cm} = C_{c2} / (1 - SD/100),$$
$$\sigma_{yc} = \sigma_y / (1 - SD/100),$$
$$q_{uc} = q_u / (1 - SD/100).$$

Dimensions of sampling equipment

Sampler	D_1 (mm)	D_2 (mm)	D_3 (mm)	t (mm)	Angle (°)	AR (%)	D_2/t (–)	ICR (–)
Standard SPT†	34.9	50.8	34.9†	15.9†	60	111.9	3.2	0†
	60.3	76.2	60.3†	15.9†	60	59.7	4.8	0†
Shelby tube	72.1	76.2	74.6	1.65	≈ 44‡	11.7	46.2	3.5
Modified Shelby tube	74.6	76.2	74.6	1.65	5	4.3	46.2	0
Sherbrooke	–	250	–	–	–	–	–	–

Table 2.1: Dimensions of typical sampling equipment

Recompression	SHANSEP
Perform CK_0U tests on specimens reconsolidated to thc insitu state of stress	Perform CK_0U test consolidating speciments well beyond in situ σ'_p to measure NC behavior and rebound to varying OCR to measure OC behavior
Preferred for High quality samples (block samples) or highly structured clays	Preffered for conventional tube samples of low OCR clays having low sensitivity
For cemented clays and weathered or heavily OC crusts	The only method to be used for NC or under-consolidated soils
Not for NC clays	Difficult to apply for high OCR soils
Plots depth specific strength values versus depth to develop s_u profile	Plots results normalized (s_u/σ'_{vc}) and forces user to explicitily evaluate in situ stress history

Table 2.2: Recompression and SHANSEP Techniques (after Ladd 1991); Advantages and limitations.

Year	Methods to define Preconsolidation Pressure	Space	Comments
1936	Casagrande Method	e - log (σ')	Graphical, subjective, most commonly used until now
1951	Burmister Method	ΔH/H - log σ'	
1955	Schmertmann Method	e - log (σ')	only for soft soil, an attempt to compesate for nominal disturbance
1969	Janbu Method	ΔH/H (or M = $1/m_v$) - σ', dσ'/dε	empirical, graphical construction
1970	Pacheco Silva Method	e - log (p')	Graphical, easy to use, good results, widely used in Brazil
1975	Sallfors	compression (%) - σ'	regression analysis
1979	Butterfield Method	log (1+e) - log (σ')	grapical, depends on critical state theory
1979	Tavernas Method	σ' * ΔH/H - σ'	regression analysis
1989	Jose et al. Method	log e - log p'	fitted lines, regression analysis
1987	Culley and Larson		regression analysis
1987	Becker et al.	ΔH/H - σ'_v	new approach, defines strain energy density
1987	Oikawa	log (1+e) - log (σ')	intersection of two fitted lines,graphical
1990	Burland	Iv = $(e-e_{100})/Cc$ - log σ'_p	empirical comparison of compression behavior of natural and remoulded soils
1991	Lebert and Horn	log σ' - e	fitted lines, regression analysis
1992	Jacobsen	$\sigma'_p = 2.5\,\sigma_k$	empirical, based on Casagrande construction
1995	Onitsuka et al.	ln (1+e) - log σ'_v	empirical, intersection of two fitted lines
1997	Strain Energy Log Stress Method, Senol, Van Zelst	ΔH/H - log σ'	regression analysis, based on Tavernas Method
2004	Dissipated strain energy method, Wang and Frost	ΔH/H - σ'v	use recompression and unload - reload curves

Table 2.3: Chronological table with the most important methods developed to define preconsolidation pressure.

Vertical Strain at σ'_{v0}	Sample Quality Level
< 1 %	A
1-2 %	B
2-4 %	C
4-8 %	D
> 8 %	E

Table 2.4: Sample quality designation used by Anderson and Kolstad (1979).

Specimen Quality Designation (SQD) (Terzaghi et al. 1996)		$\Delta e/e_0$ Criteria (Lunne et al. 1997)		
Volumetric Strain (%)	SQD	OCR = 1 – 2	OCR = 2 – 4	Rating*
		$\Delta e/e_0$	$\Delta e/e_0$	
< 1	A	< 0.04	< 0.03	Very good to excellent
1 – 2	B	0.04 – 0.07	0.03 – 0.05	Good to fair
2 – 4	C	0.07 – 0.14	0.05 – 0.10	Poor
4 – 8	D	> 0.14	> 0.10	Very poor
> 8	E			

Table 2.5: Quantification of Sample Disturbance Based on specimen volume change from Terzaghi et al. (1996) and Lunne et al. (1997).

Sampler	Length (mm)	Diameter D_w (mm)	Thick-ness t (mm)	Area ratio Ca (%)	D_w/t	Inside clearance ratio, (%)	Cutting edge angle (degree)	Sampling technique	Sites used w.r.t. Table 1
Sherbrooke block sampler	350	250	-	-	-	-	-	Preauger	All
75 mm piston (Japanese)	800	78	1.5	8.2	52	0.0	6±1	Preauger	Lierstranda
54 mm com-posite piston (NGI)	800	65	5.5	44.3	11.9	0.6	5	Displace-ment	All

Table 2.6: Summary table of the characteristics of the three different samplers used on the study by Lunne et al. (2006).

Soil Type	Compression Index, C_c
Normal consolidated clays	0,20 – 0,50
Chicago clay with silt (CL)	0,15 - 0,30
Boston blue clay (CL)	0,3 – 0,5
Vickburgs clay - dray falls into lumps (CH)	0,3 – 0,6
Swedish clay (CL – CH)	1 – 3
Canada clay from Leda (CL – CH)	1 – 4
Mexico City clay (MH)	7 – 10
Organic clays (OH)	4
Peats (Pt)	10 – 15
Organic silts and claye silts (ML – MH)	1,5 – 4,0
San Francisco sediments (CL)	0,4 – 1,2
Clay in the old San Francisco Bay	0,7 – 0,9
Bangkok clay (CH)	0,4

Table 2.7: Typical values of Compression Index, C_c for different types of soft soils (after Pestana, 2007).

Soil	Effective consolidation stress σ_{cef} [kPa]	Final effective stress in the soil σ_{ef} [kPa]	Compression Index, C_c
CL soft clay	160	200	0,34
CL hard clay	170	250	0,44
ML silt of low plasticity	230	350	0,16
CH clay of high plasticity	280	350	0,84
CH soft clay with silt layers	340	290	0,52

Table 2.8: Typical values of Compression Index, C_c for different types of soft soils and consolidation stress (after Kaufmann & Shermann, 1964).

Soil	Equations	Reference
Transformed clays	$C_c = 0.007\ (W_L - 7\%)$	Skempton 1944
Clays	$C_c = 1.15\ (e_0 - 0.35)$	Nishida 1956
Brazilian clays	$C_c = 0.256 + 0.43\ (e_0 - 0.84)$	Cozzolino 1961
Sao Paulo clays	$C_c = 0.0046\ (W_L - 9\%)$	
New York clays	$C_c = 0.009\ (W_L - 10\%)$	Terzaghi a Peck 1948
Clays of low plasticity	$C_c = 0.75\ (W_0 - 0.50)$	Sowers 1970
Taipei clays and silts	$C_c = 0.007\ (W_L - 7\%)$	Moh a kol. 1989
Clays	$C_c = 2.303\ \rho_c\ e_0\ \{1-(0.4/e_0)^2\}$	Pestana 1994
	$C_c = a\ W_L/100\ \{1-(20/W_L)^2\}$	

Table 2.9: Summary of reported empirical methods to calculate Compression Index.

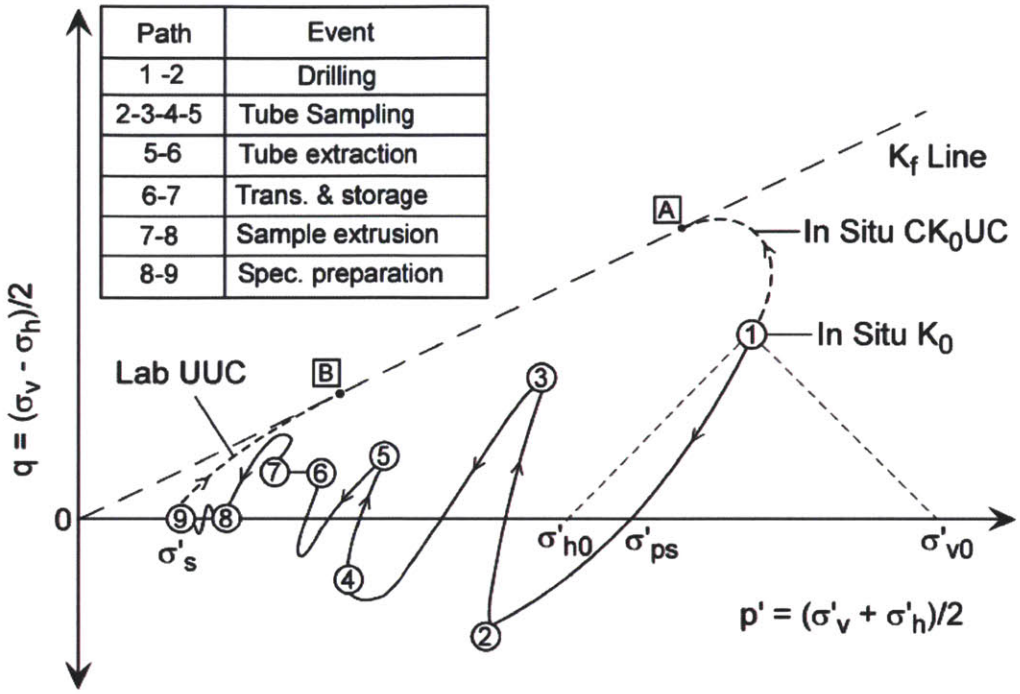

Figure 2.1: Theoretical Stress Path for a NC clay element at the centerline during sampling and specimen preparation (Ladd and Lambe, 1963).

Figure 2.2: Tube sampling using drilling mud (with a strainer for the rotary wash method (Photo: James Bay, Utah Department of Transportation Research Division 2003).

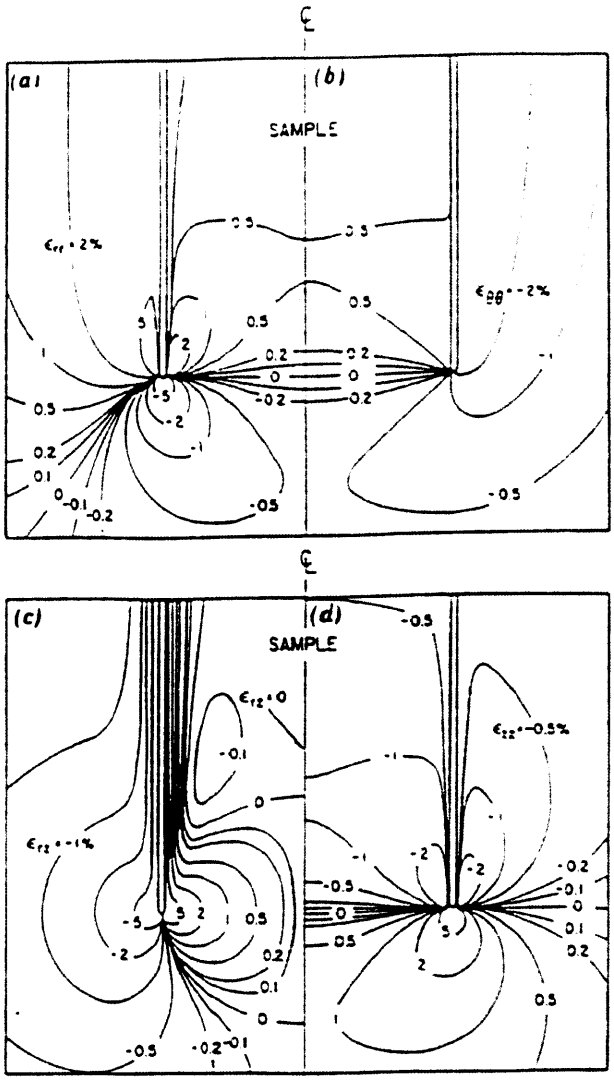

Figure 2.3: Contours of ε_{rr}, $\varepsilon_{\theta\theta}$, ε_{rz} and ε_{zz} produced by the penetration of a typical thin-walled tube sampler of B/t = 40 (Baligh et al. 1985).

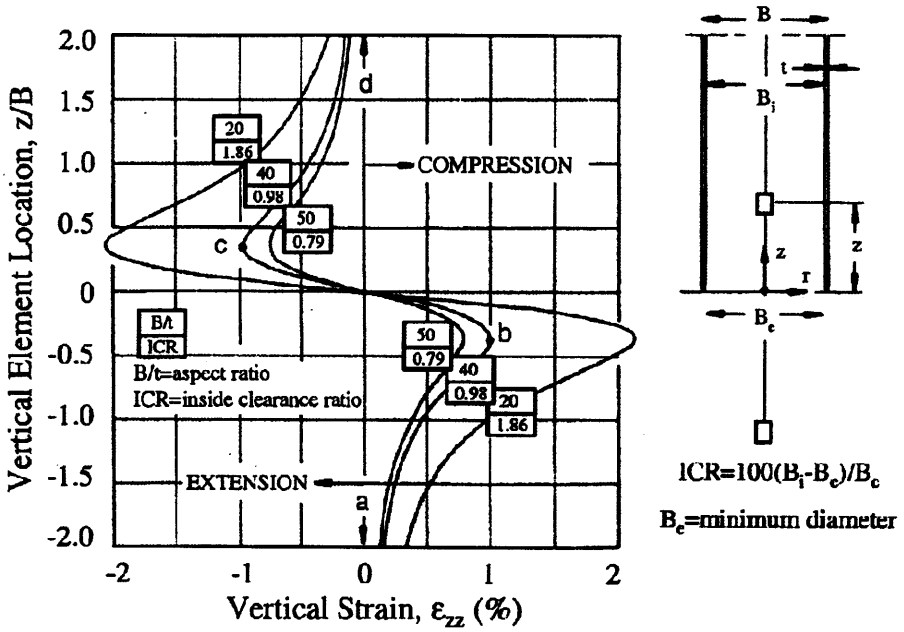

Figure 2.4: The strain path method (after Baligh et al. 1987). The axial straining that a soil element undergoes at the centerline of the tube during sampling for different B, t.

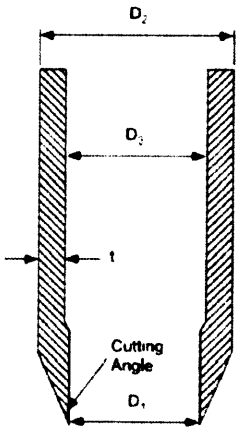

Figure 2.5: Sample tube dimensions (after DeGroot et al. 2005).

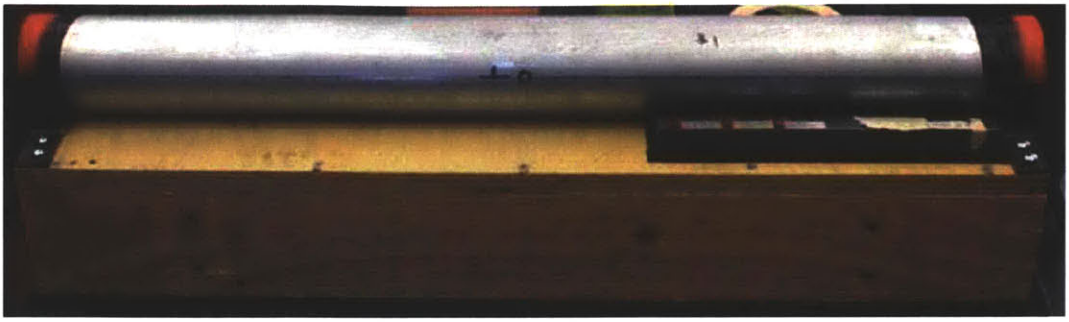

Figure 2.6: Sample tube ready to be stored.

Figure 2.7: Trimming equipment for soft clay (MIT 2010).

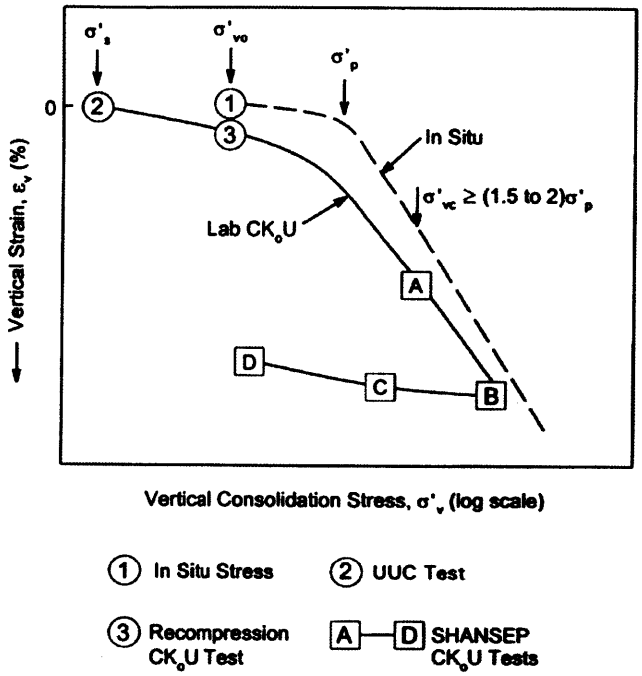

Figure 2.8: Consolidation procedures for laboratory CK_0U tests (Ladd, 1991)

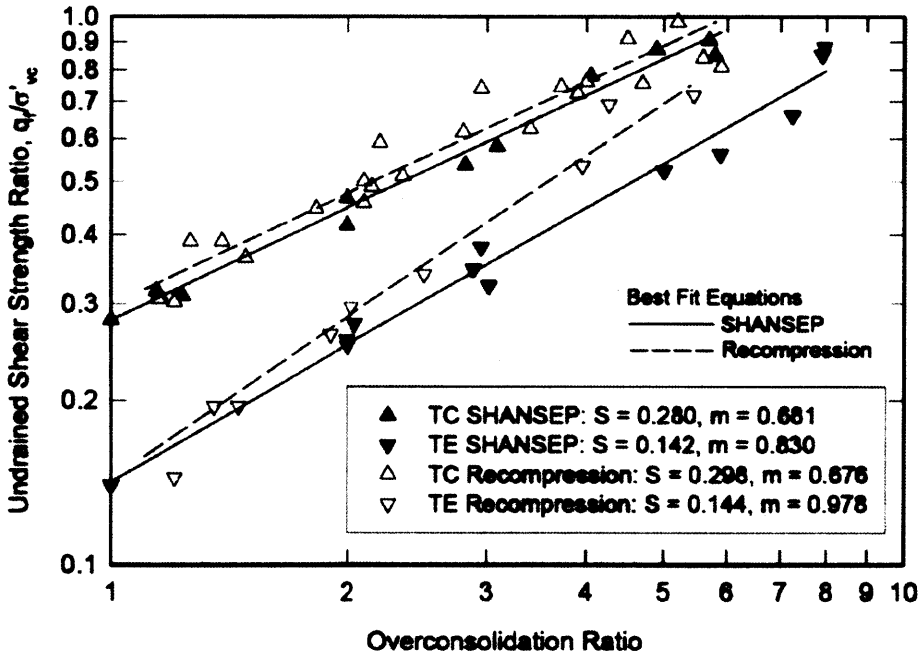

Figure 2.9: Comparison of the Undrained Streng ratios, BBC – South Boston STS for SHANSEP and Recompression for different OCRs.

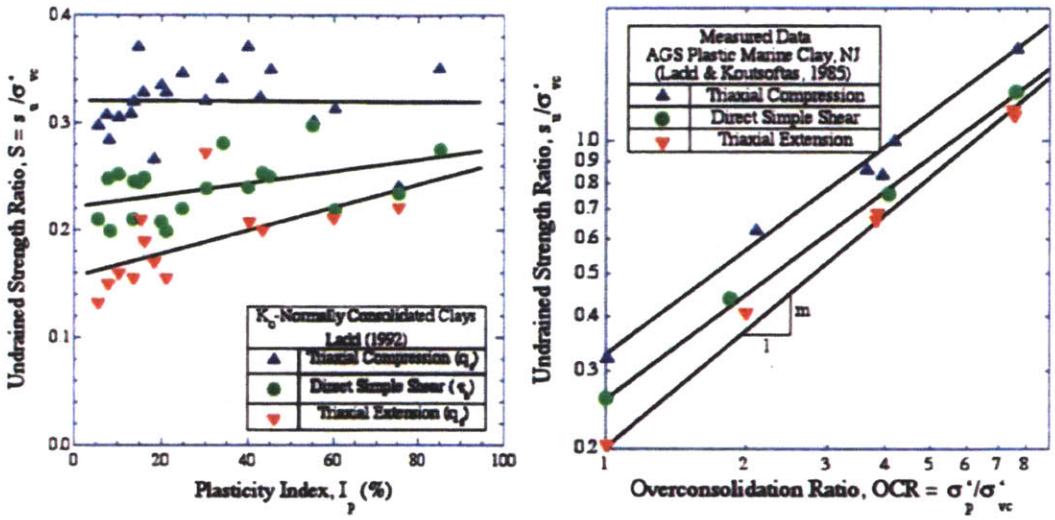

Figure 2.10: Empirical Relations SHANSEP for Undrained Shear Strength (Ladd & Foott, 1974). S is the USR for NC clays (OCR=1) and m = 0.8 ± 1.

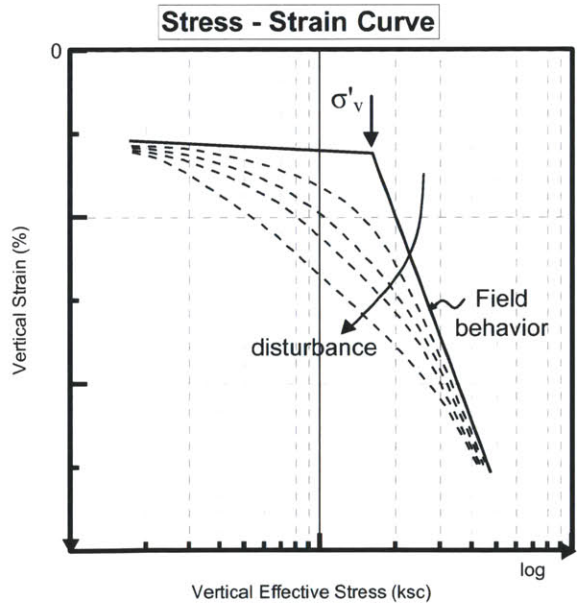

Figure 2.11: Effects of disturbance at a typical stress – strain curve.

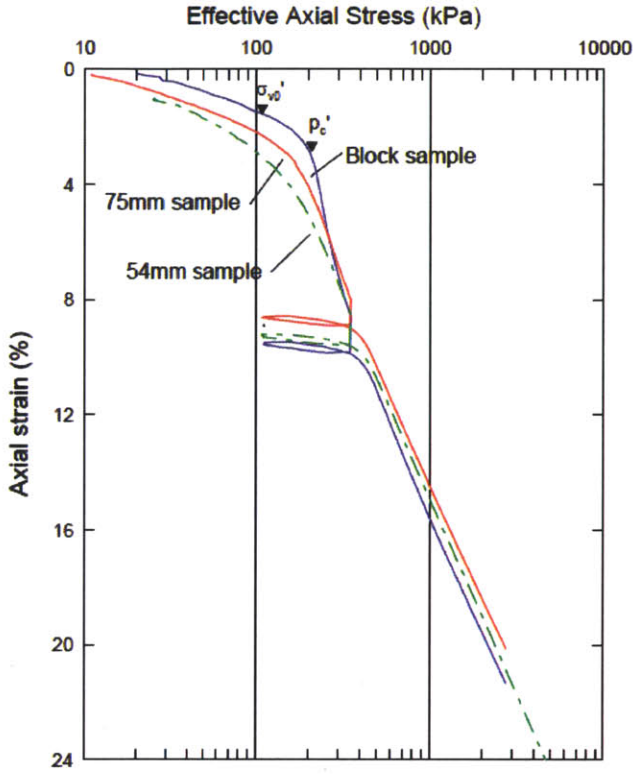

Figure 2.12: (CAU) Triaxial compression curves for specimens of Norway clay collected with three different samplers (Lunne et al. 1997).

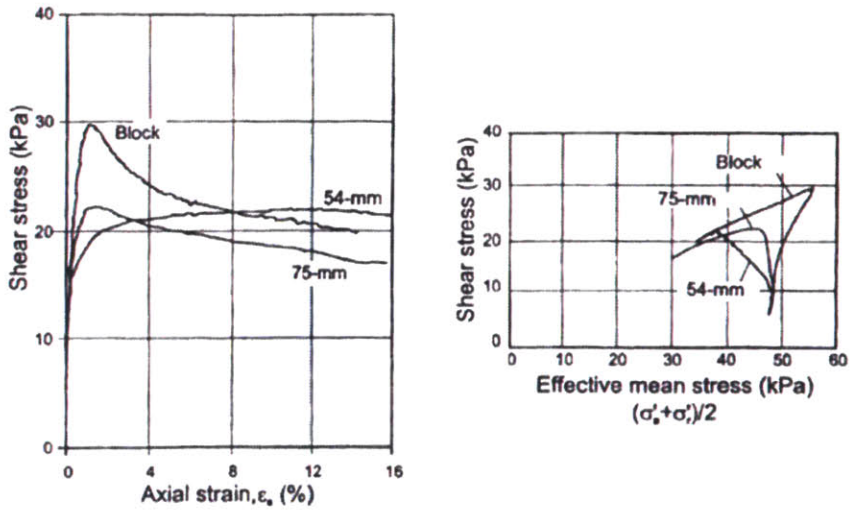

Figure 2.13: The different response in undrained shear strength for the three different samplers after reconsolidating to in situ stresses (Lunne et al. 1997).

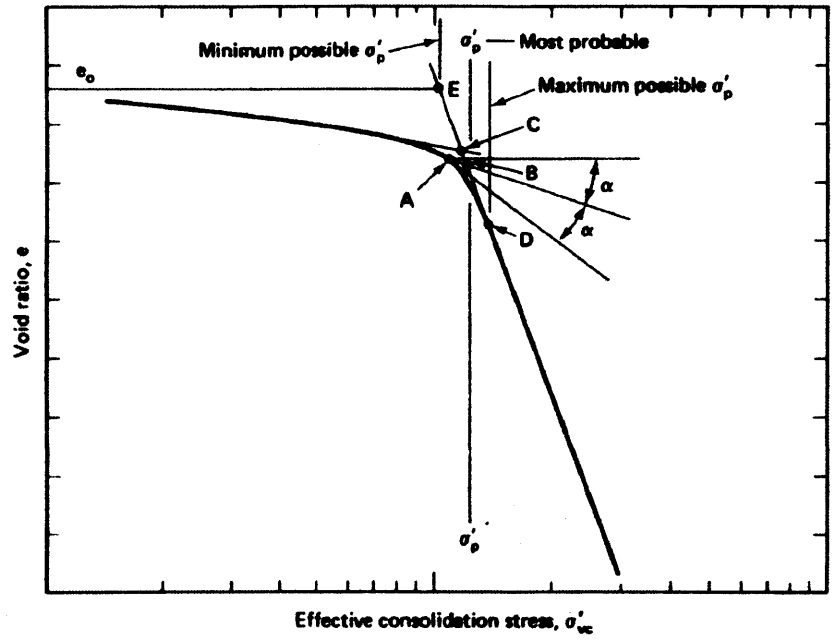

Figure 2.14: Determination of preconsolidation pressure using the Casagrande method, 1963 (after Holtz and Kovacs, 1981).

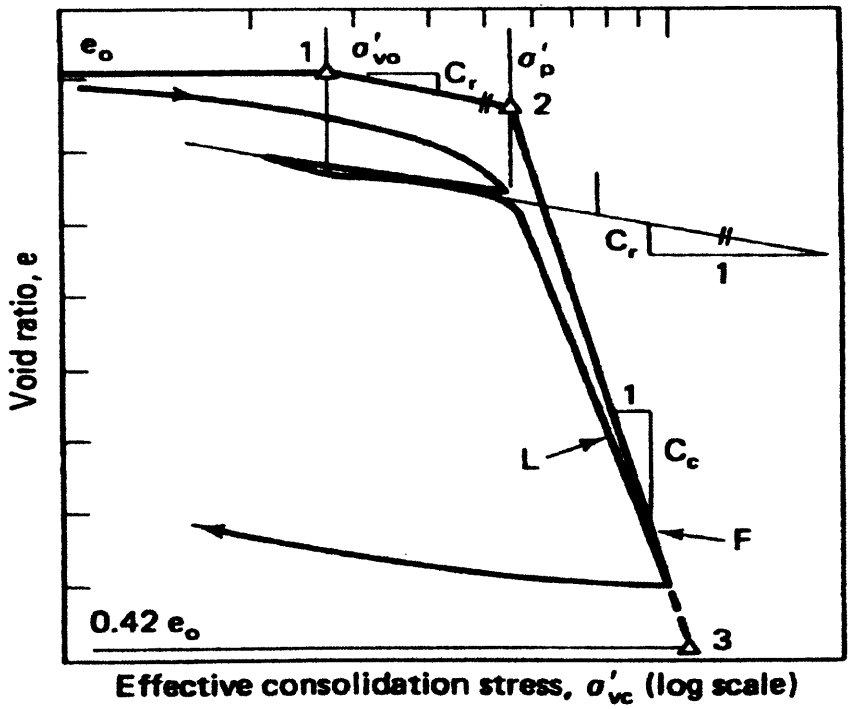

Figure 2.15: Determination of preconsolidation pressure and the Field Virgin Compression Curve using the Schmertmann Procedures for OC soils. (after Holtz and Kovacs, 1981).

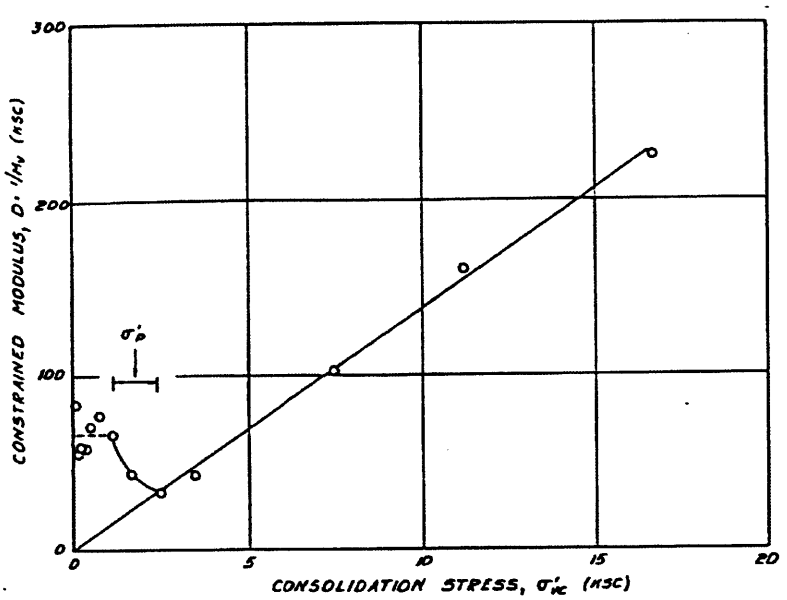

Figure 2.16: Determination of preconsolidation pressure by Janbu's Method (1969).

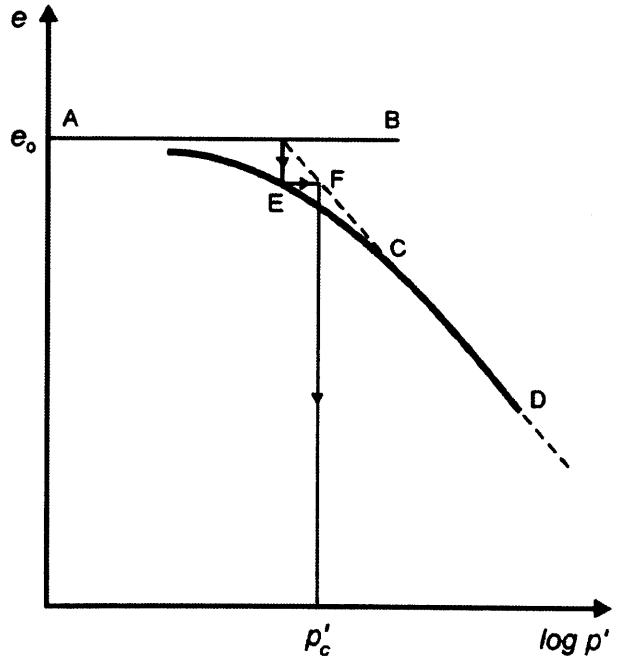

Figure 2.17: Determination of preconsolidation pressure using the Pachaco Silva (1970) empirical constructing method.

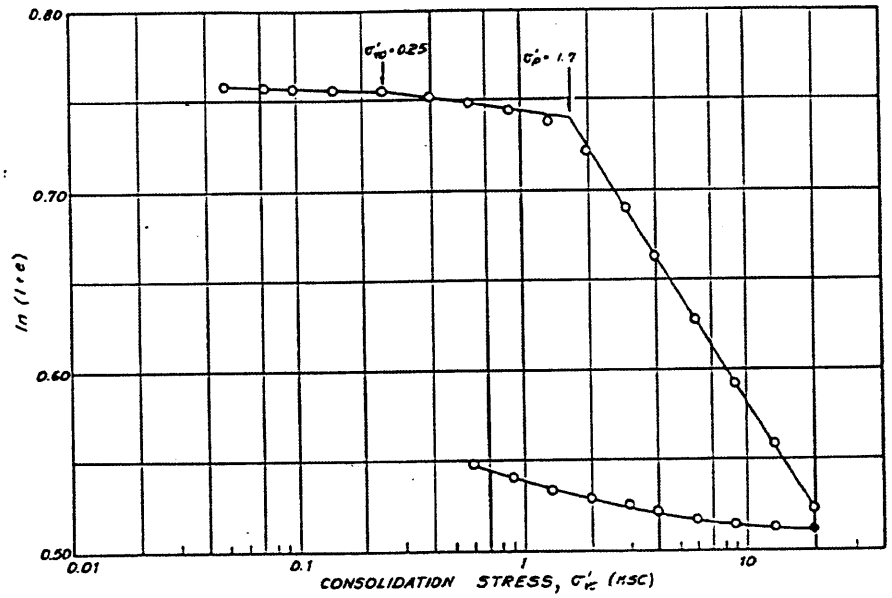

Figure 2.18: Determination of preconsolidation pressure using the Butterfield Method (1979).

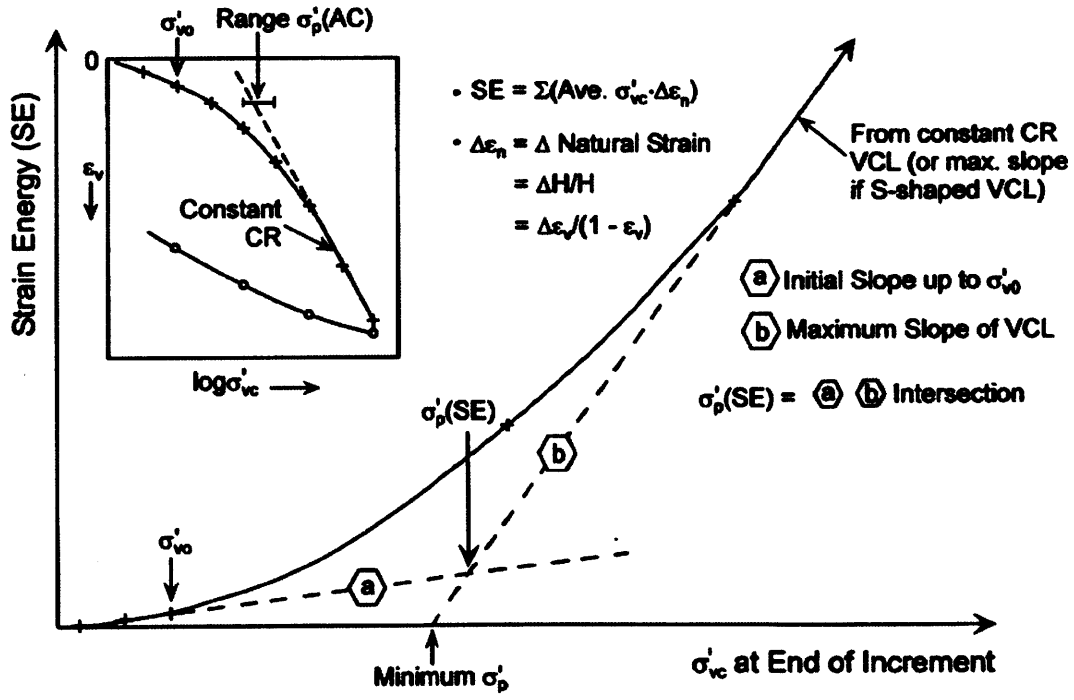

Figure 2.19: Determination of preconsolidation pressure using the Strain Energy approach (after Becker et al. 1987).

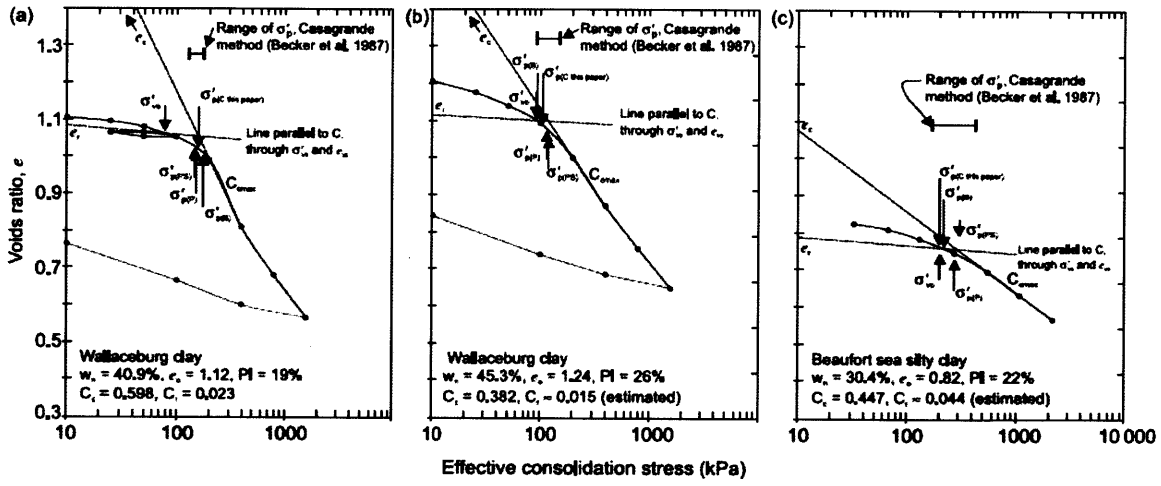

Figure 2.20: Defying preconsolidation pressure with Boone 2010, slope – intercept method. Comparison with estimates from Casagrande (1963), Strain Energy (Becker, 1987), and Pacheco Silva (1970) method.

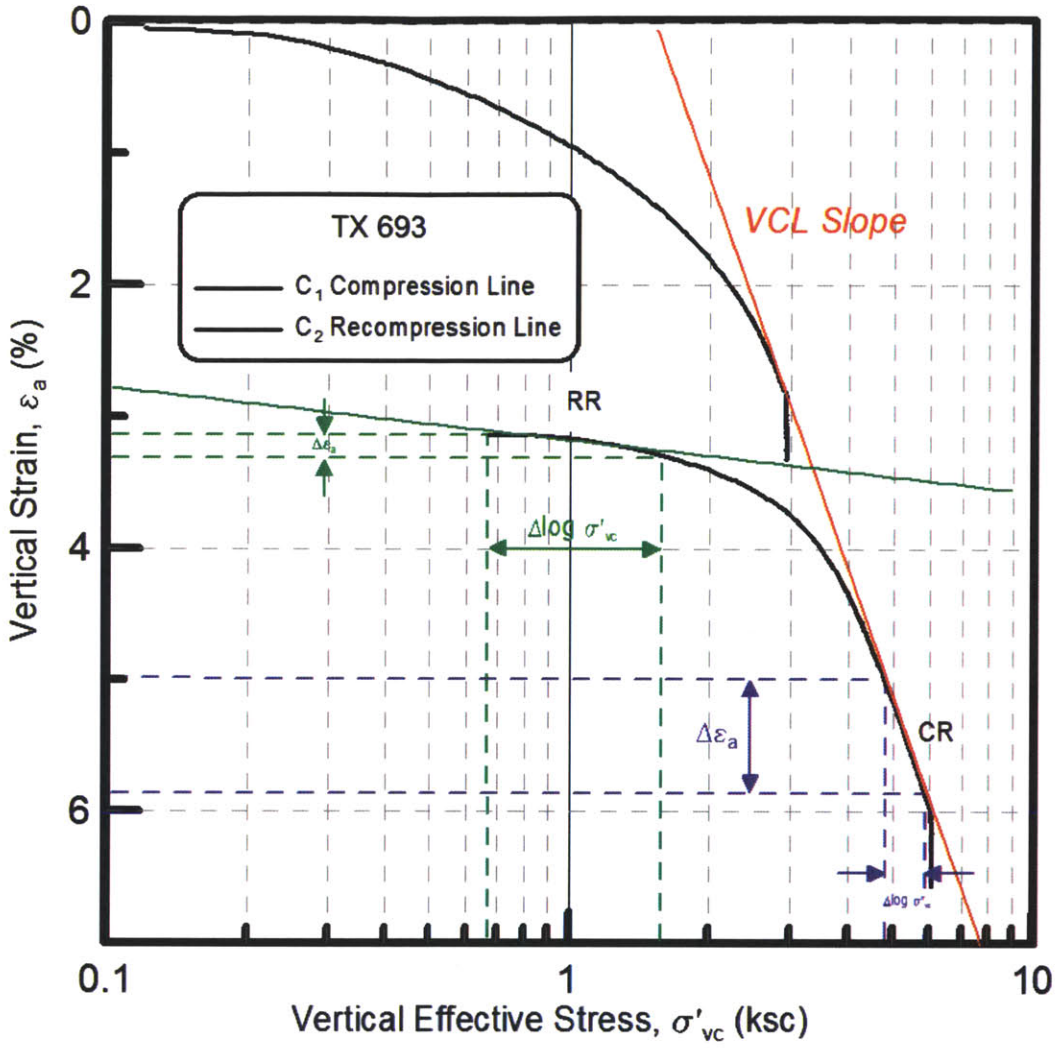

Figure 2.21: The compression and recompression Index calculation on a SFBM specimen from triaxial test TX 693.

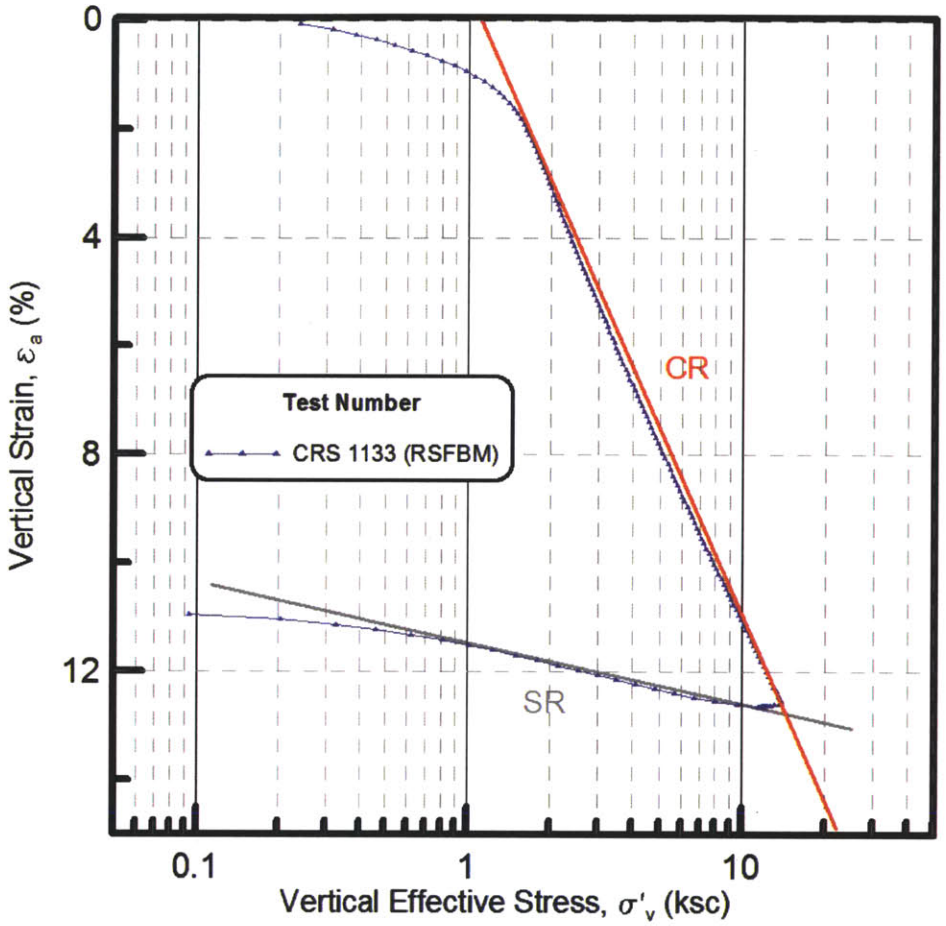

Figure 2.22: The compression (CR) and swelling ratio (SR) on a resedimented SFBM specimen from CRS test 1133.

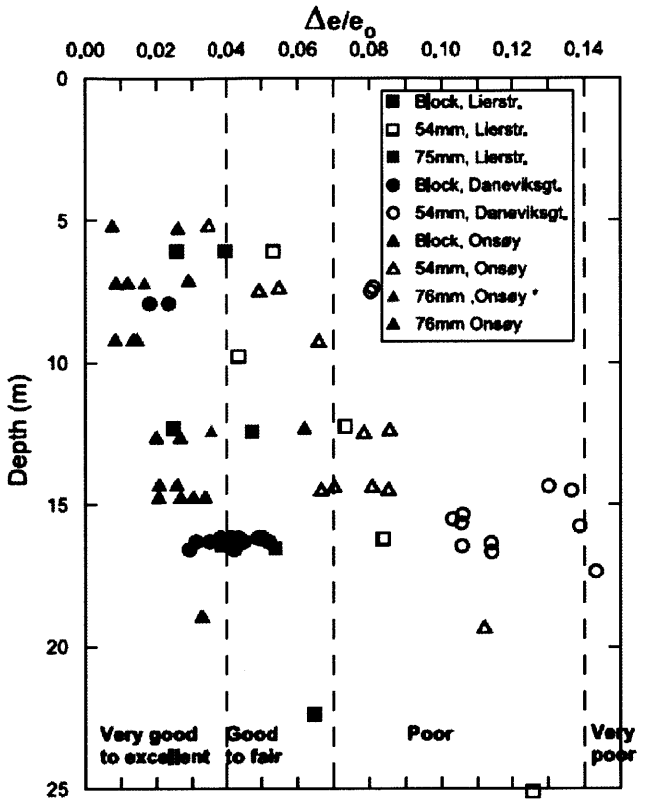

Figure 2.23: The change in void ratio $\Delta e/e_0$ Lunne et al. 1987 criteria versus depth for three different samplers (after Lunne et al. 2006).

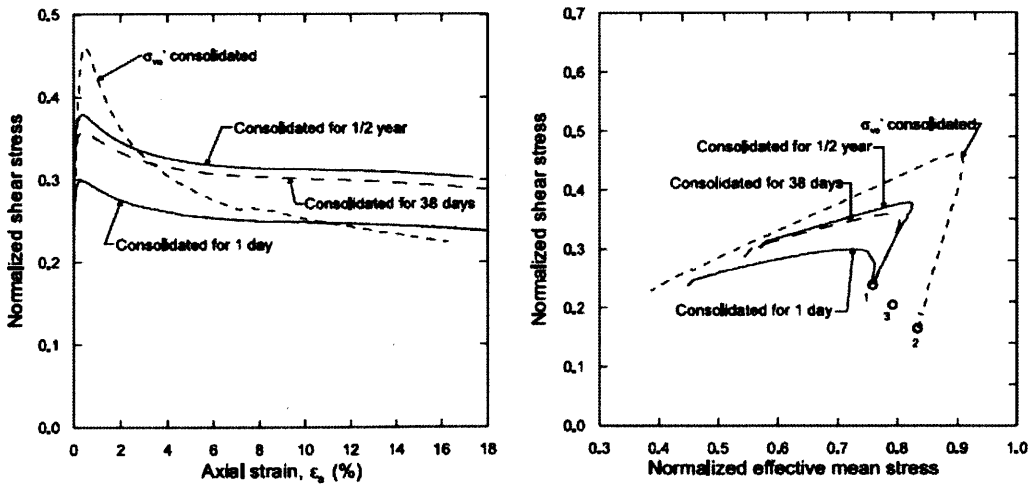

Figure 2.24: Undrained shear strength for triaxial tests on Lierstranda clay with different delayed consolidation time (Lunne et al. 2006).

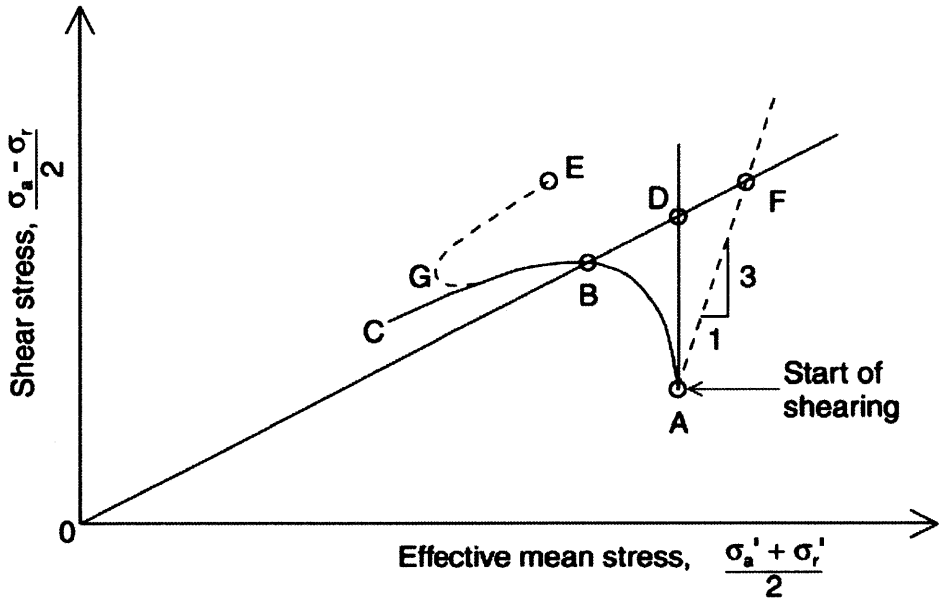

Figure 2.25: Applying the small-strain correction on CAUC tests for sample disturbance (Berre et al. 2007).

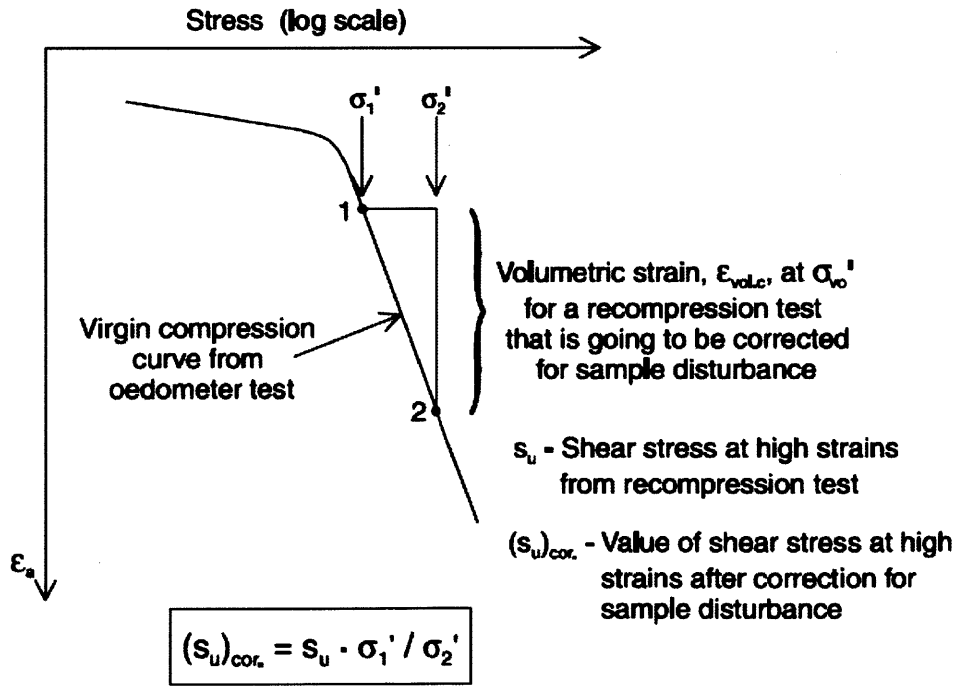

Figure 2.26: The large-strain correction of shear strength for sample disturbance in undrained tests on specimens reconsolidated to the in situ stresses.

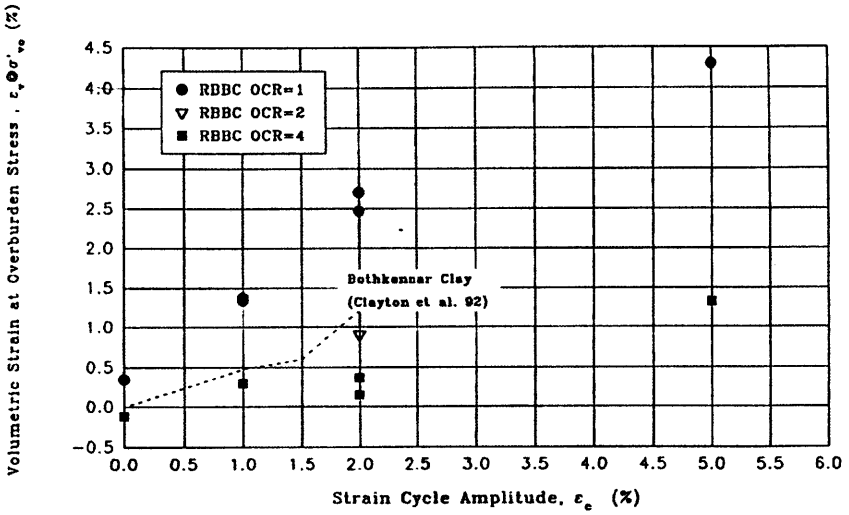

Figure 2.27: Volumetric strain versus the ISA disturbance strain amplitude (Santagata and Germaine, 1994).

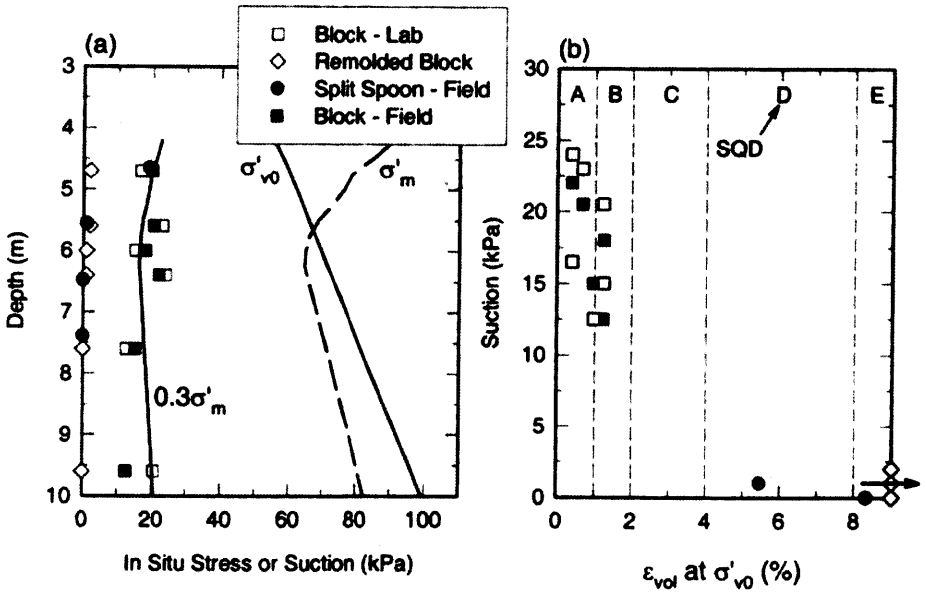

Figure 2.28: Suction Measurements versus depth and SQD values for different samples (Poirier and DeGroot, 2005).

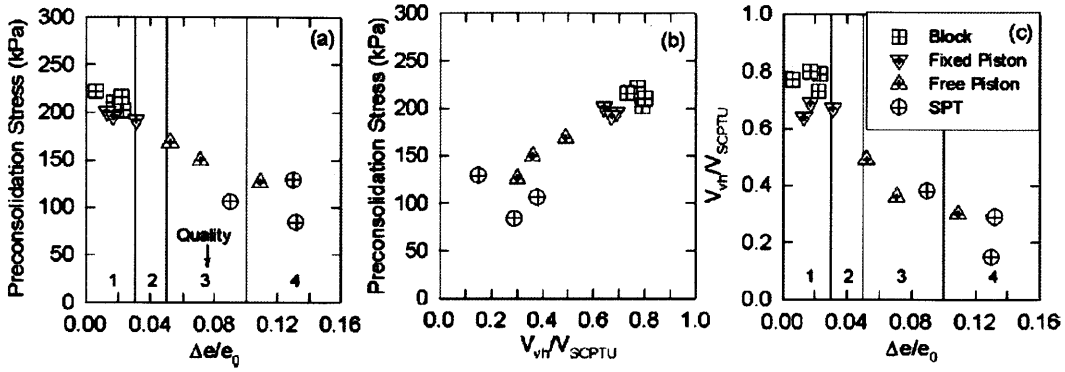

Figure 2.29: Sample quality assessment using Shear wave velocity. Comparison with Lunne et al. criteria (Landon and DeGroot, 2007).

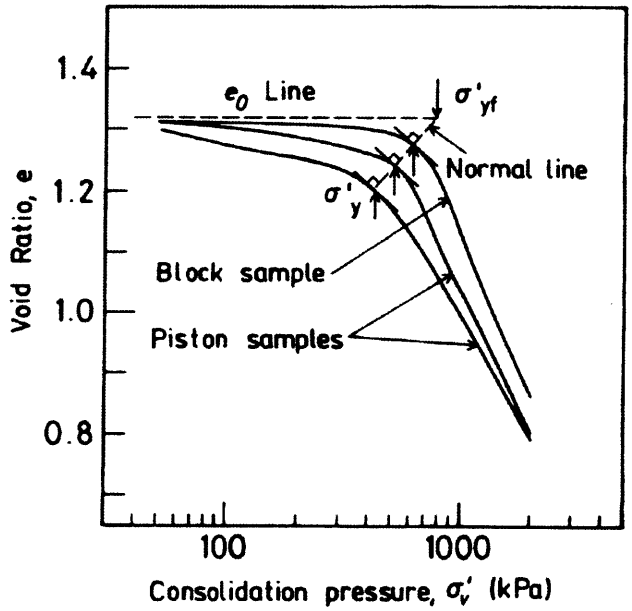

Figure 2.30: Assessment of sample disturbance using Nagaraj et al. (1990) method.

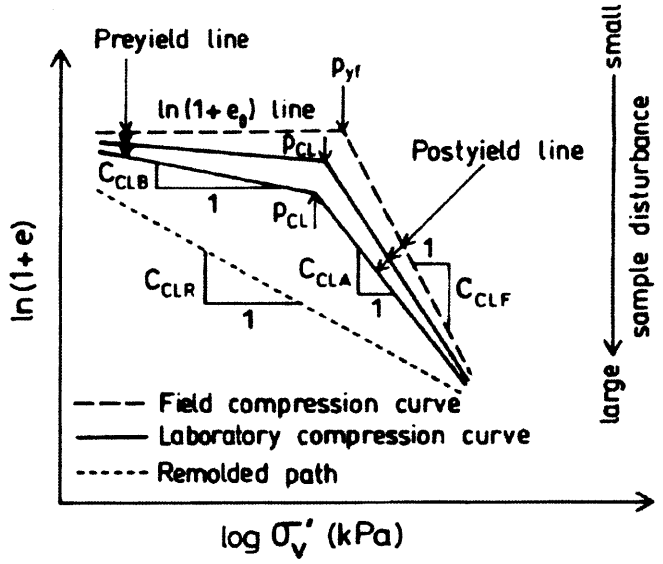

Figure 2.31: Assessment of sample disturbance using Onitsuka and Hong (1995) method.

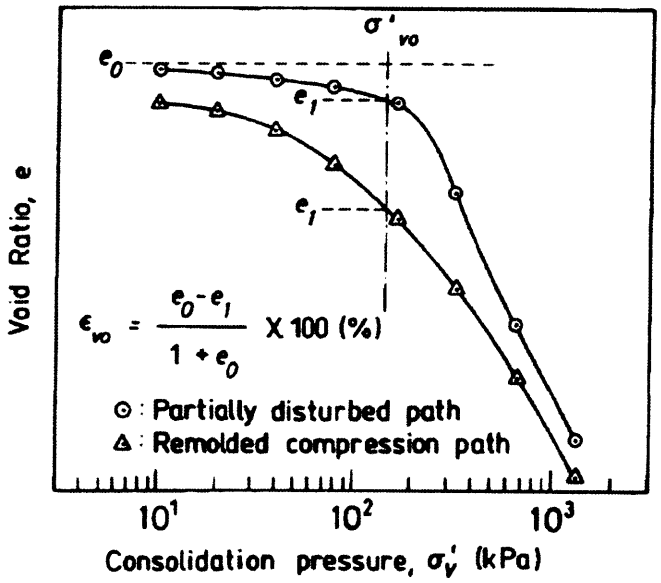

Figure 2.32: Assessment of sample disturbance using Shogaki (1996) method.

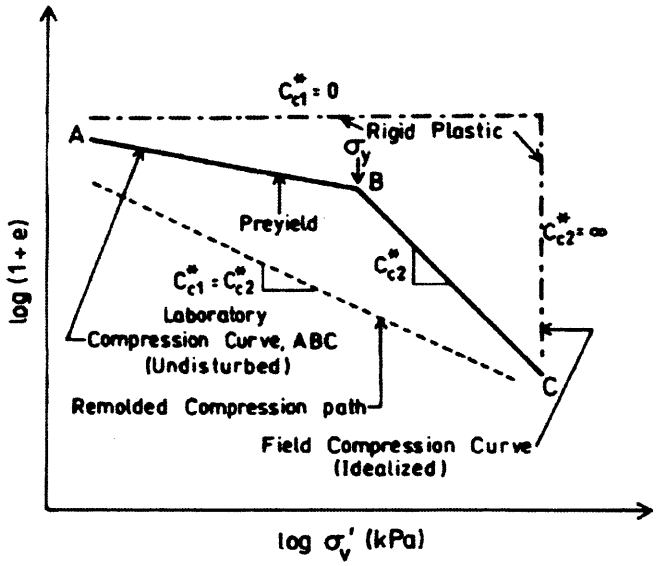

Figure 2.33: Assessment of sample disturbance using Prasad et al. (2007) method.

Chapter 3 SUPPORTING TECHNOLOGY - EQUIPMENT

3.1 Introduction

This research program is based on performing single element triaxial tests on San Francisco Bay Mud (SFBM) specimens simulating the effects of disturbance. Two low pressure MIT automated stress path triaxial cells and one high pressure cell were employed. This chapter will describe the testing equipment and technology used to perform these experiments.

Initially, disturbance effects were studied on tube samples of San Francisco Bay Mud. For the core research program, in order to be able to get more systematic results and eliminate sample variability, a homogeneous batch of SFBM was created. This material was mainly selected because of its unique properties and availability. Soil's high compressibility allows performing multiple disturbance simulation cycles on every sample, while giving the necessary strain when reconsolidated back to the virgin compression line. In addition, high undrained shear strength and low permeability set SFBM properties and behavior close to Boston Blue Clay (BBC), a material very well studied at MIT laboratories.

Section 3.2 deals with the resedimentation procedures followed in order to create the homogeneous batch of soil. The material geology, properties and the index tests performed on the samples selected to create the batch are discussed in section 3.3. Section 3.4 consists of a brief overview of MIT automated stress path cells as it was developed by Sheahan and Germaine back at 1992. The low and high pressure MIT triaxial apparatus are presented. A new suction cap built to incorporate axial extension at the high pressure cell is introduced. Instrumentation and some other essential elements used for the triaxial testing are presented at section 3.5.

3.2 Resedimented San Francisco Bay Mud

After some initial consolidation tests incorporating the effects of disturbance at tube samples of SFBM, the resedimentation process was decided. This decision was based on the initial observations and the huge scatter of preconsolidation pressure values for the same or close disturbance simulation amplitude on different tube samples. Creating a homogenous and uniform material would eliminate the variability between different tests. It would also allow comparing the disturbance's effects among triaxial tests with increasing disturbance. The resedimented material created, not only exhibits uniform characteristics, but also is completely saturated and has a more controlled stress history while it maintains the structure and the fabric of natural soil.

Resedimentation process has been used at MIT for the past 50 years mainly for Boston Blue Clay and the method has been revised by a large number of researchers. Early techniques developed by Ladd and Varallyay (1965) produced a partially saturated soil cake. Specimens were then back pressure saturated in the test apparatus with a 200 kPa of pressure. This method was later refined by Germaine (1982) and Seah (1990) to be able to produce a fully saturated soil sample and monitor the whole consolidation process while increasing productivity. The soil cake produced was around 30 cm in diameter and 12.5 cm tall. It was carefully trimmed, sealed and prepared for storing until a numerous of tests were performed from each soil cake.

For the scope of this research a new method was employed which produced individual test specimens using consolidometers, converted from oedometer apparatus. The method that will be described bellow can be divided to the following steps:

- Material selection and extrusion from the tubes
- Material cut and air-drying
- Grinding and mixing
- Preparation of the slurry
- One dimensional consolidation
- Sample extrusion and triaxial test preparation

As was already mentioned, the material for the creation of this homogeneous batch was selected due to its key characteristics; high plasticity, high compressibility, high undrained shear strength and low permeability. These characteristics allow maximum deformations at relative low pressure allowing for multiple disturbance simulations at one consolidation test. The large availability of good quality tubes of San Francisco Bay Mud (SFBM) in MIT laboratory as well as its similarities to Boston Blue Clay (BBC), a material very well studied made SFBM an ideal material for this research program.

The method of resedimentation starts with the selection of the tubes. Sixteen tubes of natural SFBM of good quality and relatively shallow depth were selected (table 3.1). Tubes were selected based on their quality as judged by their X-rays and CRS tests performed on each tube. The material was extruded and cut to smaller cylindrical pieces which is then air-dried (figure 3.1). Once the material is air dried, it is transferred to a ball mill grinder. There it is pulverized into powder to pass a #200 sieve. This is done in order to break the material down to individual clay flocks and completely erase the previous stress history and structure of the in-situ specimens. The medium size ball mill grinder was built at MIT lab by Cullen Jones (2010) (figure 3.2). It consisted of two main parts: The drive system of two horizontal rubber sheathed, keyed drive shafts connected via pulleys and a v-belt to an electric motor (3600 rpm, 120V) and the processing drum; a hexagon shaped drum with rubber lined interior, filled with 250 stainless steel balls (of 1/4" and 1/2"). The different size balls, as well as the hexagon interior of the drum, ensure the proper mixing and grinding of the material during the turnover.

Material is then manually removed and sieved to remove improperly processed material and the steel balls back to the drum. Once all the material is pulverized it is thoroughly mixed with the method of sequential batching so that it ends up to a completely homogeneous and uniform batch (figure 3.3). The batch was then stored to sealed 5 gallon containers.

Afterwards, the powder of SFBM is then mixed together with de-aired water in order to produce a thick, low viscosity slurry by the means of manual but thorough mixing (around 30 to 45 minutes to dissolve all lumps and non-uniformities). The targeted water content of the final product was around 100% which is around 1.5 times the liquid limit and agrees with Burland's (1990) recommendations. No sodium chloride was added to the slurry since no significant segregation of soil particles was observed during the sedimentation process. Slurry is sealed and left for some time to allow for a complete hydration of the clay particles. Then it is progressively siphoned into a flask were vacuum is applied to remove all the entrapped air and the air bubbles that were created during the mixing procedures. The simple set up of the two-line vacuum flask used can be seen at figure 3.4. The slurry is sufficiently de-aired as it is dropped inside the vacuum flask and by maintaining the vacuum conditions inside the flask for 15 to 30 minutes. During this time the flask is manually agitated to release any possible trapped air.

From the flask, vacuum is released and the slurry is depositioned to a consolidometer. The transfer is done carefully using a funnel to prevent any further entrapment of air inside the consolidation tube. The consolidometer used is made from an oedometer base combined with a stainless steel tube of 3.5 inch diameter and 8 inch length (figure 3.5). To reduce surface friction during the extraction of the specimen the inner walls of the consolidometer are lubricated before the deposition of the slurry. Same diameter filter papers and porous stones are placed on top and bottom of the slurry to allow drainage without soil extrusion during the consolidation process. Once all the slurry is mitigated to the consolidometer the water bath is filled with distilled water and maintained like that throughout the whole consolidation process.

The slurry is then incrementally loaded, with a Load Increment Ratio of one, to the maximum desired consolidation stress. From there, the specimen is unloaded to an OCR of 4 to ensure a coefficient of earth pressure at rest around 1 ($K_0 = \sigma'_h/\sigma'_v \approx 1$) and of course easy the extraction of the sample, minimizing sample disturbance. Doing so, at the beginning of each test, the specimen would be near to isotropic state of stress ($\sigma'_{v0} \approx \sigma'_{h0} \approx 0.25$ ksc for the low pressure apparatus). Increments are imposed using a load

hanger where free weights are placed (figure 3.4). An LVDT is employed and placed on the top cap of the consolidometer to monitor the relative vertical displacement during consolidation increments. For the low pressure triaxial apparatus, specimens are loaded to a maximum pre-consolidation stress of 100 kPa or 1 ksc and unloaded to 25 kPa or 0.25 ksc. For the high pressure apparatus specimens are consolidated to a maximum stress of 2000 kPa or 20 ksc and for the final increment also unloaded to an OCR of 4. For consolidating the samples up to2000 kPa, a bench consolidometer with level arm loading system was employed (figure 3.6). In every step, load is imposed for at least 48 to 72 hours to reach the end of primary consolidation as determined by Casagrande log time method. Figure 3.7 plots the relative displacement (cm) versus the time (hours) for a RSFBM specimen in a standard, 3.5 inch diameter consolidometer on a 4 kg free load increment. The preparation of each specimen with the above process of load increments and using double drainage consolidation lasts around two and a half to three weeks in order to reach the desired stress level. For this reason, three different consolidometers of the same diameter and height are employed in order to speed up the whole procedure.

3.3 Soil Geology - Index Tests

San Francisco Bay is a shallow estuary through which water drains from approximately 40% of California. It is located in the U.S. state of California and is being dominated by three large cities; San Francisco, Oakland and San Jose. The whole metropolitan region is a home to more than 7 million people. Water from Sierra Nevada Mountains flows through Sacramento and San Joaquin rivers into Pacific Ocean. The waterway entrance to the bay from Pacific Ocean is often called Golden Gate. Bay covers somewhere between 400 to 1,600 square miles (figure 3.8).

San Francisco Bay represents a down-warping of the Earth's crust between the San Andreas Fault to the west and the Hayward Fault to the east. During the last ice age, the basin that is now filed by the bay used to be a large valley with small hills. The rivers of this valley ran out to the sea through a canyon which is now the Golden Gate. With the

end of the ice age about 4000 ago, the sea level rose up to 300 feet and the valley was filled up with water from the Pacific to become a bay. Small hills became islands.

A large part of the bay used to be navigable until 1850's. By that time, massive amounts of sediment from hydraulic mining were released and deposited at the south part of the Bay. This was mainly done by mud and gravel dumped into Sacramento and San Joaquin Rivers. Material flowed down these rivers, progressively eroding into finer sediment until it reached the bay system. By the mid – 19^{th} century the size of the wetlands and inlets was reduced by as much as one third from deliberate filling in. This happened because, by that time, these areas were considered by most as wasted space. From the early of the 20^{th} century, a large part of the original bay was filled up with excavated soil and often built on. The entire bay profile was raised and in some areas new marshes were created. However the deep, damp soil in a large part of San Francisco Bay is subject to liquefaction. As a result, much major structural damage occurred close to the Bay during the 1989's Bay Loma Priets Earthquake.

Deposition at San Francisco Bay area has been repeatedly interrupted through time by sea-level changes. Geologists refer to the vast variety of different vintages as Young Bay Mud and Older Bay Mud. San Francisco Bay Mud originated from three general sources:

- Alluvial deposits (clay, silt and sand) from streams; unconsolidated interglacial deposits from the perimeter marshlands
- Silts and organic or inorganic detritus that formed a distinct layer in periods of high glaciation (Quaternary period – up to 2.5 million years ago).
- Human activities; mining and filling in.

Index tests were performed to the created resendimented batch of San Francisco Bay Mud in order to characterize the nature of the soil and identify its physical properties. SFBM samples selected have an average liquid limit (LL) of 73 and an average plastic limit index (I_P) of 44. The liquidity index (I_L) is 19. After the sample

preparation process and when consolidated to 1 ksc the Resedimented specimens had an initial void ratio, e_0 of 1.57±0.25 and a water content, W_n (%) of 56.5±5.

For the Specific Gravity test, three iodine flasks were employed. The test was run in accordance with the ASTM Standard D854-58 using 40 gm of soil at each calibrated flask. Soil was first mixed in a blender with about 80 gm of distilled water to create a slurry. The slurry was then de-aired and transferred into the volumetric and the rest of the flask was slowly filled up with distilled water. The three volumetrics were then stored in a cooler to equilibrate overnight (figure 3.9). After equilibrating, measurements of the volumetric mass and temperature were taken for three consecutive days. A stopper was used to cap off (in an angle so no air is trapped) the volumetric before every measurement. The dry mass of the slurry was defined once all measurements were completed. Results can be seen at table 3.2.

The final specific gravity for each measurement was computed from the equation:

$$G_{S\tau} = M_S / \{(M_B + V_{B\tau c}\, \rho_{w\tau} + M_S) - M_{B+W+S\tau}\},$$

where M_S is the mass of the dry soil, M_B the mass of the volumetric, $V_{B\tau c}$ the volume of the volumetric at temperature Tc (cm^3), $\rho_{w\tau}$ the mass density of the water (gm/cm^3) at the same temperature, and $M_{B+W+S\tau}$ the total measured mass of the volumetric with the water and the slurry. The average specific gravity for SFBM was measured to be 2.69.

For grain size analysis, a hydrometer test was run in accordance with the ASTM standard D422 using 50 gm of the material and 5 gm of Sodium Hexametaphoshate. The soil was thoroughly mixed with distilled water to create a thick slurry. The slurry was allowed to temper for a few hours and then blended with about 500 mL of distilled water for 2 minutes. The diluted slurry was transferred to 1000 cc cylinder and filled to the calibration mark with distilled water. A plunging rod was used to manually mix the 1000cc of slurry and begin the sedimentation process. Readings were taken with the hydrometer inside at the top of the meniscus for the first 2 minutes. Then the slurry was remixed, a new sedimentation process was started, taking reading for more than 2 days but now placing the hydrometer at the slurry just before each measurement. The process

can be seen at figure 3.10. Sedimentation results are presented in figure 3.11. At the end of the experiment the dry mass of the slurry was measured. The percentage of clay (particles with size diameter D < 0.09 mm) is 52%.

Atterberg Limits tests were conducted in general accordance with ASTM 4318. A Casagrande cup was used to determine the Liquid Limit (flow curve, figure 3.12, 3.13). Plastic Limit was determined using the hand rolling method (1/8 inch thread crumble). From Atterberg limit testing RSFBM showed a liquid limit of 73% and a plastic limit of 29% and could be characterized as highly plastic clay (CH). A summary of all Atterberg limits for SFBM is presented at table 3.3; where the soil plots at the Casagrande Chart can be seen at figure 3.14. The activity of the soil, as defined by Skempton (1953), was calculated from the hydrometer analysis and the PI to be:

Activity = PI / (% Mass < 2 μm) = 29/81 = 0.36

The organic content of the resedimented SFBM was determined by the loss on ignition method (LOI). The organic content analysis was performed in accordance with ASTM Standard Test Method D2974. The material was initially place overnight at the oven to dry (in a 105° oven). Then, it was transferred in a furnace at 400° C for about 24 hours. In such high temperate the organic material will burn off and by measuring the reduction in mass, the organic content can be determined. SFBM's organic content was determined to be 5.03% after it reached a constant mass in the furnace. A porcelain crucible was used to accommodate the soil. All mass measurements were determined to 0.01 g. Table 3.4 compares the organic content of SFBM to this of other very well studied clays (London Clay, Boston Blue Clay). Figure 3.15 presents the muffle furnace and the porcelain crucibles used.

A Scattering Electron Microscope (SEM) was used at MIT lab to better define the mineralogy of the SFBM batch. Results of the SEM pictures as well as the X-Ray Diffraction (XRD) spectrograph can be seen at figures 3.16 and figure 3.17. The examination of this high resolution electronic microscope can give useful information for

the grains distribution, shape and array. On the other hand, the X-Ray Diffraction provides a good analysis of the mineralogy of the material by pointing out the core elements (the Bragg's peaks at XRD results). The XRD was done using the powder method and a collimated beam of parallel X-rays of identical wavelength where the soil powder was placed in. When the beam hits a mineral's crystal lattice, the X-rays constructively and destructively interfere or diffract. The angles at which the diffracted X-ray beams of various intensities diffract were recorded and associated to the d-spacing between adjacent planes of atoms in different crystals according to Bragg's Law deviation 2θ and allowing for the identification of the different crystalline mineral.

3.4 MIT Automated Stress Path

The main phase of this research was performed using the automated low pressure triaxial cells of MIT Geotechnical lab which were originally developed by Sheahan and Germaine (1992). These automated cells allow us to load specimen through a complex strain and stress path with accuracy and efficiency. Figure 3.18 shows a schematic representation of the computer controlled triaxial apparatus that was employed. For this specific project MIT 03 and MIT 04 triaxial apparatus were used for the majority of the tests.

Each automated MIT cell consists of five main parts:

- The triaxial cell
- The load frame and the pressure volume actuator
- The motors and the motor control box
- The personal workstation
- And the Central data acquisition system

The whole mechanical system is in a wooden controlled temperature chamber of 25° C ± 0.2 SD. All the equipment and the test apparatus are located inside an air-conditioned laboratory. The cells use a 3.6 cm diameter cylindrical specimen of height 8.1 cm. Specimen is sealed with two thin membranes (unlubricated condom) and the use of O-rings.

For the low pressure apparatus, the plexiglass cell has a maximum confining pressure of about 1.5 MPa. The cell is mounted on a Wykeham Farrance load frame of a 1 tonne (9.8 kN) capacity. It has customized features such as a ball bearing bushing, a fixed top cap, top and bottom drainage, and ball valves. An internal load cell of 500 lb (2.2kN) capacity is used for direct measurement of the axial deviator force. This also eliminates the effects of piston seal friction on the load measurements. Piston enters the top of the cell through a double O-ring seal and its displacement is continuously measured with an external mounted LVDT. The cell is filled with 20 centistokes silicone oil. This nonconductive silicone oil has extremely low viscosity, is transparent and does not degrade the latex membranes that seal the soil specimen. The cell and the pore pressure are controlled by MIT- designed Pressure - Volume Actuator (PVA). A second LVDT is used at the pore PVA to compute the specimen volumetric changes. High performance pressure transducers of 200 psi (1.4 MPa) capacity are attached at the base of the apparatus to monitor the cell and the back pressure of the system. The system's valves are located at the triaxial base to reduce compliance. A schematic representation of the low pressure triaxial cell can be seen in figure 3.19.

For a few selective tests, the high pressure MIT Triaxial Cell was employed. The cell was originally built by Anderson back in 1991 for frozen soil testing. Later it was subsequently modified by Swan (1994), Da Re (2000) and Abdulhadi (2009). The chamber of this apparatus is made of steel and is designed to operate up to a confining pressure of 20 MPa. The cell encloses the soil specimen, a base pedestal, a floating top cap, top and bottom drainage lines and an internal shear-beam load cell (figure 3.20, 3.21). The top drainage line, which is connected only after the specimen with the top floating cap is in place, is made from a spiral copper tubing. This gives the system the necessary compliance and flexibility under large axial strains during consolidation and

shearing. The internal load cell used here for direct measurement of the axial deviator force has a 2,000 lb capacity. This load cell is attached to a 2.54 cm diameter hardened steel piston that enters the top of the steel chamber through a double O-ring seal. The piston's movement is monitored through an external standard LVDT of about 5 cm linear range. As with the low pressure apparatus, precision ball valves are located at the bottom of the system for compliance. Non-conductive, low viscosity silicone oil is used to fill up the cell. Thicker, commercial latex membranes of 0.31 mm are used to ensure sealing of the soil specimen to high vertical effective stresses (up to 10 – 15 MPa).

For this specific research program, the triaxial high pressure apparatus was modified to gain capability for axial extension. A Schematic of the modified high pressure triaxial apparatus can be seen on figure 3.22. A cross section of the modified apparatus appears on figure 3.23 (dimensions are in cm). A new suction cap was designed and built to ensure enough vertical uplifting force for the disturbance circle simulation phase. The new suction cap consists of three parts. The top modified floating cap that is placed on top of the soil specimen, the second top cap with an inside O-ring that is attached to the load cell, and the spiral copper tubing that allows atmospheric pressure and ensure suction between the two parts (figure 3.24). This spiral tube overpasses the load cell and connects through a hollow steel piston outside the chamber to the atmosphere. Suction is ensured through the internal O-ring between the two caps that lock in together and through the differential pressure which is created once the pressure cell is increased and during the first step of consolidation.

The triaxial state of stress at high pressure apparatus is imposed through three Pressure – Volume Actuators (PVAs). The first two, as for the low pressure cells, are used to control the cell and the back (pore) pressure. Attached to the back pressure controller, a LVDT is used to monitor the specimen volumetric change. Both the cell and the pore pressure are monitored using high performance diaphragm pressure transducers of 1,000 psi capacity. For the vertical axial force, instead of a motor, another Pressure – Volume Actuator is employed. This PVA is connected to a 9 Tonne hydraulic ram that converts fluid pressure to axial force. The hydraulic ram can, in turn, controls the

movement of the entire apparatus up against the load frame. This PVA uses low viscosity silicone oil, the same type used to fill up the cells.

As all the MIT testing systems, the high pressure apparatus is kept inside an environmental controlled chamber which is positioned in an air-conditioned MIT laboratory room (for maximum temperature control).

3.5 Computer Control and Instrumentation

Over the past 20 years, a large effort has been devoted at MIT Geotechnical Laboratory to automate geotechnical devices. The concept, first applied for triaxial cells, is described in detail by Sheahan (1991) and Sheahan & Germaine (1992). The main advantage in automation of the strength testing equipment is that it increases the flexibility and the quality control of the tests while reducing radically the required labor. Automated control is carried out by a Q-Basic program running on a PC workstation. The menu-driven program is very flexible, task specific and capable of performing all phases of the triaxial test; the initial pressure up, back pressure saturation, B-value check, consolidation along any stress path or K_0 consolidation, disturbance simulation or shearing in extension or compression.

A motor control box, receives orders (DC voltages) from the workstation to control each of the three motors of the system. The two pressure control devices controlling the cell and the pore pressure and the motor which drives the load frame. The system is based on closed-loop feedback control. This means that the electric transducers send signals to the computer which converts them, from analog to digital (AD1170 analog to digital converter), and also sends signals to engineering units to compute the actual stress-strain state of the specimen. The current state is compared with a pre-scheduled time history of the specimen (target values) while a software control algorithm computes the correcting action needed to be taken by the electric motors to keep the stress-strain state on schedule. These corrections are calculated in engineering values and are converted from digital to analog using a Strawberrytree card of 12 bit resolution (figure 3.25). The procedure is explained in more detail by Sheahan at al., 1990. The

analog signals are then sent to the individual motor control cards which rotate the motors in proportion to the voltage signal.

With regard to the high pressure apparatus, a closed loop Proportional – Integral – Derivative (PID) control algorithm was engaged. This was essential to allow the axial strain PVA to operate at very low rotational speeds. The slow rotation allowed the hydraulic load frame to operate during consolidation with accuracy and produce deformation rates as low as 0.1%/hr.

A central Data Acquisition Control Unit used for the entire MIT geotechnical laboratory transforms the information (A/D) and stores the data during the different phases of the test with rates of up to 1 Hz (figure 3.26). The system is based on a 486 microprocessor PC at Windows XP interface with an expanded channel Hewlet Packard 3497A unit. This high quality low noise system makes possible direct measurements of the load cell, pressure transducers and displacement transducers without any signal amplification. Instead, it allows a resolution of 0.1 mV for LVDTs and 1μV for pressure transducers. It is currently monitoring 180 channels simultaneously and the readings are stored to data files from where the stress-strain history of the specimen can be calculated through a reduction program.

For this research the following instrumentation was also used:

- Pressure transducers for the cell and the back pressure monitoring. These transducers, Data Instruments AB/HP type, measure absolute pressure by the deflection of a steel diaphragm instrumented with strain gages. For the low pressure apparatus they have a capacity of 200 psi (figure 3.27). For the high pressure apparatus the capacity of the transducer is up to 1,000 psi.

- An internal load cell to monitor the axial stress. The load cell used in the low pressure apparatus is a Data Instruments JP S-shaped, shear beam type with strain gauges of 500 lb capacity (figure 3.28). For the high pressure internal load cell, the capacity of the transducer used was up to 2,000 lb.

- Axial displacement to measure vertical strains. This is a Linear Variable Differential Transformer (LVDT) measuring externally the displacement of cell's piston. It is manufactured by Trans-Tek Inc (Series 240) and has a linear range of about 5 cm. The LVDT generates an output voltage when a ferromagnetic core is moving inside the LVDT casing. This output voltage can be proportionally (with a linear range of ±2.5 volts) connected to the displacement of the core inside the tube (figure 3.29).

- Volume displacement transducers to monitor specimen volume changes. This is a LVDT manyfactured by Trans-Tek Inc (Series 240) and has a linear range of about 10 cm. The displacement of this transducer times the piston area which is constant, gives in every step of the test the equivalent volumetric change for the specimen (figure 3.30).

All transducers are fed with a Direct Current (DC) of 5.5 volts (input voltage), and their signals are continuously monitored and logged by the central data acquisition system.

No	Tube	Location	Sample #	Depth (ft)	Length (inch)	Diameter (inch)	Company
1	HAAF NI - B4	Novato, CA	7	25	8	3	ARUP/PARSONS
2	HAAF NI - B10	Novato, CA	4	15	13.5	3	ARUP/PARSONS
3	CCB 44A	Town End, SF CA	9	41	32	3	ARUP/PARSONS
4	CCB 44A	Town End, SF CA	11	52	28.5	3	ARUP/PARSONS
5	CCB 29	Town End, SF CA	13	61	23.5	3	ARUP/PARSONS
6	CCB 30	Town End, SF CA	11	49	22.5	3	ARUP/PARSONS
7	CCB 18	Town End, SF CA	10	38	30.5	3	ARUP/PARSONS
8	TTB 01	151 Tremond, SF CA	27	132	18	3	ARUP/PARSONS
9	CCB 20	Town End, SF CA	12	42	9.5	2.5	ARUP/PARSONS
10	CCB 24	Town End, SF CA	15	75	9	2.5	ARUP/PARSONS
11	CCB 23	Town End, SF CA	12	52	7	2.5	ARUP/PARSONS
12	CCB 23	Town End, SF CA	9	36	6	2.5	ARUP/PARSONS
13	CCB 25 B	Town End, SF CA	12	60	9.5	2.5	ARUP/PARSONS
14	TTB 01	151 Tremond, SF CA	28	38	11	2.5	ARUP/PARSONS
15	CCB 25 B	Town End, SF CA	6	26	18	2.5	ARUP/PARSONS
16	TTB 01	151 Tremond, SF CA	30	149	18	2.5	ARUP/PARSONS

Table 3.1: Inventory of tubes used to create the homogeneous batch of SFBM.

Specific Gravity Test - SFBM

Volumetric ID : M4
Mass of Volumetric: 175.63 g

Calibration of Volumetric

Determination No.	Date	Time	Mass of bottle + water (g)	Temperature (°C)	Density of water (g/cm^3)	Volume of volumetric (cm^3)
1	18/8	12:30 PM	427.84	24.6	0.9971497	252.93
2	18/8	3:00 PM	427.84	24.4	0.9972000	252.92
3	18/8	5:30 PM	427.83	24.6	0.9971497	252.92

Mean volume 252.92
S.D. of volume 0.01

Determination No.	Date	Time	Mass of bottle+water +soil (g)	Temperature (°C)	Density of water (g/cm^3)	Specific Gravity of Soil G_{ST}	Specific Gravity of Soil G_{S20}
1	18/7/2011	11:30 AM	453.81	23.9	0.997324	2.695	2.693
2	18/7/2011	5:30 PM	453.74	24.9	0.9970735	2.694	2.691
3	19/7/2011	1:00 PM	453.76	24.3	0.997225	2.691	2.688
4	20/7/2011	11:00 AM	453.79	24	0.9972994	2.693	2.691
5	20/7/2011	12 noon	453.75	24.4	0.9972	2.690	2.688

Mass of tare+dry soil 535.51 g
Mass of tare : 494.28 g
Mass of dry soil : 41.23 g

Mean $G_{S20°}$: 2.690
SD = 0.0022

Table 3.2: Specific Gravity analysis for SFBM performed at MIT lab, 2011.

Atteberg Limits for RSFBM				
Plastic Limit	Liquid Limit	Natural Water Content	Plasticity Index	Liquidity Index
29	73	37	44	19

Table 3.3: Atteberg Limits for RSFBM as measure at MIT Geotechnical Lab, 2011.

Soil Type	Organic Content (%)
SFBM	5.03
BBC	1.37
London Clay	4.12

Table 3.4: Organic content values for typical clays (Germaine, 2010).

Figure 3.1: Tube Selection (at the left) and material air-drying (at the right) for the Resedimented San Francisco Bay Mud Batch.

Figure 3.2: Grinding of the Material using a ball mix grinder (MIT, Cullen Jones 2010).

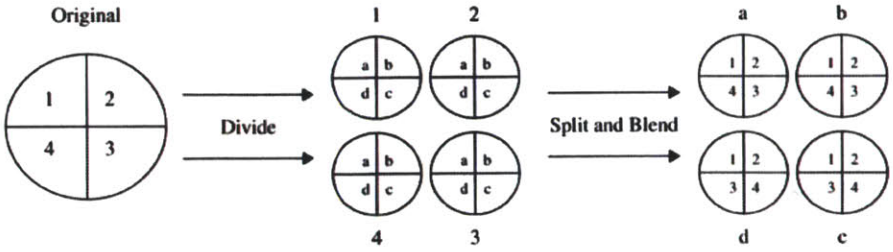

Figure 3.3: A schematic representation of the blending method used for soil mixing.

Figure 3.4: The production of a thick slurry of RSFBM ready to be de-aired through vacuum.

Figure 3.5: Incremental loading with free weights at a modified oedometer base - consolidometer.

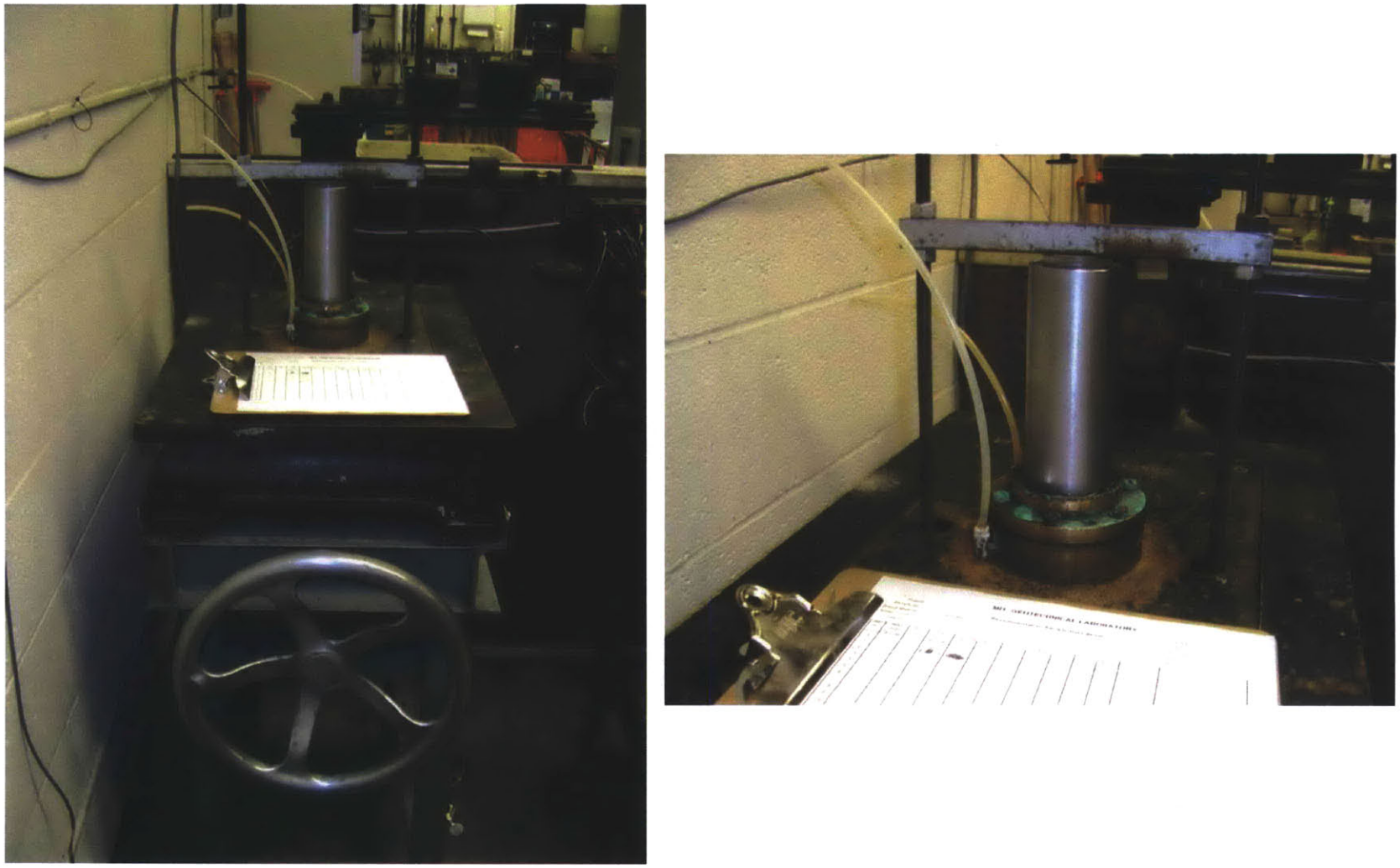

Figure 3.6: The MIT Terzaghi Load Frame with level arm loading system.

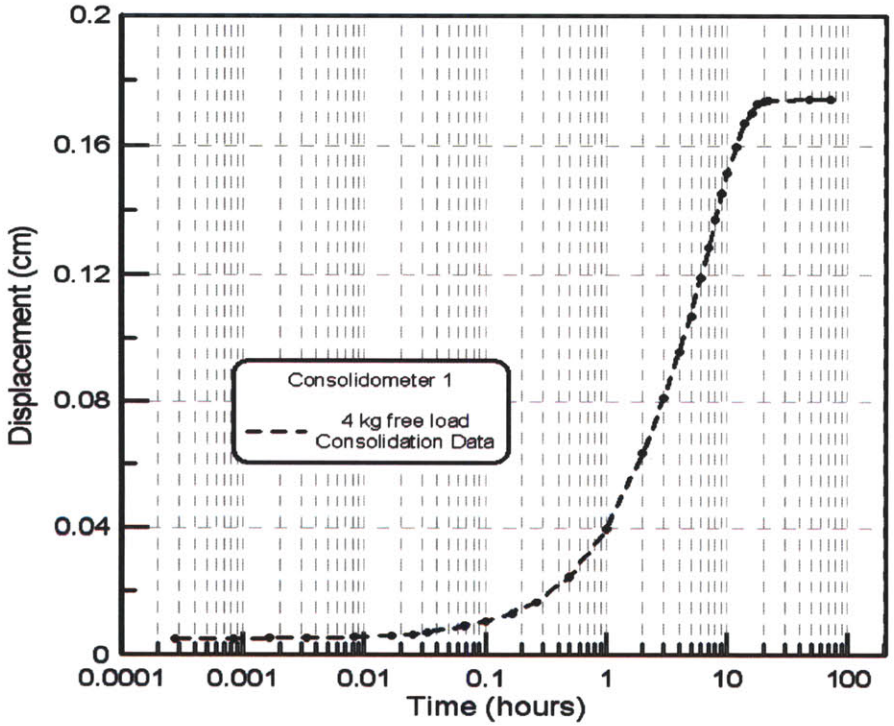

Figure 3.7: The relative displacement (cm) versus time (hours) for RSFBM at a standard 3.5inch diameter consolidometer for 4kg load increment.

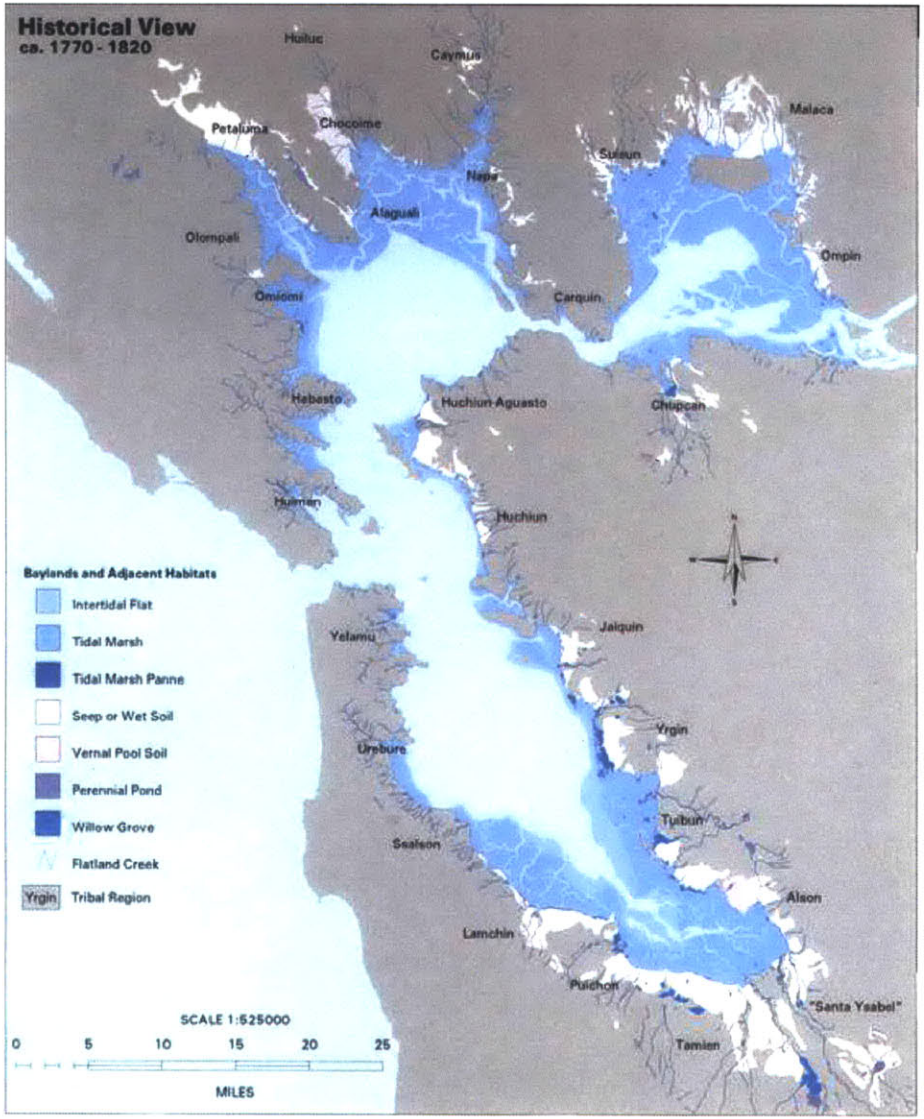

Figure 3.8: Historical view of baylands and habitats of the San Francisco Bay area.

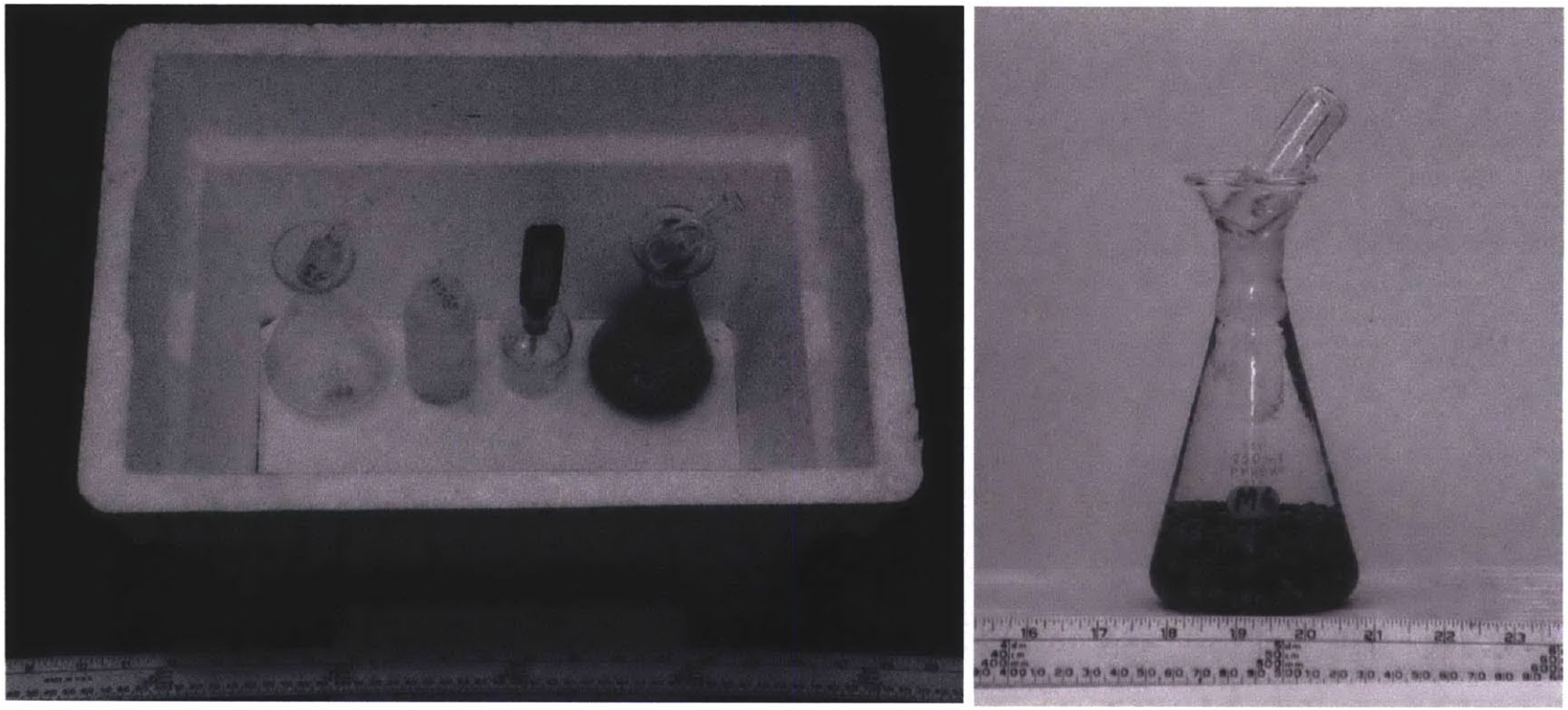

Figure 3.9: The specific gravity cooler storage container and the iodine flask with the stopper ready to be stored to equilibrate temperature (Germaine, Geotechnical Laboratory Measurements).

Figure 3.10: Sedimentation - Hydrometer analysis for RSFBM at MIT Geotechnical Lab.

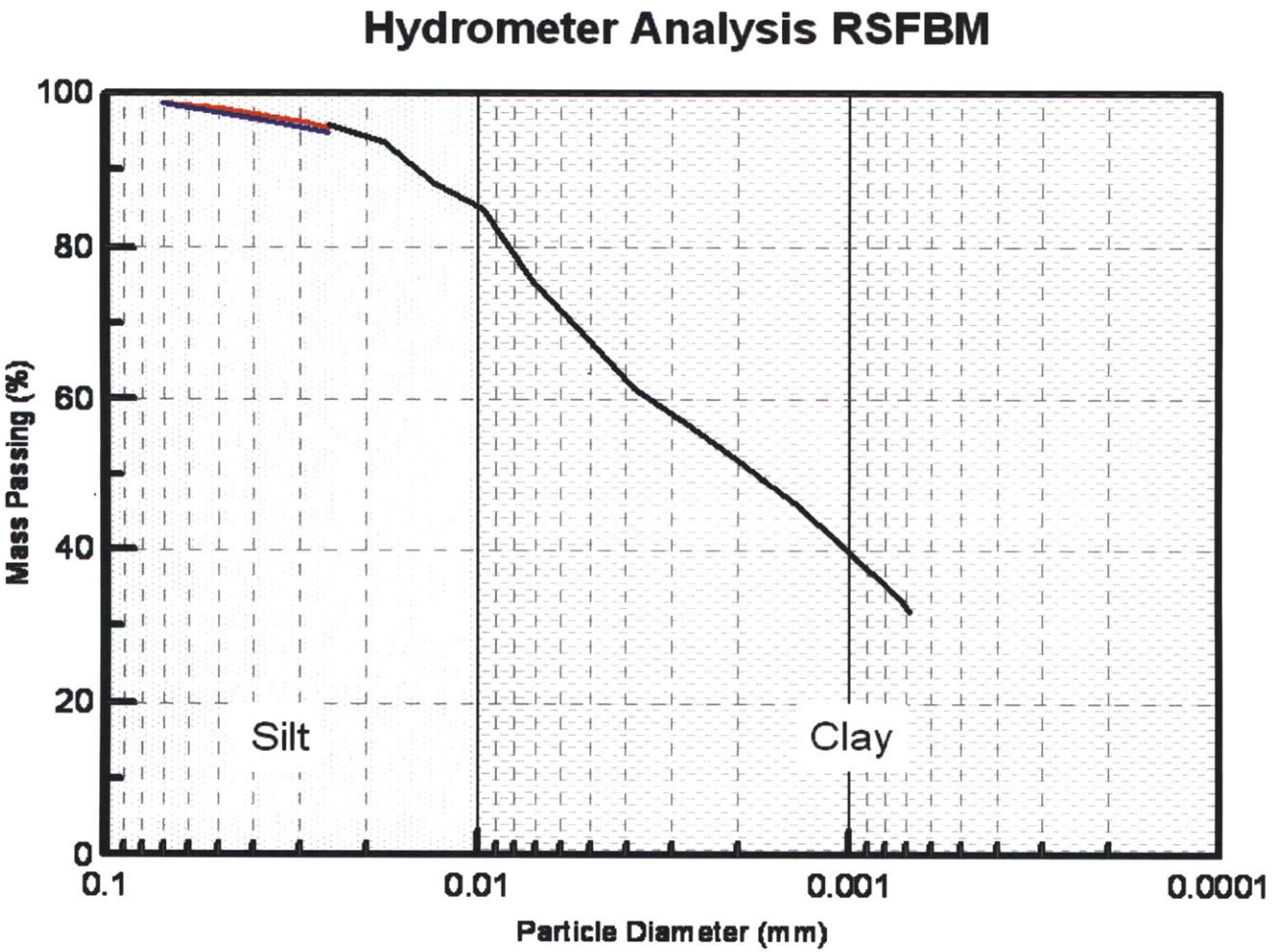

Figure 3.11: Hydrometer analysis graph for RSFBM Batch.

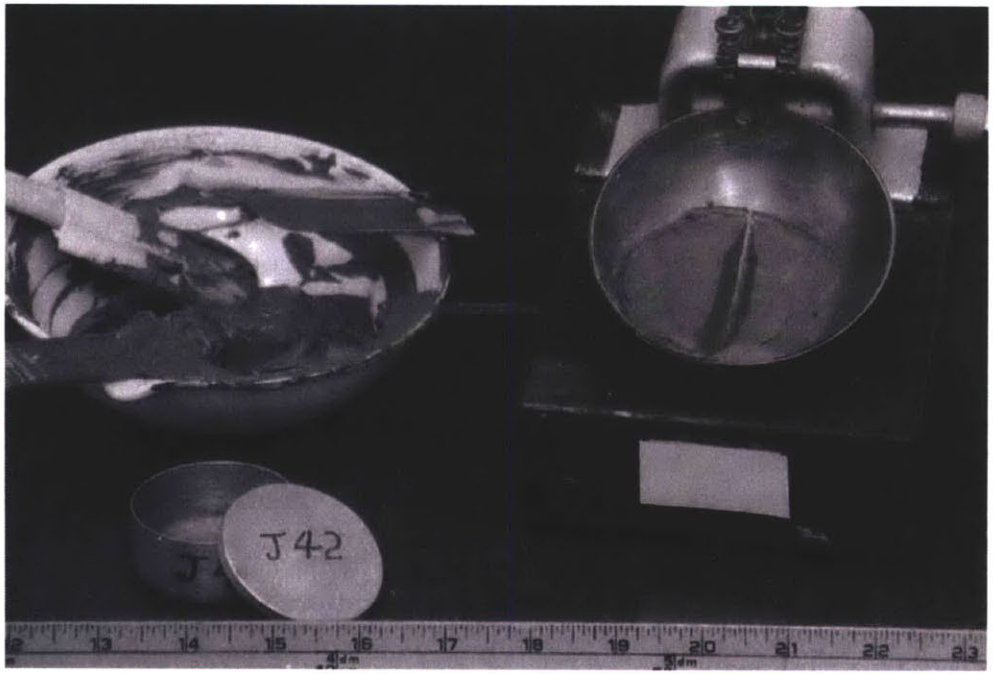

Figure 3.12: The Casagrande cup energy method to determine the liquid limit (Germaine, Geotechnical Laboratory Measurements).

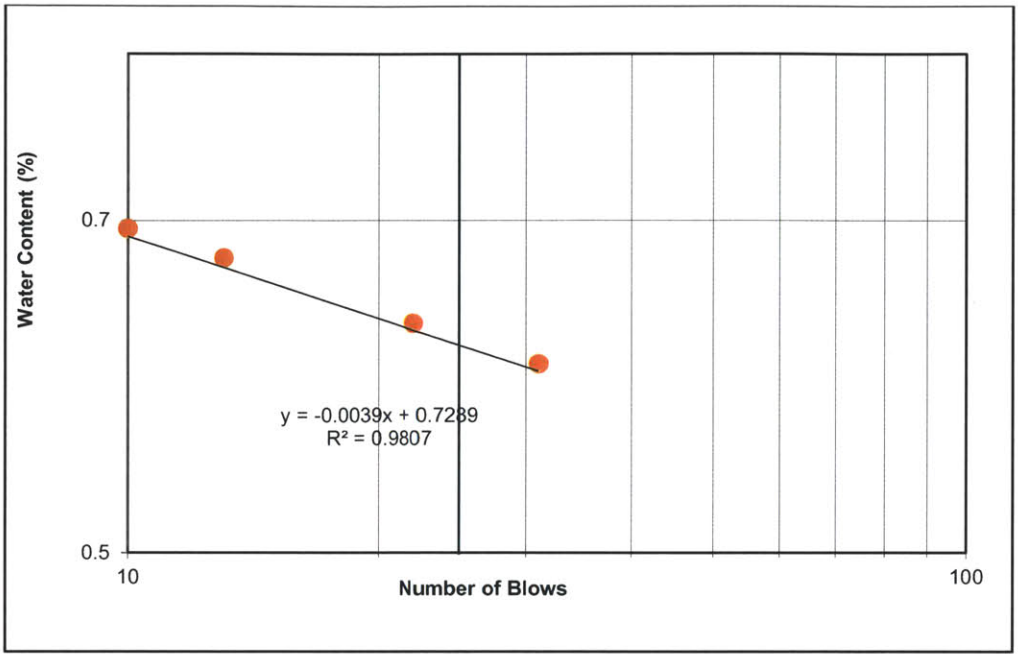

Figure 3.13: Flow curve to determine liquid limit using the Casagrande cup for SFBM.

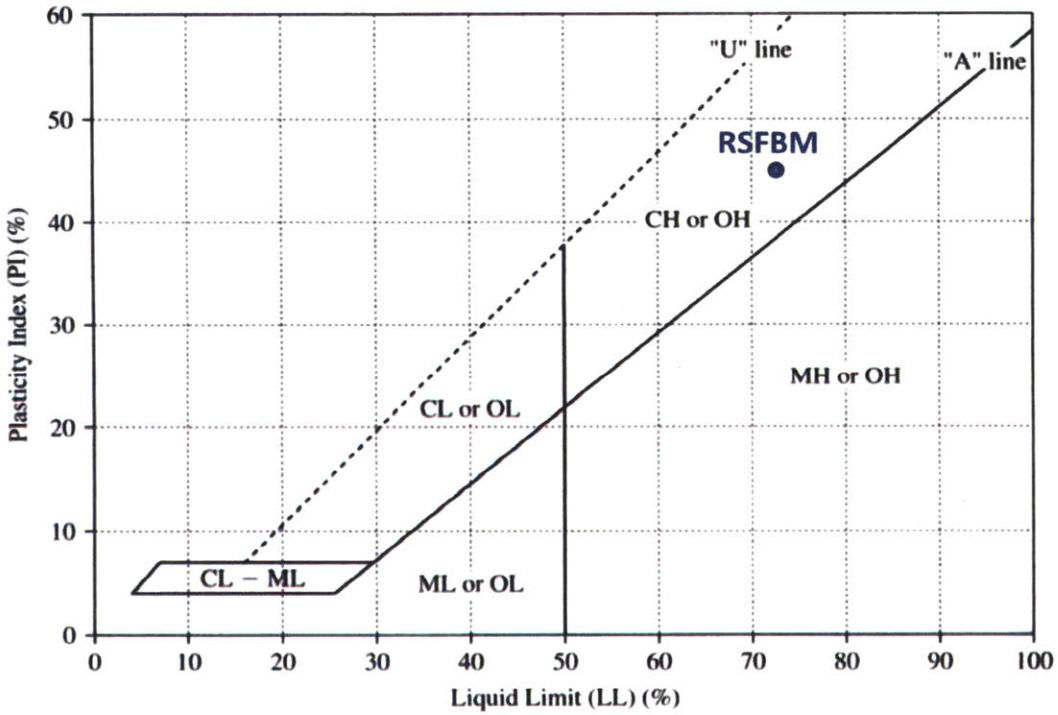

Figure 3.14: Casagrande Plasticity chart for RSFBM (High plasticity clay, CH).

Figure 3.15: A muffle furnace and porcelain crucibles; equipment to measure Organic Content by loss on ignition.

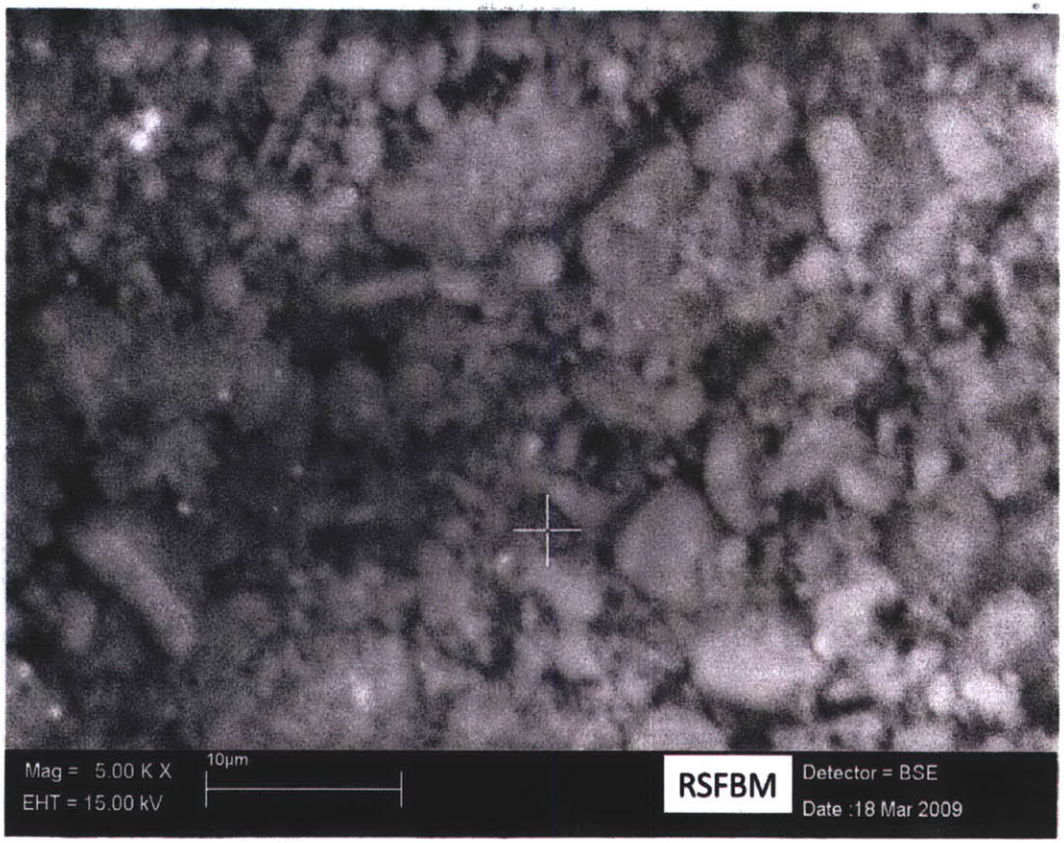

Figure 3.16: Scattering Electron Microscope (SEM) analysis for RSFBM powder at 10µm magnification.

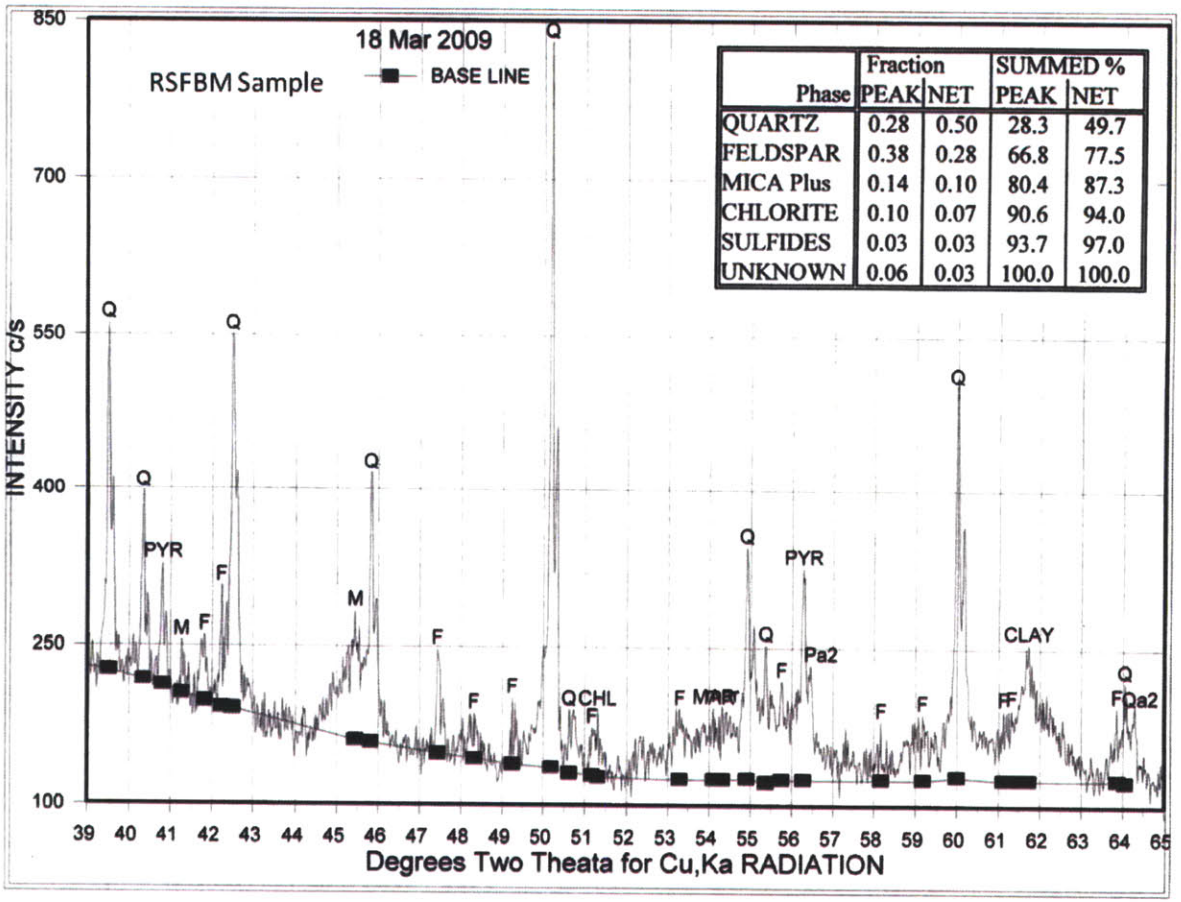

Phase	Fraction PEAK	Fraction NET	SUMMED % PEAK	SUMMED % NET
QUARTZ	0.28	0.50	28.3	49.7
FELDSPAR	0.38	0.28	66.8	77.5
MICA Plus	0.14	0.10	80.4	87.3
CHLORITE	0.10	0.07	90.6	94.0
SULFIDES	0.03	0.03	93.7	97.0
UNKNOWN	0.06	0.03	100.0	100.0

Figure 3.17: X-Ray Defraction spectrograph (XRD) results for RSFBM.

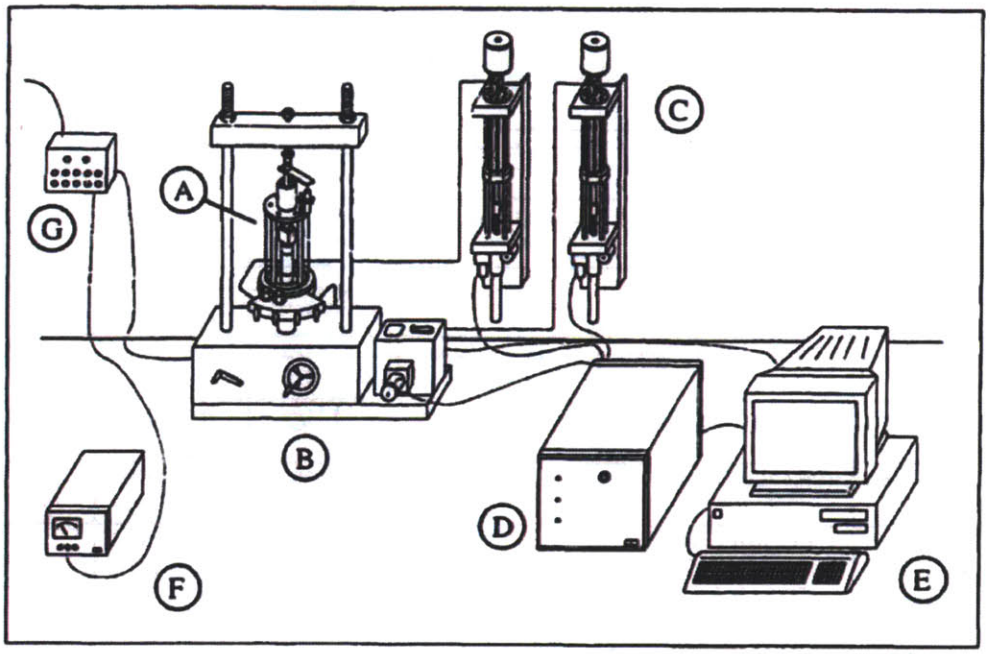

A - Triaxial Cell
B - Load Frame
C - Pressure/Volume Controllers
D - Motor Control Box
E - Personal Computer
F - DC Power Supply
G - Data Acquisition Channels

Figure 3.18: Schematic representation of the MIT automated stress path triaxial apparatus (Santagata, 1998).

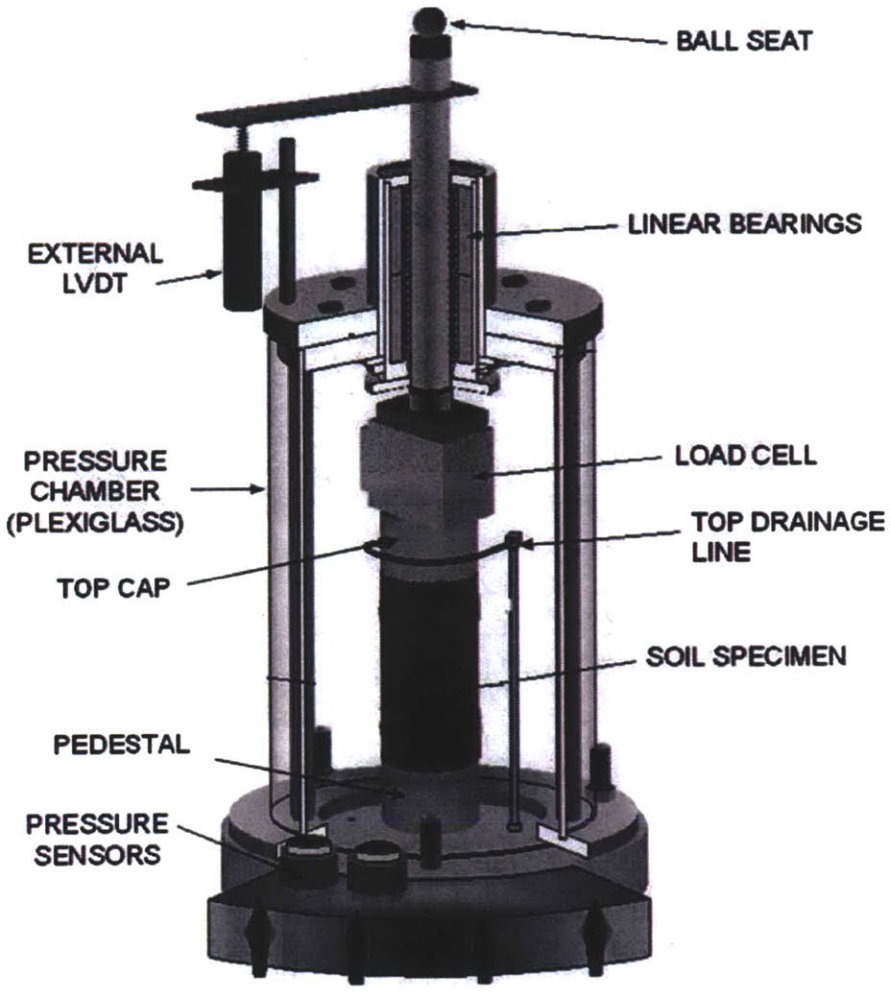

Figure 3.19: Schematic representation of the low pressure triaxial cell (Santagata, 1998).

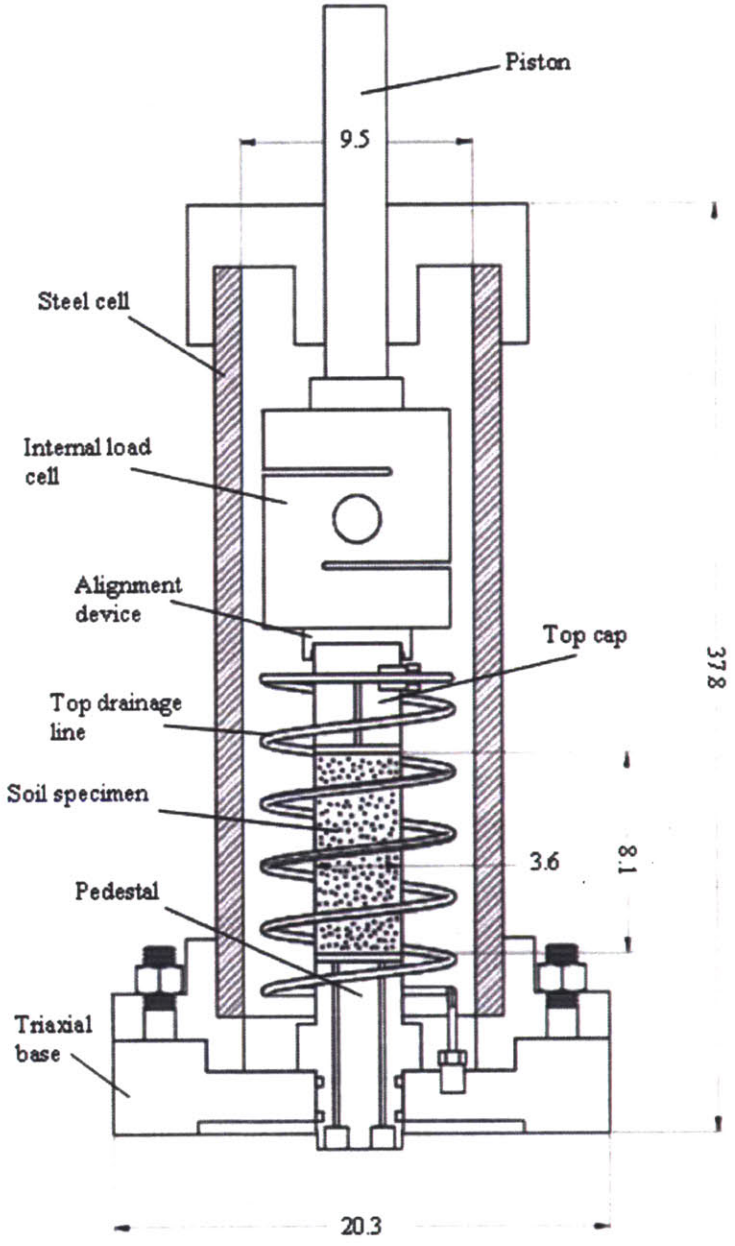

Figure 3.20: The MIT high pressure triaxial apparatus (before modification - dimensions at cm).

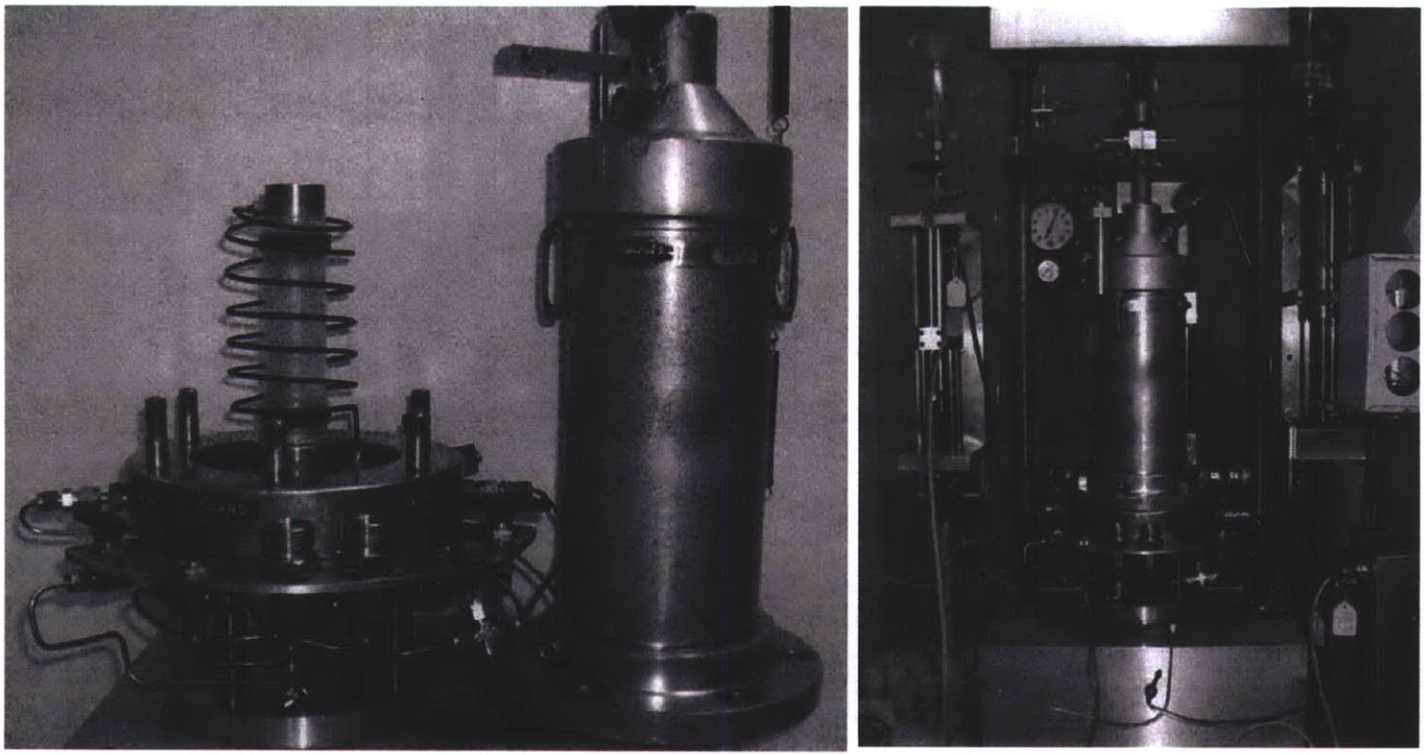

Figure 3.21: The high pressure cell during set up and inside the environmental enclosure (Abdulhadi 2009).

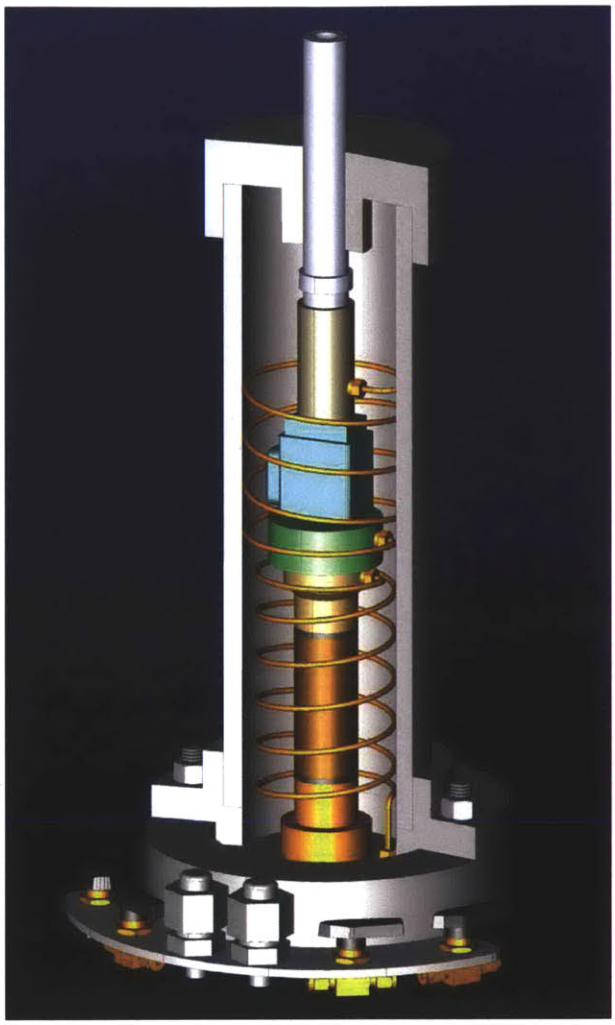

Figure 3.22: Schematic of the MIT high pressure triaxial apparatus modified to incorporate extension.

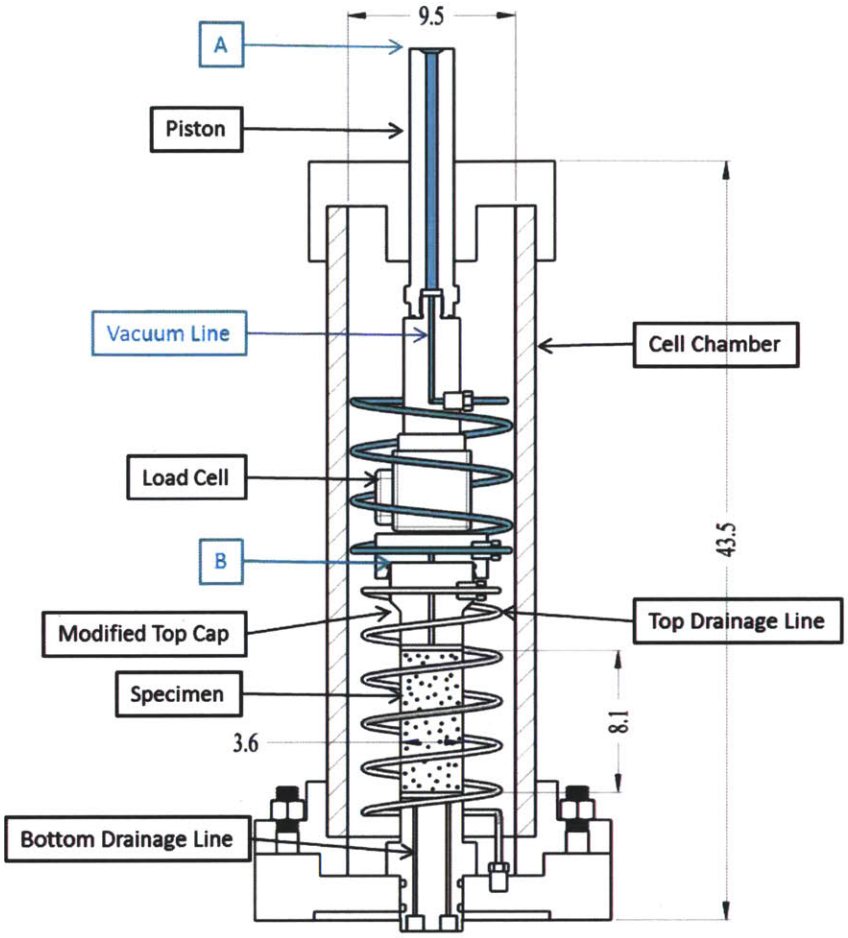

Figure 3.23: Section view of the modified high pressure triaxial apparatus (dimensions at cm).

Figure 3.24: The new suction cap and the lab bench before setting up the high pressure cell for disturbance simulation tests.

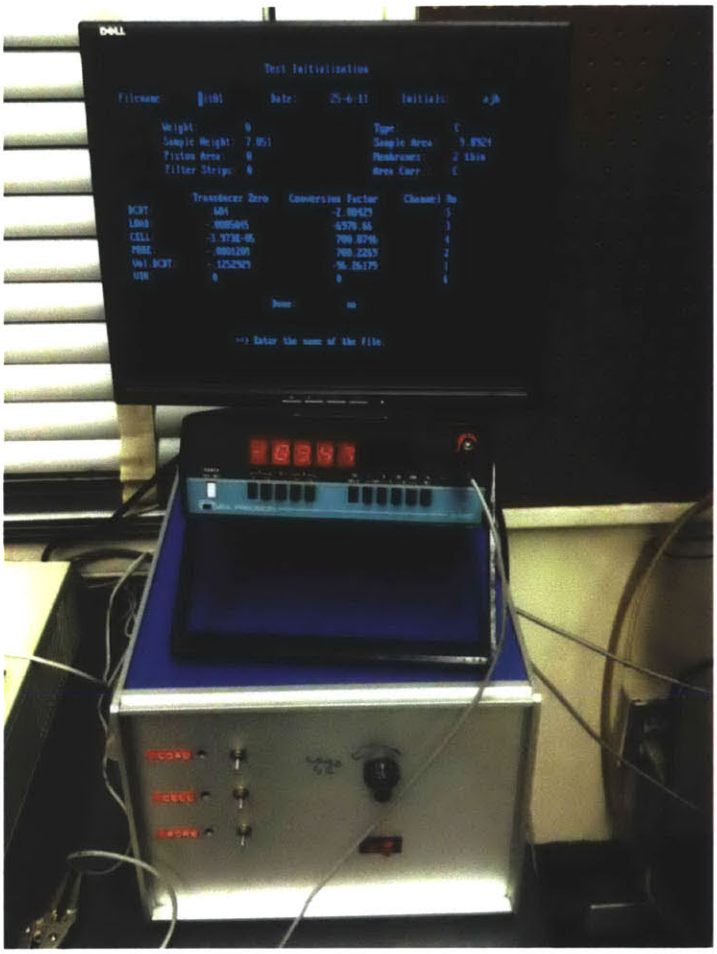

Figure 3.25: The control box and the monitoring screen for the low pressure apparatus.

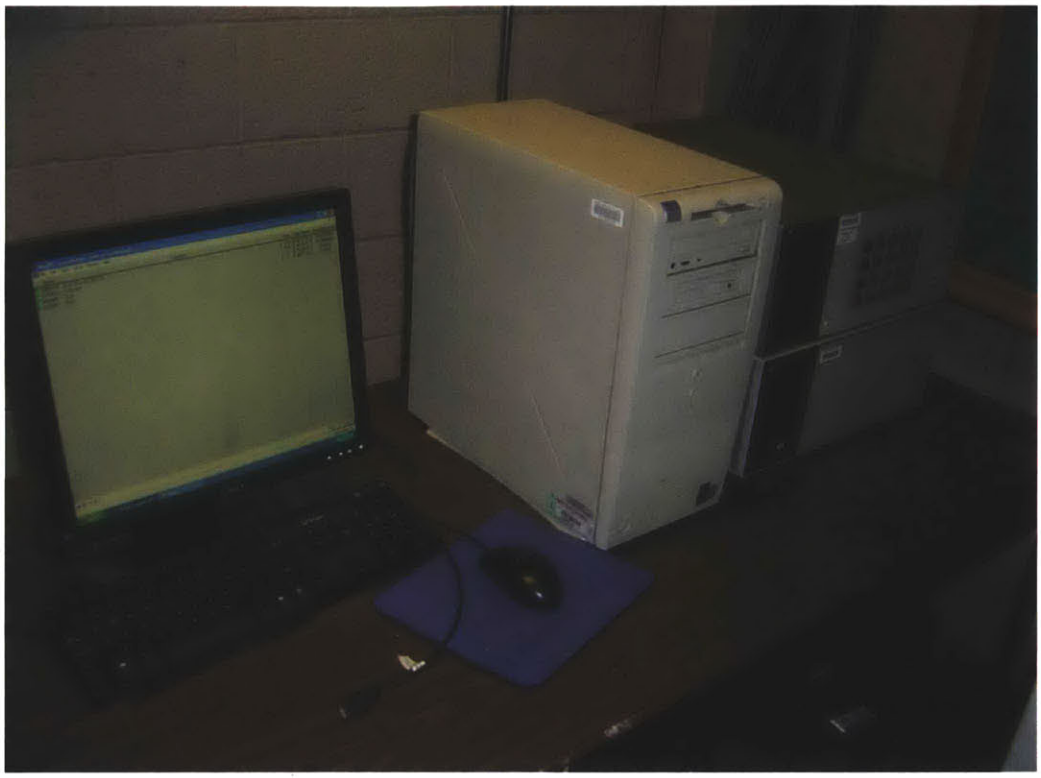

Figure 3.26: The central Data Acquisition Control Unit used at MIT geotechnical laboratory.

Figure 3.27: Pressure transducer of 200 psi attached to measure the cell and the back pressure for the low pressure triaxial cell (left) and on the lab bench (right).

Figure 3.28: Internal load cell of 500 lb capacity to monitor the axial stress.

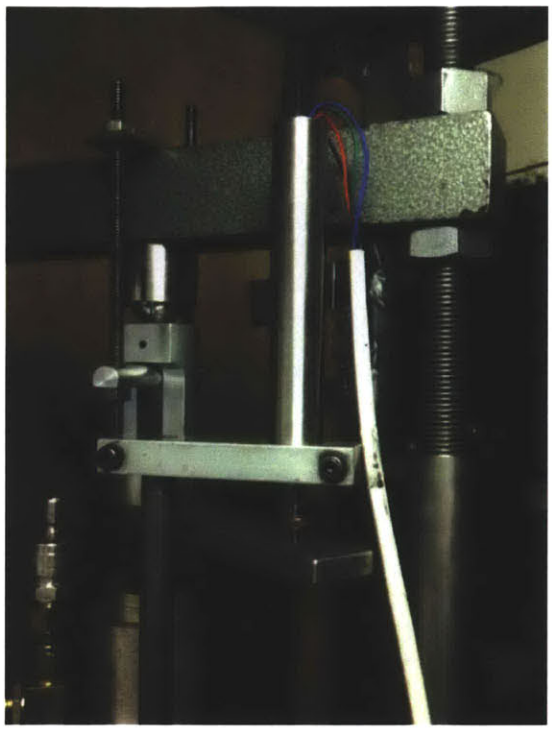

Figure 3.29: A standard external LVDT placed on top of a cell to measure axial displacement (strains) with linear range of about 5 cm.

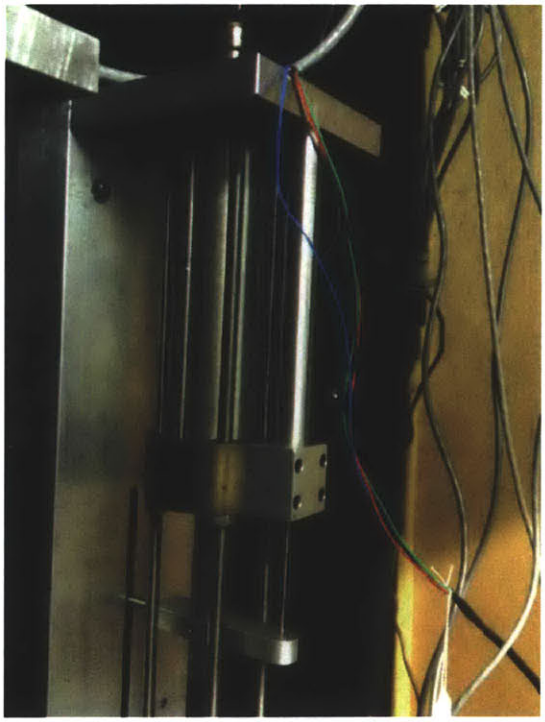

Figure 3.30: A LVDT monitoring the specimen volumetric change with linear range of about 10 cm.

Chapter 4 TESTING PROCEDURES

4.1 Introduction

The core of this experimental program has its framework based on previous work that has been done at MIT by Santagata and Germaine (1994) using Boston Blue Clay (BBC). Based on this framework, repeated simple element triaxial tests (CK_0UC-E) are performed on resedimented SFBM to K_0 consolidate the specimens well into the Virgin Compression Line (VCL). Disturbance is simulated using the Ideal Sample Approach as it was introduced by Baligh et al., 1987. The SHANSEP consolidation technique is then employed to recover the intact behavior and erase the effects of disturbance by reconsolidating the specimen well into the VCL (Ladd and Lambe, 1974). After that, every recompression phase is treated as an initial compression phase of known disturbance. The purpose of this treatment is to investigate the effect of disturbance on the compressibility parameters and preconsolidation pressure (σ'_p) for normally and slightly overconsolidated soils. Experimental procedures are discussed in detail in this chapter. These procedures were followed for the major part of this research.

Section 4.2 presents the main motives that lead to the initiation of this program. Santagata and Germaine's (1994) extensive study of sample disturbance is summarized. It focuses on the theoretical model proposed that tries to enlighten the effects of disturbance at preconsolidation pressure. The ambiguity of the value of preconsolidation pressure from site investigation data is discussed. Section 4.3 presents the triaxial test procedures for the low pressure and high pressure apparatus while section 4.4 focuses on the CRS test procedures. At last, section 4.5 presents the chambers used and their special characteristics.

4.2 Program motivation and overview

It is believed among many researchers that increasing disturbance should always be associated with a decrease of preconsolidation pressure. It is also known that increasing disturbance is always linked to a significant reduction in the sample effective stress (σ'_s) and a decrease of the VCL slope. Based on these observations, Santagata and Germaine (1994), completed a very comprehensive study to better capture the effects of disturbance on low to medium sensitivity NC clays. They investigated the effects of sample disturbance by performing single element triaxial tests on specimens of NC Boston Blue Clay. Both the Perfect Sample approach (PSA, Ladd and Lambe 1963) and the Ideal Sample Approach (ISA, Baligh et al. 1987) where employed. An effort to quantify the effects of the two reconsolidation approaches was carried through. Results from their research showed that PSA disturbance causes a modest change in engineering properties of soil. On the contrary, with ISA disturbance engineering properties of the soil changed significantly and were linked to the imposed amplitude of disturbance (figure 4.1).

Santagata concludes that the effects of disturbance on the engineering properties of NC BBC derive mainly from the following two fundamental mechanisms:

- The decrease in effective stress
- The destructuring of the soil skeleton

She meticulously compared the disturbed behavior of NC RBBC to the intact soil behavior and came up with the following observations. Disturbance can always be associated with:

- A decrease in the undrained strength
- An increase in the strain at peak and a loss of strain softening
- A reduction in small strain stiffness ($\varepsilon_a = 0.01 - 0.1\%$)
- An increase in the recompression index
- A decrease in the value of the virgin compression line (VCL)

It was also mentioned that for increasing disturbance, the undrained stress-strain curve loses all typical characteristics of NC RBBC, and the behavior is closer to that observed for intact OC RBBC (figure 4.2). This observation agrees with Ladd and Lambe's (1963) that increasing disturbance has similar effects on undrained shear behavior as those produced by swelling (figure 4.3). Santagata concludes that disturbance seems to affect to a lesser degree the value of preconsolidation pressure. However, it appears that for low to medium sensitivity clays, such as RBBC, sample disturbance can lead to an overestimation of σ'_p.

To capture the above behavior Santagata and Germaine (1994) proposed the following conceptual model to better understand the effects of disturbance on the preconsolidation pressure. They proposed that for a given VCL slope, increasing disturbance (points 1-> 2 -> 3) will cause a reduction of sample effective stress. This will make the consolidation curve start from a point further left in figure 4.4 (A) and as a result cause an increase at the preconsolidation pressure value ($\sigma'_{p1} < \sigma'_{p2} < \sigma'_{p3}$). This loss of effective stress is a result of two actions: Firstly the destructuring that the specimen undergoes when it is sheared undrained on a cycling disturbance amplitude and past its peak strength, and secondly the stress relief imposed after shearing (when the axial load goes back to zero at the end of ISA, $q = 0$).

Their second hypothesis was that for a given loss of effective stress, disturbance would cause the VCL to decrease (to be less steep – figure 4.4 (B)). As a result, starting from the same sample effective stress would cause preconsolidation pressure value to decrease with increasing disturbance ($\sigma'_{p1} > \sigma'_{p2} > \sigma'_{p3}$). This is due to the fact that in this second hypothesis the initial point of the consolidation curve is given and disturbance only influences the slope of VCL; as VCL slope decreases to the left the recompression line will meet the VCL earlier.

These two mechanisms counter act each other as far as the effect of disturbance on preconsolidation pressure is concerned. This program's main goal is to investigate how increasing disturbance can mobilize these two mechanisms and, how the two play a

role in determining the final value of preconsolidation pressure with respect to the previous maximum vertical effective stress.

Motivation for this research program is the great ambiguity that the calculated value of preconsolidation pressure has at lab reports, in NC and low OC clays. Since the preconsolidation pressure itself is one of the most important soil parameters in design and when calculating settlements, it is of great interest to try to investigate how increasing disturbance influences this value and whether a trend is identifiable while disturbance increases. It is also very significant to investigate if there is a safe procedure to try to correct the preconsolidation value and the consolidation curve of a disturbed specimen in order to retrieve its "in situ" engineering values.

A great example of this is the Haley and Aldrich report back in 1993 from Professor Charles Ladd at the CA/T South Boston Station (figure 4.5). Data of the vertical effective stress and preconsolidation pressure are plotted over depth (ft) for tube sample and block sample triaxial tests for the specific site. The Terzaghi (1996) Specimen Quality Designation criteria is presented at the left figure, while at the right the preconsolidation pressure profile selected and the tests deleted as "bad quality" samples are marked. This is an example of how easily one cans false-predicate the preconsolidation value with increasing disturbance.

Another example of how ambiguous the value of preconsolidation pressure can be is presented at figure 4.6 from Ladd's Report for the MIT Stata Center Site (2000). It is clear, from the stress history profile of this Boston Blue Clay site that the value of preconsolidation pressure can vary up to 50% at great depths where disturbance normally increases (even for the same borehole, CRS B101 or CRS B102). Of course, an interesting question would be how we can correct these false preconsolidation pressure values to derive the actual "in situ" yielding stress.

In order to investigate the role of disturbance in the actual value of preconsolidation pressure, a program of triaxial tests was conducted. The first part of this program involves triaxial tests in tube samples of San Francisco Bay Mad (SFBM). For this part, good quality tubes were selected from low depths based at X-rays and previous

CRS tests performed at each tube. The objective was to provide good NC samples of high compressibility material that would allow for multiple disturbance phase simulations at one single test. Radiography was employed in order to select good quality and representative San Francisco tube specimens. After the selection, the tube was cut, and undisturbed techniques were used to debond and extract the sample in order to have it ready to be tested at the bench. A wire saw and a miter box were used to get the sample trimmed to the desired diameter. Torvane tests were done at the top cut of each specimen. Torque from torvane test can be directly converted into shear stress in kg/cm^2. This will give a rapid, first estimate of the shear strength for each specimen prior to testing. A medium or a small size vane was used for SFBM specimens (figure 4.7).

In the second and main part of this program, a homogeneous batch of resedimented SFBM was created. The material was selected based on its properties and of course the availability of good quality sample tubes at the MIT lab. The highly compressible SFBM, with its high plasticity, high undrained shear strength and low permeability seemed a very good material to study the disturbance at different stresses, allowing for a wide range of ISA nominal disturbance values (ε_{max}), ranging from 0.5% to 10%. The resedimentation process is further explained in chapter 3.

Using resedimented material, the effects of disturbance at preconsolidation pressure were investigated initially for NC and later for OCR soils. A third phase accounting for the excessive shearing that an element would undergo outside the centerline of the tube, was implemented. The MIT high pressure triaxial apparatus was converted to incorporate extension in order to run disturbance simulations at higher stresses.

The experimental program designed in this thesis was based on the following assumptions as they derive from the ISA disturbance simulation and the SHANSEP reconsolidation technique. The first assumption is that the sampling procedure is rapid enough to be considered as an undrained process, and of course, this procedure can be simulated at the lab by a triaxial experiment. Analytical solutions on how sample disturbance can be simulated in a triaxial cell are presented by Baligh et al. (1987) on his

framework work of the Ideal Sample Approach (ISA). However, using the ISA approach, one can only account for the strain path of a soil element positioned along the centerline of the sampler. One of the main scopes of this research program was to investigate how this complex strain path alters during the penetration of a sampler once we move outside the centerline. It is of great interest to examine how the excess shearing and change in volumetric strain will influence the degree of disturbance that the rest of the tube elements are subjected to.

The third assumption derives from the SHANSEP reconsolidation technique. It was assumed that RSFBM exhibits normalized behavior. This means that when the specimen is consolidated well into the virgin compression line (VCL) and to a maximum stress (σ'_{vm}) equal or greater than 1.5 to 2 times the preconsolidation pressure (σ'_{p}) all the previous effects of disturbance are erased. Being on the VCL, the specimen is considered to be in an undisturbed state equal to that of an element of NC soil "in situ" and prior to sampling. Overconsolidated test specimens are swelled from the VCL to the desired OCR. Stress conditions on the VCL for NC specimens or on the swelling line for the OCR specimens are referred as "in situ" stresses.

4.3 Triaxial Test Procedures

Section 4.3 provides background information on the procedures used in order to set up a triaxial test in the MIT low and high pressure triaxial cells. These procedures have been very well stated over the years (Baldi et al. 1988, Germaine and Ladd 1988, Sheahan 1991, MIT subject 1.37 Geotechnical Measurements and Exploration) and are a common practice for most triaxial tests run at MIT Geotechnical laboratory.

The test procedures can be divided to the following steps:

- Cell preparation
- Specimen preparation
- Assemble cell

- Saturation and specimen consolidation/disturbance
- Disassemble
- Data processing

The cell preparation phase starts with the retraction and lock in position of the piston to an upper position. This will ensure that there is enough space for the specimen and stones during the set up. A dummy specimen can be used in advance to adjust the position for any type of test. Then water is flushed through the bottom and top drainage lines. The drainage system is checked for possible leakage by plunging the top drainage line and looking the lines and the connections for water when slightly increasing the pore pressure. The response of pore pressure transducer is checked and the zero value is recorded. The base pedestal and the top cap must be cleaned and greased thoroughly with high vacuum grease. Two rubber sleeves are placed on the top cap and pedestal in order to secure the porous stones in the right place and in alignment with the specimen (figure 4.8). Two rolling membranes (Trojan condoms) are placed on top of the rubber sleeve at the base pedestal in a sealed arrangement with greased o-rings. The o-ring stretcher is prepared with three more o-rings and placed at the bottom of the pedestal in order to be ready to seal the membranes to the top cap of the cell.

Once the rubber sleeves and the rolling membranes (condoms) are in place, the specimen can be transferred to the apparatus. Porous stones and filter papers are used on the top and bottom of the specimen. The specimen and the porous stones are aligned and the two membranes are rolled up to provide an impermeable barrier between the silicon oil in the cell and the specimen itself (figure 4.9). The load cell is connected to the base electrical connector at this stage and allowed to heat up for 20 minutes; then the zero output voltage value for the load can be recorded. After that, it is unplugged again to allow the specimen positioning. Before continuing with specimen set up one should make sure the porous stones and the filter papers are cleaned up and ready to be used. This is done by the use of ultrasounds. The pore and cell piston of the PVA should be in the right position to start the test; have enough stroke and place the LVDT within linear range. The triaxial test data sheet should also be used to record test specific values; test number, cell, dimensions, mass, zero values, calibration factors, notes at each phase etc. (figure 4.10).

For the specimen preparation a wire saw, a blade and two miter boxes are mainly used (figure 4.11). To eliminate disturbance during extrusion, for the tube samples, a wire saw is used to de-bond the soil from the walls of the tube before extrusion. All samples were extruded in the same direction that the material was pushed into the tube during sampling (the top of the tube was marked before cutting the piece to be used). For reconstituted material were lubrication is used on the walls of consolidometer, no de-bonding was required. Trimming process is performed as quickly as possible and at a humid environment to avoid moisture loss. The specimen is initially extruded manually from the consolidometer's tube section and is placed in an orthogonal miter box. The ends of specimen are cut off to create a flat surface perpendicular to the axis of the consolidometer/sample tube. The specimen diameter is reduced by trimming a layer from the perimeter to remove the excess material of tube lubrication (figure 4.12). Also, in this way the specimen is reduced on diameter if it is much greater than 8 mm large. A second cylindrical miter box, a soil lathe is used to gradually trim the specimen to the correct diameter (figure 4.13). The miter box used had two settings; one to reduce the specimen diameter to slightly larger than final size, and one defining the final diameter. The cuts were done using a wire saw and rotating the cylinder by about 5 degrees. The specimen perimeter is finalized with a razor blade. The final specimen surface should be smooth and clean of cutting in order to proceed to the next step.

Once at the correct diameter, the specimen gets wrapped with wax paper and transferred into an 81mm specimen mold and secured in place. This split mold is used as a guide to trim the ends of the specimen; first applying a wire saw and then using a razor blade. This will ultimately define the final height of the specimen (figure 4.14). Water contents are taken using the excess material from this final trim stage; two from the periphery of the specimen and one from the top and bottom cuts. In some cases trimmed material was also used to perform index tests (Chapter 3). The blade used to finalize the surface of the specimen is a 10" Eastman Cloth Cutting Razor blade.

It should be mentioned that trimming does not only bring the specimen to the correct dimensions for testing but also allows the removal of the perimeter, more

disturbed soil. The final dimensions of the cylindrical specimen are 3.5 cm in diameter and 8 cm at height. The total mass (specimen and split mold), as well as the exact dimensions of the specimen after trimming, are recorded using a digital scale and a caliper. The height and the diameter of the specimen are defined by an average of 3 measurements (at top, middle and bottom of the specimen without the wax paper).

Prior to testing in the low pressure apparatus, specimens were batch consolidated to 100 KPa (1ksc) and unloaded to an OCR of 4. For the high pressure apparatus, specimens were batch consolidated to 2000 KPa (20 ksc) and unloaded to an OCR of 4. The resulting sample for the high pressure tube was stiff but still it could be trimmed with a wire saw and a blade. Material (RSFBM) for these high pressures appeared to be much more brittle.

Once the specimen is ready, it is placed on the base pedestal with filter papers and porous stones at the top and the bottom. The piston is lowered to touch the specimen and locked in place. The first prophylactic membrane is rolled up and sealed against the top cap by two greased o-rings. Then, the second prophylactic membrane is rolled up and placed over the two first o-rings. A third o-ring is placed between the first two creating a secure seal. The cylindrical Plexiglas chamber is placed around the cell making sure both o-ring surfaces are clean to ensure no leak. The top plate of the cell is placed and secured with sealed bolts. The load frame is lowered in place and the remaining equipment and the external LVDT are assembled (figure 4.15). The triaxial cell is filled with silicone oil and the zero value for cell (corresponds at the cell pressure when filling up the cell up to the middle of the specimen height) and axial LVDT are recorded (figure 4.16, 4.17). With the triaxial cell ready, the specimen dimension, zero values and calibration factors for all transducers are input into the set-up Q-Basic computer program.

For the high pressure apparatus the set up and assembly of the cell takes place on a mobile cart (figure 4.18). For this cell, a dry setup is adopted to avoid swelling. Specimen is placed on the pedestal using semi-dry porous stones and dry filter paper at the top and bottom. A rubber sleeve is used at the pedestal and free cap with vacuum grease to cover the porous stones and filters and align everything together. The modified

free cap (to incorporate extension) is placed on the specimen; the sleeves are unfolded to cover the perimeter of the porous stones. Using a vacuum membrane stretcher a thick commercial latex membrane is fixed in place with two O-rings at the top and bottom cap. A second condom membrane is placed above the first and one O-ring is used between the first two at the top and bottom of the specimen. An alignment device is employed to secure the free cap in place when shooting the O-rings and after every step when a membrane is applied (figure 4.19).

Once the specimen is sealed with the double membrane and aligned, the top spiral drainage is attached to the base of the apparatus and the top cap. The alignment device is used again to check for consistency (figure 4.20). A large O-ring is placed at the bottom of the apparatus and the steel chamber is put on making sure there is enough height inside the cell in order not to smash the sample. The internal load cell is connected when resting the steel chamber on the bolds of the cell base. The load zero value is recorded after a 20 minute period is allowed for the electric wires to warm up. Then the chamber is lowered in place and secured by tightening the bolts. The whole apparatus is transferred from the mobile cart to the load frame using a wooden bridge (figure 4.21).

The piston clamp is released and the piston is slowly lowered until it makes contact with the specimen. Then small force is imposed monitoring the load cell in order to make sure the top cap and the cap of the load frame is fully in contact. This will ensure that vacuum will be created between the two surfaces for the uplift force to be imposed during the undrained extension phase. The cell is filled with silicon oil and the cell pressure transducer is attached. Imposing a slight pressure on the cell of about 50 kPa, the pore pressure lines are vacuumed from air. Then the vacuumed is removed while water is used to flush pore and back pressure lines and valves. Pore pressure transducer is attached. The top assembly and the external LVDT are attached to the piston while the load frame is lowered in place. The remaining zero values are recorded and put into the computer program; the axial, the volumetric and the cell zero values (the cell zero value is recorded while filling up the cell chamber up to the middle of specimen's height).

Once the set-up program has the correct input values the actual testing can begin. This can be double-checked by the actual values the program reads after the new input zero values. The first phase for triaxial testing starts with the Pressure up. Here, with the drainage lines closed a hydrostatic total stress of about 0.3 to 0.4 ksc for the low pressure apparatus is applied overnight. This will establish a small positive pore pressure. The difference between the cell and the pore pressure gives an initial effective stress that for the RSFBM specimens is about 0.25 σ'_p (0.25 ksc for specimens consolidated in the lab to 1ksc). This is an estimate of the initial sampling effective stress, $\sigma'_s = \sigma_v - u$. For the high pressure apparatus the initial stress applied was up to 3 or 4 ksc in order to get a response on the pore pressure.

The second phase is the back pressure saturation. Initially, the back pressure is equalized to the pore pressure of the specimen, the drainage lines opened and the pressure is incrementally raised to 2 ksc (through isotropic loading $\Delta\sigma_1 = \Delta\sigma_3 = \Delta u$). The initial effective stress is maintained constant while increasing the pore in 30 minutes increments of 0.5 ksc. When the targeted stress has been reached, a B-value parameter check ($\Delta u/\Delta\sigma_3$) ensures saturation of the system above 85 to 90%. This B- value is lower than ASTM Standards recommendation (95%) but was found to be sufficient for the saturation of the MIT triaxial systems. B- value calculation is based at the Skempton's empirical equation (1954):

$$\Delta u = B\{ \Delta\sigma_3 + A (\Delta\sigma_1 - \Delta\sigma_3)\},$$

where A and B, are empirical "pore-pressure coefficients" to express the change in pore pressure Δu, under changes in total stresses, $\Delta\sigma_1$ and $\Delta\sigma_3$. Coefficient A describes the shear induced change in pore pressure as a function of deviator stress ($\Delta\sigma_1 - \Delta\sigma_3$) and its value depends on the overconsolidation ratio (OCR). By isotropic loading where ($\Delta\sigma_1 - \Delta\sigma_3$) = 0, the above equation can be simplified to $\Delta u / \Delta\sigma_3 = B$. So, for completely saturated soils (S = degree of saturation = $v_{water}/ v_{voids} = 1$), an increase in cell pressure should cause an equal reaction at the pore pressure, depending on soil stiffness.

The B-value check for the triaxial cell starts with drainage valves closed and by imposing a pressure increment of 0.25 ksc in a single increment while recording the pore pressure reaction. The computer calculates the B-value for 2 minutes and then reports a final value. The backpressure saturation of the system is significant since it allows more accurate measurements of pore pressure and volume changes during the next phases of the test. This is done by removing the trapped air in the specimen's voids, porous stones and drainage line and by securing the system from possible miscalculations due to air compressibility. Axial and volumetric strains are recorded at the end of this stage to ensure the good quality of the test specimen. For an ideal measurement of sampling effective stress, σ'_s, minimum swelling should occur. This for RSFBM is around 1.5 - 2% volumetric strain at 2 ksc back pressure.

Triaxial specimens are then K_0-consolidated well into Virgin Compression Line and at a stress level more than 1.5 times greater than the preconsolidation pressure, $\sigma'_{vc} > 1.5\ \sigma'_p$. The constant rate of axial deformation selected for most tests for RSFBM is 0.15%/hr. This low rate ensures that no significant excess pore pressure will build up during consolidation. During the K_0-consolidation, the program increases the cell pressure insuring the zero lateral strain condition (the area of the specimen remains the same) and tries to equilibrate volumetric to axial strains. So it is essential before every consolidation phase to reset the volumetric strain to be equal to the axial strain. Once the maximum stress condition has been reached, it is held for 24 hours to allow for equilibration and some secondary compression.

In the case of overconsolidated specimens, the specimen is then rebounded (unloaded) to the desired OCR. This can be done after defining the exact targeted vertical and horizontal condition and using stress path consolidation with the same but now negative constant strain rate (-0.15%/hr). In order to do this the pre-sheared K_0 is estimated for the corresponding value of OCR.

The approximate correlation to calculate $K_{0\,OC}$ that is used, was proposed by Schmidt back at 1966:

$$K_{0\,OC} = K_{0\,NC}\,(OCR)^n\ ,$$

where for RSFBM is an approximation of $n \approx 0.4$. $K_{0\,NC}$ was calculated from the previous K_0 consolidation phase of the test. Thus a different value of $K_{0\,NC}$ is used for each test.

After unloading to the desire OCR the system holds stresses overnight for secondary compression.

Once the specimen reaches the desired stress level a disturbance simulation is imposed. A leak check is performed by closing the top and bottom drainage lines and monitoring the pore pressure for 30 minutes. This is done before every disturbance cycle simulation. Then the specimen undergoes a cycling strain deformation to simulate the straining that a soil element undergoes at the centerline of the tube during sampling (Baligh et al. 1987). An axial strain rate of 0.5% is used and the deformation strain amplitude is defined (ε_{max} %). Disturbance simulations from 0.5% strain amplitude to up to 10% strain were performed. During this phase, the specimen is sheared undrained to compression (from 0% to ε_{max} % axial strain), extension (from ε_{max} % to $-\varepsilon_{max}$ %), and to compression back to 0% axial strain. The phase ends with unloading back to hydrostatic conditions (0 axial deviator load) to account for the complete stress relief after sampling. It is very significant for this complex step of disturbance simulation that the user only assigns to the program a strain rate and strain cycle amplitude. All the reversals in deformation as well as the unloading to hydrostatic conditions are performed under computer control reducing significantly the test labor. The final stresses at the end of ISA Disturbance are maintained overnight.

After each disturbance phase, a new recompression phase follows in most tests. SHANSHEP reconsolidation technique is used to erase the effects of imposed disturbance and recover the intact behavior of the soil (after Ladd and Lambe, 1974). For this step, the back pressure PVA is set to the pore pressure of the specimen at the end of the disturbance cycle and the volume deformation is reset to be equal to the axial strain. This can be done by manually changing the zero value of the input file using the set up program. Drainage lines are opened. The specimen then follows a K_0 consolidation as

described earlier but to higher stresses and until it is well into its virgin compression line (up to 7 ksc) at approximately 15% strain for the first recompression phase on the low pressure apparatus.

In most cases if there are no stroke constrains or cell pressure limitations a second disturbance phase and then another recompression phase would follow. This for RSFBM normally occurs at stresses up to 12 to 15 ksc reaching maximum axial strain deformations of around 22%. After the second reconsolidation the test would either terminated or, if needed, a third disturbance or an undrained shearing will take place as described above. The shearing rate of axial strain is constant in all tests and through different phases and is approximately 0.5%/hr. A typical triaxial test for RSFBM will be further analyzed at Chapter 5.

Upon completion of each test the final readings are recorded. The cell pressure and back pressure are slowly released (the pore pressure drainage lines stay closed so that no swelling occurs). The piston is locked in place and the cell chamber is drained of the silicon oil by the use of air pressure. The top of the cell, the clamp and the external LVDT are disassembled. The plexiglass cylinder is removed. The excess oil on the load cell and the top cap are cleaned using paper towels and the membranes and the o-rings are carefully removed to release the specimen from the cell. All equipment is thoroughly cleaned up. Filter papers and stones are also removed to be cleaned with the ultrasound. After that they are stored in a water bath for future use. The specimen mass is determined and put in the oven to dry out. The final dry mass of the specimen is also measured after one day in the oven and used for phase relation calculation.

After finishing the experiment, all data files for the different test phases are collected from the MIT Geotechnical Data Acquisition System. A QBasic program similar to the one used for automated control is then used to edit the collected values and convert them to engineering values. The program uses as input the initial normalized zero readings, the calibration factors of the different instrumentation (pressure transducers, axial and volumetric LVDTs and load) and the specimen dimensions. The reduction program takes the voltage readings during consolidation or shearing (disturbance) and

creates an output file where effective stresses, vertical and volumetric strains, void ratio, pore pressure, p' and q, stress ratio K and total work are calculated with time. For undrained shear or disturbance data, everything is normalized to the maximum vertical effective stress σ'_{vm} at the end of the previous consolidation phase.

4.4 CRS Test procedures

Constant rate of stress consolidation was originally developed by Smith and Whals back at 1969. Two years later Wissa et al. (1971) developed the MIT CRS device to perform quick consolidation test (figure 4.22). The device incorporates a cell camber, a load cell and a rolling diaphragm seal. It allows back pressure saturation and produces fast 1-D consolidation curves with a much better accuracy and less effort than the conventional oedometer tests.

For the CRS tests, a specimen 2.5 cm tall was separated from the resedimented material prepared in the consolidometer. For the trimming, a miter box and a cutting shoe is used (figure 4.23). The cutting shoe and specimen ring are greased on the inside to reduce friction. The insert distance of the recess tool and one filter paper is measured. Then the ring is placed on top of the specimen and slowly pushed through the soil mass. The excess material is removed using a spatula. The specimen ring connects to the cutting shoe once it is filled completely with the soil mass. Then the assembly is removed from the trimming stand. The front of the cutting shoe is finalized using a wire saw and a sharpened straight blade. Water content is obtained from the trimmings. A filter paper is placed at the surface of the specimen inside the cutting shoe. Then a recess tool is used to push the specimen into the ring and create a gap on the top. The excess soil is trimmed from the bottom with a wire saw and finished with a blade. The mass of the specimen, ring and filter as well as the height of the specimen are determined. During this process the use of the cutter and the recess tool produce a specimen of about 1.25 cm height and 1.76 cm in diameter.

Once the specimen is ready, a wet assembly method is used to set up the CRS apparatus (figure 4.24). The base is filled with distilled water and the bottom stone and

filter are inserted. Any excess water is removed with a paper towel. The response of the load cell and the pore and cell pressure transducers are checked. The specimen is positioned on top of the stone. Two greased O-rings are used at the bottom of the specimen ring to seal the assembly (one thick, one thin). The top semi-dry stone is placed on the specimen. The cell chamber is positioned and centered in place with the piston locked and external displacement transducer attached. Piston is lower into contact with the specimen and locked in place. A small positive load is imposed to the specimen to keep it in confinement (1-2 pounds). For the low stress CRS equipment a 500 lb load cell was used, while for the high pressure CRS a load cell of 10,000 lb capacity was equipped. The cell is filled with distilled water opening the bottom drainage and cell pressure volume controller valves; all the remaining zero values are recorded and used for the input file of the computer program.

The cell chamber is connected to a PVA to maintain the cell pressure during testing. Test starts with the back pressure saturation phase. An initial cell pressure equal to the pressure applied by the piston due to its weight is imposed. After a few hours and once the difference between the axial and the cell pressure is determined, one can pressurize the system incrementally to the desired back pressure level. The same difference between the axial stress and the cell pressure are maintained during the pressure up. The system is left to equilibrate overnight. After back pressure saturation, the bottom drainage line is closed and the specimen is consolidated at a constant rate of strain. For a typical CRS consolidation a constant rate of 0.15%/hour is imposed. 24 hours of secondary compression follow after each step. System goes to hold stress for the excess pore pressures to dissipate. Unload – reload cycles at predefined stresses where imposed between K_0 consolidation phases. To unload a stress path consolidation to a specific OCR is applied with an unloading rate of -0.2%/hour.

For a constant rate of strain consolidation, there is an excess pore pressure generated at the bottom of the specimen. This allows the calculation of an average axial effective stress, $\sigma'_{average} = \sigma_a - 2/3 \cdot u_e$.

Where σ_a is the applied axial stress and u_e is the measured excess pore pressure at the bottom of the specimen. The specimen is inside a metal ring so there is zero lateral strain, ε_v (%) = ε_a(%). This limitation makes easy the conversion of axial strain to void ratio.

4.5 Apparatuses Characteristics

For this research program the following devices were used:

- Triaxial low pressure apparatus; MIT 03 and MIT 04
- Triaxial high pressure apparatus MIT 07
- CRS apparatus

Their electrical characteristics are presented at tables 4.1 to 4.4. Measurements, calibration factors, linear range, resolution and stability are stated. The resolution and stability calculations are based on the MIT central data acquisition system. The calibration factor calculations are based on the specimen and apparatus dimensions. All instrumentation used in this study have excellent hysteresis, non-linearity and repeatability characteristics. Load and pressure transducers were extremely rigid so compressibility did not affect any of the results. Linear calibration factors were used in all devices and appeared to be consistent for a long period of time. Zero values were recorded before every test for an input voltage of 5.5 volts and also used at the input file of the data reduction program. Consistency was checked among tests for each cell.

TX MIT03	Measurement	Calibration Factor	Linear Range	Resolution	Stability
Pressure Transducer	Pore Pressure	70.393 Mpa/v/v	1.4 MPa (200 psi)	0.01 kPa (0.001 mV)	0.1 kPa (0.01 mV)
Pressure Transducer	Cell Pressure	-70.075 Mpa/v/v	1.4 MPa (200 psi)	0.01 kPa (0.001 mV)	0.1 kPa (0.01 mV)
Internal Load Cell	Axial Load	-82.433 kN/v/v	2.2 kN	0.01 N (0.001 mV)	0.1 N (0.01 mV)
External LVDT	Axial Strain	-2.492 cm/v/v	2.5 cm	±0.0006% (0.1 mV)	±0.006% (1 mV)
Volumetric LVDT	Volumetric Strain	22.487 cm^3/v/v	45 cm^3	±0.0005% (0.1 mV)	±0.005% (1 mV)

Table 4.1: Instrumentation characteristics for the low pressure triaxial cell MIT03.

TX MIT04	Measurement	Calibration Factor	Linear Range	Resolution	Stability
Pressure Transducer	Pore Pressure	70.785 Mpa/v/v	1.4 MPa (200 psi)	0.01 kPa (0.001 mV)	0.1 kPa (0.01 mV)
Pressure Transducer	Cell Pressure	-70.447 Mpa/v/v	1.4 MPa (200 psi)	0.01 kPa (0.001 mV)	0.1 kPa (0.01 mV)
Internal Load Cell	Axial Load	67.763 kN/v/v	2.2 kN	0.01 N (0.001 mV)	0.1 N (0.01 mV)
External LVDT	Axial Strain	-3.436 cm/v/v	2.5 cm	±0.0006% (0.1 mV)	±0.006% (1 mV)
Volumetric LVDT	Volumetric Strain	22.599 cm^3/v/v	45 cm^3	±0.0005% (0.1 mV)	±0.005% (1 mV)

Table 4.2: Instrumentation characteristics for the low pressure triaxial cell MIT04.

TX MIT07	Measurement	Calibration Factor	Linear Range	Resolution	Stability
Pressure Transducer	Pore Pressure	354.101 Mpa/v/v	7 MPa (200 psi)	0.01 kPa (0.001 mV)	0.1 kPa (0.01 mV)
Pressure Transducer	Cell Pressure	352.461 Mpa/v/v	7 MPa (200 psi)	0.01 kPa (0.001 mV)	0.1 kPa (0.01 mV)
Internal Load Cell	Axial Load	-297.544 kN/v/v	8.9 kN	0.01 N (0.001 mV)	0.1 N (0.01 mV)
External LVDT	Axial Strain	3.295 cm/v/v	2.5 cm	±0.0006% (0.1 mV)	±0.006% (1 mV)
Volumetric LVDT	Volumetric Strain	22.078 cm^3/v/v	45 cm^3	±0.0005% (0.1 mV)	±0.005% (1 mV)

Table 4.3: Instrumentation characteristics for the high pressure triaxial cell MIT07.

GEOJACK CRS	Measurement	Calibration Factor	Linear Range	Resolution	Stability
Pressure Transducer	Pore Pressure	20.942 Mpa/v/v	1.4 MPa (200 psi)	0.01 kPa (0.001 mV)	0.1 kPa (0.01 mV)
Pressure Transducer	Cell Pressure	-14.008 Mpa/v/v	1.4 MPa (200 psi)	0.01 kPa (0.001 mV)	0.1 kPa (0.01 mV)
Load Cell	Axial Load	54.757 kN/v/v	2.2 kN	0.01 N (0.001 mV)	0.1 N (0.01 mV)
External LVDT	Axial Strain	-0.519 cm/v/v	2.5 cm	±0.0006% (0.1 mV)	±0.006% (1 mV)

Table 4.4: Instrumentation characteristics for the GEOJACK CRS apparatus.

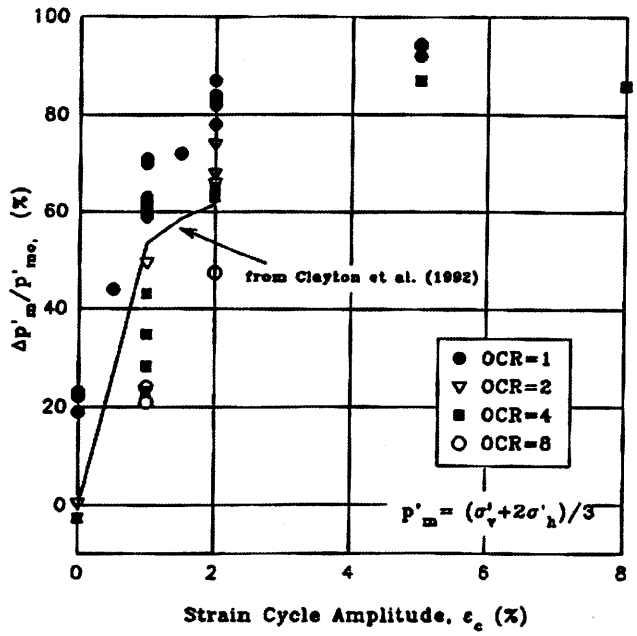

Figure 4.1: Loss in Mean Effective Stress versus disturbance strain amplitude due to PSA and ISA for NC and OCR RBBC (Santaga and Germaine, 1994).

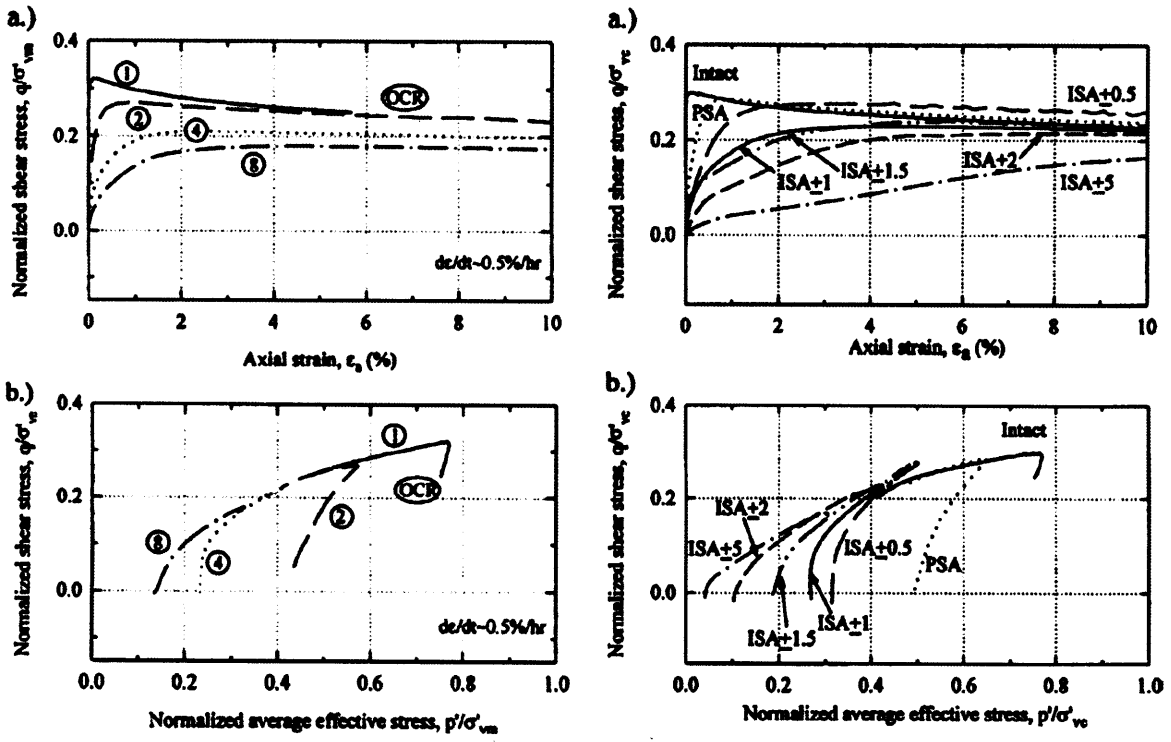

Figure 4.2: Effects of OCR (left) and disturbance (right) on the (a) stress-strain curves and (b) the stress paths for RBBC (Santagata and Germaine, 2002).

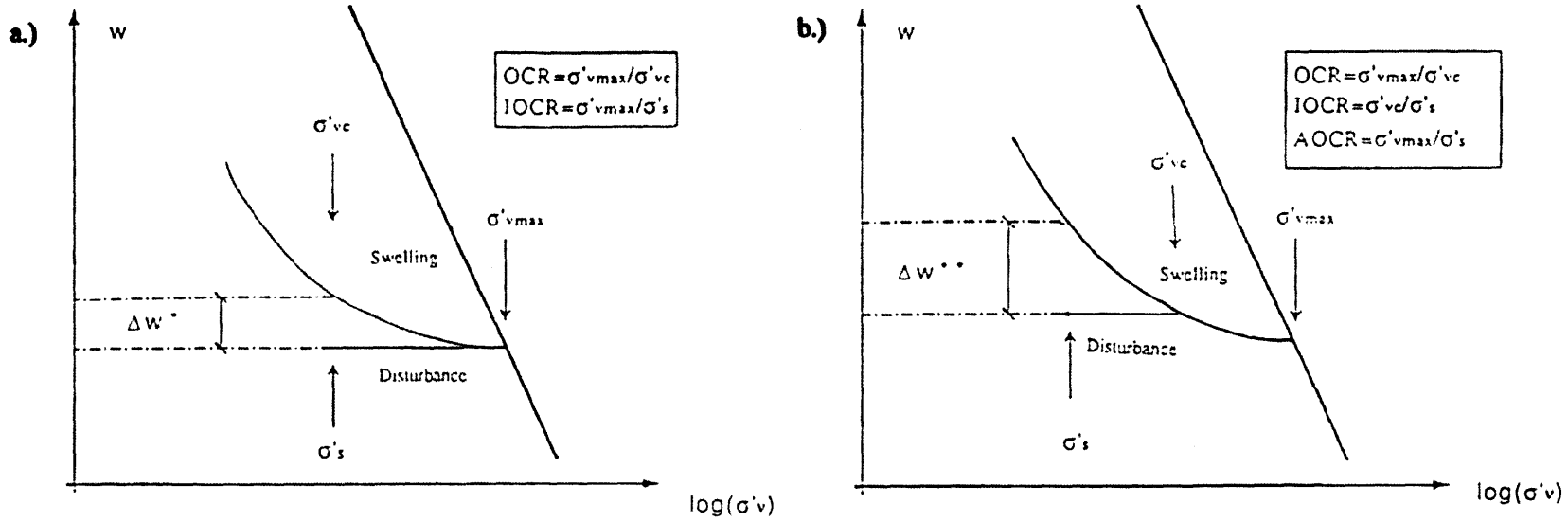

Figure 4.3: Schematic representation of effects of swelling and disturbance for NC RBBC (left) and OC RBBC (right)

(Santagata and Germaine, 1994).

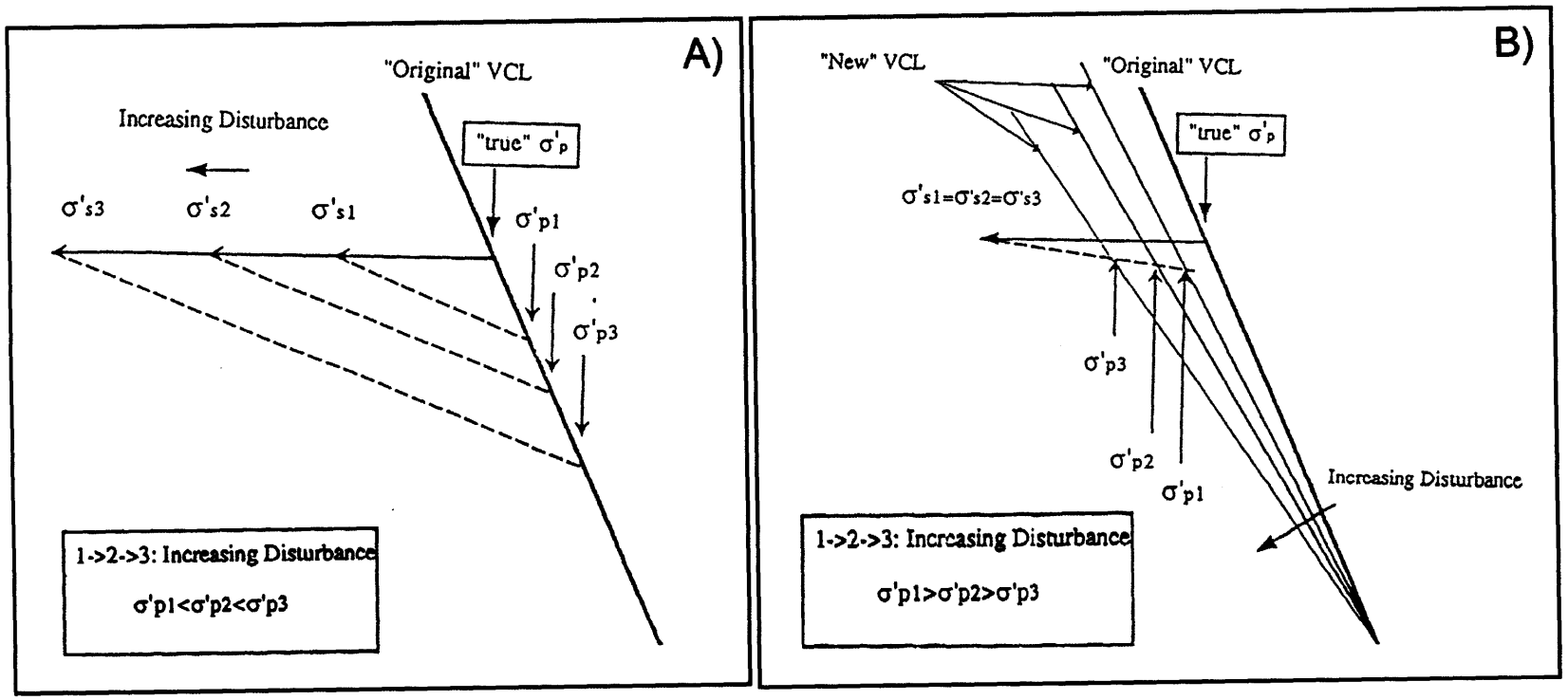

Figure 4.4: Simplified Model describing the effect of disturbance at preconsolidation pressure (Santagata and Germaine, 2002).

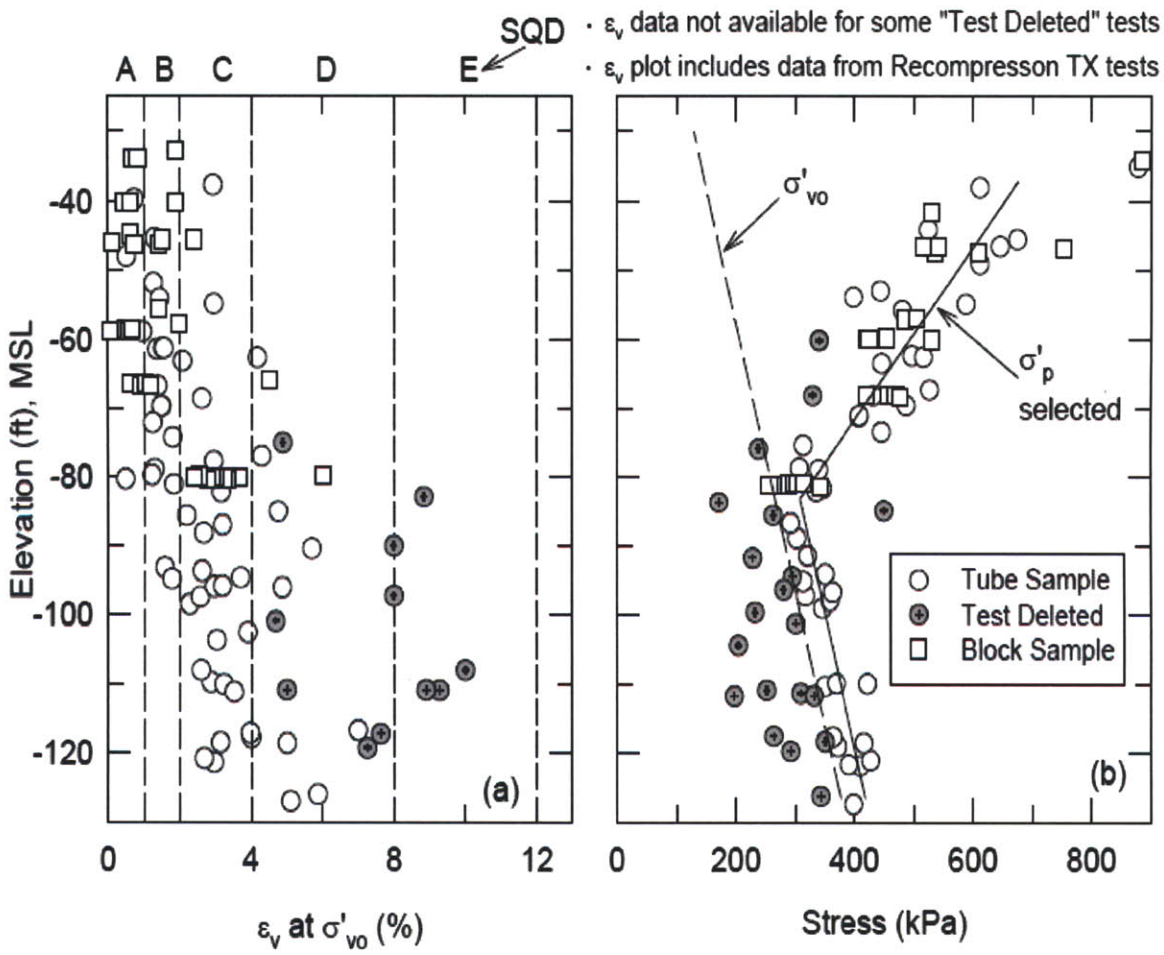

Figure 4.5: Comparison of SQD and Stress history versus depth; data of BBC from CA/T South Boston (after Ladd et al. 1999).

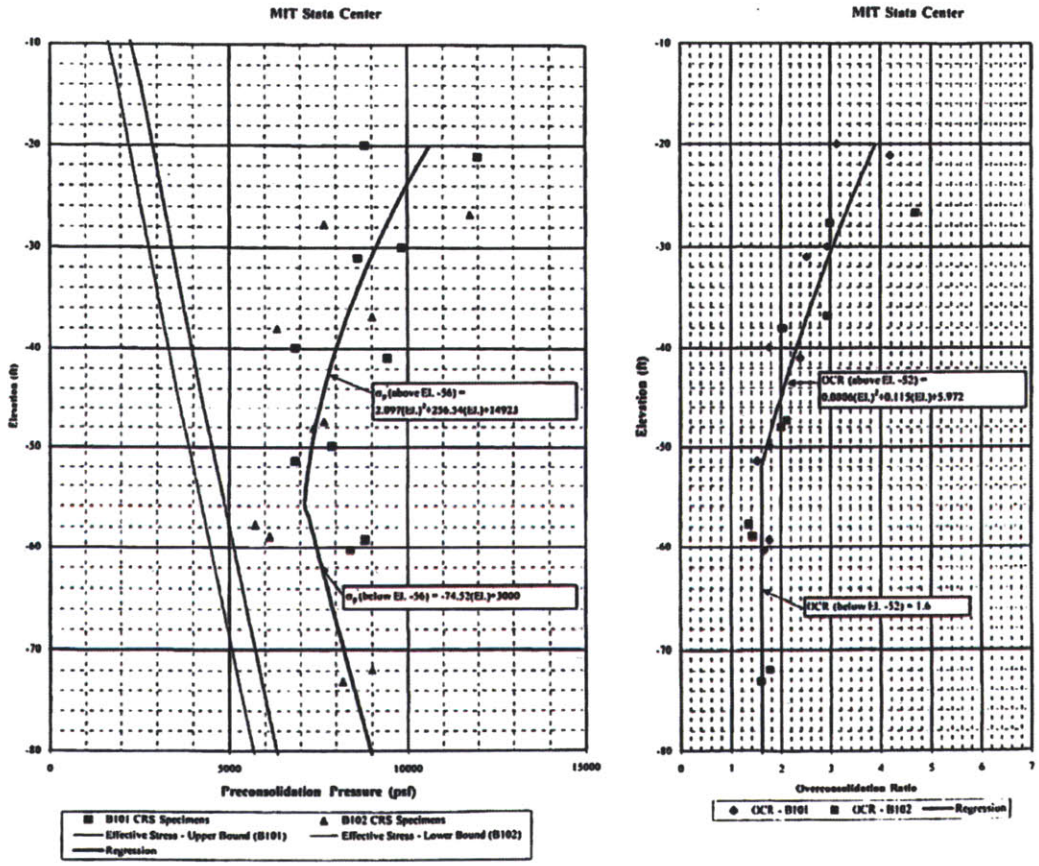

Figure 4.6: Stress history profile for BBC from the MIT Stata Center (Ladd Report, 2000).

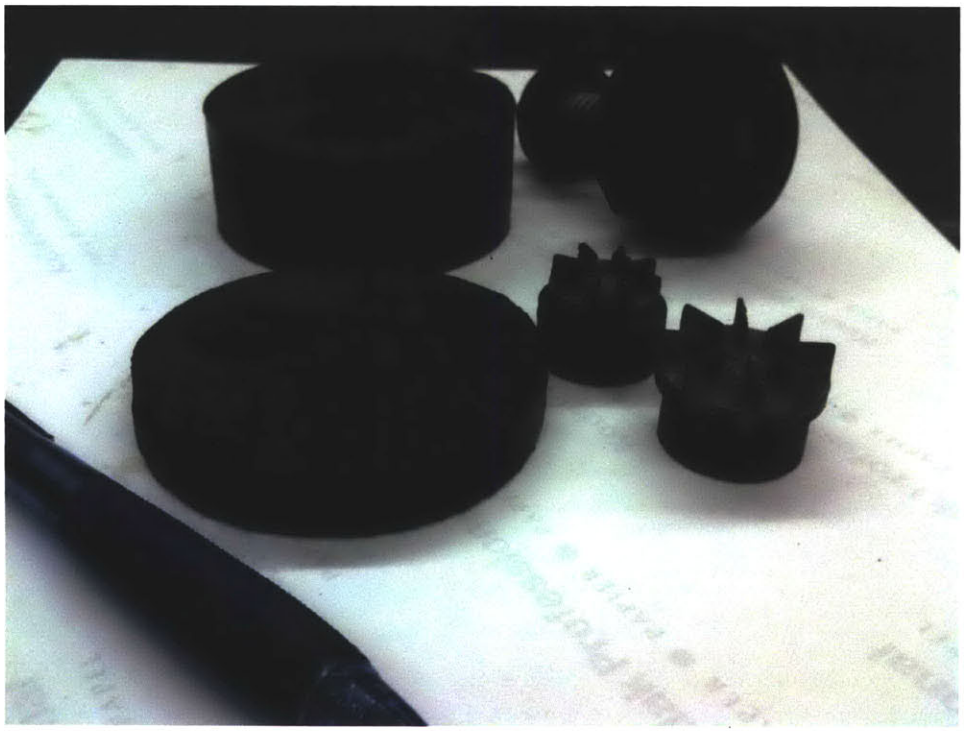

Figure 4.7: The Torvane testing device; using a small and medium vane on SFBM to estimate shear strength.

Figure 4.8: The pedestal and top cap with the rubber sleeves and rolled condom in place.

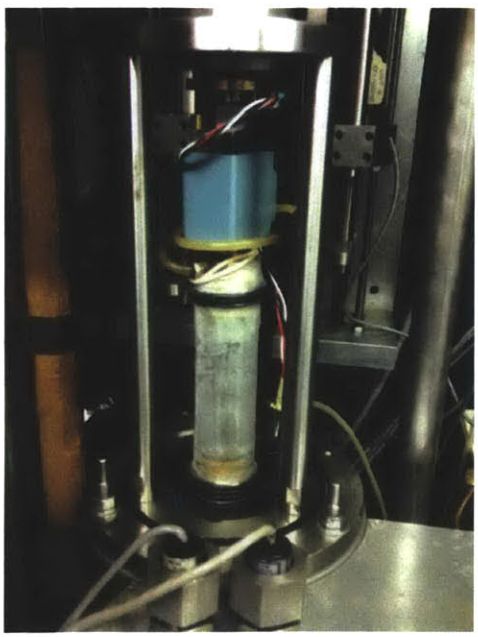

Figure 4.9: The specimen with the prophylactic membrane positioned to provide an impermeable barrier between the soil and the cell fluid.

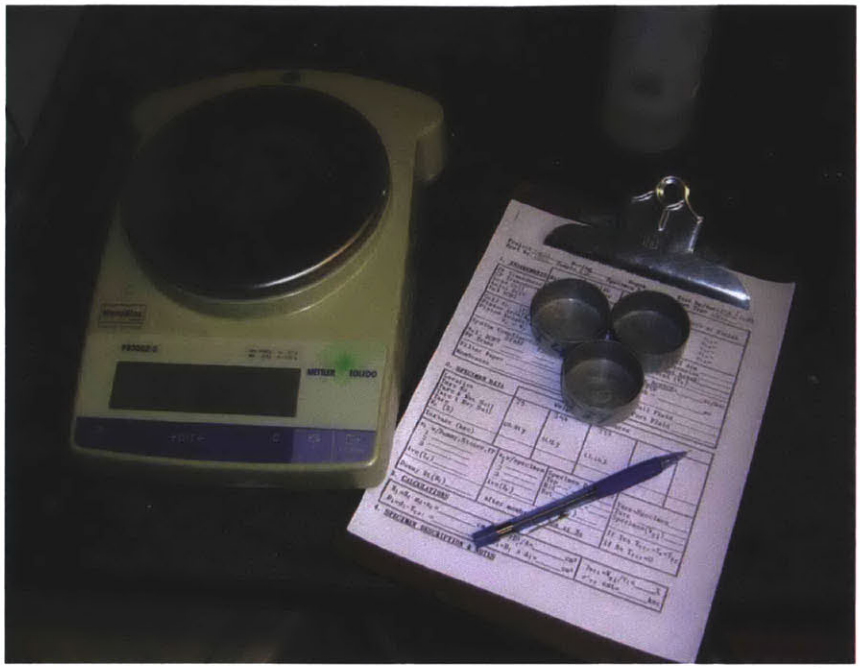

Figure 4.10: Preparation of Triaxial Testing; the spreadsheet, tares and scale to take mass measurements.

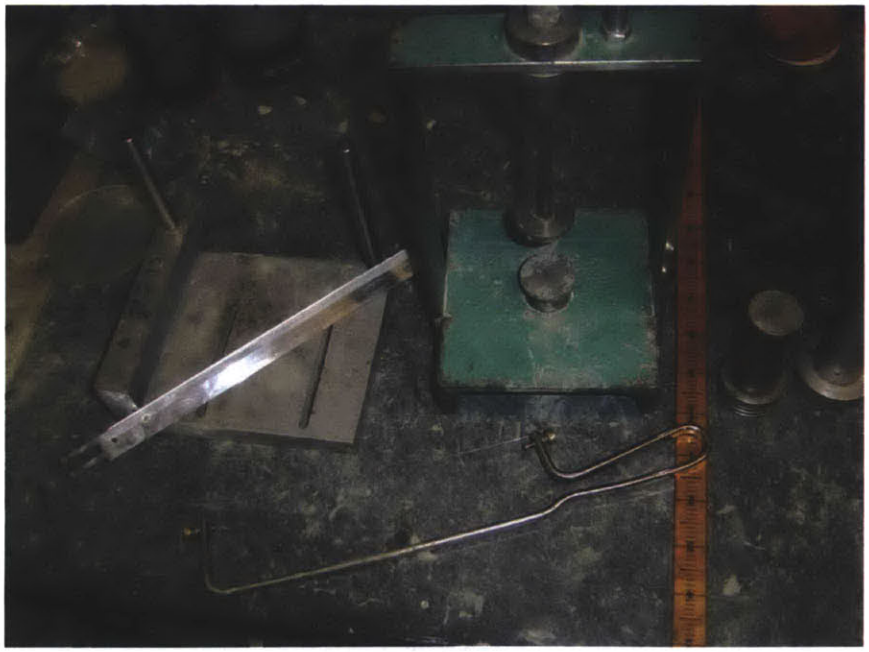

Figure 4.11: Typical MIT Lab bench before trimming; the miter box, the cylindrical (green) miter box, a wire saw and a blade.

Figure 4.12: Extrusion of the material from consolidometer and transfer to the first miter box.

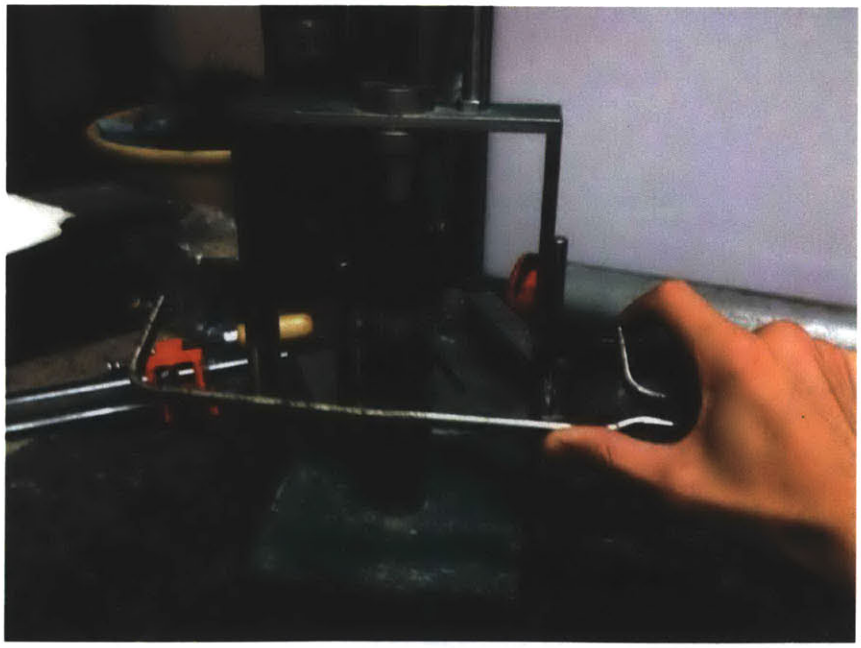

Figure 4.13: Trimming with a wire saw to the final diameter (specimen of RSFBM).

Figure 4.14: The use of a split mold to define the final height of the specimen.

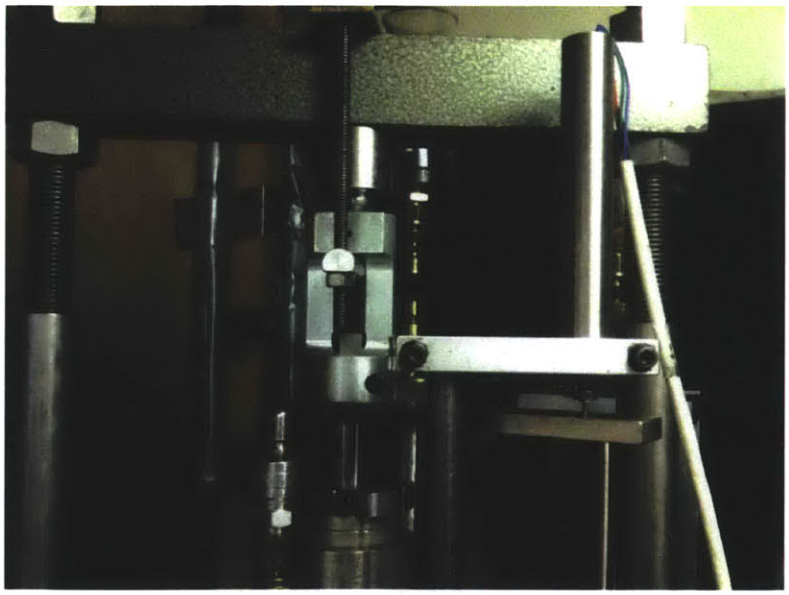

Figure 4.15: The upper components of the triaxial cell; loading frame, top assembly, piston, piston clamp, and the axial LVDT

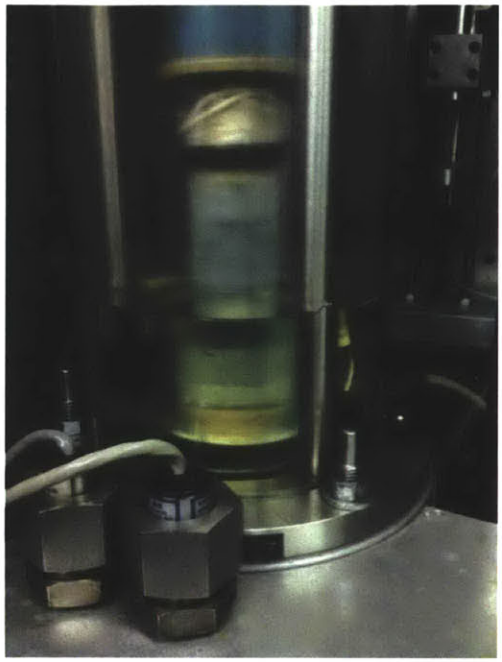

Figure 4.16: Recording cell zero value while filling up the cell to the middle of the specimen.

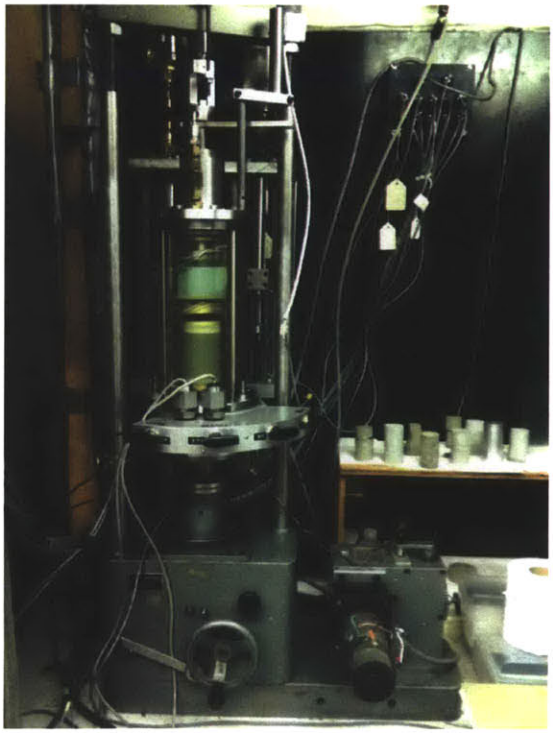

Figure 4.17: The low pressure triaxial cell fully assembled, with a specimen in place and the cell filled up.

Figure 4.18: The base of the high pressure triaxial apparatus resting on the mobile cart.

Figure 4.19: A specimen sealed with the two latex membranes with alignment frame holding top cap.

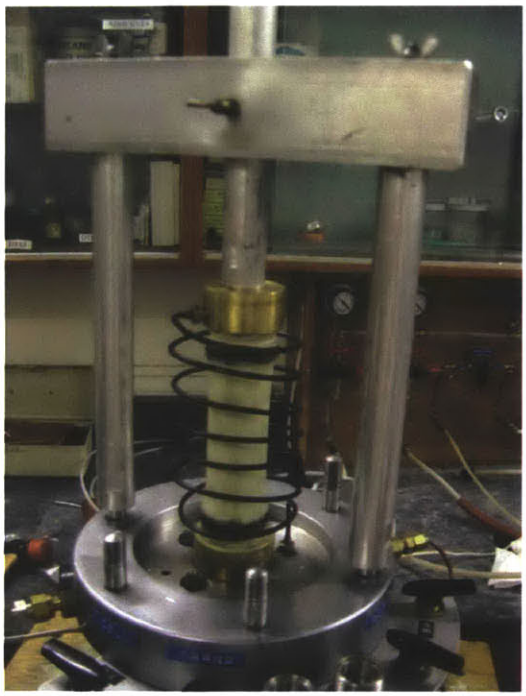

Figure 4.20: A specimen with the free top cap and the spiral top drainage line attached.

Figure 4.21: Transferring the high pressure apparatus inside the load frame using a wooden bridge.

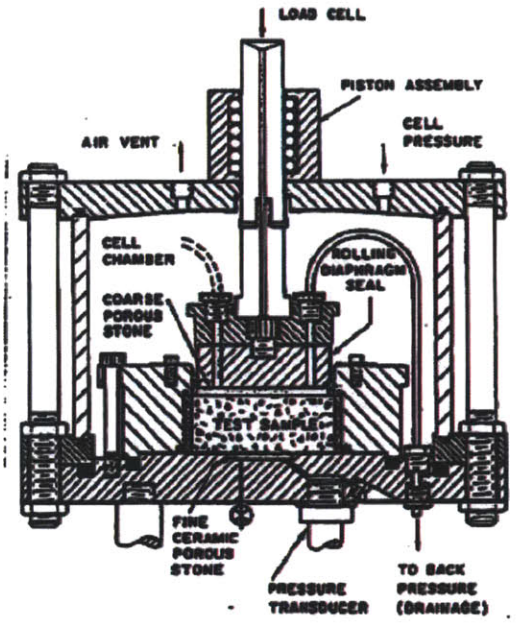

Figure 4.22: The MIT CRS apparatus (Wissa et al., 1971).

Figure 4.23: The miter box, cutting ring and spatula used for trimming the CRS specimen.

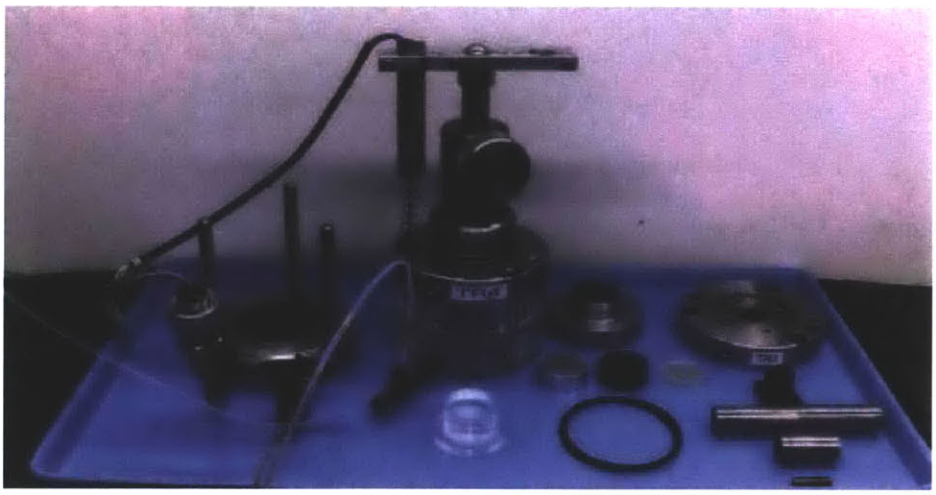

Figure 4.24: A typical MIT CRS chamber and its assembly.

Chapter 5 EXPERIMENTAL PROGRAM & INTERPRETATION METHODS

5.1 Introduction

The purpose of this experimental program is to better understand the mechanical behavior of San Francisco Bay Mud and to investigate the effects of disturbance on preconsolidation pressure for normally consolidated (NC) and low overconsolidated (OCR) samples. All tests performed for this study were run using the automated triaxial equipment developed at MIT and described on section 3.4. Some of the results will be compared with previous work that has already been done on sample disturbance from Santagata and Germaine, 1994 using Boston Blue Clay.

An extensive K_0 consolidation triaxial testing program (CK_0UC) is first applied on NC SFBM tube samples. Previous research programs and tests on SFBM have shown that, within a certain range of stresses, SFBM exhibits normalized behavior. This means that when it is consolidated well above the Preconsolidation Pressure and into the Virgin Compression Line (VCL) the effects of disturbance are entirely removed. The behavior of the soil in such state (consolidated to a stress well beyond the preconsolidation pressure) can be considered representative of the intact behavior of SFBM. Information for the "in situ" compression ratio CR or the lateral stress coefficient K_0, can be derived from the last portion of the compression curves and when well into the VCL. Shear properties can be derived from the initial compression phase of disturbance simulation (undrained strength).

Section 5.2 presents an overview of the research program and the phase relation calculations for the intact and resedimented material used. Section 5.3 analyzes the K_0 consolidation Constant Rate of Strain tests performed on SFBM. These tests will serve as a guideline to establish the strain - stress level trends and overall behavior of SFBM. For the resedimented material, two CRS tests, one on a low pressure CRS apparatus and one at a high pressure apparatus are analyzed. Section 5.4.1 introduces the analysis of a typical triaxial test with multiple disturbance simulation phases. The compression behavior of a NC SFBM specimen is analyzed. The section states how the preconsolidation pressure σ'_p, lateral stress ratio K_0, compression and recompression ratio calculations were carried out. The disturbance

simulation results for NC SFBM are reviewed. Section 5.4.2 analyzes the compression behavior of NC SFBM over a wider range of stresses and in the high pressure MIT apparatus. Consolidation and disturbance simulation results are compared with those of the low pressure triaxial cells. Stress dependencies become obvious on many consolidation parameters. Section 5.4.3 presents results from overconsolidated RSFBM specimens. The K_0 consolidation behavior and the disturbance simulation results for typical OC RSFBM specimens are reviewed. The effects of OCR on disturbance simulation effects and other consolidation parameters are analyzed. For a large portion of this research program, disturbance is simulated with respect to the ISA method (Baligh et al. 1987). This method accounts for the disturbance that an element, sitting on the centerline of the sampling tube, will undergo. In section 5.5, a new methodology is proposed in order to be able to account for the excess shearing and the volumetric change that are imposed on an element sitting beyond the centerline of the tube during sampling. This is done by allowing for some swelling to occur after ISA phase. The results of this combined disturbance are discussed. Section 5.6 presents the effective stress paths of the NC, OC and account for an element outside the center line of the sampling tube/swelling (ΔV) typical tests in the MIT p', q space. The different disturbance paths, as well as the differences in failure mode, are analyzed. Results are compared with previous work of Santagata and Germaine (1994) on BBC. At last, section 5.7 introduces the modified compression and recompression indices*. These indices are proposed to better capture the changes at the shape of the compression curve during extensive disturbance.

5.2 General Review of Tests and phase relation

For the core of this program, low pressure standard MIT automated triaxial cells were used to K_0-consolidate San Francisco Bay Mud specimens. Intact specimens and resedimented material was tested. Testing procedures are described in detail in Chapter 3. For resedimentation, the specimen is always loaded in the consolidometer to a maximum stress of 1 ksc and maintained at this stress for about 36 hours before being unloaded to an OCR of 4. In practice, however, the stress applied using dead weight can be slightly different. Also, the maximum stress might be maintained for a longer period of time. Bearing in mind the material's

compressibility and organic content, it was observed that the two above parameters resulted in specimens with slightly different preconsolidation pressure values. This would also justify at some extent the variability observed on the initial void ratio for the different specimens.

The main part of this research program consists of a total of 45 triaxial tests. Summary table 5.1 presents all triaxial tests performed on tube samples of SFBM and before creating a homogeneous batch of soil. Table 5.2 presents all the tests performed on the resedimented batch of SFBM that was created to identify more efficiently the effects of disturbance, leaving out non-uniformities or irregularities of tube samples. Three triaxial tests were also performed using the modified high pressure MIT apparatus. These tests highlight the effect of stress level, and low void ratio, on the ISA disturbance simulation. For these tests, specimens were initially 1-D consolidated to 20 ksc and then unloaded to an OCR of 4.

Table 5.3 consists of the phase relationship calculations for all the tube specimens of SFBM used for this research. The table presents the initial water content (w_c %), the initial void ratio (e_0), the initial degree of saturation, the wet and dry density and the height of solids. For these intact SFBM specimens, an average initial water content of $w_c = 31.36\%$ and an initial void ratio of $e_0 = 0.89$ is observed. Table 5.4 presents the resedimented specimens tested from intact tube samples. For the resedimented material, the average initial water content is about $w_c = 52.74\%$ and the initial void ratio is $e_0 = 1.52$. The high standard deviation that is observed in these tests (SD = ±5.22% for w_c and, SD = ±0.13 for e_0) is attributed to the fact that, during this phase, the resedimentation procedures for San Francisco Bay Mud were calibrated. A couple of resedimentation techniques were better refined during these initial triaxial tests (for example, how to better mix the slurry, how to efficiently de-air the soil after mixing and how to avoid trapping air bubbles during the relocation of the slurry into the consolidometer).

Table 5.5 and 5.6 present the phase relation calculations for the resedimented material of SFBM created using a homogeneous batch of soil. The main phase of testing was conducted based on this homogeneous batch of soil. The specimens tested in the low pressure apparatus were initially consolidated to 1 ksc and are summarized on table 5.5. Their initial water content is calculated to be $w_c = 53.94\%$ with a standard deviation of SD = 1.91%. Their initial void ratio is calculated to $e_0 = 1.53$ with a SD of 0.04. The standard deviation from this core testing phase is significantly lower than for individual tube specimens in table 5.4. This is a result of the nature

of the material used among these later tests; it is completely homogeneous, while the resedimentation and consolidation techniques are, to a great extent, standardized and refined.

Table 5.6 shows the phase relation calculations for test specimens prepared for the new modified high pressure triaxial apparatus. All specimens prepared to be tested in the high pressure apparatus were incrementally consolidated to 10 ksc and then unloaded to an OCR of 4. For these three tests presented here, an average initial water content of w_c = 36.77% and an initial void ratio of e_0 = 1.04 are calculated.

5.3 Constant Rate of Strain Tests

Constant rate of strain (CRS) tests were performed as the first step of this research program in order to establish the overall K_0 consolidation intact behavior and stress level trends of San Francisco Bay Mud. These results will be later used as a baseline in order to compare results from triaxial tests.

CRS Tests were conducted in the MIT low pressure and high pressure Constant Rate of Strain systems. The experimental test results of two typical tests for the resedimented SFBM batch can be seen in figure 5.1 and 5.2. The first figure shows the compression behavior in a void ratio – log stress (e-log σ'_v) space and the second figure shows the compression behavior in a vertical strain – log stress (ε_a-log σ'_v) space. CRS 1133 corresponds to the low pressure cell and CRS 1148 corresponds to the high pressure cell. Good repeatability in the behavior of RSFBM is obvious. The initial void ratio e_0 for both tests is around 1.53 while their stress history is almost the same. CRS 1133 was monotonically consolidated to a stress well beyond the preconsolidation pressure, at about 10.5 ksc stress, and then unloaded to a high OCR. On the other hand, CRS 1148 includes two unload – reload circles on predefined stress levels, and it is consolidated to a much higher stress. All RSFBM specimens were loaded well into the VCL to about 2.5 or more times the preconsolidation pressure (in accordance with SHANSEP) and at a constant rate of 5%/hour. To unload to a specific OCR a rate of -5%/hour is applied. The shape of these compression curves from the two tests, and their compression and recompression coefficients, will later be compared with the compression and recompression coefficients from the triaxial testing program.

The two compression curves change drastically between the pre-yield and post-yield region of the compression curve allowing for a good estimation of the preconsolidation pressure, σ'_p. The same distinct change in the compression behavior is observed for the unload–reloaded circles and the overconsolidated and normally consolidated region of the recompression curve. The preconsolidation value for the initial compression curves is slightly higher (about 1.2 ksc) than this observed from triaxial data. This difference can be attributed to the fact that the CRS specimens were normally cut off from the specimens prepared for the triaxial tests, stored for a few days or weeks, and then tested. For storing purposes, specimens were sealed in a double ziplok bag with a humid paper towel in between. The whole package was stored in a protected, insulated container with a constant moisture source. The container and the specimens are located inside a temperature controlled MIT lab.

San Francisco Bay Mud is also sensitive to strain rates effects. For this research program, a minimum rate of 0.15%/hour was imposed for the consolidation of triaxial tests. This appears to be the minimum rate in order not to allow any secondary compression to interfere with the test. Low strain rate will also result in a relatively low but distinct excess pore pressure. On SFBM specimens, a shift on the VCL slope was noted with increasing consolidation rate after Korchaiyapruk and Germaine, 2007 (figure 5.3). This strong strain rate dependency might explain some of the differences noted on VCL between the CRS and the triaxial tests.

The recompression index, C_r, the swelling index, C_s, and the compression index, C_c, are also noted on the compression behavior figures, 5.1, 5.2. The recompression index, C_r, is the slope defined from the unload – reload loop. The swelling index, C_s, is defined from the unloading to a low OCR at the end of each test, while the compression index, C_c is defined from the slope of VCL.

In order to get a clear notion on how these indices are changing, when moving along the strain-stress (ε_a-log σ'_v) or void ratio-stress (e-log σ'_v) compression curves for RSFBM, the slopes of the two curves are plotted versus stress level for different test phases (unload, reload, VCL consolidation). Figure 5.4 presents the calculated slope of all K_0 consolidation compression curves for the two tests mentioned above (CRS 1133, CRS 1148). The coefficient of compressibility, C_c, is calculated as the slope of the compression curve in an e-log σ'_v space, and

when the specimen is consolidated well into the VCL slope (in the figure, these would be only the data points that define the fit line):

$$C_c = \frac{\Delta e}{\Delta\{log_{10}(\sigma_v')\}}$$

As it can be seen in figure 5.4, for RSFBM the compression index depends upon stress level. For stress level of 1 ksc, C_c is about 0.6 and reduces with increasing stress to 0.4 for stresses of about 100 ksc (dotted line). The blue-color data points correspond to the low pressure MIT CRS 1133 test while the black data correspond to the high pressure CRS 1148 test.

Figure 5.5 shows the recompression (C_r) and swelling index (C_s) versus the vertical effective stress. Although these indices tend to be calculated over a wider range of stress (for example, the recompression index should normally be calculated as the slope of the total unload - reload loop), the first derivative is used in this case in order to observe how the slope of unload – reload curves changes with stress. Results for the recompression index (C_r) indicate that it starts from about 0.01 – 0.02 and increases with stress up to around 0.12 - 0.15 as the specimen moves towards its yielding point; dotted lines (the preconsolidation pressure).

The swelling index (C_s) follows a different trend; now the curve starts from high stresses to lower stresses. At the beginning, it slightly increases up to 0.06 – 0.08 depending on the stress level and then decreases with increasing the vertical effective stress to about 0.02. These first estimates on the compression indexes, C_c, C_r and C_s, will be used in chapter 6 in order to compare the calculated slopes from triaxial tests for different disturbance simulation amplitudes.

Figure 5.6 shows the relationship between the vertical hydraulic conductivity (k_v) and the void ratio for the low and high pressure CRS apparatus. The hydraulic conductivity, k_v (cm/sec) decreases with decreasing void ratio and as the vertical consolidation stress increases. At void ratio e = 1.5, the hydraulic conductivity is about $1\times E^{-7}$ (σ'_v = 0.23 ksc) and for a void ratio e = 0.9 decreases to about $1\times E^{-9}$ (σ'_v = 13.5 ksc) following a bi-linear behavior (CRS 1133, low pressure apparatus). Respectively, for the high pressure CRS test 1148 hydraulic conductivity starts from the same point and reduces to about $1\times E^{-10}$ for a void ratio e = 0.4 at about σ'_v = 200 ksc. For the high pressure data points (CRS 1148), a jump presented on the relationship of void

ratios e = 0.82 and e = 0.35 is due to the unload - reload circle that were imposed. It must also be mentioned that the data from the low and high pressure apparatus are in strong agreement with other CRS tests performed on the same material.

Figure 5.7 presents the change in the vertical coefficient of consolidation (c_v) versus stress level from the low and high pressure CRS tests mentioned above. In general, the coefficient of consolidation decreases with vertical effective stress. This decrease is much more apparent in the recompression part of the consolidation curve and up until the preconsolidation pressure where it drops sharply. Then, the coefficient of consolidation, c_v, value increases within the normally consolidation region, and as the specimen consolidates well into the virgin compression line; test CRS 1133 and 1148 after the first unload - reload circle, for stress levels σ'_v = 0.25 to 13.5. On higher consolidation stresses, the coefficient of consolidation, c_v value, seems to continuously reduce with increasing consolidation stress; test 1148, for stress levels σ'_v = 13.5 to 400.

5.4 Triaxial Testing

For the majority of the triaxial tests performed during this research program, two low pressure triaxial cells were used; MIT03 and MIT04. Instrumentation characteristics for the two cells are presented in tables 4.1 and 4.2. A summary of the compression curves for the triaxial tests performed on each apparatus for the homogeneous batch of SFBM is presented at figure 5.8. Data for MIT03 are plotted on the left figure at a void ratio – log (stress) scale. Data for MIT04 are plotted on the right. Data were plotted on void ratio e – log stress σ'_{vc} scale in order to be able to compare them and normalize everything to a unique VCL. The lateral stress ratio, K_0 for this series of tests versus stress level for MIT 03 and MIT04 are plotted at figure 5.9. From these summary figures, the lateral stress ratio for the RSFBM batch was found to be at a range of K_0 = 0.39 - 0.48. The summary plots at these two figures, 5.8 and 5.9 served in many cases as a verification of set up's or test's good quality. A test varying a lot from these VCL slopes or K_0 values, especially when using resedimented material and maintaining proper repeatability at test procedures was excluded as a fault test.

It must be mentioned that, between the two cells, some small differences in stress – strain behavior were noticed. In general MIT03 was found to produce slightly steeper VCL slopes, giving more strains for the same stress level. However, this can be attributed to the fact that controllers of the cell and pore pressure at this apparatus were a bit more unstable, often resulting in a small isolation back and forth of the motors and thus producing more strains. This irregularity of the apparatus can also be noticed as many of the tests for MIT03 do not lie exactly on the general VCL (blue line). On the other hand, MIT04 produced much more systematic results and fewer problems during the set-up or the testing. Thus, the latter was preferred for testing the majority of the more complex triaxial tests.

The consolidation results of a typical triaxial test, for a resedimented specimen of SFBM, are presented at figure 5.10. The figure shows the decrease of void ratio (e) versus the imposed vertical effective stress, σ'_{vc}. By plotting the consolidation test results in this space, results from different consolidation tests can be directly associated. To do that we normalize most engineering values to the vertical consolidation stress. The typical triaxial test presented here has the following phases:

- Initial consolidation phase, C1
- Disturbance simulation, S1
- Recompression phase, C2
- 2nd disturbance phase, S2
- Recompression phase, C3
- 3rd disturbance phase or
  undrained shear to failure

5.4.1.a Compression behavior and Preconsolidation Pressure on NC SFBM

During the initial phase of the TX test, the K_0 consolidation phase (C_1), the specimen is loaded to a maximum effective stress, σ'_{vcm} of 1.5 to 2.5 times the previous maximum consolidation stress. Once the maximum stress has been reached the specimen is left for 12 to 24 hours of secondary compression. For the initial consolidation phase, this would be 1.5 to 2.5 times the 1 ksc that the specimen was consolidated to, during resedimentation. This will ensure that our specimen is consolidated well into the Virgin Compression Line (VCL) and according with SHANSEP reconsolidation technique experience normalized behavior. An axial strain rate, ε_α, of 0.15%/hour was used for all three consolidation phases of the test. For this specific test, TX 878, a preconsolidation pressure $\sigma'_{p,}$ value of 0.68 ksc is observed. This low preconsolidation pressure value is attributable to several accumulative factors; the actual consolidation stress imposed at the consolidometer during resedimentation of specimen is lower than that calculated (different combinations of free weights are used during this process), the sample is not left for an adequate time (3 to 4 days) on maximum load to go to secondary compression, some built up side wall friction on the consolidometer might also play a role in the low preconsolidation pressure value observed (although lubrication was used in the consolidometer inner wall before the set up).

Figure 5.11 describes the lateral stress ratio, K_0, variation during the three consolidation phases for increasing stress. It can be seen that, as consolidation progresses, K_0 decreases towards a minimum value and as the soil passes the preconsolidation pressure and moves well into the VCL portion of the curve. The initial K_0 value for all phases is about 1 since the state of stresses is isotropic before each consolidation phase. This value decreases to a minimum of around 0.39 for C_1 consolidation and slightly increases with stress as the specimen is consolidated well into the VCL slope. For each recompression phase, a hold stress period of about 12 to 24 is imposed where K_0 remains constant as the imposed stresses do not change. This value of K_0 corresponding to the VCL state is referred to as the normally consolidated value $K_{0(NC)}$.

Lateral Stress Ratio, K_0, for RSFBM was observed to be consistent and ranging from 0.39 to 0.48 for all the tests performed for this research program. The equivalent K_0 value for resedimented Boston Blue Clay (RBBC) is a bit higher and about 0.44 to 0.52 (Abdulhadi and

Germaine, 2009). As it is consistently verified in the present study and from Abdulhadi and Germaine (2009), there is a constant increase on lateral stress ratio during K_0-consolidation with increasing the vertical consolidation stress. So for every recompression phase across all tests performed the K_0 value is observed to be slightly higher than for the previous consolidation phase. For this research program, the $K_{0\,(NC)}$ is reported as the average value of lateral stress ratio K measured during the 12 to 24 hours of hold stress phase and secondary compression, just after each consolidation phase. This was done for all compression and recompression phases in all tests for several reasons; to make sure that the specimen is consolidated well into the VCL and all the effects of previous disturbance have been erased, to investigate how the lateral stress ratio (K_0) changes with progressing destructuring of the soil and stress level, and to investigate how these changes affect the undrained strength and the disturbance mode during shearing.

As mentioned above, some significant scatter in the measured values of $K_{0\,(NC)}$ was observed, even for the resedimented SFBM batch used. This variation can be justified to some extent from the variation in the initial water content and initial void ratio values determined for the different specimens. Increasing stress seems also to influence the measured K_0 to some extent and a clear relationship between K_0 and stress level was established. The stress level dependences will be summarized and presented on Chapter 6.

For defining the preconsolidation pressure, σ'_p, at every consolidation phase, the Strain Energy approach is adopted (after Becker et al. 1987). The total work per unit volume is plotted versus the vertical effective stress (Figure 5.12 for C_1 consolidation phase). The total work applied to the specimen can be calculated as:

$$\text{Work} = \Sigma\left[\left(\frac{\sigma_i - \sigma_{i+1}}{2}\right)\cdot \ln\left(\frac{1-\varepsilon_{i+1}}{1-\varepsilon_i}\right)\right]$$

In this graph, two fitted linear portions of data are defined. The first, pre-yield portion corresponds to the initial loading of the compression phase where the specimen is supposed to act as more of an elastic material (red fitted line on figure 5.12). The second linear portion of the compression curve corresponds to the virgin compression line (VCL) where the soil has a constant, more plastic behavior (blue fitted line). Much of the deformation happening along the VCL is irreversible and consists of reorientation of particles, movement or sliding and less of the compression of the particles themselves or the double layering of the clay particles. Fitting the

two lines and finding their point of intersection, gives a point corresponding to the preconsolidation pressure value. Some curves, especially with increasing disturbance, appear to be more rounded but for most cases, they exhibit a clear break between the pre – yield and post – yield behavior. This allows determination of the preconsolidation pressure using the Strain Energy method with confidence.

It must be noted that, across all tests in this research, the VCL fitted line was uniquely defined without much subjective judgment involved. However, for normally consolidated samples and in cases where large disturbance amplitudes were imposed, it was not possible to define a unique VCL for all three consolidation phases. This was attributed to the fact that large disturbance amplitudes tend to significantly alter the soil structure. In the example of triaxial test TX 878, figure 5.10, a unique VCL can be defined throughout the whole range of the increasing vertical effective stress. The imposed disturbance simulation of 0.5% strain was not significant to notably change the compressibility of the soil on the post-preconsolidation pressure region, for the three consolidation steps. This can also be expressed by the small change in the compression behavior for the three consolidation phases (compression index, $C_c = CR \cdot (1 + e_0)$. Observed values were within the limits observed on the CRS tests (for low stress level):

$C_{c1} = 0.5123$,
$C_{c2} = 0.5410$,
$C_{c3} = 0.5549$.

On the other hand, the linear fit for the initial, pre – preconsolidation pressure portion of the consolidation curve cannot be objectively defined (red fitted line). For most specimens, three lines were determined: a minimum fitted line corresponding to an almost horizontal line, and a line with a maximum possible fitted slope. A final fit for this initial portion of the consolidation curve is defined as the line bisecting the angle created from maximum and minimum slopes. The consolidation data and their fitted lines were plotted both in work – stress space and void ratio – log (stress) space to check for consistency (figure 5.13). This was mainly done as it is commonly known that by just using only linear stress space, the Strain Energy method (Baligh et al. 1987) tends to somewhat overestimate the value of preconsolidation pressure (Boone, 2010). Using a minimum and maximum slope for the fitted line on the initial portion of the consolidation curve,

would result in the calculation of a minimum and maximum value of preconsolidation pressure. For the majority of the tests, this range was of the order of ± 10% or less and it is in agreement with previous observations on Boston Blue Clay (Santagata and Germaine, 1994). The Casagrande construction method (1963) is also employed in some cases to verify the Strain Energy Approach (figure 5.14).

The data points used for the fitted lines in both cases are actual raw data (no curve fitting was used to smooth the data for the consolidation curves). Because of this, keeping a sufficient number of data for every linear fit was also a concern. For RSFBM specimens, the initial linear fit line of the consolidation curve, in most cases, is calculated from about 50 data points, while the VCL slope used about 150 or more. Bearing in mind that for the consolidation phase, data are recorded every 3 minutes means that the initial slope was calculated from about 2.5 hours of consolidation data, while the VCL slope was calculated from about 8 hours or more of consolidation data.

It is widely accepted that increasing disturbance leads to more rounded compression curve. This will have a profound effect on the estimation of the recompression index and will make the determination of the preconsolidation pressure more difficult. For small disturbance simulation amplitudes, as in test TX 878, the error in estimating the preconsolidation pressure was about 2%. This is expected to increase by increasing disturbance. Using the Strain Energy approach, the fitted line with the minimum slope would give a minimum value of preconsolidation pressure of $\sigma'_p = 0.693$, and the fitted line with the maximum slope would give a maximum value of $\sigma'_p = 0.732$. Using the same set of data on the void ratio e – log (stress) space would give three estimates for the recompression index C_r. For most tests on this research program only the best estimate of recompression index ratio C_r is reported. For TX 878, the recompression indices for the three compression phases were found to be (where again $C_r = RR/(1+e_0)$):

$C_{r1} = 0.0168$,

$C_{r2} = 0.0183$,

$C_{r3} = 0.0179$.

These recompression coefficients agree with the limits found from the CRS tests, for low and high pressure cells, presented earlier for the RSFBM specimens.

5.4.1.b Disturbance Simulation on NC SFBM

Disturbance simulation for the present research program is simulated using the Ideal Sample Approach (ISA), as was proposed by Baligh et al. (1987). ISA simulates the penetration of the tube sampler in the soil mass and the extrusion of the soil from the tube. On the other hand, Perfect Sample Approach (PSA), that was proposed a few decades earlier after Ladd and Lambe (1963), simulates only the release of the in situ shear stress which occurs when the soil is transferred from the anisotropic in situ state of stress to the isotropic state after tube extrusion and when it sits to the lab bench ready to be tested. Figure 5.15 is an example of the stress strain curves of disturbance simulations during PSA and ISA simulation on NC resedimented BBC (after Santagata and Germaine, 1994).

The ISA effects of disturbance can be simulated in a triaxial cell and has 4 distinct parts. The soil element is initially sheared in compression up to a maximum strain, ε_{max}. This strain corresponds to the geometry of the sampling tube B/t; where B is the diameter of the sampling tube and t is the wall thickness (figure 5.16). For example, a ratio B/t = 20 corresponds to a typical sampler and the maximum strain would be around ε_{max} = 2%. In figure 5.17 the initial compression phase corresponds to points 1 – 2. The second phase, points 2 – 3 correspond to shear in extension that the soil element undergoes as it moves near to the sampler. At this undrained extension phase, the specimens are unloaded to a strain of - ε_{max}. Finally, as the sampler progresses, the soil element is subjected again to compression when seated well inside the tube. This phase is represented in the lab by an undrained compression phase back to zero axial strain, ε = 0% (path points 3 – 4). Finally, to account for the release of stress when sample is extruded from the tube, the specimen is unloaded to zero axial stress (path points 4 – 5).

In figure 5.17 the ISA disturbance phases after the first consolidation, and after the recompression phases are plotted, S_1, S_2, S_3. The data are for ISA+0.5% on a SFBM tube specimen. A small difference can be clearly noted at maximum stress for the three different disturbances. S_1 disturbance that took place first and at lower consolidation stress level had the

higher undrained strength. S_3 disturbance that took place at the end of the experiment and at higher consolidation stress level had the lower undrained strength. It should be noted that the shear stress values, q, on the plot are normalized to the maximum vertical effective consolidation stress, σ'_{vc}.

Figure 5.18 presents the ISA disturbance for NC RSFBM specimens of increasing amplitudes (after Baligh et al. 1987). The axial strain ε_a (%) is plotted versus the normalized shear stress, q/σ'_{vcm}. The disturbance amplitude or axial strain increases from 0.5% for TX 878 to up to 4.5% strain for TX 977. The maximum shear stress across most of the disturbance simulations is reached by about 0.3% axial strain. There also seems to be a variation in the maximum shear stress, but this can be attributed to the difference in stress level among the test. Normally for a large disturbance simulation circle we need to consolidate the specimen to a higher stress. So, on this figure the increase of the disturbance amplitude, causes the maximum shear strength to decrease due to the stress level effect. It should also be noted that after the disturbance steps 1 – 2, 2 – 3 and 3 – 4, the remaining shear stress on the specimen decreases with increasing disturbance. This means that, for larger disturbance amplitudes, less unloading will have to take place to bring the specimen back to hydrostatic position.

5.4.2.a Compression behavior and Preconsolidation Pressure on NC SFBM using the modified high pressure apparatus

In order to develop a broader understanding of the effect of ISA disturbance simulation over a wider range of stresses, the MIT high pressure triaxial cell was used. Modifications were required to incorporate extension capabilities and impose the Ideal Sample Approach. For this, a modified suction cap was designed and built. Results from two typical tests from the modified high pressure apparatus are presented in figures 5.19 and 5.20. Specimens to be tested in the high pressure apparatus were prior 1-D consolidated up to 10 ksc stress using a modified oedometer base – consolidometer and the MIT Terzaghi load frame with level arm loading system to apply the weight (chapter 3). Specimens were then unloaded to an OCR of 4.

Figure 5.19 presents the consolidation behavior of two typical tests (TX 1076 and TX 1088) in a log vertical effective stress – void ratio (e – log σ'_{vc}) space. Both tests have an initial

consolidation phase (C_1), a disturbance phase (S_1), and a final recompression phase (C_2). The initial void ratio for both tests is about $e_{0\ initial} = 1$. As the stress increases they both reach their preconsolidation pressure (yielding stress) at about 8 to 9 ksc, a value less than the 10 ksc that the specimens were initially consolidated at the modified oedometer base. The author believes that this is primarily attributed to the side friction developed during 1-D consolidation of the slurry (eventhough lubrication was used at the inside walls of the consolidometer), and secondary comes as a result of the difficulty to align the top cap with free weights at the initial consolidation steps. These two factors, coupled with small mistakes, i.e. at the imposed hanging loads or misjudging loading time, may alter the actual final consolidation stress of the resedimented specimen. In the initial consolidation phase, the specimen was consolidated well beyond the preconsolidation pressure (σ'_p) and at a maximum vertical effective stress of about 40 to 45 ksc to ensure that it is well into the VCL and all the previous effects of disturbance have been erased. As far as the vertical axial strain is concerned (figure 5.20), the first consolidation phase was up to about 12.5%. Consolidating to high stresses using the high pressure cell, had an obvious impact at the compressibility parameters of the soil, resulting in a flattening of the slope of VCL increasing the stress level. This behavior agrees with the change in VCL slope that was observed with stress level in the high pressure CRS tests performed.

In both triaxial tests presented in the figures above, a large disturbance simulation amplitude was imposed (3.5% and 4.5% axial strain). Then, a recompression phase is imposed again well beyond the preconsolidation pressure, and up to about 100 – 140 ksc vertical consolidation stress. The initial void ratio for this recompression phase is about $e_{0\ initial} = 0.74$ at about 8 ksc stress and the final void ratio is about $e_{final} = 0.54$. The final vertical axial strain for both tests is about 22%, which is near the maximum stroke of the high pressure MIT triaxial piston. The calculated preconsolidation pressure for the two tests was near the previous maximum effective stress from C_1, and was calculated to be at about 30 ksc for TX 1076 and about 33 ksc for TX 1088.

Figure 5.21 shows the change in lateral stress ratio, K_0 versus vertical effective stress for the different consolidation phases for TX 1076 and TX 1087. The trend, as before is the following; K_0 value initially decreases from a value around 1 and up to the preconsolidation pressure to a minimum, and then slightly increases as the specimen moves into the VCL. During consolidation onto the VCL, the lateral stress ratio, K_0 value, increases slightly with stress and

then remains constant during the overnight hold stress period. For the high pressure apparatus and for stress level from about 50 – 200 ksc, the lateral stress ratio is about 0.57. This value is much higher than the average K_0 value calculated in the low pressure triaxial apparatus that is of about 0.43 (for a vertical consolidation stress from 5 to 10 ksc). The noticed difference is an extension of the stress level trend that is noticed through the whole triaxial test program; the lateral stress ratio value, K_0, increases as the vertical consolidation stress increases (figure 6.6).

5.4.2.b Disturbance Simulation on NC SFBM using the high pressure triaxial apparatus

The high pressure MIT triaxial apparatus was modified during this research program to incorporate extension capability using a modified suction cap. Results from the NC RSFBM specimens for TX 1076 and TX 1087 can be seen in figure 5.22. The disturbance simulation axial strain, ε_a, is plotted versus the normalized shear stress, q/σ'_{vcm}. Results indicate that, at higher stresses, the soil experiences a more ductile response (close to the one seen by OC specimens); the peak shear stress is significantly lower and less apparent while the strain at maximum shear stress has also increased. The differences between the tests performed on the high pressure triaxial apparatus versus the low pressure triaxial cells can be more clearly reviewed in figure 5.23. There, in addition to TX 1076 and TX 1087 disturbance simulation, TX 901 and TX977 are plotted. These tests have exactly the same disturbance simulation amplitudes (3.5% and 4.5% axial strain) and are noted on the figure with dotted lines. The two low pressure triaxial tests present a more brittle response and greater softening at large strains (> 15%). It must be noted that for TX 1076, a smaller disturbance simulation circle was performed inside the larger disturbance amplitude of 3.5% strain that seems to have almost no effect on the following recompression curve, C_2.

5.4.3.a Compression behavior and Preconsolidation Pressure on OC SFBM

After running a series of tests on NC tube samples and Resedimented material of San Francisco Bay Mud (RSFBM), it was decided to test the effects of disturbance on mechanically overconsolidated specimens. A total of 18 triaxial tests were performed at a nominal OCR = 2 and an OCR = 4. From these tests, 11 were on the final resedimented batch (table 5.2). A typical test performed on OCR = 4 RSFBM is presented at figure 5.24. The figure shows the stress history of a specimen for triaxial test TX 942. The decrease in void ratio, e, is plotted versus the log of vertical effective stress, σ'_{vc}.

The test has the following discrete phases:

- Initial consolidation phase, C1
- Drained unload to an OCR of 4
- Disturbance simulation, S1
- Recompression phase, C2
- Drained unload to an OCR of 4
- 2nd disturbance phase, S2
- Recompression phase, C3

For a mechanically overconsolidated specimen, after every consolidation phase the specimen is unloaded to a specific OCR value using stress path consolidation and an unload strain rate of ε = - 0.15 %. To do this, a new lateral stress ratio for the overconsolidated targeted state, $K_{0\,(OC)}$, is defined using the normally consolidated lateral stress ratio, $K_{0\,(NC)}$ from the previous consolidation step. Defining $K_{0\,(OC)}$ then allows for calculation of the horizontal stress for the targeted OCR. The relationship used is the following:

$$K_{0\,(OC)} = K_{0\,(NC)} \cdot OCR^{n},$$

after Schmidt (1966), O'Neil (1985) and Sheahan (1991) recommendations. For RSFBM parameter n was assumed to be equal to 0.4 for all specimens. The computer then follows a straight stress path from NC condition to the targeted σ'_{vc} and $K_{0\,(OC)}$.

At the end of each consolidation phase, the test goes again on a 12 to 24 hours hold stress to allow for dissipation and equilibration of the excess pore pressure along the specimen. This increased the duration of most of these tests to up to two weeks time. On every compression curve, the initial sampling effective stress, σ'_s, the preconsolidation pressure, σ'_p, and the maximum vertical effective stress, σ'_{vc}, are defined. The maximum vertical effective stress, σ'_{vc}, is the average stress corresponding to the hold stress time (secondary compression) that the specimen is imposed. At the end of the secondary compression the void ratio, e_{final}, is calculated. Then based on this void ratio, the vertical effective stress corresponding to the VCL slope is calculated. This would be the maximum vertical effective stress, σ'_{vcm} (figure 6.1). This final maximum vertical effective stress, σ'_{vcm}, is the stress that is later used to normalize everything to the VCL, such as the preconsolidation pressure, strains and loss of effective stress. The undrained shear strength, q, is the only SFBM property throughout this research that is always normalized to the σ'_{vc} and not the interpreted maximum vertical effective stress, accounting also for secondary compression, σ'_{vcm}.

Mesri and Choi (1979, 1984) note that during secondary compression aging of clays, the preconsolidation increases. This time depended mechanical behavior during secondary compression includes particle rearrangements, natural formation and transformation of minerals, such as organic matters, induration and weathering. To account for this aging of the soil they proposed the following equation to compute the critical pressure resulting from secondary aging, σ'_{vc}:

$$\frac{\sigma'_{vc}}{\sigma'_{vi}} = \left[\frac{t}{t_p}\right]^{\frac{C_a/C_c}{1-C_r/C_c}}$$

where σ'_{vi} is the imposed effective stress at which secondary compression takes place, t_p is the time required to complete primary consolidation, t is the time required to complete secondary compression, C_r is the recompression index from σ'_{vi} to σ'_{vc}, C_c is the compression index, and C_a the secondary compressibility index.

Typical values for Organic clays and silts for C_a/C_c is 0.05, while for inorganic clays and silts is 0.04. For RSFBM a C_a/C_c of 0.05 was assumed since the material is 10% organic. A typical value for clays mentioned from Mesri is $C_r/C_c = 0.01$. The above relationship is used only in few triaxial tests on this research program and compared with the values of maximum vertical effective stress, σ'_{vcm}, that is calculated using linear extrapolation to the VCL slope. Results are presented in table 5.8. On the present triaxial testing program t_p is assumed to be the time till the end of secondary compression and creep during the 12 to 24 hours of hold stress; t is assumed to be the time till the end of K_0 consolidation phase, just before the hold stress period. For all calculations typical values of $C_a/C_c = 0.1$ and $C_r/C_c = 0.05$ are used. Results indicate that Mesri & Choi (1984) method to account for secondary compression gave values of σ'_{vcm} consistently lower than those proposed using the VCL extrapolation method of figure 6.1.

When unloading to a specific OCR like in figure 5.24, the maximum vertical effective stress for the mechanically overconsolidated case is defined as σ'_{vcu}. It must be pointed out that even though the magnitude of disturbance is much higher for TX 942 (than that of NC case in figure 5.10), the effects on this OCR of 4 specimen are much less apparent. In the triaxial example for TX 878 the disturbance simulation amplitude was 0.5% where here, at TX 942 was about 2.5% axial strain. However in this second case, the loss of effective stress ($\Delta\sigma'$) is significantly lower than that of NC specimen. Some destructuring and a difference in the VCL slope are also noticeable from the stress - strain history. The lateral stress ratio, K_0 is around 0.4 and within the calculated range for most tests. The typical trend of decreasing K_0 to a certain value up to preconsolidation pressure and then remaining constant, with a slight increase with consolidation stress, is accurate within low stress triaxial tests (figure 5.25).

5.4.3.b Disturbance Simulation on OC SFBM

Figure 5.26 presents the ISA disturbance for overconsolidated RSFBM specimens of increasing amplitudes. Axial strain, ε_a %, versus the normalized shear stress, q/σ'_{vcm}, is plotted for triaxial tests of increasing disturbance amplitude. TX 915 has a minimum ISA amplitude of 0.5% while TX 965 has a maximum ISA amplitude of 5%. The stress strain curves on OC specimens have some distinct differences compared to the NC specimens. The curves seem to increase monotonically up to the maximum axial strain. The behavior is much more ductile, and for most cases, the maximum shear strength is mobilized near the maximum axial strain. The maximum normalized shear strength for OCR = 4 specimens is around 1.2 compared to the NC specimens that had normalized shear strength of about 0.38. For low ISA disturbance amplitudes, as of test TX 915 (0.5% strain), only a fraction of this shear strength was activated. A decrease of the remaining load at 0% axial strain (end of disturbance strain cycle) of disturbance with increasing strain amplitude is observed on OC specimens as was the case for NC specimens. A small decrease in the peak value of the normalized shear stress, q/σ'_{vc}, is due to the consolidation stress effect; increasing the vertical consolidation stress, decreases the peak undrained shear stress.

To better understand the effect of overconsolidation ratio on the ISA disturbance simulation, the axial strain, ε_a %, versus the normalized shear stress, q/σ'_{vc}, is plotted for triaxial tests of the same ISA amplitude and different OCR. Figure 5.27 presents three tests of different OCR; TX 879 of OCR = 1, TX 976 of OCR = 2 and TX 916 of OCR = 4. All tests have an ISA strain of 1.5% and are sheared with a rate of 0.5%/hour. The effect of increasing OCR on the stress strain curves is obvious. The maximum normalized shear strength increases significantly with OCR. The strain needed to mobilize this maximum shear strength also increases with OCR. For NC specimens, there is an increase in stress up to a maximum value and then a strain softening. On the other hand, for OCR = 4 specimens, the stress increases monotonically up to the maximum imposed strain. For an OCR = 2 the behavior is intermediate. The shear strength is mobilized at a strain of about 1 to 1.5% and this value is maintained almost up to the maximum imposed strain. The strain softening is much less apparent than that of the NC specimens.

5.5 Account for Swelling

The Ideal Sample Approach (ISA), after Baligh et al. (1987), simulates sample disturbance in the triaxial cell accounting for two main factors. These are the loss in effective stress and the straining that a soil element resting on the center line of the tube undergoes during sampling. In the triaxial cell, this is simulated by an undrained cycle of shearing; shear the specimen in compression up to a certain strain ε_i %, reverse the motor and shear in extension up to a strain $-\varepsilon_i$%, shear back in compression so that the total disturbance straining comes back to zero, ε_{total} = 0%, and finally unload the specimen back to hydrostatic conditions (zero shear stress).

However, disturbance simulation when running a triaxial test is imposed on a large area of the tube sample rather than just on an element at the center line of the sampling tube. Additionally, even though there is some symmetry over the area of the specimen tested, excess shearing and redistribution of water during sampling can have a significant effect on the quality of the specimen. Bearing this in mind, one should also account for these volume changes when simulating disturbance in the lab. To better understand the redistribution of water inside the tube during sampling, a soil slice from a recent tube sample of SFBM was cut off. Water content measurements were taken radially in order to be able to drawn the water content, w_c(%), profile along the diameter of the tube (figure 5.28). It must be noted that the average water content, w_c (%), in the figure is hypothetical (the actual average value is not known).

During the time of transportation and storage, the pore pressure equilibrates and this results in the variation of water content inside the tube. These radial measurements were a first indication of how water content is redistributed during sampling. Near the edges of the sample tube where extensive shearing is expected, the water content is found to be much lower than that of the center of the tube. This in effect means that, during sampling, there are higher pore pressures close to the sample tube. The pore pressure increase is much more significant near the edges of the tube where extensive shearing is also present than that of the centerline of the tube. This will cause an expansion of the soil mass near the centerline and a contraction of soil near the edges. Thus, triaxial specimens taken from the center of the sample tube are expected to have greater water content than that observed "in situ". The zones of extensive shearing, where disturbance and contraction are present (near the edges of sampling tube), and the water

mitigation towards the center of the sampling tube, where expansion is expected, can be perceived in figure 5.29.

In almost all lab tests, the highly disturbed material near the edges of the sample tube is removed during trimming procedures. However, some shearing effects and radial water mitigation must alter - to some extent - sample quality. Water mitigation has an increasing significance with increasing the stress level or the reduction of void ratio, e_0. This mechanism can also explain the noticeable very bad quality of many samples especially in great depths. Simply with ISA straining in triaxial tests this high disturbance effect cannot be simulated in total. One should also apply some volumetric change after each imposed ISA simulation to account for this radial volumetric difference, the shearing and the redistribution of water content inside the tube.

Santagata et al. (2006), investigated the effects of the sampler tip geometry and of the ratio of tube diameter to thickness, B/t, on Sample Quality. Field Boston Blue Clay (BBC) data were also compared to the ISA triaxial element test results performed on NC RBBC. Figure 5.30 shows 3 different tip geometries of sampler that were used to collect field samples and investigate the effects of disturbance in the lab (Sinfield, 1994). Figure 5.31 plots the normalized sampling effective stress for all the different sampler geometries and ratios, B/t, versus disturbance. The ISA strain cycle amplitude, ε_c (%), is calculated from the Baligh et al. (1987) approximate equation for the maximum axial strain in compression and extension at the centerline of the sampling tube, ε_{zzMAX}:

$\varepsilon_c = \varepsilon_{zzMAX} = 0.385 \cdot t/B$, that is valid when $B/t >> 1$.

The sampling effective stress is normalized to the vertical effective stress, σ'_{vc}, acting on the clay layer prior to the beginning of the sampling operation. Different symbols are used for the three different tip geometries presented in figure 5.32. The symbol sizes refer to different ratios of the tube diameter, B, to the actual specimen diameter, D. The large symbols correspond to a $B/D = 2$ (approximately what is used in triaxial tests), the medium symbols correspond to a

B/D = 1.3 to 1.8, and the small symbols correspond to a ratio B/D < 1.2. In the figure, the RBBC ISA disturbance simulation path for triaxial testing is presented (dotted line). From the results it is clear that the ISA disturbance simulation in the lab gives significantly higher sampling effective stress compared to field data. Also as the ratio B/D decreases, the expected disturbance, as it is measured from the loss of effective stress, increases. This makes sense, as it is known that moving from the center of the tube to the edge, the disturbance presented on the layers and soil structure becomes greater.

The reconsolidation strain, ε_v (%), was also plotted versus the ISA strain cycle amplitude, ε_c (%), for the 3 different geometries and the ISA disturbance simulation from triaxial tests in the lab. The reconsolidation strain is a direct measurement of disturbance from Terzaghi et al. (1996) qualitative criterion. Results indicated again that the expected - in the field reconsolidation strains are much higher than that reproduced from the ISA triaxial simulation. A clear difference was also observed in the Specimen Quality using Shelby tip samplers and blunt tip samplers. Shelby tip sampler consistently reproduced lower reconsolidation strains and gave higher sampling effective stress.

Results from Santagata et al., 2006, are a strong indication that the ISA disturbance simulation, in the lab, using triaxial tests can only reproduce some effects of disturbance. In reality, the disturbance from a give tube sampler (with a given ratio B/t), is expected to create greater reconsolidation strains and give a lower sampling effective stress. It is also clear that the ratio B/D, the sampler diameter to the specimen diameter plays a significant role on the specimen quality. From all the above, it was decided to account for the disturbance on an element on the outside of the centerline of the sampling tube. This means that after ISA simulation, a second step should be introduced accounting for the volumetric, that an element on given distance from the centerline undergoes.

In order to gain some insight on the importance of this increase in water content on the actual specimen tested on the triaxial apparatus, few inceptive tests were run applying some volumetric change after each disturbance simulation with the ISA. This simulated the effects of disturbance on an element sitting outside the center line of the sample tube. Some of the initial

challenges to this were that there are no actual measurements on how much this volumetric mitigation inside the tube is. The only available data were from measuring the water content on a tube after the dissipation of pore pressure and after transportation and storing (but without knowing the initial exact water content). It was also challenging to find a correct way to replicate this process in the lab. A hypothetical volumetric change and its effect on the consolidation behavior of the specimen can be seen in figure 5.33. In this figure the black consolidation line is from a NC RSFBM specimen of imposed disturbance 6% axial strain. The black line is the actual recompression line after the disturbance. The blue, dotted line is the hypothetical recompression line when the water content increases after disturbance (swelling). The recompression coefficient, C_r, is expected to be greater since the soil structure "loosens", and the coefficient of consolidation, C_c, is expected to be smaller. On the opposite case, if we allow some water to drain out from the specimens, the hypothetical recompression path is expected to be as presented with the pink dotted line. Initially the response will be stiffer up to VCL and preconsolidation pressure, where the specimen will collapse, resulting in a higher coefficient of consolidation, C_c.

To overcome these difficulties on the initial tests, small disturbance simulation amplitudes were used. Then, the normalized loss of effective stress is compared to that of other tests of higher disturbance amplitudes (5% or more). For example for an ISA of 0.5% one should expect a normalized loss of effective stress of 0.6 while for an ISA of 5% one should expect a normalized loss of effective stress of 0.95 (results Chapter 6). So, a designed test to account for volumetric change, ΔV, would be to impose an ISA of 0.5% and then increase the pore pressure of the specimen such that the final loss of effective stress is increased to about 0.95%. To accomplish this, after each disturbance simulation the new stress conditions were calculated. Then the back pressure of the system was equalized to the pore pressure of the system and the drainage lines were opened. The new stresses were imposed in a single step and the specimen was allowed to swell overtime. Then it was left overnight at hold stress to equilibrate.

A typical test of disturbance simulation that accounts for the effect of swelling (volumetric change, ΔV) can be seen in figure 5.34. It should be mentioned that the loss of effective stress during this step (black and purple line) is almost immediate. However, the specimen experiences a change in the void ratio over time as it stabilizes to the new effective stress (sometime this process takes up to 12 hours). This makes sense, as the time required for

swelling depends on the soil's coefficient of consolidation, c_v. Once swelling has subsided, a new recompression phase takes place. The recompression curve will then be used to determine the effects of this combined disturbance on the stress – strain history and compressibility parameters of the soil. The effect of this second disturbance step, accounting for volumetric change, ΔV, and how this is imposed, is presented in figure 5.35. The figure plots the change in vertical effective stress (black line on the upper diagram), pore pressure (blue line, on the middle diagram) and void ratio (red line, on the lower diagram) versus time in logarithmic scale in second. The effect of the sudden, step increase of pore pressure on vertical effective stress and void ratio is presented. The total vertical stress remains constant, so an increase on pore pressure causes equal decrease on the vertical effective stress. Also, the void ratio increases logarithmically towards a certain value.

As results in the next Chapter will point out, during this process both the reduction in sampling effective stress and the change in the VCL slope appear to be significant. This means that the specimen structure changes to a greater extent when allowing for volumetric changes to occur. A small increase of lateral stress ratio, K_0, was also noticed on every recompression curve but the trend overall is in agreement with the general trend observed for K_0-consolidation in the low pressure MIT apparatuses (figure 5.36).

The value of preconsolidation pressure, σ'_p, is in most cases over-predicted when accounting for volumetric changes. This contradicts the theory since it is expected to have more disturbed soil from the center to the edges on a sampling tube. However, as water is injected into the specimen, there is an increase of the pore pressure and with time, of the void ratio. More fluid between the clay particles leads to fewer interparticle forces (lower effective stress) and thus, leads to more ductile response. More rounded recompression curves are expected. With the same logic, when we have lower void ratios or higher stresses, the clay particles are re-oriented and closer together is such a way that more bonds are formatted. Thus initial a rigid response is expected that will lead to a sudden collapse of the soil skeleton when stress increases beyond the preconsolidation pressure.

This overestimation of preconsolidation pressure can be explained from Santagata and Germaine (1994) conceptual model. The author believes that, for SFBM, the loss of effective stress effect, when accounting for a volume change, ΔV, was much more significant than the soil

destructuring (as it depicts on the change the shape of the compression curve) and so resulted in an overall increase of the preconsolidation pressure value, σ'_p.

5.6 The MIT p', q space

The effective stress paths for the three triaxial specimens presented in Chapter 5 can be seen at figures 5.37 to 5.40. Figure 5.37 presents the state of stress on the MIT p' – q space, in terms of mean stress and maximum shear on the normally consolidated specimen for triaxial test TX 878 C2. Where:

$$p' = \frac{\sigma'_v + \sigma'_h}{2} \; and \; q = \frac{\sigma_v - \sigma_h}{2}$$

The specimen, starts from a hydrostatic state of stress where q = 0, and follows the K_0 consolidation line. Before each consolidation step, the volumetric strain is reset to match the axial strain. Then the axial strain is increased while the control program maintains the volumetric strain equal to the axial strain as consolidation progresses (to maintain the boundary conditions). The pore pressure is held constant during the whole K_0 consolidation phase. The drainage valves remain open allowing the consolidation and drainage of water to the back pressure system in order to maintain the equilibrium between axial and volumetric strain.

After K_0 consolidation and the overnight hold stress for TX 878 a disturbance simulation phase was performed. The disturbance simulation is essentially an undrained cycle of shearing at a constant rate of axial strain of about 0.5%/hour. The cell pressure is maintained constant during this phase and the pore pressure responds to the increase of the axial stress under undrained conditions. Pore pressure valves are closed keeping the volumetric change of the specimen zero. Here, the failure envelop appears to move almost vertical towards the failure envelope. The path of disturbance in p' – q space is noted with a red line. Normally consolidated specimens show a contractive behavior and the failure envelope meets the failure line to the left as on figure 5.37. The shearing also results in an increased pore pressure which will be comparable to the final calculated loss of effective stress during disturbance. Increasing the vertical consolidation stress is observed to slightly increasing the final K_0 value. This causes a small decrease in the peak

strength. It must be noted that at the end of the disturbance simulation the specimen has zero shear load on it and lies on the x – axis on the p' – q space (q = 0).

Santagata and Germaine (1994) implement similar observations, as far as the effective stress path is concerned. Figure 5.38 presents the normalized stress path of a NC BBC specimen when applying the ISA disturbance of 1 % axial strain and when applying the Perfect Sample Approach method. The effective stress path for PSA is of course much simpler since it accounts only for the stress relief during sampling.

The effective stress path in the MIT p' – q space for the Overconsolidated specimen (OC) TX 942 can be seen in figure 5.39. As above, there is the initial K_0 consolidation (black line) up to the maximum vertical effective stress that is maintained during hold stress for 12 to 24 hours. Then the specimen is mechanically unloaded to a target value of vertical and horizontal stress that will give the desired OCR = 4 ratio (blue line). A second hold stress period is allowed for secondary compression after unloading to the specific OCR. Then, the specimen is disturbed by imposing the ISA undrained shear cycle (red line). The OC specimen dilates during the first compression phase of the ISA undrained shearing, but ends up having positive pore pressure. The failure envelope for the OCR of 4 has now changed and yields to the right until it meets the failure line. Again, after the cycle of straining is imposed, disturbance simulation unloads the specimen to zero shear stress (q = 0).

Figure 5.40 presents the effective stress path for the combined disturbance simulation (ISA and ΔV) at the MIT p' – q space. The change in volumetric strain, ΔV (pink line, points 3 to 4), is incorporated after the K_0 consolidation (points 1 to 2) and the ISA disturbance simulation. The ISA simulation (points 2 to 3) initially shears the NC specimen to almost 45° up until the failure envelope. From there it goes through the compression – extension – compression – unloading steps and rests on the x – axis as normal (where q = 0). Increasing the pore pressure of the specimen after the disturbance cycle moves the specimen's stress point resting on the x - axis further reducing the sampling effective stress. These combined paths (ISA and account for ΔV) in figure 5.40 agree more with the hypothetical stress path of sampling disturbance as was proposed by Ladd and Lambe (1963). Accounting for volumetric change, ΔV, brings the sampling effective stress of the specimen, σ'_s, closer to zero and can simulate the effect of

multiple steps on the hypothetical stress path such as transportation and storage of the sample or the specimen preparation.

5.7 Quantification of Disturbance using the Compression Indices*

All triaxial tests start from a small positive or negative axial strain. This value depends on the amount of the initial effective stress that is applied on the specimen prior to and during back pressure saturation. This value for most specimens is about ¼ of the preconsolidation pressure or the previous maximum consolidation stress but can vary with specimen preparation procedures. Also, after disturbance simulation is imposed using the ISA (Baligh et al. 1987), the specimen is left to equilibrate overnight for about 8 to 16 hours. Then, the back pressure of the system is equilibrated to the pore pressure of the specimen and the drainage lines open to be able to start the next consolidation phase. All the above procedures influence the initial measured sampling effective stress, σ'_s, on the different consolidation phases of the triaxial test.

Small alterations when the initial effective stress is defined during the set up, or a difference in the creeping of soil after disturbance, or even small mistakes when equalizing the back to the pore pressure of the specimen, can alter the sampling or initial effective stress. The slope of the recompression line is defined with the recompression index, C_r. In many cases, and when the initial part of the slope is used to calculate the recompression index, C_r, mistakes are significant. This can lead to a miscalculation on the value of preconsolidation pressure itself. In cases of large disturbance simulation amplitudes ($\varepsilon_a \geq 5\%$), where the sampling effective stress tends to go to zero, the problem is even greater; Small mistakes significantly change the measured σ'_s and the recompression index, or recompression ratio, C_r or RR, is a very small number, sometimes difficult to define on a semi-logarithmic scale.

In tests where large disturbance amplitudes (ISA > 5%) are imposed, defining the VCL slope is not always trivial. In many cases, even when reconsolidating well beyond the preconsolidation pressure ($\sigma'_{vc} >> 2.5\ \sigma'_p$) the specimen appears not to have reached its "true" VCL. This of course will result in an underestimation of the preconsolidation pressure value.

To overcome these difficulties a new method is developed to quantify disturbance on resedimented San Francisco Bay Mud specimens (RSFBM). The compression index* and the recompression index* are proposed as objective measures of the slope of the compression curve in the vicinity of the preconsolidation pressure. These indices correspond to the slope of the compression curve just before and after the calculated preconsolidation pressure, σ'_p, and are calculated as shown in figure 5.41 and 5.42.

The compression curves are plotted on a semi – logarithmic scale of void ratio, e, versus the vertical effective stress, σ'_{vc}. Applying the strain energy approach, the preconsolidation pressure and the void ratio on the measured curve at this stress level are defined. The given stress corresponding to σ'_p is multiplied by a constant number, n and its inverse, 1/n. This defines point A where the stress is σ'_p/n and point C where stress is $\sigma'_p \cdot n$. Finding the equivalent void ratios from the consolidation curve one can define the stress history at these 3 points, A, B, and C. The recompression index* is the slope of line AB while the compression index* is defined from slope BC. Since the scale on the X-axis is logarithmic, point A and C would have the same horizontal distance from point B, the point corresponding to the preconsolidation pressure. Also, by keeping the same distance (keeping the parameter n constant among different tests), it is possible to compare the compression and recompression indexes of different compression curves. This is a direct outcome from the logarithmic properties. So the horizontal distance from A to B and from B to C for any give number would be:

$$X_A - X_B = logX \cdot n - logX = \log(\frac{X \cdot n}{X}) = \log n$$

And

$$X_B - X_C = logX - log\frac{X}{n} = \log(\frac{X}{\frac{X}{n}}) = \log n$$

Taking advantage of the above outcome, one can easily define points of equal horizontal distance from the preconsolidation pressure. Then the slopes of the curves AB and BC can give a clear understanding of the extent to which the curvature of the compression curve changes near the preconsolidation pressure. Later on results from RSFBM will attempt to quantify the

statement that "increase in disturbance cause more rounded compression curves" based on these two proposed indexes.

The ratio of the recompression to compression index would be an indication of the angle$A\hat{B}C$. This comes from the fact that angle $A\hat{B}C$ can be expressed as a function of the compression and recompression index, C_r^* and C_c^*. On figure 5.42 the angle$A\hat{B}C$ would be:

$$A\hat{B}C = 180^o - \varphi\,(C_c^*) + \varphi(C_r^*)$$

where φ is the angle of the compression or recompression slope to the horizontal line.

Even though the above equation recommends that the angle ABC is analog to the difference of the two slopes since the scale is semi - logarithmic results showed a better consistency when using the ratio of the two indices, C_r^*/C_c^*.

To define the boundaries in this new methodology, two concepts are introduced (chapter 2). The first is the theoretical concept of rigid – plastic behavior material (Nagaraj et al., 2003). This is the model of a completely rigid material up to preconsolidation pressure and then completely plastic just after the preconsolidation pressure. The indices ratio of such a material tends to zero.

For the rigid – plastic behavior material, $C_r^*/C_c^* \to 0$.

On the other hand, for a completely remolded material, one would expect to see no difference on the compression behavior before and after the preconsolidation pressure. So, for this case C_r* equals C_c*. This is in accordance with the concept of Intrinsic State Line (ISL) as it was introduced from Burland (1990).

For a completely remolded material, $C_r^*/C_c^* \to 1$.

It must be noted that for a "typical clay" the indices ratio is, $C_r^*/C_c^* \approx 0.1$.

Disturbance ε (%)	Intact	Resedimented	
	NC	NC	OCR 4
0.5	TX693	-	-
1	TX694	TX795	-
1.5	TX720	-	TX839
2	TX695, TX703	-	-
2.5	TX717	-	-
3	TX698, TX714	TX802	TX814
3.5	-	-	TX841
4	TX701	-	-
5	TX721	-	-
5.5	-	-	TX852
6	TX785	TX867	-
10	TX731	-	-
Total	12	3	4

Table 5.1: Summary Table of triaxial tests performed on intact tube samples of SFBM.

Disturbance ε (%)	NC	OCR 2	OCR 4	Account for ΔV
0.5	TX878	TX1024	TX915	TX1044
0.8	TX911	-	-	-
1	-	-	TX964	TX1052
1.5	TX879	TX976	TX916	-
2.5	TX902	TX1025	TX942	TX 1060
3.5	TX901	TX1017	TX943	TX1058
4.5	TX977	-	-	-
5	-	TX1028	TX965	-
6	TX912	-	-	-
Total	7	5	6	4

Table 5.2: Summary Table of triaxial tests performed on the RSFBM homogeneous batch of soil.

TEST No.	TX 693	TX694	TX695	TX698	TX701	TX703	TX714	TX715	TX717	TX718	TX720	TX721	TX726	TX731	Average Values	Standard Deviation
Inital Water Content (%)	32.58	30.51	31.18	31.72	31.51	31.46	31.46	31.10	31.01	30.02	30.02	34.44	31.69	30.29	31.36	1.14
Initial Void Ratio	0.920	0.861	0.869	0.900	0.880	0.934	0.911	0.880	0.864	0.847	0.866	0.972	0.881	0.845	0.89	0.04
Inital Saturation (%)	98.46	99.67	99.70	97.96	99.59	93.68	96.97	98.22	99.79	98.51	96.41	98.46	99.96	99.70	98.29	1.82
Wet Density (gm/cc)	1.920	1.960	1.951	1.927	1.945	1.890	1.912	1.938	1.954	1.957	1.937	1.895	1.946	1.964	1.94	0.02
Dry Density (gm/cc)	1.448	1.502	1.487	1.463	1.479	1.438	1.454	1.478	1.492	1.505	1.490	1.409	1.478	1.507	1.47	0.03
Height of solids	4.4317	4.3945	4.2976	4.2719	4.3213	4.2037	4.2487	4.3187	4.3569	4.3959	4.3529	4.1152	4.2935	4.3764	4.31	0.08

Table 5.3: Phase relationship calculations for triaxial tests performed on intact tube specimens of SFBM.

TEST No.	TX795	TX802	TX814	TX838	TX839	TX841	TX852	TX867	Average Values	Standard Deviation
Inital Water Content (%)	60.95	51.65	54.81	53.63	46.18	57.88	50.61	46.18	52.74	5.22
Initial Void Ratio	1.729	1.459	1.538	1.494	1.483	1.675	1.496	1.306	1.52	0.13
Inital Saturation (%)	97.99	98.44	99.04	99.82	86.58	96.07	94.06	98.27	96.28	4.32
Wet Density (gm/cc)	1.639	1.715	1.695	1.713	1.637	1.641	1.678	1.762	1.68	0.04
Dry Density (gm/cc)	1.019	1.131	1.095	1.115	1.120	1.039	1.114	1.205	1.10	0.06
Height of solids	2.8104	3.3088	3.2242	3.2263	3.1183	3.0324	3.0770	3.5077	3.16	0.21

Table 5.4: Phase relationship calculations performed on RSFBM specimens from single tubes.

TEST No.	TX 878	TX 879	TX901	TX902	TX911	TX912	TX915	TX916	TX942	TX943	TX964	TX965	TX976	TX977	TX995
Inital Water Content (%)	**56.12**	**57.17**	**56.41**	**57.39**	**57.88**	**56.98**	**53.85**	**53.60**	**54.84**	**56.87**	**52.36**	**52.73**	**54.08**	**53.41**	**53.27**
Initial Void Ratio	**1.572**	**1.581**	**1.542**	**1.607**	**1.617**	**1.582**	**1.558**	**1.558**	**1.555**	**1.567**	**1.522**	**1.525**	**1.494**	**1.485**	**1.517**
Inital Saturation (%)	**99.22**	**100.51**	**99.88**	**99.26**	**99.50**	**98.37**	**96.06**	**95.63**	**98.02**	**100.87**	**95.63**	**96.14**	**100.63**	**99.98**	**97.62**
Wet Density (gm/cc)	1.687	1.693	1.699	1.678	1.677	1.679	1.672	1.669	1.685	1.699	1.679	1.682	1.717	1.716	1.693
Dry Density (gm/cc)	1.081	1.077	1.094	1.066	1.062	1.077	1.087	1.087	1.088	1.083	1.102	1.101	1.115	1.119	1.104
Height of solids	3.1581	3.1452	3.0489	3.1080	3.1099	3.1378	3.1663	3.1714	3.1710	3.1470	3.2440	3.2338	3.2491	3.2604	3.2137

TX1017	TX1024	TX1025	TX1028	TX1029	TX1044	TX1049	TX1052	TX1058	TX1060	TX1071	TX1088	Average Values	Standard Deviation
53.70	**52.44**	**52.05**	**52.56**	**52.54**	**54.50**	**53.63**	**52.74**	**52.01**	**51.12**	**51.36**	**52.68**	53.94	1.91
1.546	**1.480**	**1.508**	**1.499**	**1.526**	**1.570**	**1.497**	**1.475**	**1.461**	**1.482**	**1.503**	**1.525**	1.53	0.04
96.55	**98.51**	**95.95**	**97.50**	**95.72**	**96.50**	**99.60**	**99.39**	**98.99**	**95.89**	**95.02**	**96.05**	97.89	1.86
1.678	1.709	1.685	1.697	1.679	1.671	1.710	1.716	1.717	1.693	1.681	1.681	1.69	0.02
1.092	1.121	1.108	1.113	1.101	1.082	1.113	1.123	1.130	1.120	1.111	1.101	1.10	0.02
3.1910	3.2767	3.2409	3.2437	3.2160	3.0623	3.2454	3.2790	3.2908	3.1558	3.1388	3.2185	3.19	0.07

Table 5.5: Phase relationship calculations performed on specimens from the homogeneous batch of RSFBM (for the low pressure apparatus).

TEST No.	TX1055	TX1076	TX1087	Average Values	Standard Deviation
Inital Water Content (%)	38.59	35.02	36.68	36.77	1.78
Initial Void Ratio	1.088	1.020	1.026	1.04	0.04
Inital Saturation (%)	98.62	95.47	99.42	97.84	2.09
Wet Density (gm/cc)	1.845	1.858	1.876	1.86	0.02
Dry Density (gm/cc)	1.332	1.376	1.372	1.36	0.02
Height of solids	3.8117	4.0268	3.9992	3.95	0.12

Table 5.6: Phase relationship calculations performed on specimens from the homogeneous batch of RSFBM (high pressure apparatus).

		Intact Specimens	Reconsolidated Specimens	
Phase Relation	units		Low Pressure	High Pressure
Initial Water Content	(%)	31.36	53.94	36.77
Initial Void Ratio		0.89	1.53	1.04
Initial Satudation	(%)	98.29	97.89	97.84
Wet Density	gm/cc	1.94	1.681	1.86
Dry Density	gm/cc	1.47	1.101	1.36
Height of Solids		4.31	3.2185	3.95

Table 5.7: Phase relationship calculations for intact and resedimented SFBM.

Test	Phase	σ'_{vc}	t_p/t	C_a/C_c	C_r/C_c	σ'_{vcm}	
						Mesri & Choi	MIT
TX 878	**C1**	1.11	1.41	0.1	0.05	1.16	1.22
	C2	2.42	1.28	0.1	0.05	2.48	2.62
TX 879	**C1**	1.31	1.41	0.1	0.05	1.36	1.43
	C2	2.88	1.32	0.1	0.05	2.96	3.17
	C3	7.99	1.38	0.1	0.05	8.27	8.71
TX 1017	**C1**	29.65	1.50	0.1	0.05	30.94	38.68
	C2	99.31	1.09	0.1	0.05	100.23	107.43

Table 5.8: The critical pressure calculations accounting for secondary compression aging (Mesri & Choi, 1984).

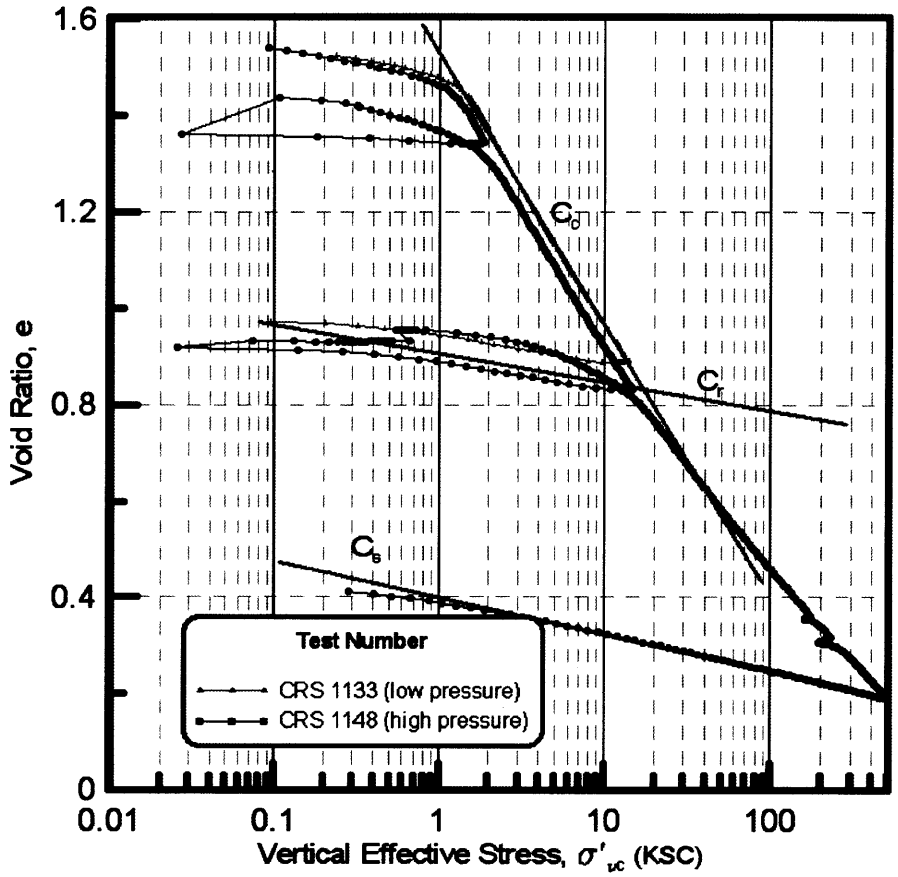

Figure 5.1: Compression behavior in e-log σ'_v space for RSFBM from CRS tests.

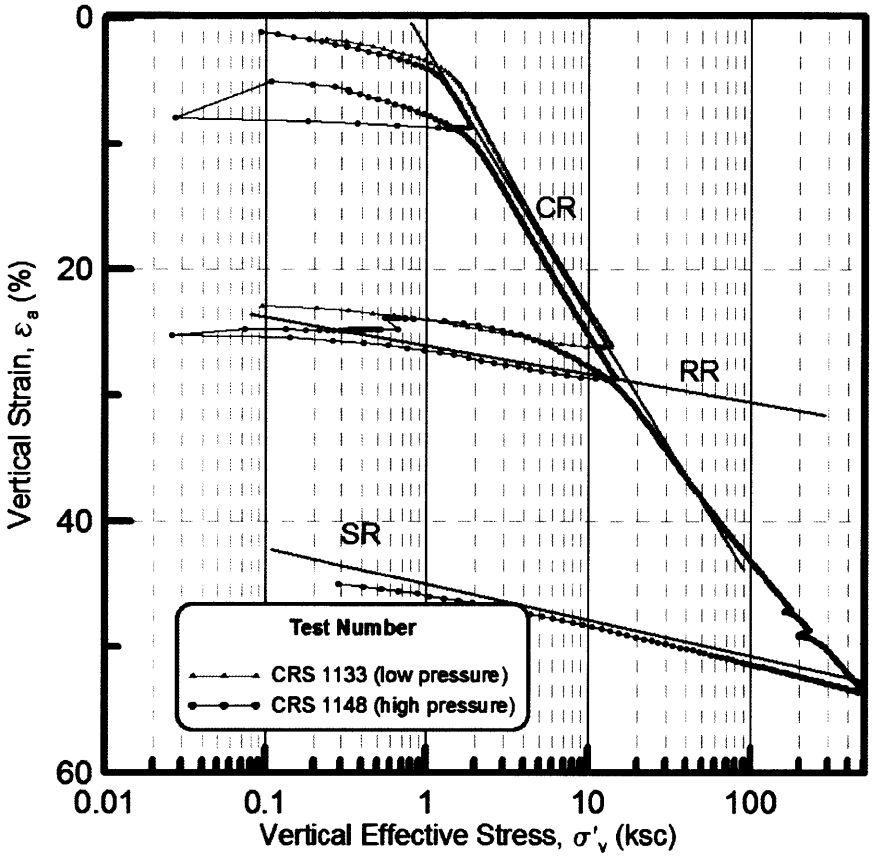

Figure 5.2: Compression behavior in ε_a-log σ'_v space for RSFBM from CRS tests.

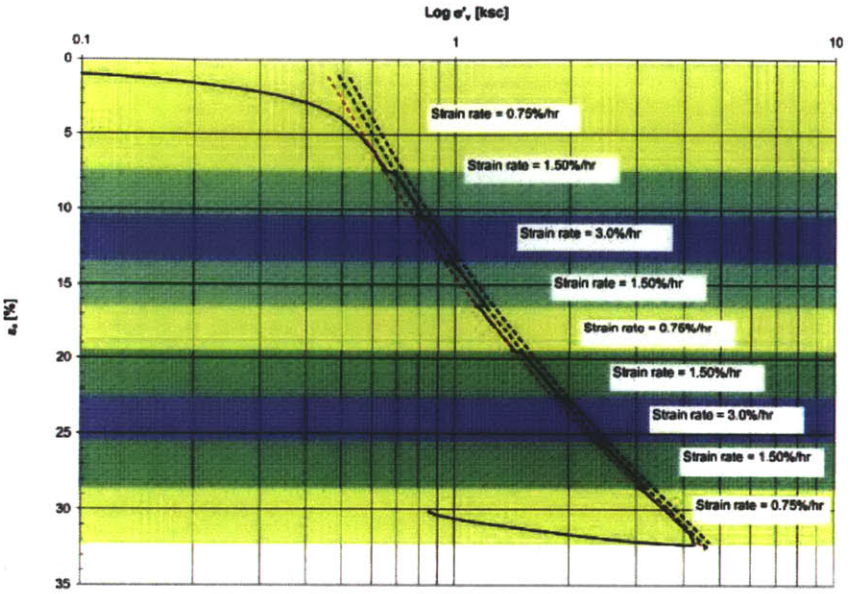

Figure 5.3: Strain Rate sensitivity compression test for SFBM (Korchaiyapruk and Germaine, 2007).

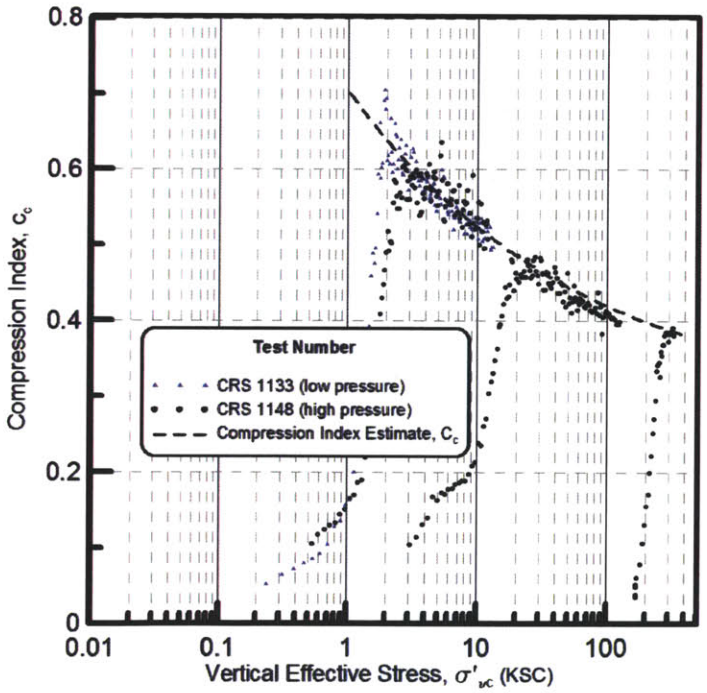

Figure 5.4: The change in the compression curve slope versus vertical effective stress for CRS tests on RSFBM. The dot line corresponds to the interpreted Compression index, C_c.

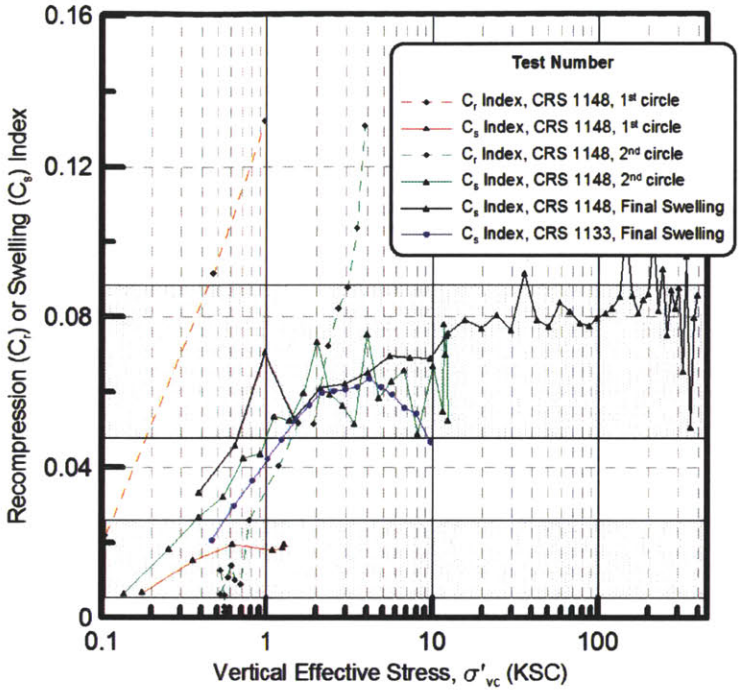

Figure 5.5: The Recompression index (C_r), and Swelling index (C_s) versus vertical effective stress for CRS tests on RSFBM.

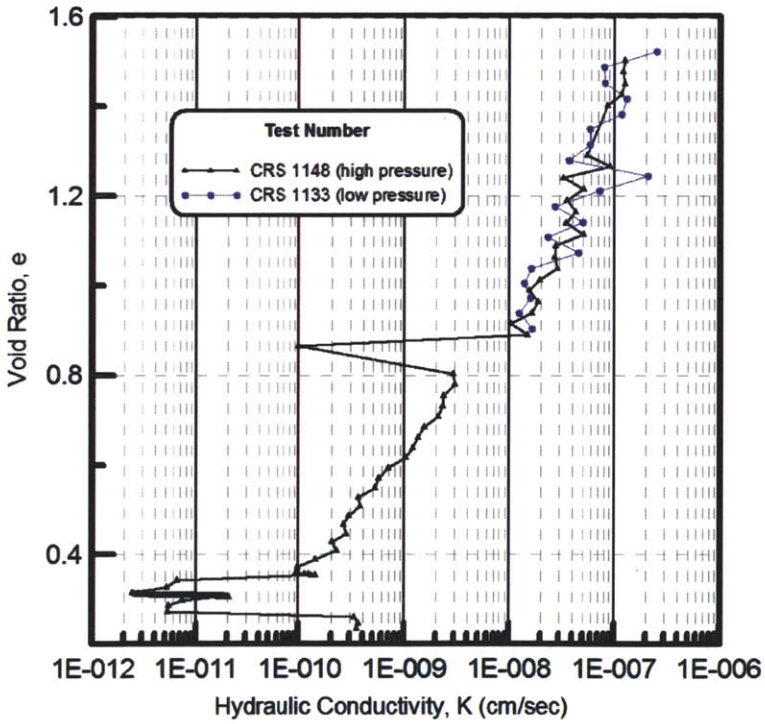

Figure 5.6: Relationship between hydraulic conductivity and void ratio for RSFBM from CRS tests.

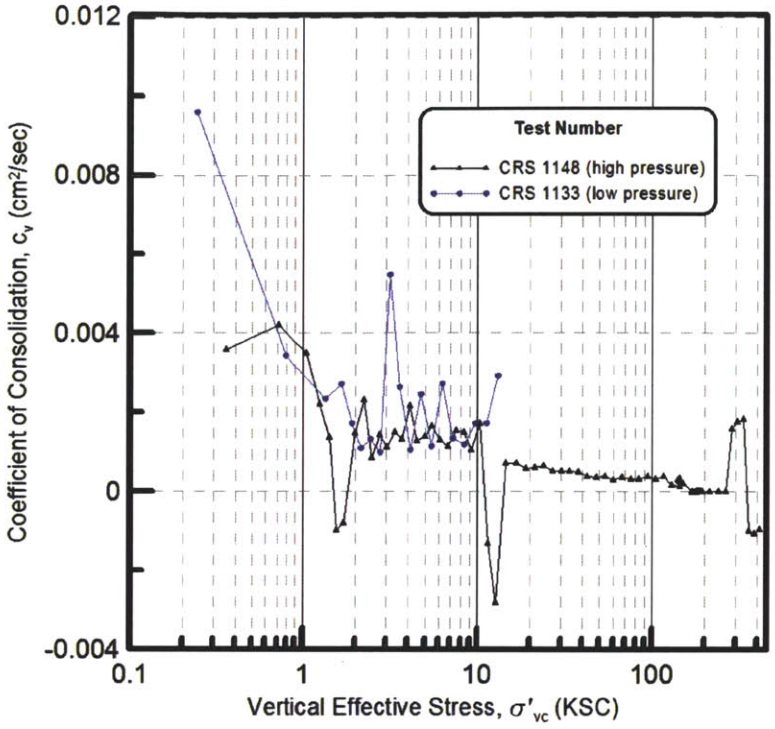

Figure 5.7: The Coefficient of consolidation versus stress level for RSFBM from CRS tests.

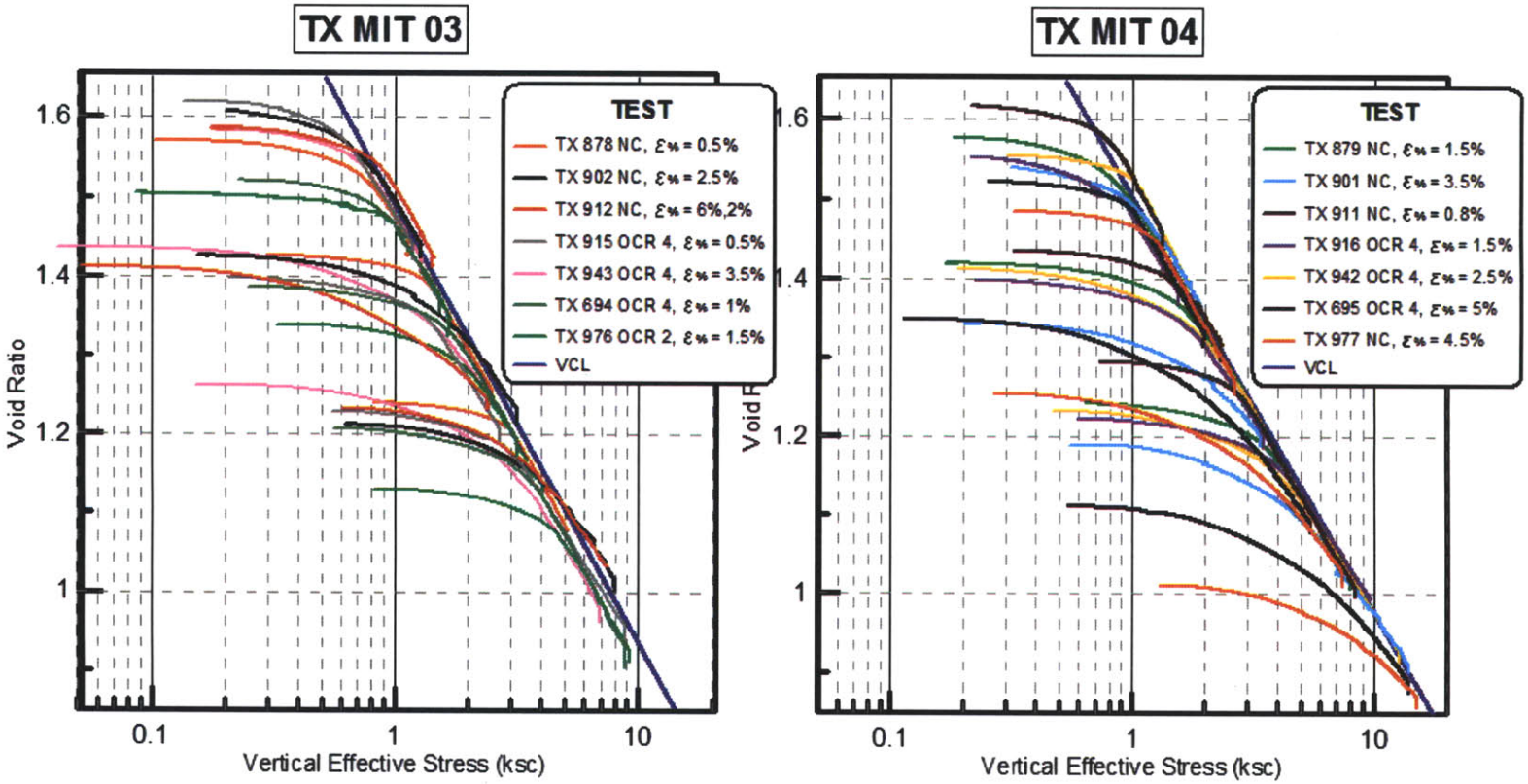

Figure 5.8: The consolidation curves for TX tests of RSFBM performed on the low pressure triaxial cells; MIT03 and MIT04.

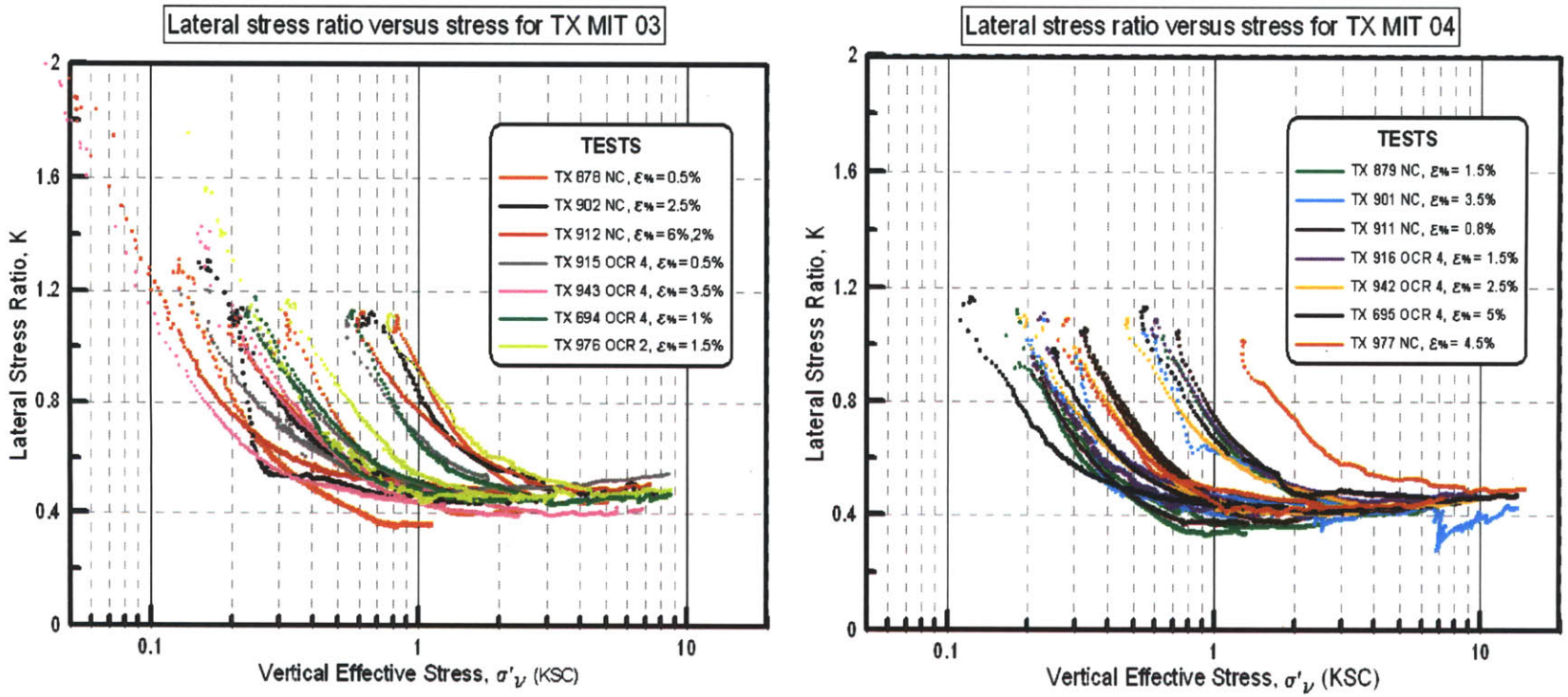

Figure 5.9: The Lateral Stress Ratio K_0 vs. Vertical effective stress for TX consolidation tests performed at the low pressure cells; MIT03 and MIT04.

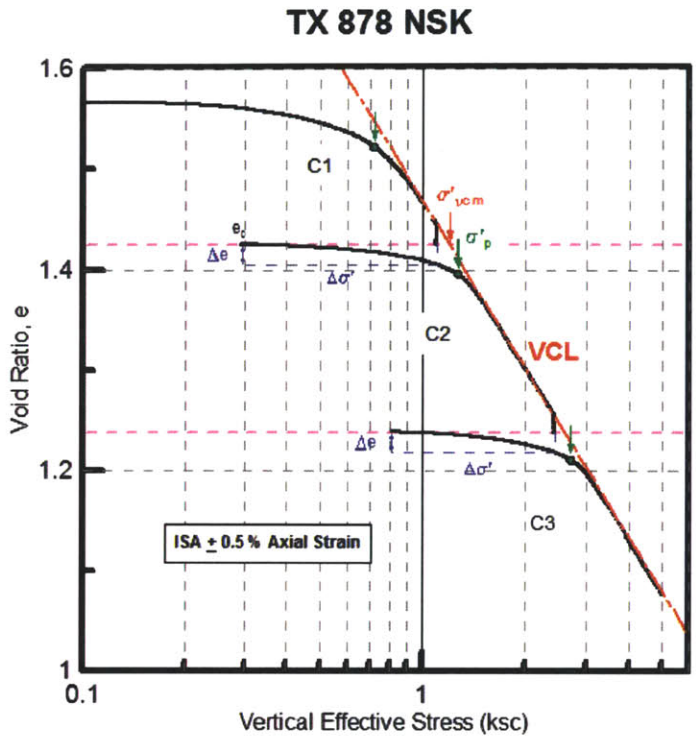

Figure 5.10: A typical CK_0UC test of NC RSFBM with multiple disturbance phases.

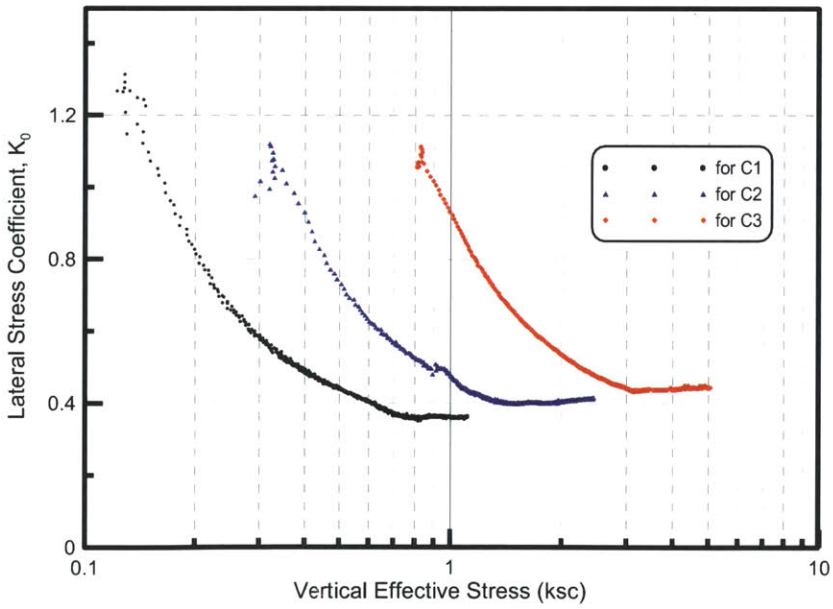

Figure 5.11: Lateral Stress Ratio vs. Vertical Effective Stress during K_0 – consolidation of RSFBM (TX 878).

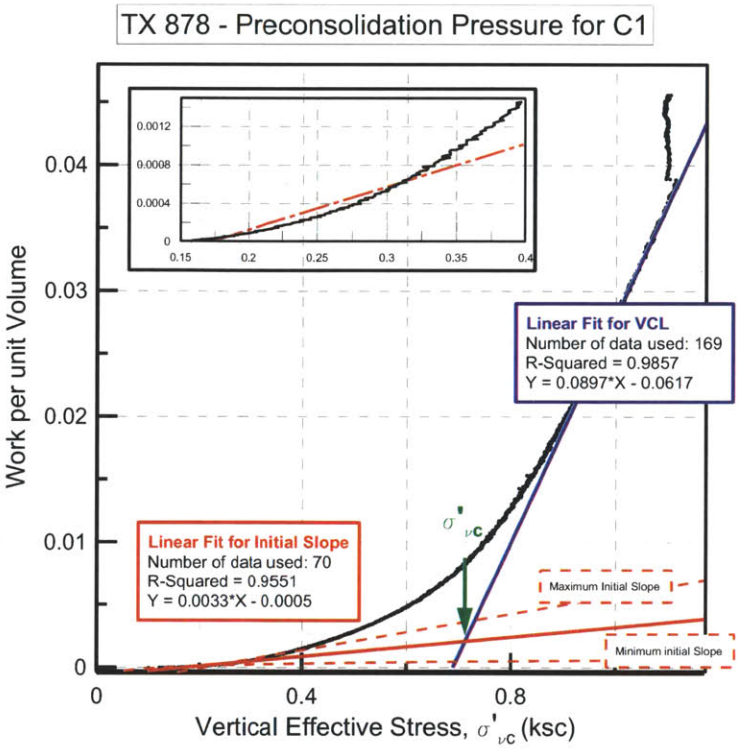

Figure 5.12: Applying the Strain Energy Method for C1 consolidation phase, TX 878.

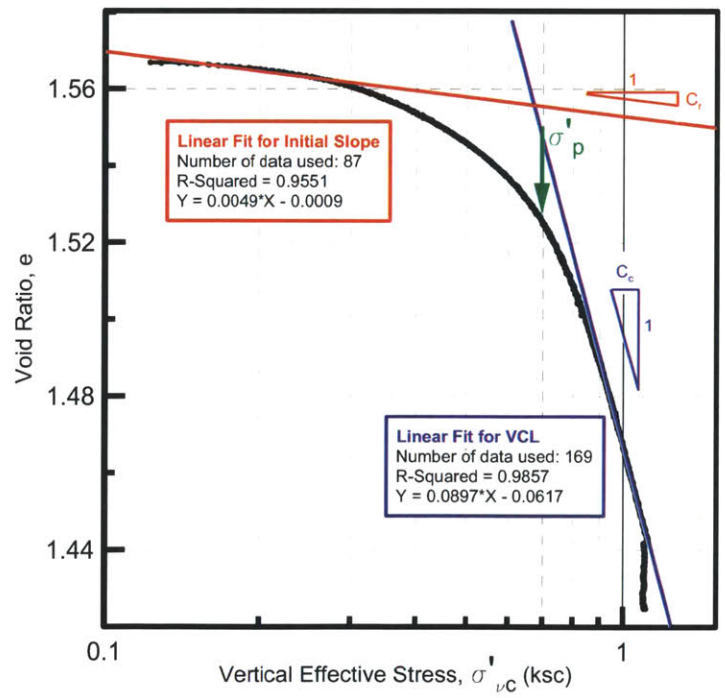

Figure 5.13: Defining the preconsolidation pressure on compression curve, TX 878 C1.

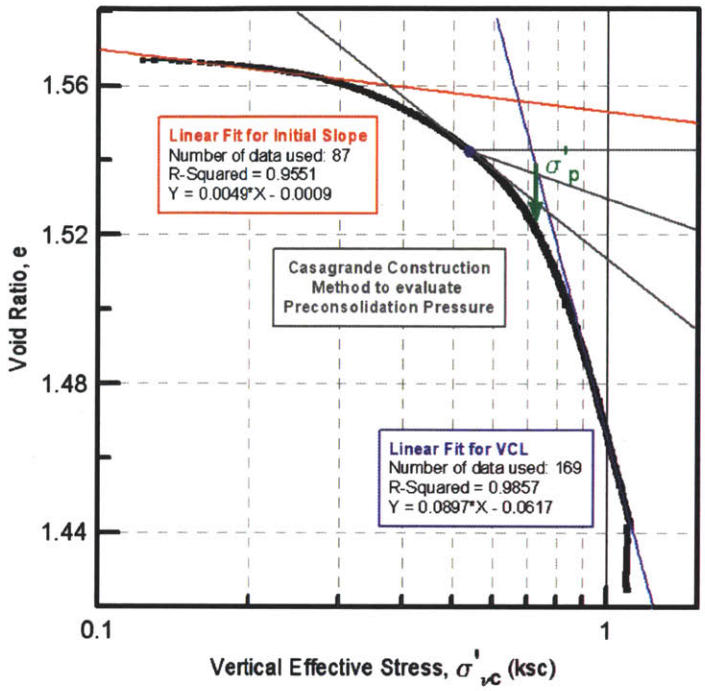

Figure 5.14: Defining the preconsolidation using the Casagrande Method (1963) for TX878 C1.

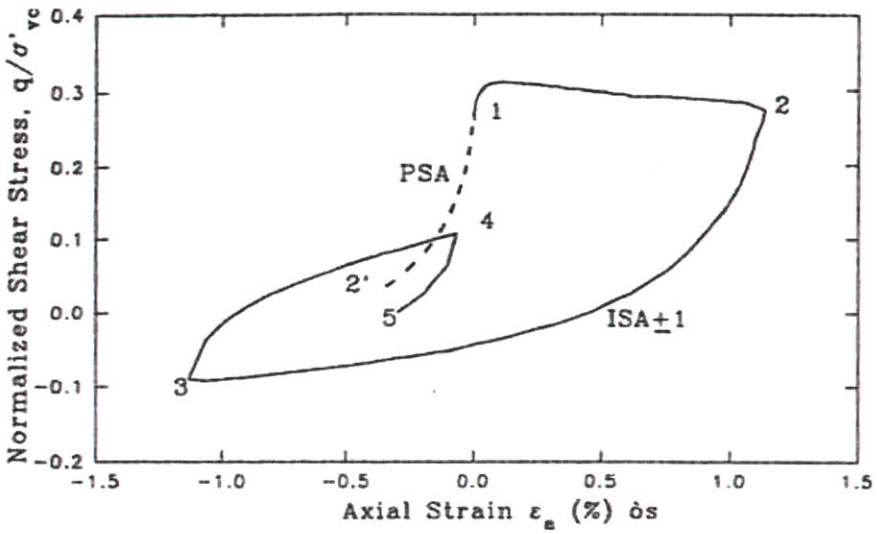

Figure 5.15: Stress Strain curves during PSA and ISA Disturbance of NC RBBC (Santagata and Germaine, 1994).

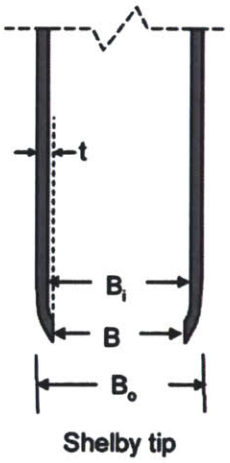

Figure 5.16: Schematic representation of a typical Shelby sampling tube; where B is the diameter of the tube and t is the wall thickness (Santagata et al. 2006).

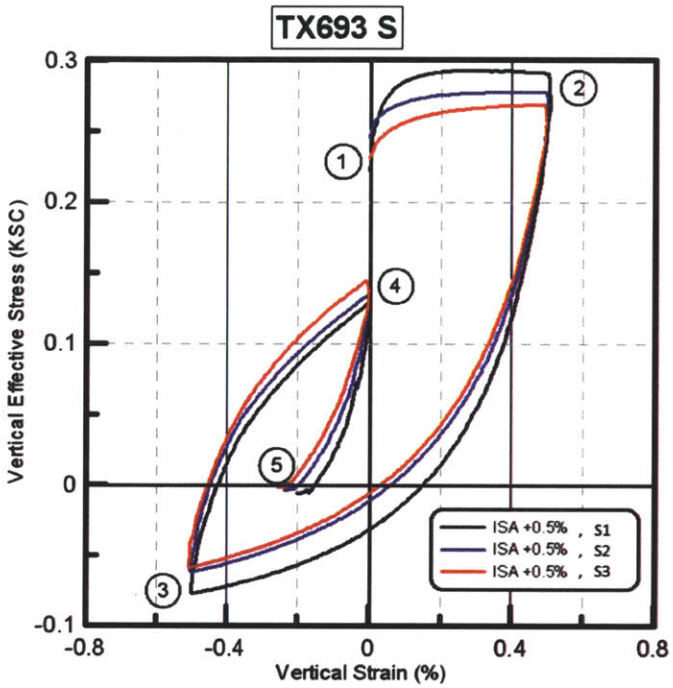

Figure 5.17: Stress strain curves during ISA±0.5% Disturbance for a NC SFBM tube specimen, TX 693.

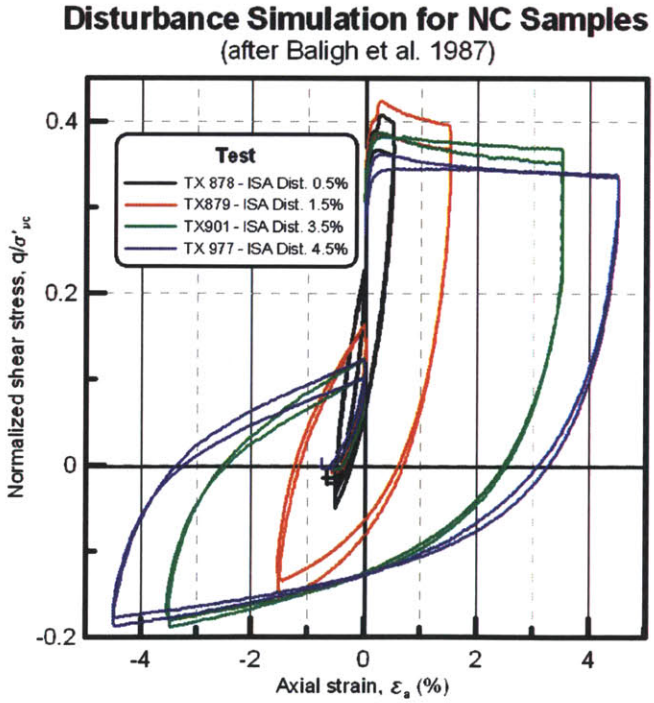

Figure 5.18: Disturbance simulation on Normally Consolidated Resedimented SFBM specimens for different amplitudes of the ISA (after Baligh et al. 1987).

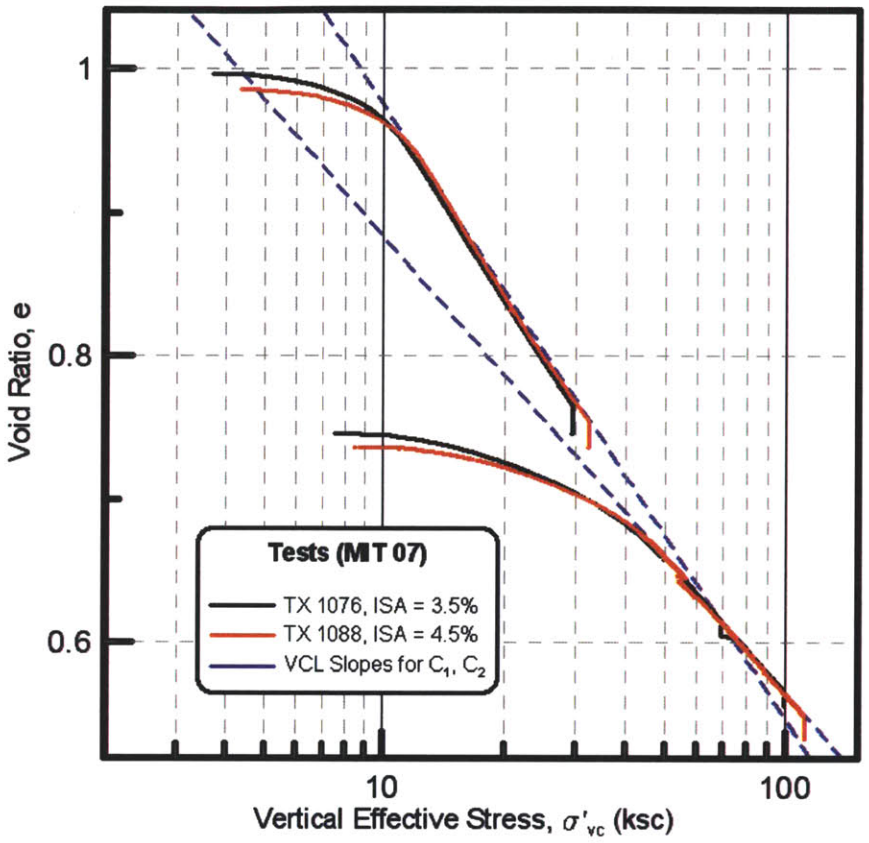

Figure 5.19: A typical CK_0UC test of NC RSFBM on the modified high pressure MIT triaxial cell (e – log σ'_{vc}).

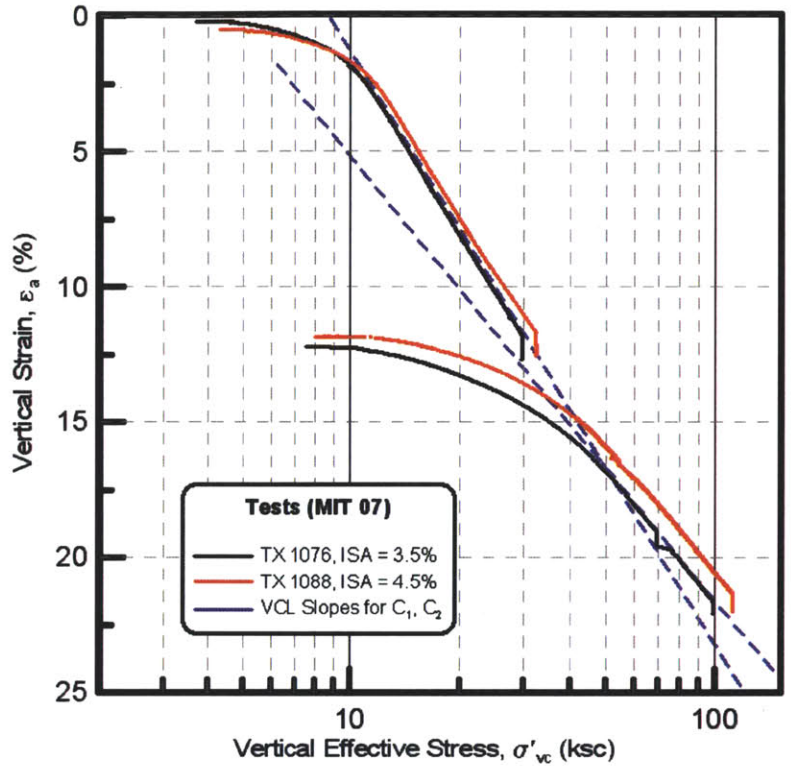

Figure 5.20: A typical CK_0UC test of NC RSFBM on the modified high pressure MIT triaxial cell (ε_a – log σ'_{vc}).

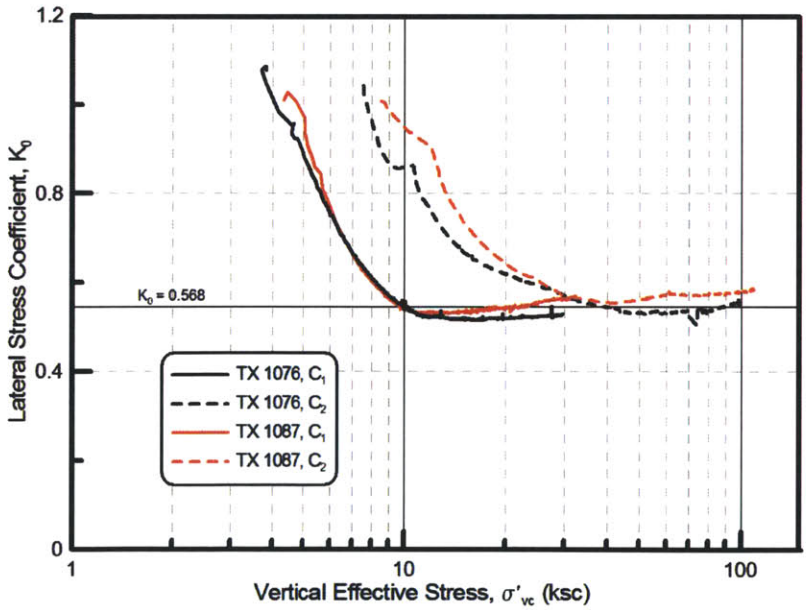

Figure 5.21: Lateral Stress Ratio vs. Vertical Effective Stress during K_0 – consolidation of RSFBM on the high pressure MIT triaxial cell.

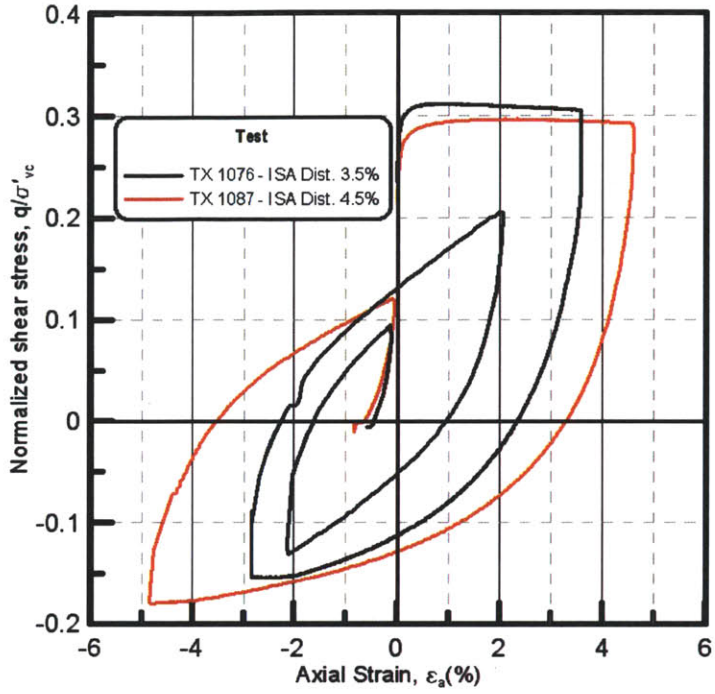

Figure 5.22: Disturbance simulation on Normally Consolidated Resedimented SFBM specimens for different amplitudes of the ISA on the modified high pressure MIT triaxial cell (after Baligh et al. 1987).

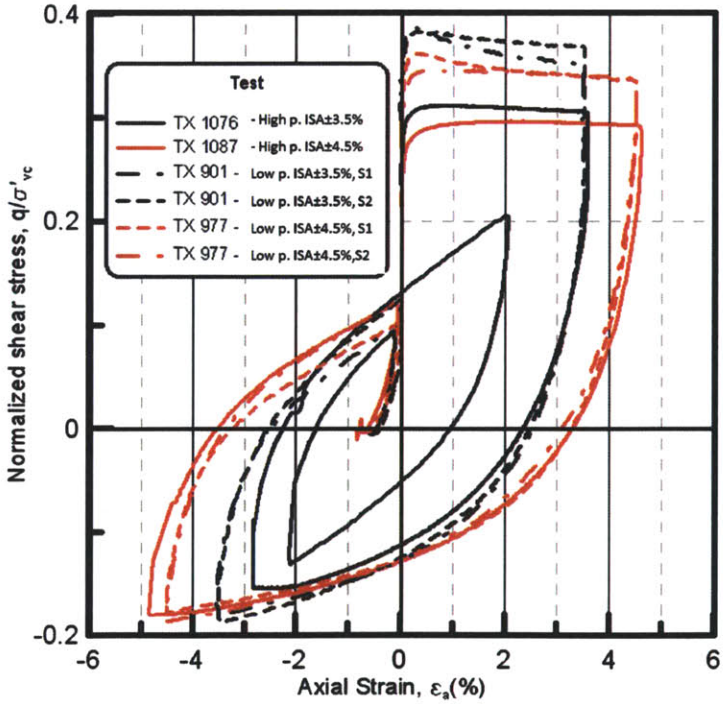

Figure 5.23: Comparison of ISA on low pressure and high pressure MIT triaxial cells for RSFBM.

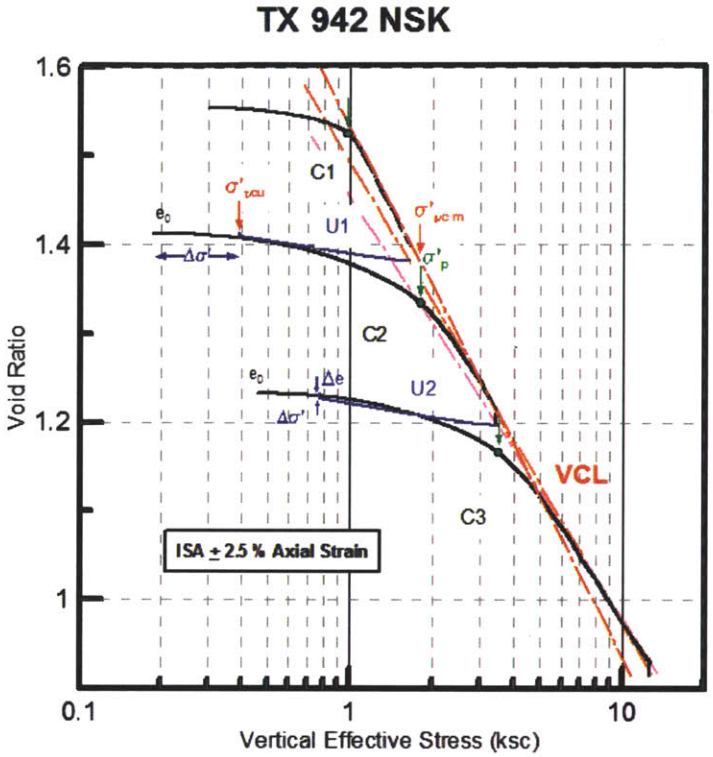

Figure 5.24: A typical CK_0UC test of RSFBM of OCR of 2 with multiple disturbance phases.

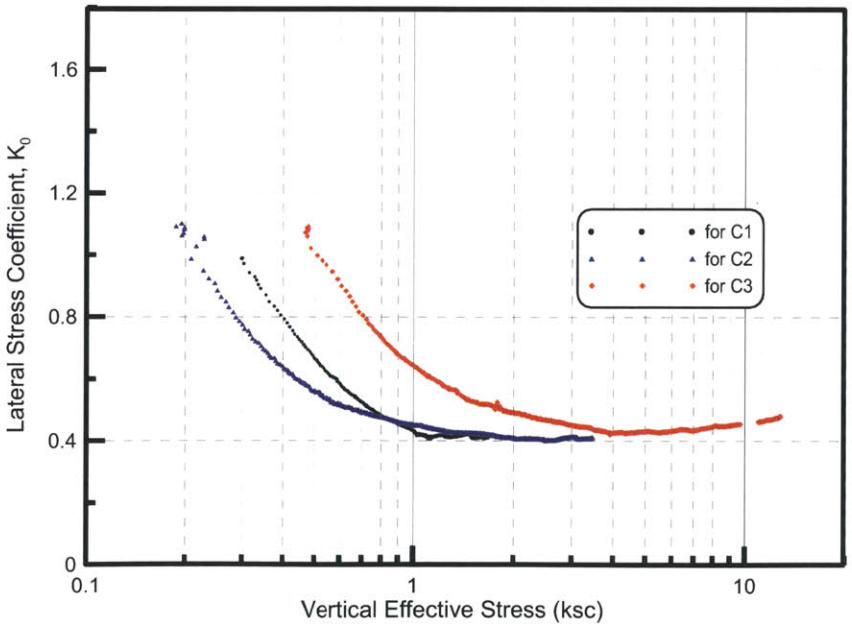

Figure 5.25: Lateral Stress Ratio vs. Vertical Effective Stress during K_0 – consolidation of RSFBM (TX942).

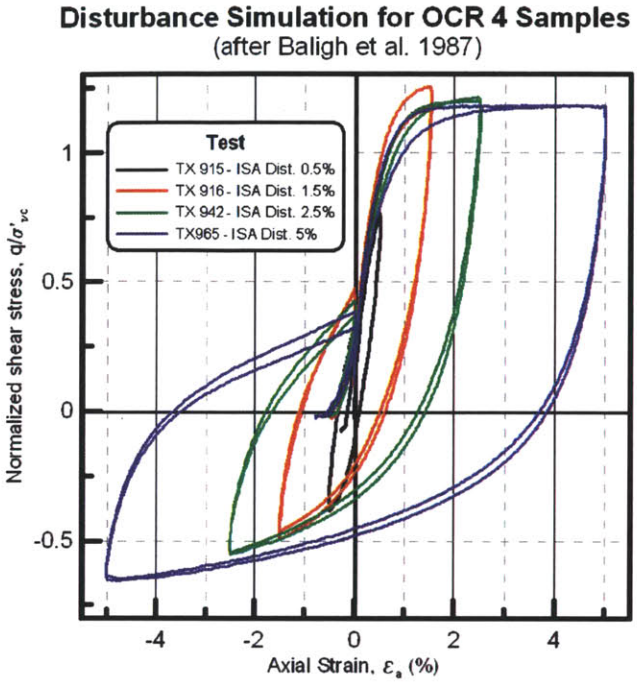

Figure 5.26: Disturbance simulation on Overconsolidated Resedimented SFBM specimens for different amplitudes of the ISA (after Baligh et al. 1987).

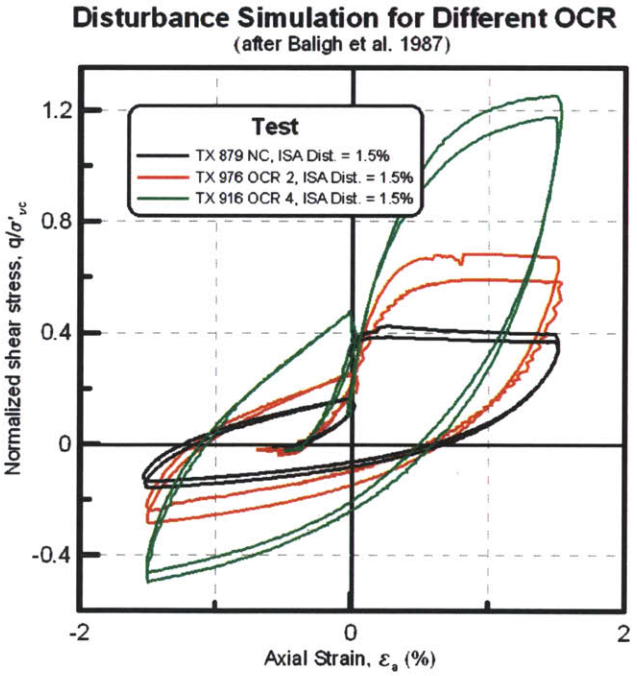

Figure 5.27: Disturbance simulation in respect with ISA on Resedimented SFBM specimens for different OCR.

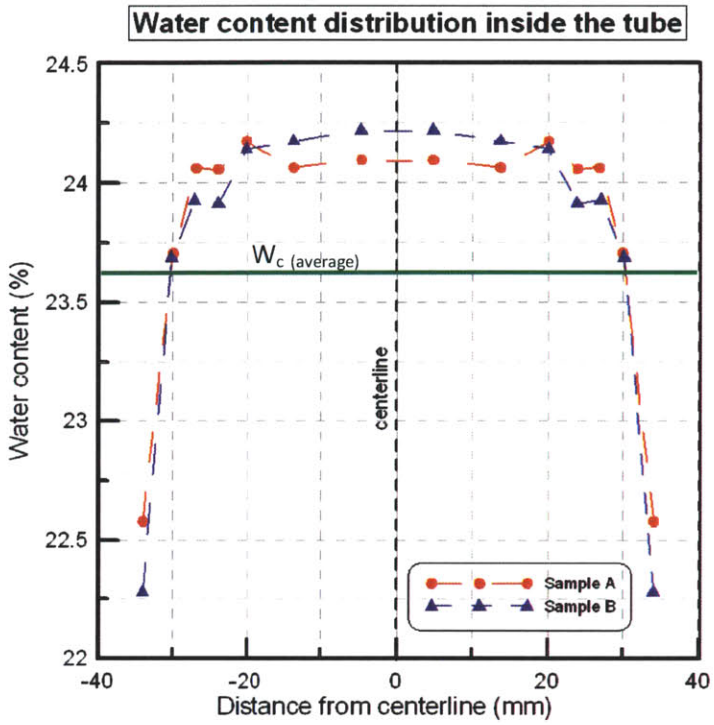

Figure 5.28: Water Content W_c (%) measurements radially on a sample tube of SFFM.

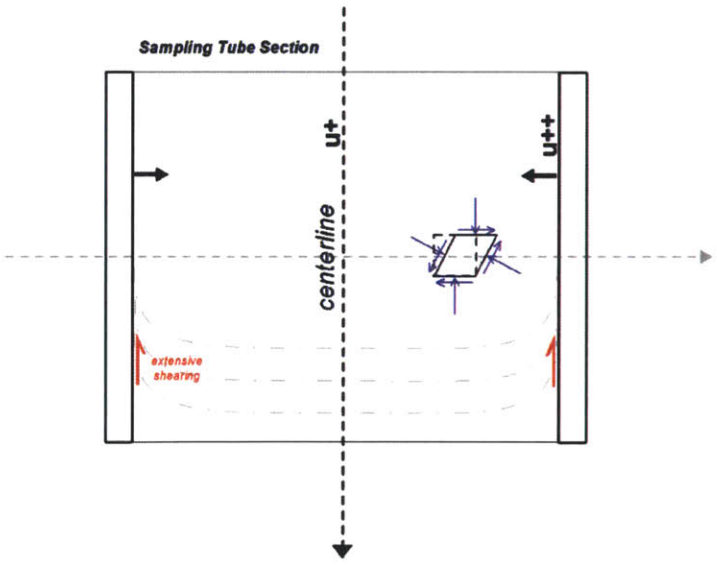

Figure 5.29: Schematic representation of an element of soil outside the centerline of a sample tube.

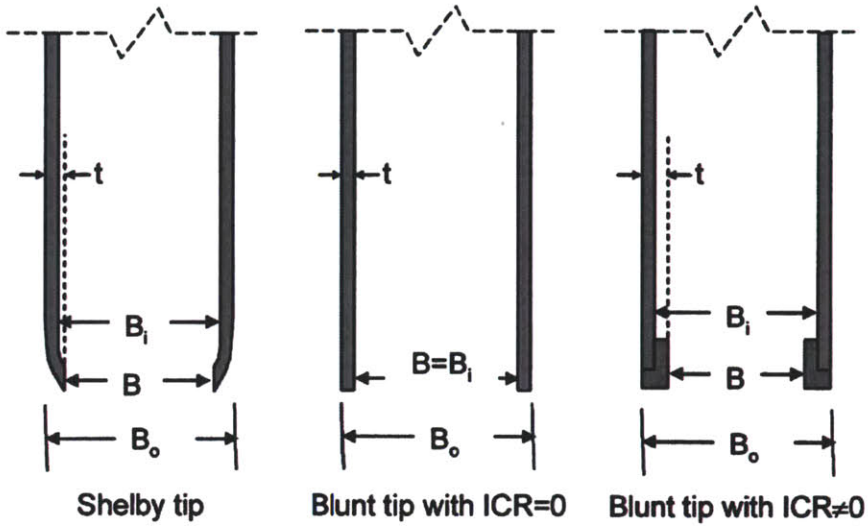

Figure 5.30: Typical sampler tip geometries (Santagata et al., 2006).

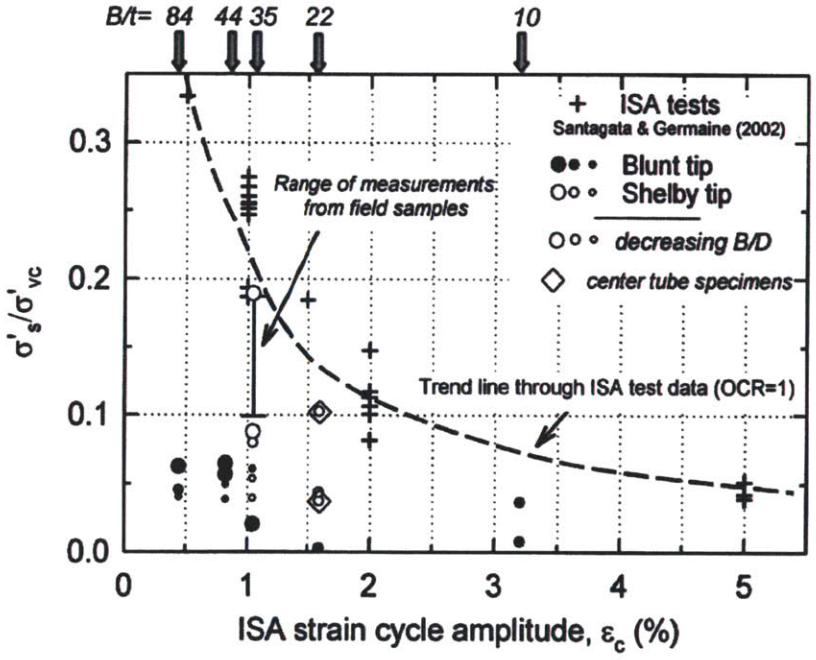

Figure 5.31: The ISA lab sampling effective stress versus field data from South Boston site (Santagata et al., 2006).

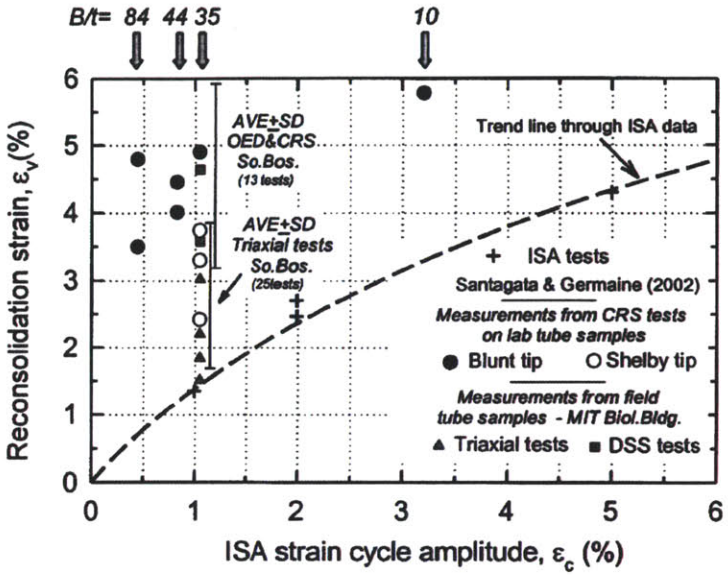

Figure 5.32: Lab reconsolidation strains from ISA disturbance simulation versus field data (Santagata et al., 2006).

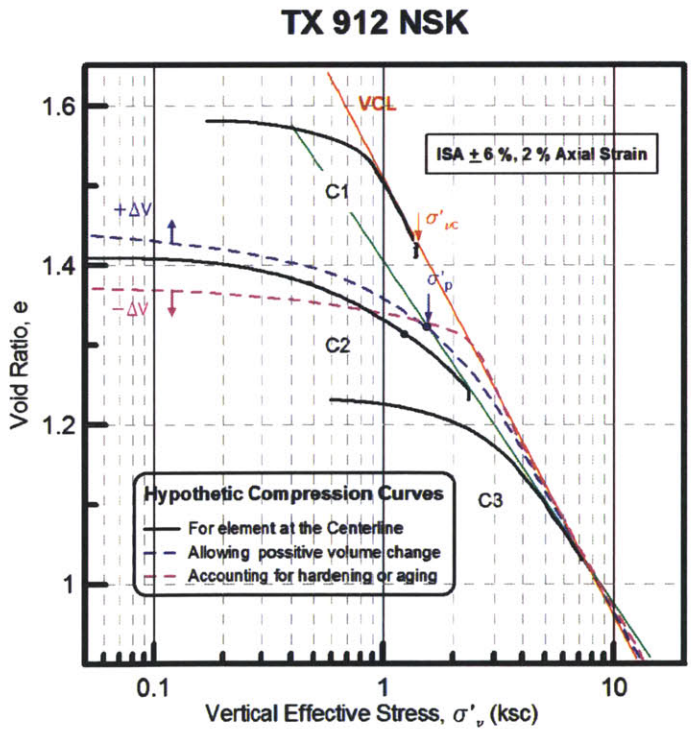

Figure 5.33: Hypothetic compression behavior when allowing for volumetric change to occur after disturbance.

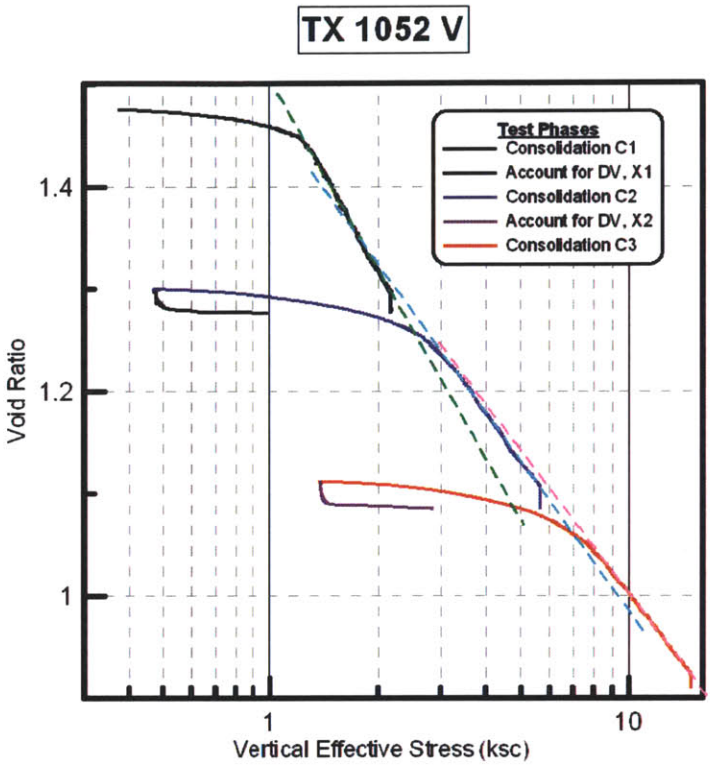

Figure 5.34: A typical CK_0UC test of RSFBM accounting for Volumetric Changes after disturbance.

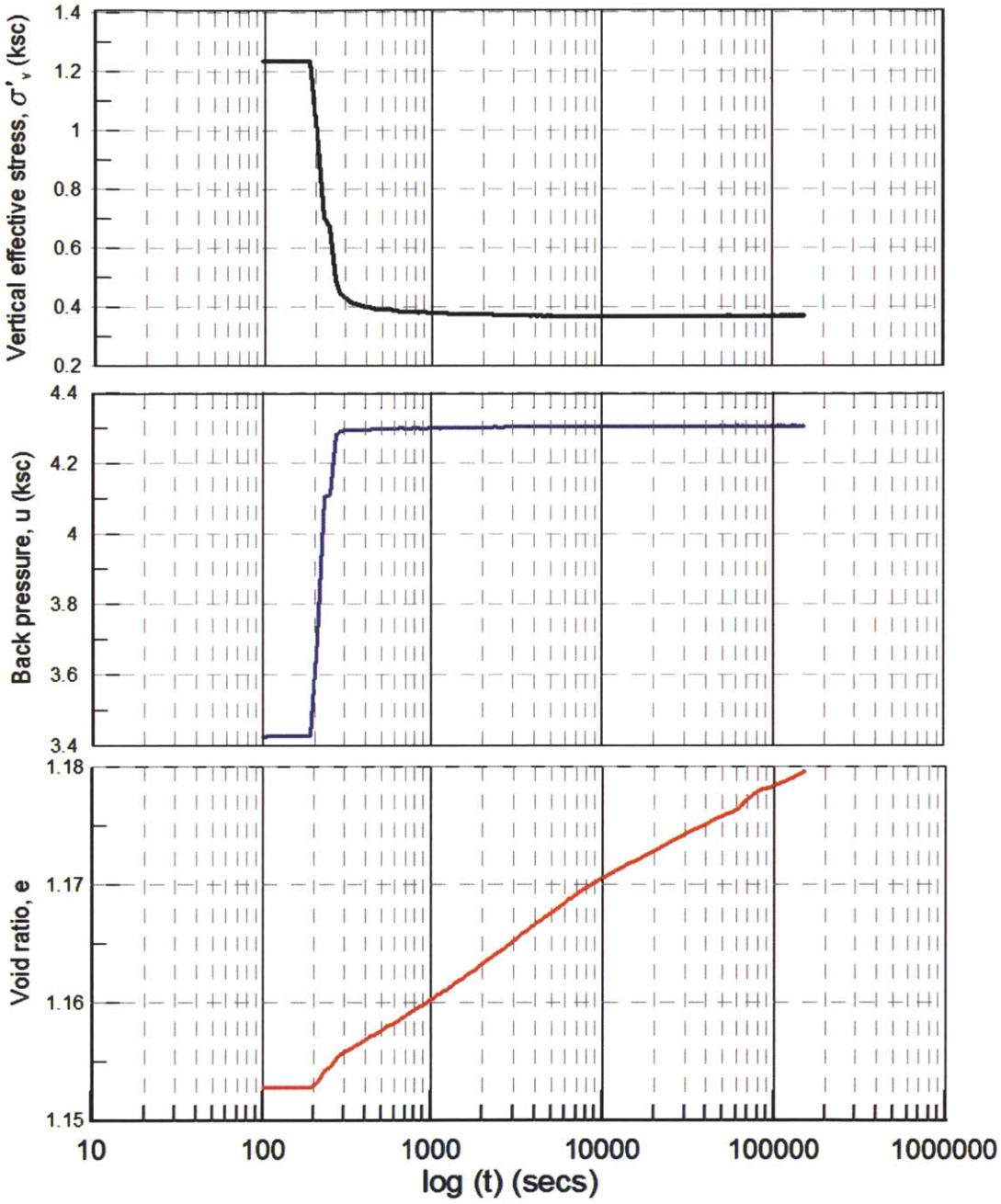

Figure 5.35: The effect of swelling during time for the vertical effective stress, the pore pressure and the void ratio. From TX 1058 on RSFBM (initial ISA±3.5%).

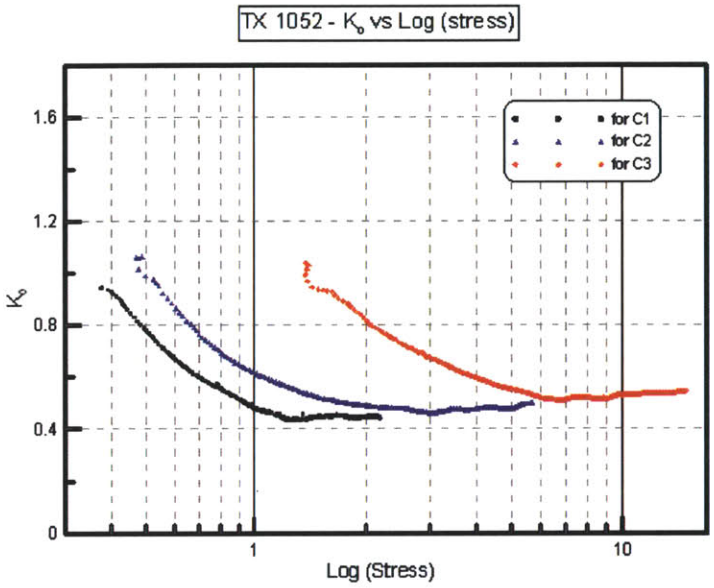

Figure 5.36: Lateral Stress Ratio vs. Vertical Effective Stress during K_0 – consolidation of RSFBM (TX 1052).

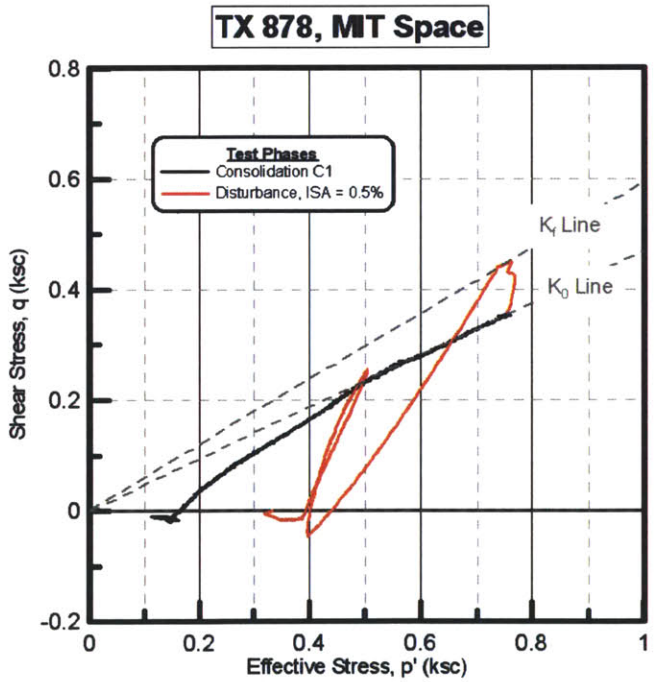

Figure 5.37: The effective stress path of an NC RSFBM specimen for the K_0 consolidation and disturbance simulation phase.

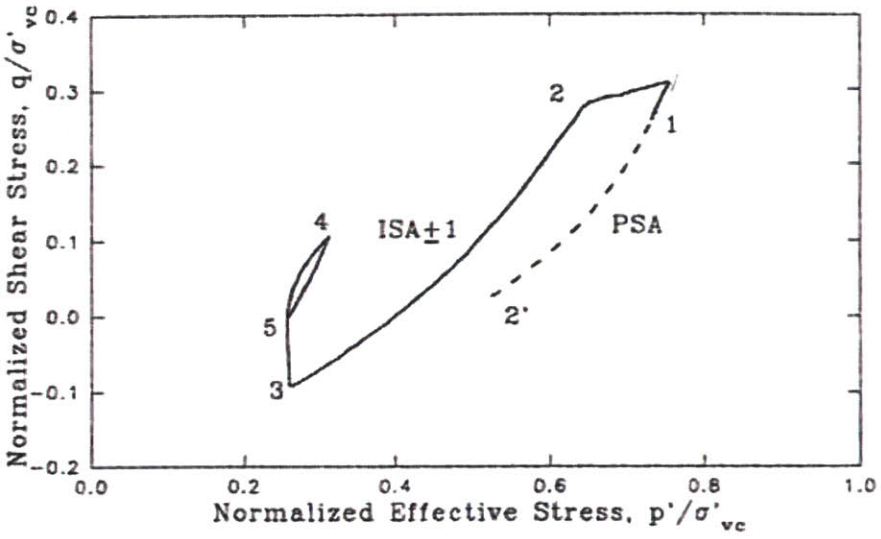

Figure 5.38: The effective stress path during ISA and PSA disturbance simulation for RBBC (Santagata and Germaine, 1994).

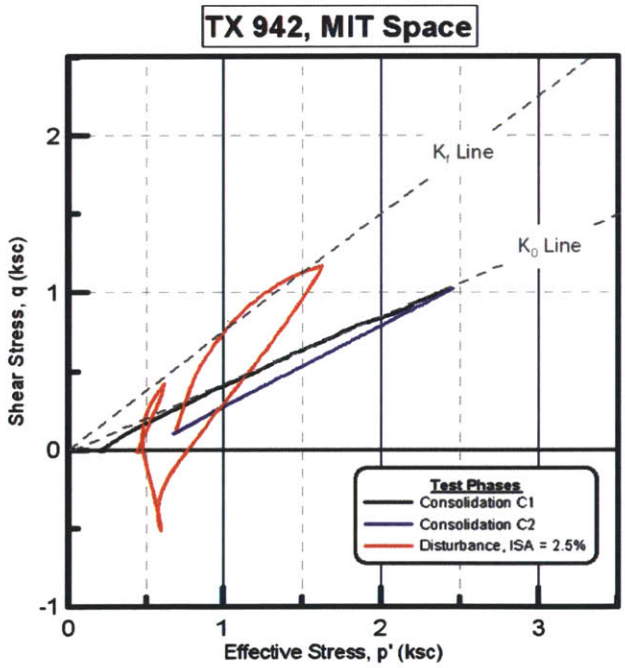

Figure 5.39: The effective stress path of an OC RSFBM specimen for the K_0 consolidation, unload and disturbance simulation phase.

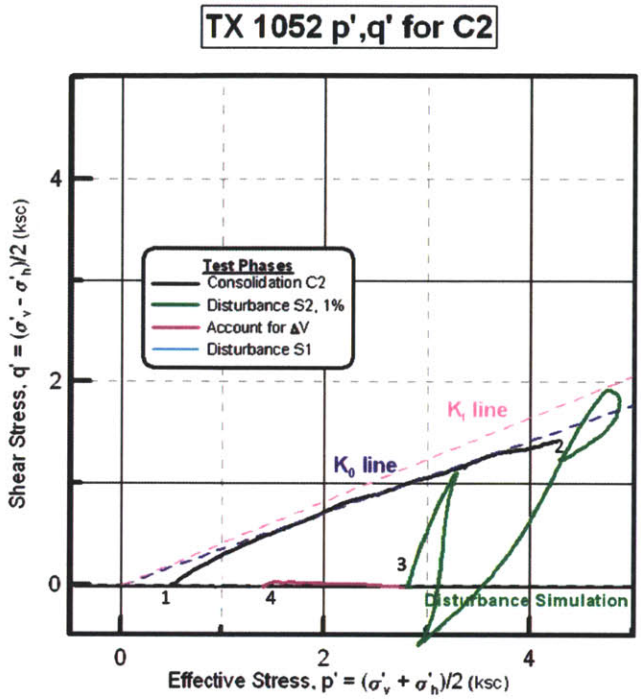

Figure 5.40: The effective stress path of an NC RSFBM specimen for the K_0 consolidation, disturbance simulation and account for ΔV phase.

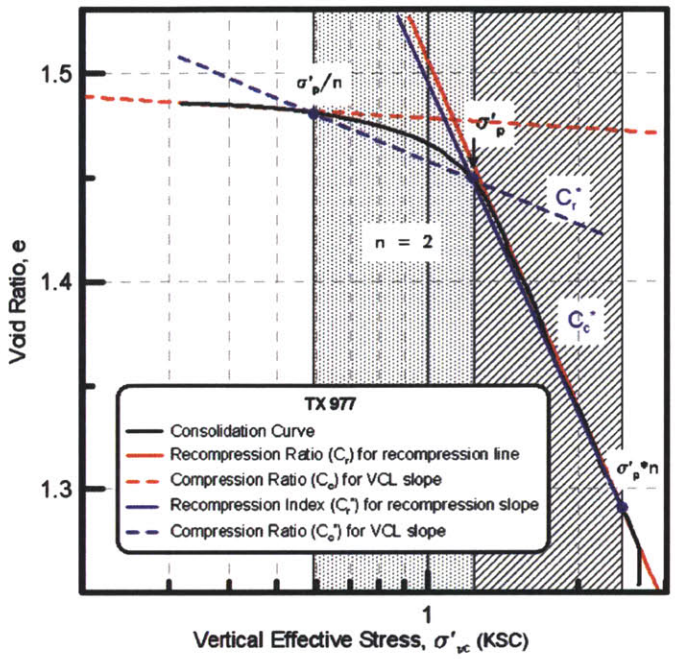

Figure 5.41: Compression and Recompression Ratio vs. Compression and Recompression Indices.

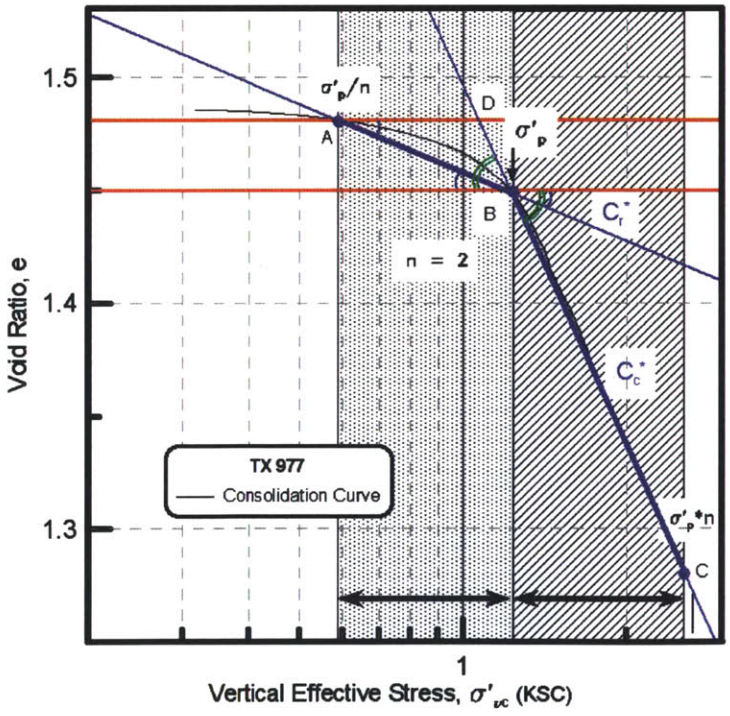

Figure 5.42: Calculating Compression and Recompression Indexes for C1 consolidation curve (TX 977).

Chapter 6 INTERPRETATION OF RESULTS

6.1 Introduction

This chapter analyzes and interprets the results from the series of triaxial tests performed to investigate the effects of disturbance on preconsolidation pressure for Resedimented San Francisco Bay Mud (RSFBM). It complements Chapter 5 and will provide useful results on the effects of ISA disturbance on Normally Consolidated (NC) and low Overconsolidated (OC) SFBM specimens. The effects of stress level and the effects of swelling after disturbance will be discussed.

In parallel, investigating the effects of disturbance on preconsolidation pressure, some strong stress dependences were noticed in the behavior of SFBM specimens. Section 6.2 presents how stress level affects the engineering properties of the specimens. This will help the reader understand the engineering behavior of the examined soil and how disturbance influences this behavior at different stress levels. Section 6.3 introduces the implementation of ISA on different OCR specimens and different stress levels. The effects of these two parameters on the shape of the disturbance simulation circle and the alterations they cause to the recompression behavior are discussed. Section 6.4 presents the change in lateral stress ratio, K_0, and how this influences the undrained strength. The undrained strength is connected to the strain at failure for different OCR, stress level and disturbance amplitudes. Section 6.5 quantifies the main effects of disturbance. The loss of effective stress is analyzed for specimens of different disturbance and OCR. The normalized preconsolidation pressure is calculated for each recompression curve after imposing the disturbance. Specimen Quality Designation, (SQD, after Lunne et al. 1997) is used as a qualitative, "rule of thumb" method in order to draw initial conclusions in specimen quality. Tube SFBM specimens and resedimented material are used in order to investigate the effects of disturbance on preconsolidation pressure. Finally, section 6.6 presents the test results for Recompression Index, C_r^* and Compression Index, C_c^* versus disturbance amplitude. A new method to quantify disturbance based simply on the shape of the compression curve is proposed. The method is based on the generally accepted observation that "increasing disturbance causes more rounded compression curves".

6.2 Effect of stress level on the consolidation curve and the undrained shear strength

This research program consists of two main phases. The initial phase involves running disturbance simulation triaxial tests on tube samples of SFBM. A summary table of this phase was presented on table 6.1, 6.2 and 6.3. For every test and each consolidation phase, the following information is defined:

- The imposed ISA amplitude, ε_a (%)
- The preconsolidation pressure, σ'_p, as it is calculated using to the Strain Energy Method in chapter 5. The best estimate preconsolidation pressure value is reported for every consolidation phase of each TX test.
- The previous maximum effective stresses, σ'_{vc} and σ'_{vcm}. The first one is the vertical effective stress as measured in the lab at the end of K_0 consolidation. The second is the vertical consolidation stress corresponding to the Virgin Compression Line (VCL) for e_{max} at the end of secondary compression, and after holding stress for 12 to 24 hours (figure 6.1).
- The sampling effective stress, σ'_s at the beginning of each consolidation phase.
- The loss of effective stress, $\Delta\sigma'$ is measured as the difference between the maximum vertical effective stress, σ'_{vcm}, on the pre-disturbance K_0-consolidation phase and the sampling effective stress, σ'_s, of the next recompression phase.
- The normalized loss of effective stress, $\Delta\sigma'/\sigma'_{vcm}$ and the normalized preconsolidation stress, σ'_p/σ'_{vcm}.

- The void ratio, e, is defined at the initial sampling effective stress (σ'_s), on the preconsolidation pressure (σ'_p) and at the maximum vertical consolidation stress (σ'_{vcm} or σ'_{vc}). For simplicity are not reported in the tables.
- The compression and recompression indices are calculated based on chapter 5.7 and figure 5.41. The method presented is using a constant, n = 2, to calculate the points of interest on the compression curve before and after the preconsolidation pressure.

Figure 6.1 presents the initial K_0-consolidation for triaxial test TX 955 in a void ratio – log stress space. It is a typical example of how the maximum vertical effective stress is calculated based on the interpreted VCL equation and the minimum void ratio at the end of the secondary compression (12 – 24 hours of hold stress). This value, σ'_{vcm}, is the calculated stress on log fitted line for VCL data points, and has a void ratio e_{min}. This vertical effective stress, σ'_{vcm}, is used in order to normalize and compare all different specimen parameters and effects of disturbance. From now onwards, when throughout this interpretation the writer refers to the calculation of the previous maximum effective stress or normalized values are calculated, the vertical consolidation stress used is σ'_{vcm} and not σ'_{vc}. This applies to all SFBM properties except the undrained shear strength, q, which is always normalized to σ'_{vc}. In many cases, when the consolidation phases are over a wide range of stresses, the definition of VCL slope is not straight forward. These are cases where, because of increasing stress, the VCL has a concave up shape rather than a straight line shape. This, for RSFBM, is more obvious when the change of void ratio is about 0.1 or more. A typical example of a concave up VCL shape is presented in figure 6.2. The interpreted VCL for low and high stresses for this compression curve are:

VCL_1: $e = - 0.4158 \log (\sigma'_v) + 1.3578$, $r^2 = 0.9991$, for $\sigma'_v = 17 – 24$ ksc

&

VCL_2: $e = - 0.3733 \log (\sigma'_v) + 1.3003$, $r^2 = 0.9996$, for $\sigma'_v = 24 – 31$ ksc

Both curves are based on around 250 data points which would correspond to 12.5 hours of consolidation data when taking readings every 3 mins. When increasing the vertical consolidation stress from 20 to 28 ksc the change of VCL slope is 0.0425. In cases where a concave up consolidation curve is obvious only the end consolidation, data are used to calculate the maximum vertical effective stress σ'_{vcm} (for the example of high pressure TX 1087, VCL_2 is used).

Figure 6.3 plots the decrease in the normalized undrained strength, caused by increasing vertical consolidation stress, σ'_{vcm}. The data presented here are from the ISA disturbance simulation on NC resedimented SFBM from the homogeneous batch of soil created for this research. The relationship is consistent among the disturbance simulation circles at different

stress level on the same specimen, and among multiple RSFBM specimens of different imposed ISA disturbance amplitudes. As already mentioned in Chapter 5, increasing the vertical consolidation curve causes more ductile undrained response, a decrease in the undrained peak strength, a small increase in the strain at peak shear and a loss of strain softening. Some scattering of data for relatively low vertical consolidation stresses is observed mainly due to the different lateral stress ratios, K_0. Secondary, these differences maybe caused by small differences on the initial strain rate imposed during the ISA simulation; the strain rate was initially controlled manually and slowly increased from zero until it passed the peak undrained strength where it was set to be 0.5%/hour for the rest of the disturbance simulation circle. For the high pressure apparatus, the undrained strength is calculated to be as low as 0.3 for a vertical consolidation stress of 30 ksc. The observations on the high pressure cell agree with the general trend of the decreasing normalized undrained shear stress with an increase on the vertical consolidation stress.

6.3 Effect of OCR on the ISA disturbance and the undrained shear strength

A clear relationship for the normalized undrained strength can also be defined versus the overconsolidation ratio for the RSFBM specimens. This relationship is close to previous observations on BBC specimens. The relationship for RSFBM specimens is presented in figure 6.4 and is found to be:

$$s_u/\sigma'_{vc} = 0.381 \cdot (OCR)^{0.787}$$

The equivalent relationship for BBC is after Abdulhadi &Germaine, 2009.

$$s_u/\sigma'_{vc} = 0.296 \cdot (OCR)^{0.741}$$

This equation is valid for resedimented specimens of SFBM and an ISA disturbance of 1% or more. For ISA = 0.5% although the trend is similar to the imposed axial strain is not

enough to mobilize the maximum undrained strength. So, the maximum normalized undrained shear strength in these cases is less than the one calculated from the above equation for the equivalent OCR. Figure 6.5 plots the ISA disturbance circle (0.5% axial strain) versus the axial strain for both tube and resedimented SFBM specimens. As in Chapter 5, the increase in strength is obvious with increasing OCR even in this very low disturbance simulation amplitude. Also, there is a noted difference in the undrained shear strength between the tube specimen (s_u/σ'_{vc} = 0.35) and the resedimented specimen (s_u/σ'_{vc} = 0.4). This is true for most of the parallel tests run in this research program from intact and resedimented material, for increasing ISA disturbance amplitude. The difference is attributed to the soil structure of each specimen and the variation on initial void ratios; for the intact specimens the average initial void ratio is about e_0 = 0.89 (w_c = 31%) and for the resedimented specimens is e_0 = 1.53 (w_c = 54%).

6.4 Effect of lateral stress ratio K_0 on the ISA disturbance and the undrained shear strength

Lateral stress ratio is found to be dependent on the vertical consolidation stress, σ'_{vc}. The variation in the lateral stress ratio, K_0, with increasing vertical consolidation stress is presented in figure 6.6 for the majority of resedimented triaxial tests. This variation in K_0 seems to be directly connected to the differences on normalized undrained strength, s_u/σ'_{vc} observed with stress level. Especially in low stresses, the same variability that was noted in figure 6.3 for undrained strength is also observed here. Lateral stress ratio seems to increase logarithmically while increasing the vertical consolidation strength. Figure 6.6 presents the tests run in the low pressure apparatus. A linear fit is calculated for the majority of data points on NC RSFBM. It also presents the lateral stress ratio, K_0 of triaxial tests accounting for swelling after the ISA disturbance simulations. For these tests, an increased K_0 value is observed (green, triangle data points). This may have its roots in the fact that in order to impose a certain volumetric change (ΔV), the pore pressure of the specimen is increased by a certain value, $\Delta\sigma'$. Knowing that $K_0 = \sigma'_h / \sigma'_v$, increasing the vertical and horizontal stress by the same value, $\Delta\sigma'$ will always result in a higher lateral stress ratio value, $K_0' = (\sigma'_h + \Delta\sigma') / (\sigma'_v + \Delta\sigma')$. The linear relationship in figure 6.6 describing the

lateral stress ratio, K_0 versus the vertical consolidation stress for normally consolidated RSFBM specimens on the low pressure apparatus, is calculated to be:

$$K_0 = 0.4064 + 0.0053 \cdot \sigma'_{vc}\ ,\ r^2 = 0.583$$

where σ'_{vc} is on ksc.

Figure 6.7 presents the combined data from the low pressure and high pressure MIT triaxial cells. Here, it is clear that the increase in Lateral stress ratio, K_0, versus the vertical consolidation stress σ'_{vc} is logarithmic rather than linear. The interpreted fitted line is:

$$K_0 = 0.0862 \cdot \log(\sigma'_{vc}) + 0.395\ ,$$

$r^2 = 0.640$, for both low and high pressure RSFBM tests.

Based on the previous stress level dependencies, a clear relationship is defined between the lateral strength ratio, K_0, and the normalized undrained strength, s_u/σ'_{vc}. Data for normally consolidated (NC) specimens of RSFBM (black trend line) and data for resedimented BBC (red trend line) are presented on figure 6.8. Both materials follow the same trend; increasing the Lateral stress ratio, K_0, results in a lower undrained strength ratio. The undrained strength ratio of RSFBM is about 0.4 for low Lateral stress ratio of about 0.35 and decreases to 0.3 for a Lateral stress ratio as high as 0.55. It is also noted that the change in K_0 for RSFBM specimens has less influence on the undrained shear strength ratio of the specimens than that of BBC specimens. The equation for RSFBM is calculated through the majority of the NC specimens tested during this research program which are presented in table 5.2, and though the different consolidation phases for each test (C_1, C_2, and C_3). Data from high pressure triaxial apparatus are in agreement with the interpreted line (blue diamond data points):

$$s_u/\sigma'_{vc} = 0.584 - 0.512 \cdot K_0$$

For RBBC, the equivalent relationship was found to be (Abdulhadi &Germaine, 2009):

$$^{s_u}/_{\sigma'_{vc}} = 0.84 - 1.01 \cdot K_0$$

where K_0 is the Lateral stress ratio calculated as the average lateral stress ratio value during hold stress and secondary compression, at the end of each consolidation phase (12 to 24 hours).

6.4.1 The ISA disturbance and the strain at failure

The vertical consolidation stress, overconsolidation ratio and lateral stress ratio, have at the same time a direct impact to the strain at failure. In general, high values of normalized undrained strength are coupled with low strains at failure. This would correspond to a brittle and sudden loss of shear strength of the soil. It is also expected to cause significant strain softening at large strains (>10%). Such behavior is normally observed on NC, high quality samples (i.e. block samples).

On the contrary, the low undrained shear strength is coupled with higher strains at failure. When increasing disturbance, OCR or, to some extent, vertical consolidation stress, the undrained response of the specimen becomes ductile. This means that more strain is required to mobilize the peak shear strength and after that, the strain softening is much less apparent. Such behavior is expected at high consolidation stresses, or from low quality, or high OCR samples.

To verify the above, the normalized undrained strength (s_u/σ'_{vc}) is plotted versus the strain at failure (ε_f %) for RSFBM specimens in figure 6.9. At this figure, only selected results from the NC specimens are plotted. The results in the figure are representative of the general trend noted for NC RSFBM specimens. The dots are numbered with 1 if they belong to a first disturbance simulation phase and with 2 if they belong to a second disturbance simulation phase. Disturbance simulation phases that belong to the same triaxial test are connected with a straight line. In the middle of each line, in blue color, the amplitude of the ISA simulation is noted. For the tests described in the figure, a maximum undrained strength of 0.43 and a minimum of 0.33 are calculated. The strain at failure did not exceed 0.5% even when imposing extremely large disturbance simulation amplitudes. The maximum values of s_u/σ'_{vc} are observed for a strain at failure around 0.225%. For the high pressure triaxial cell, the calculated strains at failure were, as expected higher; 0.75 and 1.54 with an undrained strength of 0.31 and 0.29 respectively. The

data presented confirm that strain at failure increases while normalized undrained strength ratio decreases. It can also be seen that in most cases, the second ISA simulation results in a lower undrained strength and a higher strain at failure. There is no clear relationship between the disturbance simulation amplitude and the extent of this change on the undrained strength or the strain at failure. So, this noticed difference, from the first to the second disturbance circle, can be attributed to the change in the vertical consolidation stress (stress level effect). If the first imposed disturbance has an effect on the second imposed disturbance, it would mean that consolidating well into the VCL, well passing the preconsolidation pressure - is not actually erasing all the effects of disturbance. Thus would be opposite to the fundamentals of SHANSHEP reconsolidation technique.

In order to better understand why a more ductile response is observed on a latter disturbance simulation phase the same data were plotted on a strain at failure (ε_f %) - vertical consolidation stress (σ'_{vc}) space. Figure 6.10 presents the strain at failure increase with increasing the vertical consolidation stress. A better estimate, polynomial curve is drawn over the data corresponding to the 1st disturbance simulation circle (black dotted line) and over the 2nd disturbance simulation circle (red dotted line). It should be noted that the second ISA disturbance is performed at greater stresses, so the two lines are similar, but the one corresponding to the 2nd disturbance simulation data points is shifted to the right. This suggests that reconsolidation does not completely erase the effects of the previous disturbance cycle.

Figure 6.11 plots the disturbance simulation amplitude (ε_a %) versus the strain at failure. This illustrates how the overconsolidation ratio (OCR) influences the ISA imposed. Round data points (black dots) stand for NC RSFBM specimens, triangle data points (blue color) stand for specimens unloaded to an OCR of 2, and diamond data points (red color) represent specimens unloaded to an OCR of 4. From the figure, it can be seen that for NC or low OCR specimens the strain at failure is around 0.25, while it remains constant when the disturbance circle amplitude, ε_a %, is increased (a weak trend is observed only with increasing vertical consolidation stress). For an OCR of 2, the peak shear strength can be mobilized only when applying a disturbance simulation greater than 1% axial strain. When doing so, the strain at failure is constant with ISA disturbance amplitude, ε_a %, and about 1 to 1.2%. For disturbance simulation circles of less than 1%, the strain is not enough to mobilize the peak strength. In this case, the effects of disturbance

are expected to be much less significant. For an OCR of 4 (red diamond and inverse triangle symbols), it can be seen that the maximum strain at failure increases with disturbance amplitude following a 1:1 straight line. This means that up to 4 to 4.5% strain, the specimen has not reached its maximum shear strength (reverse triangle data points). The undrained shear stress would monotonically increase up to the maximum applied disturbance amplitudes. The effect of disturbance for an OCR of 4 and for disturbance simulation circles up to 4 to 4.5% strain would be less significant. This will also be verified from the effects of disturbance on the consolidation curve and preconsolidation pressure for high OCR RSFBM specimens. Only for disturbance amplitudes more than 5% strain, the ISA mobilizes the peak shear stress (diamond red data points).

6.4.2 Observations on the imposed ISA disturbance simulation cycles

To sum up, the following effects were observed as far as the normalized undrained strength (s_u/σ'_{vc}) is concerned:

- It decreases with increasing vertical consolidation stress, σ'_{vc}. This decrease is coupled with the change of K_0 with stress level. One should look on both the effects of stress level and Lateral stress ratio to come up with a good approximation of the normalized undrained shear strength.

- It decreases when the lateral stress ratio, K_0, increases. The K_0 is defined from the previous consolidation step and increases with increasing the stress level. A direct linear relationship can be defined with accuracy between the two parameters, K_0 and σ_u/σ'_{vc}. The strength vs. K_0 correlation is stronger than the strength vs. stress correlation which implies that the strength is controlled by K_0.

- It increases when the OCR value increases. A SHANSEP equation applies to RSFBM specimens. In this research program, the parameters S and m in SHANSEP equation were defined to be 0.381 and 0.787 respectively.

- When the normalized undrained strength decreases, an increase on the strain at failure is expected.

- Strain at failure increases when the vertical consolidation stress increases.

- Strain at failure increases when the OCR increases. For OCR ≥ 4, the strain at failure equals the disturbance simulation amplitude. This limits the maximum vertical consolidation strength s_u/σ'_{vc}, and minimizes the effects of disturbance.

6.5.1 Effect of disturbance on preconsolidation pressure for tube SFBM specimens

The main topic of this research is to investigate the effects of disturbance on preconsolidation pressure, σ'_p. Figure 6.12 plots the normalized loss on effective stress, $\Delta\sigma'/\sigma'_{vcm}$, for a given disturbance simulation circle, ε_a %. Figure 6.13 presents the normalized preconsolidation pressure (σ'_p/σ'_{vcm}) versus the normalized loss at effective stress ($\Delta\sigma'/\sigma'_{vcm}$). Both parameters σ'_p and $\Delta\sigma'$ are normalized to interpreted maximum vertical consolidation stress on the VCL curve, as calculated using the procedure presented in figure 6.1. The grey dots in both diagrams correspond to specimens of SFBM from tubes with similar depth and location as those used to produce the homogeneous soil batch for resedimentation. The purple dots correspond to resedimented material created by a single tube while the yellow, triangle data points correspond to resedimented material created by a single tube and unloaded to an OCR of 4. These tests were the incentive to produce the systematic study and lead to the analysis of the results using the homogeneous batch of soil. Also, during these initial resedimented tests, the resedimentation procedures were refined (the pulverization, the mixing with water to a slurry and the consolidation process).

From the results using tube SFBM samples, few clear but very important results are concluded relatively to sample disturbance. Starting with the diagram in figure 6.12, it can be seen that the increase in disturbance can always be associated with an increase in the loss of the normalized effective stresses. As this loss of stress increase, the sampling effective stress, σ'_s, decreases. For the NC tube specimens (grey dots) and low disturbance simulation amplitudes

(0.5%) this loss increases logarithmically and varies from around 0.68 to 1. For the tube specimens of SFBM and disturbance more than 3% amplitude, the loss of the normalized effective stress is up to 0.97%. In order to do a first comparison between the effects of disturbance on NC tube specimens of SFBM and on resedimented material, four tests were run applying different ISA disturbance circles and using resedimented material from single tubes. Results indicate that the loss at effective stress at the case of RSFBM were slightly less significant; the normalized loss of effective stress for a low disturbance amplitude (0.5%) on RSFBM is almost the same as for intact specimens, 0.69. However, it increases less with increasing disturbance, following again a logarithmical line up to about 0.92 for disturbance simulation circle of 6% or more.

The author believes that the difference on the effects of disturbance can be attributed to the fact that during the resedimentation process the soil specimens end up to have a much more simple and homogeneous structure than that of specimens from the tubes. Having a uniform particle arrangement, the specimens would be less prompt to disturbance. The material created would have a more ductile response than how it behaves "in situ". As a result, greater ISA amplitudes would be needed to mobilize a given amount of loss of effective stresses. Three more test were performed using resedimented material but now unloading to an OCR of 4 before the ISA disturbance. Results show that, for these OCR specimens, a new logarithmic curve could be drawn, corresponding to even lower normalized loss at effective stresses. The $\Delta\sigma'/\sigma'_{vcm}$ in this case started as low as 0.1 for an ISA disturbance of 1.5% and went up to 0.7 for an ISA of 5.5% strain.

Figure 6.13 shows the Preconsolidation Pressure, σ'_p/σ'_{vcm}, versus the Normalized Loss of Effective Stress, $\Delta\sigma'/\sigma'_{vcm}$, for intact NC SFBM and resedimented NC and OCR 4 tube specimens of SFBM. From the NC tube specimens, it can be seen that as the loss at effective stress increases, the scatter of data significantly increases. This means that for highly disturbed samples (loss of effective stress more than 0.9), defining preconsolidation pressure with accuracy becomes not a trivial problem. In most cases where there was a distinct decrease in the VCL slope, the preconsolidation pressure ended up to be less than 1. For cases where there was a considerable loss of effective stress and the decrease in the VCL was not that significant (e.g. one could get a unique VCL between the compression and recompression phase), the normalized preconsolidation pressure value would be even greater than that of 1 or 1.1. This contradicts the

general idea that increasing disturbance will always cause a decrease in the preconsolidation pressure value. It seems that, with medium sensitivity clays (such as SFBM or BBC), the value of preconsolidation pressure depends on the two mechanisms that act on the compression curve, as they are proposed by Santagata and Germaine (2006): the loss of effective stress and the change in the VCL slope. When the first is more eminent, the preconsolidation value is overpredicted ($\sigma'_p/\sigma'_{vm} \geq 1$). When the change of VCL slope is more eminent, then the preconsolidation pressure is underpredicted ($\sigma'_p/\sigma'_{vm} \leq 1$).

For the resedimented material from a single tube and an OCR of 4 tests, the reduction of effective stresses is much less significant and so, the preconsolidation pressure value would always be about 1, independently of disturbance.

6.5.2 Effect of disturbance on preconsolidation pressure for resedimented SFBM batch specimens

In a more systematic pattern, resedimented material of SFBM from a homogeneous batch of soil was used to better understand and quantify the effects of disturbance on preconsolidation pressure and compressibility parameters. The main results of this research are presented on figures 6.14 to 6.20.

Initially the normalized loss of effective stress is plotted versus the disturbance simulation amplitude in figure 6.14. The normally consolidated specimens are marked as black dots in this figure. These are data where, disturbance simulation was directly applied after the each K_0 consolidation phase. When imposing ISA of 0.5% axial strain, the normalized loss of effective stress is up to 0.69, while for ISA of up to 6% axial strain, the normalized loss of effective stress is about 0.96. Triaxial tests with simulation of ISA disturbance were also run for overconsolidated, resedimented SFBM specimens. In these cases, specimens are K_0 consolidated to a specific stress and then unloaded to the desired OCR (of 2 or 4). After that, the disturbance simulation circle is imposed. The triangle blue color data correspond to an OCR of 2 and the red, diamond data correspond to an OCR of 4. Clearly, increases the OCR will decrease the normalized loss of effective stress imposed by a certain amount of disturbance. For a small level of axial strain (0.5%) and an OCR of 2, the loss of effective stress is about 0.3. The value

increases logarithmically to about 0.8 and for an ISA of 5% or more. For an OCR of 4 and ISA of 0.5 the loss of effective stress is about 0.1 and increases with increasing disturbance up to 0.7 for ISA of 5% axial strain. When investigating the effect of disturbance on the loss of effective stresses, some stress dependencies were observed. In most tests, ISA disturbance was constant for all three disturbance simulation circles (S_1, S_2 and S_3). So, for every test, up to two or three different data points on the same ISA disturbance, but at a different consolidation stress level can be introduced. In general, the higher values of normalized loss of effective stress correspond to the first ISA disturbance simulation - lower vertical consolidation stress – while, the data points below, correspond to the second ISA imposed on higher consolidation stress. Data show that one could draw contours parallel to the logarithmic lines for NC, OCR of 2 and OCR of 4, that would relate to different consolidation stress level (grey doted lines). In general, low consolidation stress (of about 1 ksc) would shift the curve up, while increasing stress would shift the curve down (e.g. 20 ksc or more).

Figure 6.15 presents the normalized total loss of effective stress ($\Delta\sigma'/\sigma'_{vcm}$) versus the disturbance simulation circle (ε_a %). The total loss of effective stress is measured as the reduction of effective stress from the end of the NC previous K_0 consolidation phase to the start of the new recompression phase. This means that for an OCR specimen would both include the reduction of effective stresses due to the unloading to the specific OCR and the disturbance cycle. In the case of accounting for swelling the reduction of the effective stress due to ISA disturbance and due to allowing for swelling are also included. A clear trend is revealed. ISA disturbance is uniquely matched to a certain amount of loss of effective stress. When some other causes have already been taken away some of the possible loss of effective stress, such as unloading to a specific OCR, then disturbance would cause such a reduction on effective stress to match a value close to this of an NC soils (or the total loss of effective stress for the specific disturbance simulation circle as it can be calculated in figure 6.15). A small increase on the total loss of normalized effective stress is expected with OCR. This can be justified from the fact that, when OCR increases, the imposed disturbance happens at slightly lower stress. So, the total loss of effective stress is expected to be on a line slightly higher to that of the NC specimens (e.g. for a disturbance simulation circle of 0.5% axial strain the NC specimen gives a loss of effective stress of about 0.7, while for an OCR of 4 the total loss is about 0.8). The difference decreases

when disturbance increases while for an ISA circle of 5% axial strain or more, the two values are identical.

In order to verify the findings of this research program, and connect the methods used here to those methods researchers and consultants quantify disturbance, the Specimen Quality Designation method (SQD) is employed. The SQD method is applied as proposed by Lunne et al. (1997); the normalized difference of void ratio is calculated up to the previous maximum effective stress – "in situ stress", σ'_{vc}. For the NC specimens, this relates to the maximum vertical consolidation stress corresponding to the VCL slope. For the OC specimens, the maximum vertical consolidation stress would be the vertical effective stress on hold stress before imposing the ISA simulation. Figure 6.16 presents the SQD for NC, OCR of 2 and OCR of 4 RSFBM specimens versus the disturbance circle amplitude, ε %. For NC specimens, as disturbance simulation amplitude varies from 0.5% to 2% axial strain, a SQD of 1, excellent quality samples is calculated. For ISA circle up to about 5.5% axial strain, the specimens fall into the 2 category, very good sample quality category. Above that, when an ISA disturbance circle of 6% axial strain or more is imposed, specimens are characterized as fair to good, 3 category. For an OCR of 2 or an OCR of 4, all specimens with up to 5% axial strain imposed disturbance, are in the excellent specimen quality, 1 category.

Figure 6.17 presents the SQD versus the disturbance simulation amplitude (ε %), but now the change in void ratio is calculated up to the maximum vertical consolidation stress of the K_0 consolidation to the VCL (instead of the vertical consolidation stress after unloading to the specific OCR). Of course, for the NC specimens the two diagrams would be exactly the same. For the OC specimens, there would be a difference. In this case, OCR of 2 specimens have a SQD of 1 for ISA disturbance of 0.5% axial strain. On the ISA disturbance increase up to 5% axial strain, specimens follow an almost linear increase to a maximum SQD of 6.5 corresponding to 3 category, fair category specimen. For an OCR of 4 and for ISA of 0.5% a SQD of about 0.2 or less is observed. This value also increases when disturbance increases, and it is almost linear in its relationship and reaches to an SQD of 5.5, for an ISA disturbance amplitude of 5% axial strain. This would again give specimens starting from 1, excellent category, up to 3, fair category samples. It must be noted that for OC specimens, the limits between the SQD categories are slightly different to those of the NC case. In figure 6.16 the SQD categories are marked based on the NC soil limits, while in figure 6.17 the limits are marked for the case of OC specimens. The

SQD as it is calculated in figure 6.17 leads to 3 lines for NC, OC of 2 and OCR of 4 specimens, almost parallel to each other. NC specimens appear to have the greatest calculated SQD. Then the SQD decreases with increasing OCR; thus, the effects of disturbance are less eminent with increasing the OCR. The difference between OC data point in the figure 6.16 and 6.17 corresponds to the change in void ratio Δe that is caused due to the unload of specimen to a specific OCR.

As previously stated, a major focus of this research is to investigate the effects of disturbance at preconsolidation pressure. Figure 6.18 presents the normalized preconsolidation pressure (σ'_p/σ_{vcm}) versus the disturbance simulation amplitude, ε_a %. The data are from the resedimented homogeneous batch that was created for the main phase of the research. Data on black color correspond to the NC specimens, where disturbance is imposed after the K_0-consolidation phase. Surprisingly, for ISA simulation amplitudes from 0.5 to up to 5% axial strain, the value of the normalized preconsolidation pressure remains constant and slightly above 1 (around 1.05 to 1.1). For larger disturbance simulations ($\varepsilon > 5\%$) where the destructuring, as expressed by the change in the VCL slope, is the dominant mechanism, the preconsolidation value is in general underestimated. For example, for an ISA of 6%, the normalized preconsolidation pressure for a NC RSFBM is about 0.78. Almost same behavior is observed for specimens with an OCR = 2. The normalized preconsolidation pressure value is constant with disturbance and up to about 4% axial strain. It is clear, even for NC or OCR of 2, that increasing disturbance makes the estimation of preconsolidation pressure more difficult.

Moving to specimens of OCR = 4 (blue, triangle data points) and imposing disturbance simulations up to 5% axial strains, added significantly on the understanding of how the mechanisms that influence the value of preconsolidation pressure work. Firstly, increasing OCR to 4, disturbance up to 5% axial strain seems to have almost no effect on σ'_p. However, there is an overall small decrease in the average value of preconsolidation pressure, σ'_p, for overconsolidated specimens in comparison to the NC or even OCR = 2 specimens; the normalized preconsolidation pressure, σ'_p/σ'_{cvm}, for the average of data points is 0.99. Coming back to Santagata and Germaine's conceptual model, this can be explained as follows; for OC specimens there is a relatively small change in loss of effective stress even when large disturbance simulations amplitudes are applied (in most cases for an OCR of 4, the specimen is not sheared to failure during ISA disturbance simulation). Therefore, the decrease in the VCL

slope is the main mechanism to define the actual value of preconsolidation pressure. Increasing disturbance causes a decrease of VCL slope, which, even though small compared to decrease of VCL slope for NC specimens, causes the calculated value of preconsolidation pressure to slightly decrease. Overall, it should be made clear that disturbance seems to have no clear effect on the value of preconsolidation pressure, unless imposed disturbance amplitudes are relatively large (more than 5% axial strain). Especially for overconsolidated specimens of OCR = 4, disturbance effects are negligible even for high disturbance amplitudes. Judging on the results of the overall data, it can be said that disturbance increases the ambiguity of the value of preconsolidation pressure, and objective estimates become more challenging.

Figure 6.19 presents the normalized preconsolidation pressure (σ'_p/σ'_{vcm}) for increasing loss of effective stress ($\Delta\sigma'/\sigma'_{vcm}$). This figure shows the effect of loss in effective stress in preconsolidation pressure more clearly. For high OCR specimens (red, diamond data, OCR = 4) the loss of effective stress is minimum and the majority of data are on the left hand side of the graph ($\Delta\sigma'/\sigma'_{vcm}$ = 0 – 0.8). With decreasing OCR, the losses of effective stress from ISA disturbance become greater while the normalized preconsolidation pressure increases. OCR = 2 specimens have $\Delta\sigma'/\sigma'_{vcm}$ = 0.25 to 0.8, while NC specimens have loss of effective stress from 0.69 up to 0.97 with all data points gathered on the right part of the diagram. It is apparent that results of preconsolidation pressure become more systematic when OCR increases. A small decrease in the preconsolidation pressure for higher OCR specimens is also observed. Increasing the loss of effective stress makes the ambiguity of preconsolidation pressure value to increase; for loss of effective stress up to about 0.6, the preconsolidation data are for all tests about 1, where for greater losses the value of preconsolidation pressure can be anything in between 0.78 to 1.2. It is more likely thought that the normalized preconsolidation value is biased to the high side unless the normalized loss of effective stress is very close to 1, for very high ISA disturbance simulations. In such cases the loss of effective stress is more than 0.95, and the VCL slope decreases significantly so the value of σ'_p/σ'_{vcm} is underpredicted.

Figure 6.20 plots the normalized preconsolidation pressure versus the SQD (Lunne et al. 1997) that corresponds to the normalized change in void ratio $\Delta e/e_0$ up to the maximum vertical consolidation stress, σ'_{vcm}. The different zones of SQD (1, 2 and 3 categories) are marked on the plot using the OC specimen limits as they are proposed by Lunne et al. 1997 (1st from 0 to 3%, 2nd from 3rd category to 5% and 3 from 5% or more). Here, it is clear that for NC or low OCR

RSFBM specimens increasing the SQD of the specimens, the margins of the calculated values of preconsolidation pressure increase. Allowing for some volumetric change to occur (+ΔV) always results in low reconsolidation strains or change in void ratio, Δe. These tests also resulted in high values of normalized preconsolidation pressure, σ'_p/σ'_{vcm} (the loss of effective stress is much more significant than the change in VCL slope).

6.6 Effect of disturbance on the shape of the compression curve

A great portion of this research focuses on how the shape of the compression curve changes for different disturbance simulation amplitudes for NC and OC specimens. Using the conventional indices it is clear that subjective judgment is needed especially when calculating the recompression index. The most solid conclusion when dealing with disturbance is that it always leads to more rounded compression curves. The increase in recompression strain with increasing disturbance is also very well stated (SQD method, to quantify soil destructuring). This is why defining preconsolidation pressure becomes more ambiguous with increasing disturbance. As the shape of the compression curve becomes more rounded, the transitioning phase between elastic and plastic behavior increases, and the difference between the two manners is less noticeable. In order to be able to better understand the soil behavior near the preconsolidation pressure, and to quantify the increase in the compression curvature with disturbance the modified recompression and compression indices are proposed. This research used a constant number of n = 2 to define two points; one on the recompression and one on the VCL part of the compression curve. These two points will be used along with the preconsolidation pressure to define the recompression and compression indices*. Results on how these indices change when disturbance increases are presented in figure 6.21 and 6.22.

Figure 6.21 presents the change in modified recompression index, C_r* for increasing the disturbance simulation amplitude, ε_a %. NC specimens, OCR = 2, OCR = 4, and accounting for swelling specimens. The modified recompression index for small disturbance simulation cycles, 0.5% axial strain is about 0.060. This value increases logarithmically up to 0.20 for disturbance simulation amplitudes of 4% or more. A logarithmic best fit is planned in the figure marked with a blue dotted line. Also, some scatter in the data points is observed for disturbance circles of

more than 3.5% axial strain, especially for NC specimens or specimens of OCR = 2. Overconsolidation ratio, seems to have no significant effect on the modified recompression ratio, C_r^*; for low disturbance cycles, specimens with OCR = 4 give a slightly higher recompression index. This difference decreases when disturbance increases. A minimum theoretical value of recompression index equals $C_r^* = 0.02$ for 0% disturbance simulation amplitude. This is obtained from the initial slope of a typical unloading curve to an OCR of 2 from CRS tests on RSFBM. The value can only be used as a lower limit of recompression index (it is not calculated over a wide range of stresses as the modified recompression index). In the figure, two NC RSFBM data points are plotted for 0% disturbance with much higher recompression index. This is due to the fact that the specimens where probably disturbed to some extent during the set up. Some tests, especially for an OCR of 2 or 4 and for relatively high disturbance simulation amplitudes (e.g. $\varepsilon_a = 3.5\%$) appear to give different recompression indices for ISA simulations imposed on different stress level. This can be explained simply from the fact, that in higher stress level, the same degree of disturbance is expected to cause slightly more rounded compression curves. So, in general, the second recompression phase is expected to give a lower recompression index in comparison to the first recompression phase of the same disturbance (stress level effect on the reloading slope).

The modified compression index (C_c^*) versus the disturbance simulation amplitude (ε_a %) for the resedimented SFBM specimens tested from the homogeneous batch of soil created, are presented in figure 6.22. Here, a difference is observed when OCR increases. For NC specimens (marked as black color dots), the modified compression ratio index starts from a maximum value of about 0.60 (disturbance amplitude of 0.5% axial strain) and decreases with increasing disturbance to 0.235 for disturbance amplitudes of 6%. For specimens of OCR = 2 (blue, triangle data points), the compression index for 0.5% disturbance circle is about 0.21. This value decreases with increasing disturbance amplitude to a minimum value of 0.30 and disturbance simulation of 5% axial strain. Following a similar trend, specimens with OCR = 4 have a maximum C_c^* value of 0.51 and a minimum value of about 0.32. Fitted lines in data points for NC, OCR = 2 and OCR = 4 are presented in the same figure with black, blue and red color respectively. All lines follow an exponential decay form. Increasing disturbance seems to have a more detrimental effect in NC or low OCR specimens. Stress level effects were also observed on the modified compression index, C_c^*, versus disturbance. For higher vertical consolidation stress,

such as the high pressure apparatus tests (grey cross data), the modified recompression index significantly decreases.

Finally, in order to quantify the fact that "increasing disturbance causes more rounded compression curves" the ratio of the two indices is applied. Figure 6.23 presents the ratio of modified recompression index to the modified compression index (C_r^*/C_c^*) versus disturbance simulation circle (ε_a %). The ratio of these two indices increases proportionally to the angle that is defined between the point A & C and the preconsolidation pressure (point B) in figure 5.39. This angle is a very good indication of the curvature of the compression curve, and predictor of imposed disturbance. From the aggregation of the data points from NC, OCR = 2 and OCR = 4 RSFBM specimens, a linear relationship between C_r^*/C_c^* and disturbance can be defined. For low disturbance simulation amplitudes (0.5% axial strain) the indices ratio is about 0.21 to 0.17. Increasing disturbance makes the indices ratio rise up to about 0.62 for disturbance simulation amplitude of 6%. NC specimens (black dots), OCR = 2 specimens (blue, triangles symbols), OCR = 4 specimens (red, diamond shape symbols) and tests with accounting for swelling (green reverse triangle symbols) are plotted in the figure. It must be noted that little difference is observed among the specimens under different OCR. The ratio of recompression to compression indices seems to be uniquely related to disturbance for RSFBM specimens, with no noticeable difference when increasing the OCR.

This unique relationship can be used in order to back calculate the disturbance in NC and low OC RSFBM samples, simply by taking the compression and recompression indices ratio from the shape of each compression curve. Those lab data are in agreement with many theoretical concepts; e.g. the concept of rigid – plastic behavior as it was proposed by Nagaraj back at 2007. He also proposed that the disturbance could be quantified by the ratio of pre-yield to post-yield slope for a compression path of the same test (SD% = C_{c1}/C_{c2}, figure 2.31). The advantage of this method is the fact that, once a relationship between C_r^*/C_c^* and disturbance amplitude ε% is defined, one can very easily estimate the disturbance simply by examining the compression curve slopes before and after the preconsolidation pressure. However, defining the two slopes C_r^* and C_c^* is, to some extend directly related to defined the preconsolidation pressure, which is by definition somewhat subjective (even when the user is very experienced or even when Strain Energy Method is employed). In cases where the preconsolidation pressure is underestimated, the interpreted yielding point in the compression curve would actually move to

the left; so both the recompression index and the compression index are expected to decrease, causing the mistake in the ratio C_r^*/C_c^* to be smaller. Consecutively, in cases where the preconsolidation pressure is overestimated, the interpreted yielding point in the compression curve would move to the right; this will make both the interpreted recompression and compression index to increase and so the miscalculation in the ratio C_r^*/C_c^* would be less significant. It should also be pointed out that the present results must not be used on soils with different properties. Different soil samples, or even SFBM specimens of different location, might give a different relationship between disturbance, ε_a %, and indices ratio, C_r^*/C_c^*. One, should expect to run a couple of triaxial tests with multiple ISA disturbance simulation circles before a unique relationship between C_r^*/C_c^* and ε % can be defined. Also, the modified indices used in this research must not be confused with the standard indices characterizing the initial recompression curve (C_r) and the VCL slope (C_c). Running 4-5 triaxial tests with multiple disturbance simulation circles requires a lot of time and effort (in many cases a single test can take up to 2 weeks) and this can be restrictive for using the proposed method in routine applications. However, the method itself provides a great illustration of how one can determine the imposed disturbance on a specimen simply by examining the shape of its compression curve. Theoretically, one can aggregate all reported compression curves from studies on a given soft clay and, simply by plotting the C_r^*/C_c^* ratio versus SQD or imposed disturbance, come up with a solid criterion of quantifying disturbance. It should be noted that the imposed ISA disturbance is fixed for a given sample geometry. Here, the typical specimen dimensions used for TX testing were height, h =8.1 cm, and diameter, d = 3.5 cm.

In order to verify the proposed method, the same analysis was carried out for the initial tests that were run on intact SFBM specimens. Figure 6.24 presents the indices' ratio C_r^*/C_c^* versus disturbance amplitude, ε_a %, for tube specimens of SFBM and resedimented SFBM. Results indicate that a new linear relationship can be defined between the indices' ratio and disturbance for the tube specimens. The fitted line is almost parallel to the one for the resedimented material, but it is now shifted up. For tube specimens and disturbance circle of 0.5%, the indices' ratio, C_r^*/C_c^*, is about 0.3. This value increases with increasing disturbance up to 0.8 and for disturbance of 6% axial strain. The equations of the two lines, as well as their square ratio are calculated to be:

$C_r^*/C_c^* = 0.085 \cdot \varepsilon_a + 0.142$, with $r^2 = 0.929$, for resedimented SFBM specimens

&

$C_r^*/C_c^* = 0.089 \cdot \varepsilon_a + 0.280$, with $r^2 = 0.902$, for tube SFBM specimens.

The difference between the two lines justifies that the effects of disturbance are more apparent on the intact specimens of SFBM. Intact specimens seem to alter their soil structure more for a given disturbance, resulting in more rounded compression curves. This will also lead to a greater ratio of the recompression to the compression index, C_r^*/C_c^*, which as said before, is analog to the increase of the angle formed between the recompression and the compression slope. This points out that when processing the material during resedimentation, its sensitivity decreases. The produced resedimented batch of soil ends up being less susceptible to disturbance effects.

Test No	No of Disturbance simulations	ISA, ε_a	σ_p'	σ'_{vc}	σ'_{vcm}	σ_s'	$\Delta\sigma'$	$\Delta\sigma'/\sigma'_{vcm}$	σ_p'/σ'_{vcm}
Units		%	ksc	ksc	ksc	ksc	ksc		
TX689	1	0.45	2.65	6.05	6.68	0.34	4.62	0.69	1.08
NC	2	0.5	7.22	13.04	14.98	2.06			
MIT03									
TX693	1	0.5	1.75	3.13	3.26	0.12	2.44	0.75	1.04
NC	2	0.5	3.38	6.72	7.06	0.82	5.46	0.77	0.97
MIT03	3	0.5	6.86	12.65	13.22	1.60			
TX694	1	1	2.39	3.26	3.49	0.12	3.15	0.90	0.85
NC	2	1	2.97	6.19	6.60	0.34	5.44	0.82	0.95
MIT03	3	1	6.27		12.41	1.16			
TX695	1	2	1.91	2.99	3.17	0.11	3.01	0.95	0.93
NC	2	2	2.95	6.84	7.29	0.17	6.65	0.91	0.78
MIT03	3	2	5.67		12.35	0.65			
TX698	1	2.5	1.09	2.01	2.03	0.03	2.03	1.00	1.24
NC	2	2.5	2.52	7.97	8.53	0.01	8.28	0.97	0.58
MIT03	3	2.5	4.92		16.42	0.25			
TX701	1	4	1.64	2.10	2.31	0.27	2.28	0.99	1.11
NC	2	4	2.57	7.13	7.95	0.02	7.81	0.98	0.67
MIT03	3	4	5.33		14.88	0.14			
TX703	1	2	1.34	1.99	2.05	0.27	2.03	0.99	1.10
NC	2	2	2.26	7.42	8.09	0.02	7.95	0.98	0.72
MIT03	3	5	5.81		13.96	0.14			
TX712	1	4	2.41	3.36	3.64	0.16	3.59	0.99	0.90
NC	2	2	3.28	7.89	8.95	0.05	8.26	0.92	0.75
MIT03	3		6.67		12.63	0.69			
TX714	1	3	1.46	3.68	3.70	0.14	3.61	0.97	0.97
NC	2	2	3.58	7.42	8.06	0.10	7.42	0.92	0.81
MIT04	3	3	6.56		12.87	0.64			
tx717	1	2.5	1.62	2.95	3.20	0.14	2.87	0.90	1.25
NC	2	2.5	3.99	7.93	8.69	0.33	8.28	0.95	0.68
MIT04	3	2.5	5.90		13.10	0.41			
TX720	1	1.75	3.29	6.70	7.53	0.16	6.81	0.90	0.96
NC	2	1.75	7.20	11.93	12.92	0.72			
MIT04									
TX721	1	1.75	2.40	3.24	3.61	0.22	3.31	0.92	0.76
NC	2	5	2.74	7.40	7.59	0.30	7.47	0.99	0.68
MIT04	3	5	5.18		13.64	0.11			
TX726	1	3.5	1.59	3.46	3.61	0.22	3.31	0.92	1.06
NC	2	5	3.84	7.90	7.59	0.30	7.47	0.99	0.69
MIT04	3	2.5	5.25		13.64	0.11			
TX731	1	10	2.66	7.90	8.71	0.16	8.59	0.99	0.59
NC	2	10	5.16	11.89	13.47	0.12			
MIT04									

Table 6.1: Calculation Table of Triaxial Tests performed on intact specimens of SFBM.

Test No	No of Disturbance simulations	ISA, ε_a	σ_p'	σ'_{vc}	σ'_{vcm}	σ_S'	$\Delta\sigma'$	$\Delta\sigma'/\sigma'_{vcm}$	σ_p'/σ'_{vcm}
Units		%	ksc	ksc	ksc	ksc	ksc		
TX795	1	1	0.69	1.70	1.98	0.24	1.27	0.64	1.12
NC	2	1	2.22	3.43	4.02	0.70	2.39	0.60	1.03
MIT02	3		4.15	6.05	6.67	1.62			
TX802	1	3	1.09	2.97	3.26	0.30	2.56	0.79	0.94
NC	2		3.06	6.35	6.82	0.70			
MIT04									
TX814	1	0.5	0.75	1.88	2.12	0.24	1.80	0.85	0.96
NC	2		2.05	7.30	8.14	0.32			
MIT04									
TX867	1	6	0.70	0.93	1.15	0.22	1.07	0.93	1.03
NC	2		1.18	2.75	3.03	0.08			
MIT03									

Table 6.2: Calculation Table of Triaxial Tests performed on resedimented tube specimens of SFBM.

Test No	No of Disturbance simulations	ISA, ε_a	σ_p'	σ'_{vc}	σ'_{vcm}	σ'_{vc_u}	σ_S'	$\Delta\sigma'$	$\Delta\sigma'/\sigma'_{vcm}$	σ_p'/σ'_{vcm}
Units		%	ksc	ksc	ksc	ksc	ksc	ksc		
TX839	1	1.5	0.94	2.05	2.33	0.52	6.50	0.06	0.11	0.96
OCR4	2	1.5	2.23	5.72	6.27	1.99	0.62	0.09	0.04	1.04
MIT04	3		6.50	14.15	14.23		1.70			
TX841	1	3.5	0.62	1.45	1.72	0.32	5.35	0.17	0.53	0.99
OCR4	2	3.5	1.70	4.84	6.78	1.09	0.80	0.37	0.34	0.79
MIT04	3		5.35	14.76	16.57		2.15			
TX852	1	5.5	0.80	1.85	2.03	0.50	0.26	0.34	0.69	1.06
OCR4	2	5.5	2.15	5.66	6.38	1.42	0.15	0.89	0.63	0.99
MIT02	3		6.30	12.87	13.55		0.53			

Table 6.3: Calculation Table of Triaxial Tests performed on OCR 4, RSFBM tube specimens.

Test No	No of Disturbance simulations	ISA, ε_a	σ_p'	σ'_{vc}	σ'_{vcm}	σ_S'	$\Delta e/e_0$	$\Delta\sigma'$	$\Delta\sigma'/\sigma'_{vcm}$	σ_p'/σ'_{vcm}
Units		%	ksc	ksc	ksc	ksc		ksc		
TX878	1	0.5	0.72	1.10	1.22	0.14	1.81	0.90	0.74	1.04
NC	2	0.5	1.27	2.42	2.62	0.32	1.99	1.80	0.69	1.06
MIT03	3		2.77	5.03	5.05	0.82				
TX879	1	1.5	0.81	1.31	1.43	0.19	3.13	1.24	0.87	1.04
NC	2	1.5	1.49	2.88	3.17	0.18	3.49	2.53	0.80	1.06
MIT04	3		3.36	7.99	8.71	0.64				
TX901	1	3.5	1.03	1.94	2.11	0.31	5.53	1.91	0.91	0.76
NC	2	3.5	1.61	3.45	3.74	0.20	5.53	3.19	0.85	1.12
MIT04	3		4.18	13.89	14.77	0.55				
TX902	1	2.5	0.71	1.24	1.36	0.22	4.59	1.20	0.89	1.05
NC	2	2.5	1.42	3.09	3.44	0.16	4.73	2.81	0.82	1.09
MIT03	3		3.75	7.81	8.40	0.62				
TX911	1	0.8	0.78	1.33	1.46	0.21	2.69	1.13	0.78	1.13
NC	2	0.8	1.65	2.32	2.48	0.32	2.46	1.74	0.70	1.05
MIT04	3		2.60	8.40	8.64	0.74				
TX912	1	6	0.86	1.40	1.49	0.18	7.94	1.43	0.96	0.75
NC	2	2	1.12	2.35	2.64	0.06	3.73	2.03	0.77	1.15
MIT03	3		3.04	7.29	7.33	0.61				
TX977	1	4.5	1.17	2.65	2.85	0.32	6.32	2.57	0.90	1.05
NC	2	4.5	2.99	7.38	8.18	0.28	5.79	6.90	0.84	0.80
MIT04	3		6.51	14.89	16.80	1.28				

Table 6.4: Calculation Table of Triaxial Tests performed on NC RSFBM batch specimens.

Test No	No of Disturbance simulations	ISA, ε_a	σ_p'	σ'_{vc}	σ'_{vcm}	σ'_{vc_u}	σ_S'	$\Delta e/e_0$	$\Delta\sigma'$	$\Delta\sigma'/\sigma'_{vcm}$	σ_p'/σ'_{vcm}
Units		%	ksc	ksc	ksc	ksc	ksc		ksc		
TX976	1	1.5	0.94	1.55	1.78	0.72	0.08	2.95	0.37	0.51	1.01
OCR2	2	1.5	1.80	3.81	4.13	1.85	0.35	3.41	1.04	0.56	1.01
MIT03	3		4.16	8.71	9.17		0.81				
TX1017	1	3.5	0.76	1.69	1.74	0.51	0.21	5.42	0.41	0.80	1.14
OCR2	2	3.5	1.98	4.81	5.18	0.90	0.10	5.31	0.70	0.78	0.80
MIT04	3		4.16	14.80	15.70		0.20				
TX1024	1	0.5	1.09	2.23	2.38	1.08	0.35	1.31	0.37	0.34	1.04
OCR2	2	0.5	2.47	6.16	6.60	3.00	0.71	1.26	0.79	0.26	1.03
MIT04	3		6.80	17.52	20.19		2.21				
TX1025	1	2.5	1.04	2.69	2.88	1.27	0.28	3.24	0.86	0.68	1.14
OCR2	2	2.5	3.27	8.43	9.55		0.41				
MIT01											
TX1028	1	5	1.02	1.99	2.13	0.96	0.36	6.34	0.73	0.77	1.17
OCR2	2	5	2.50	5.69	6.21	2.76	0.22	6.85	2.09	0.76	0.94
MIT04	3		5.85	14.81	16.15		0.68				

Table 6.5: Calculation Table of Triaxial Tests performed on OCR 2, RSFBM batch specimens.

Test No	No of Disturbance simulations	ISA, ε_a	σ_p'	σ'_{vc}	σ'_{vcm}	σ'_{vc_u}	σ_S'	$\Delta e/e_0$	$\Delta\sigma'$	$\Delta\sigma'/\sigma'_{vc\_u}$	σ_p'/σ'_{vcm}
Units		%	ksc	ksc	ksc	ksc	ksc		ksc		
TX915	1	0.5	0.54	1.15	1.26	0.24	0.17	0.23	0.03	0.13	0.99
OCR4	2	0.5	1.25	2.62	2.84	0.56	0.21	0.78	0.01	0.02	0.96
MIT03	3		2.73	8.60			0.55				
TX916	1	1.5	0.87	1.54	1.65	0.35	0.21	2.00	0.11	0.31	0.98
OCR4	2	1.5	1.62	3.49	3.82	0.79	0.24	1.65	0.16	0.20	0.98
MIT04	3		3.74	9.63	9.73		0.63				
TX942	1	2.5	0.96	1.67	1.78	0.39	0.30	3.30	0.19	0.49	0.97
OCR4	2	2.5	1.72	3.45	3.75	0.78	0.20	3.21	0.32	0.41	1.00
MIT04	3		3.74	12.69	13.59		0.46				
TX943	1	3.5	0.67	1.25	1.35	0.24	0.20	4.62	0.19	0.79	0.96
OCR4	2	3.5	1.29	2.34	2.58	0.50	0.05	4.87	0.33	0.66	1.08
MIT03	3		2.78	6.78	7.34		0.17				
TX964	1	1	0.84	1.48	1.56	0.30	0.23	1.38	0.06	0.20	0.98
OCR4	2	1	1.53	3.11	3.39	0.69	0.24	2.42	0.12	0.17	0.99
MIT03	3		3.34	8.62	9.71		0.57				
TX965	1	5	0.94	1.98	2.11	0.45	0.25	7.17	0.33	0.73	0.99
OCR4	2	5	2.08	5.43	5.86	1.25	0.12	5.24	0.70	0.56	1.00
MIT04	3		5.85	13.83	15.29		0.55				

Table 6.6: Calculation Table of Triaxial Tests performed on OCR 4, RSFBM batch specimens.

Test No	No of Disturbance simulations	ISA, ε_a	σ_p'	σ'_{vc}	σ'_{vcm}	σ_S'	$\Delta\sigma'$	$\Delta\sigma'/\sigma'_{vcm}$	σ_p'/σ'_{vcm}
Units		%	ksc	ksc	ksc	ksc	ksc		
TX1044	1	1	0.80	1.36	1.40	0.36	0.94	0.67	1.37
ΔV	2	1	1.93	4.61	4.98	0.46	2.35	0.47	1.24
MIT04	3		6.15	14.78	15.71	2.63	15.33	0.98	
TX1049	1	0.5	1.16	2.34	2.51	0.38	1.37	0.55	1.22
ΔV	2	0.5	3.07	6.83	7.35	1.14	4.52	0.61	1.08
MIT04	3		7.92	14.81	16.08	2.84	15.70	0.98	
TX1052	1	1	1.20	2.18	2.31	0.38	1.84	0.80	1.11
ΔV	2	1	2.56	5.67	6.16	0.47	4.78	0.78	1.05
MIT04	3		6.45	14.78	15.96	1.37	15.61	0.98	
TX1058	1	3.5	1.30	2.15	2.24	0.34	2.15	0.96	0.89
ΔV	2	3.5	1.98	4.14	4.38	0.09	4.01	0.92	1.17
MIT04	3		5.12	14.76	15.82	0.37	15.47	0.98	
TX1060	1	2.5	0.96	1.69	1.85	0.36	1.79	0.97	0.90
ΔV	2	2.5	1.66	4.32	4.69	0.06	4.69	1.00	0.90
MIT04	3		4.20	11.74					

Table 6.7: Calculation Table of Triaxial Tests performed on RSFBM batch specimens, accounting for ΔV.

Test No	No of Disturbance simulations	ISA, ε_a	σ_p'	σ'_{vc}	σ'_{vcm}	σ_S'	$\Delta\sigma'$	$\Delta\sigma'/\sigma'_{vcm}$	σ_p'/σ'_{vcm}
Units		%	ksc	ksc	ksc	ksc	ksc		
TX1076	1	3.5	9.56	29.65	38.68	3.84	34.84	0.900724	0.851344
NC	2		32.93	99.31	107.43	7.56	99.87	0.929629	
MIT07									
TX1087	1	4.5	10.38	33.36	40.02	4.33	35.69	0.891804	0.910045
NC	2		36.42	111.07	81.44	8.48	72.96	0.895874	
MIT07									

Table 6.8: Calculation Table of Triaxial Tests performed on RSFBM batch specimens, using high pressure apparatus.

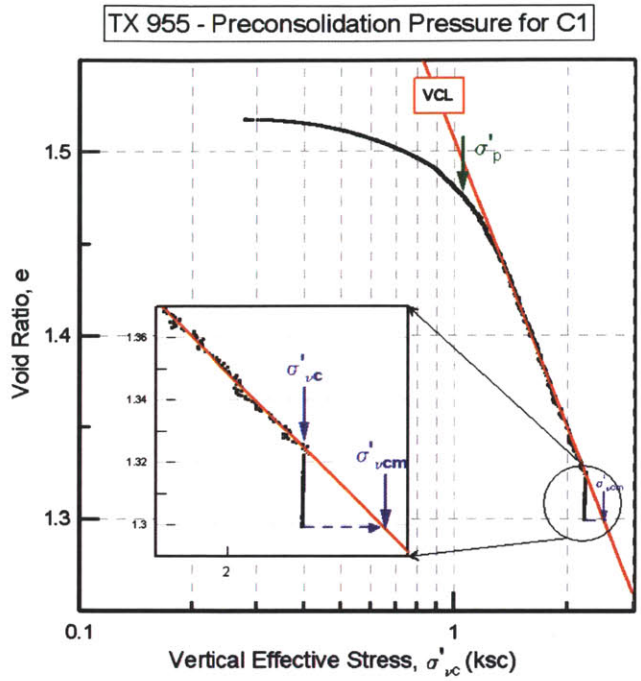

Figure 6.1: The preconsolidation pressure and maximum vertical effective stress on a stress strain consolidation curve (TX 955).

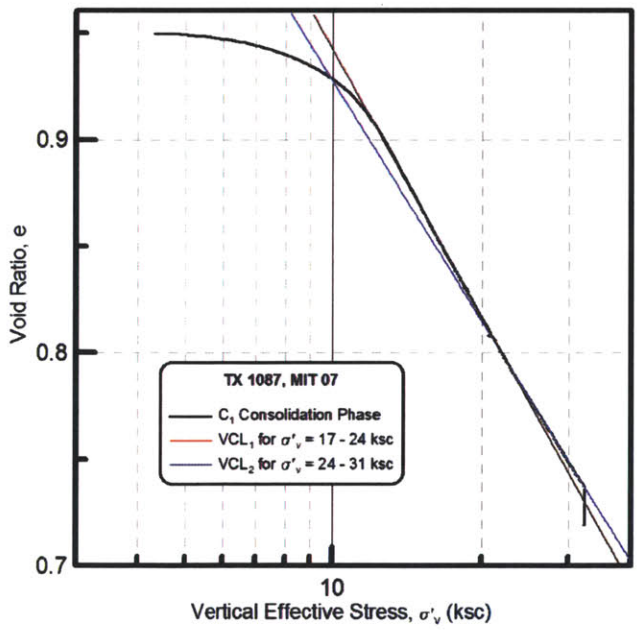

Figure 6.2: TX consolidation phase for the high pressure triaxial cell. The change on VCL slope with increasing stress level.

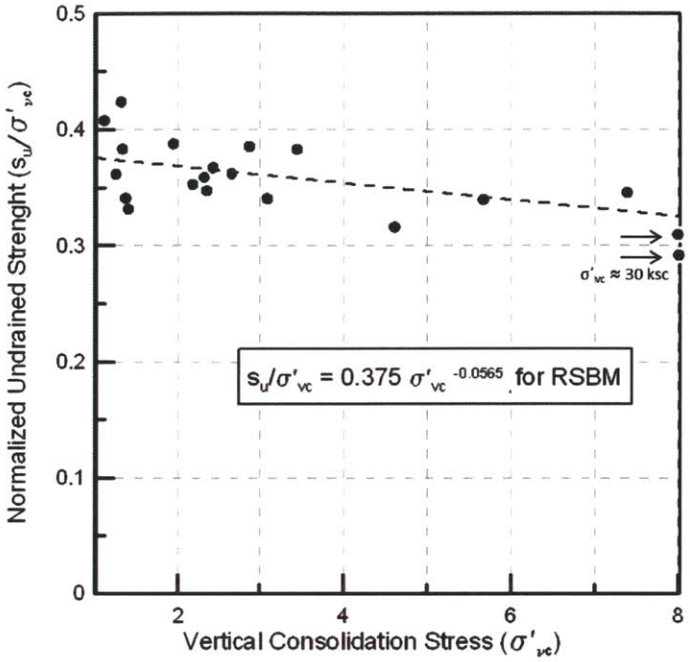

Figure 6.3: The effect of vertical effective stress (σ'_{vc}) on the normalized undrained strength (s_u/σ'_{vc}) for RSFBM specimens.

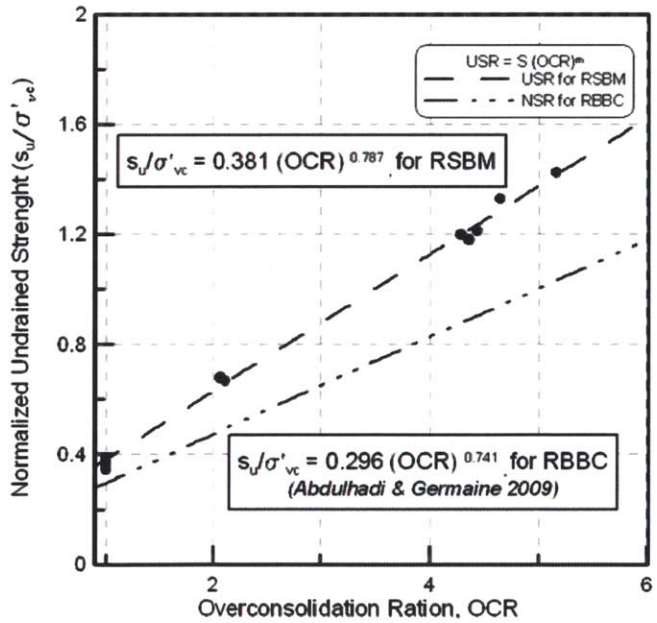

Figure 6.4: The normalized undrained strength (s_u/σ'_{vc}) versus the overconsolidation ratio (OCR) for RSFBM and RBBC specimens.

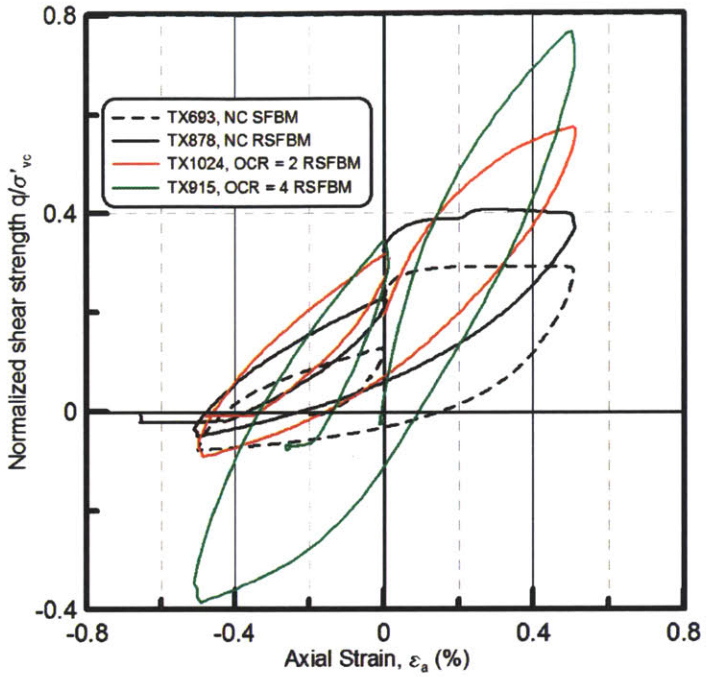

Figure 6.5: Disturbance simulation with ISA = 0.5 % on intact and resedimented NC SFBM specimens and RSFBM specimens of different OCR.

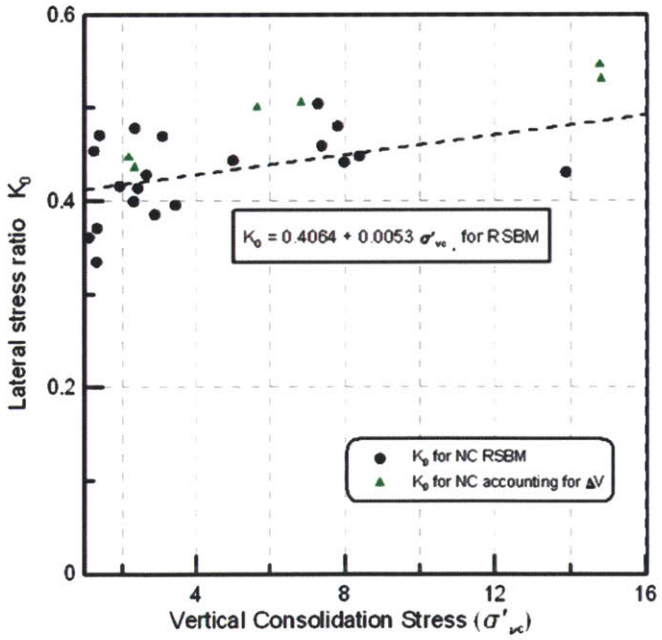

Figure 6.6: The effect of stress level on lateral stress ratio, K_0 for the low pressure apparatus on RSFBM specimens.

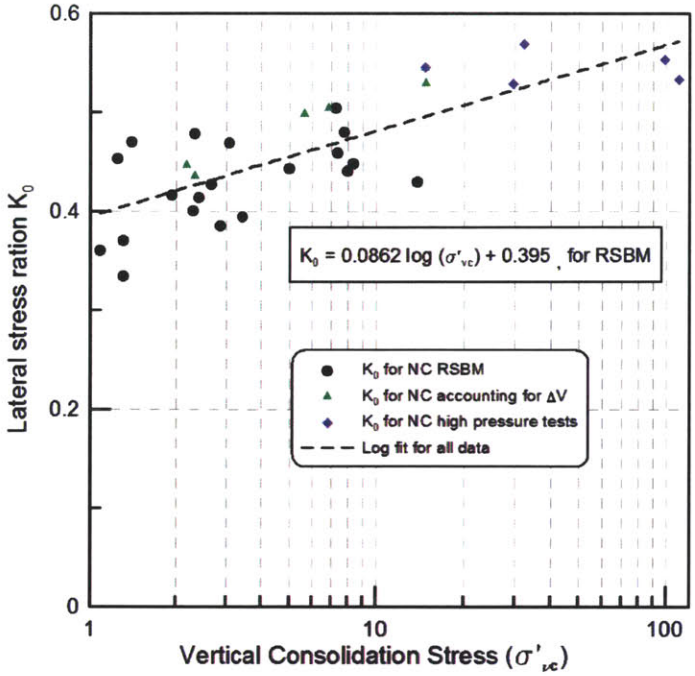

Figure 6.7: The effect of stress level on lateral stress ratio, K_0 for low and high pressure triaxial tests on RSFBM specimens.

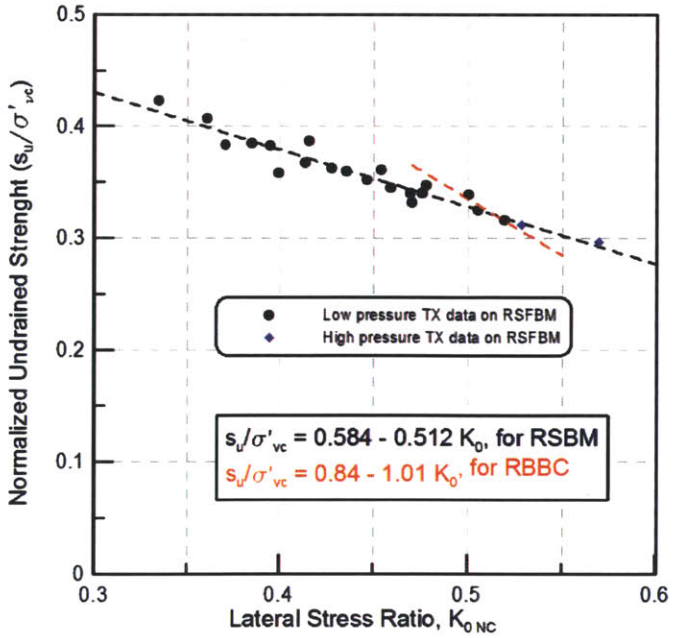

Figure 6.8: The effect of K_0 on normalized undrained strength s_u/σ'_{vc} from low and high pressure TX tests on RSFBM specimens.

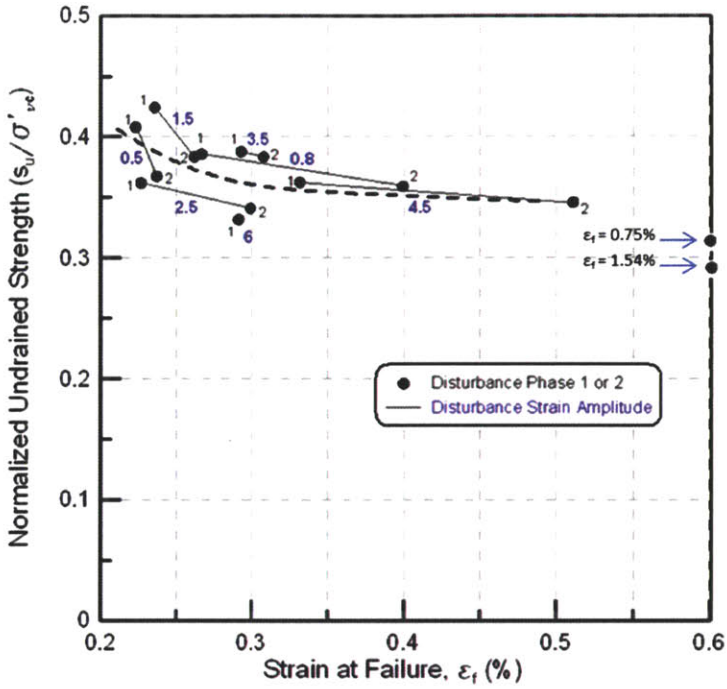

Figure 6.9: The normalized undrained strength versus the stain at failure for NC RSFBM specimens.

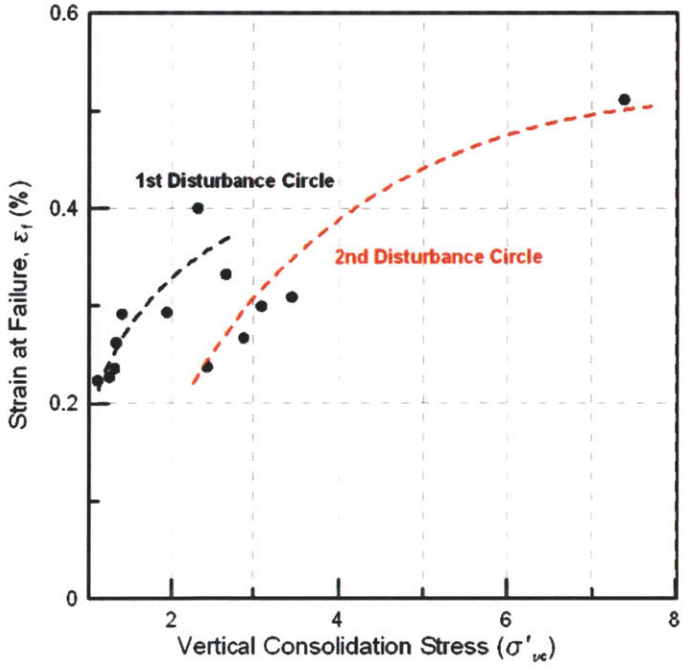

Figure 6.10: The strain at failure versus the vertical consolidation stress for the 1st and 2nd disturbance simulation circle on NC RSFBM specimens for the low pressure MIT apparatus.

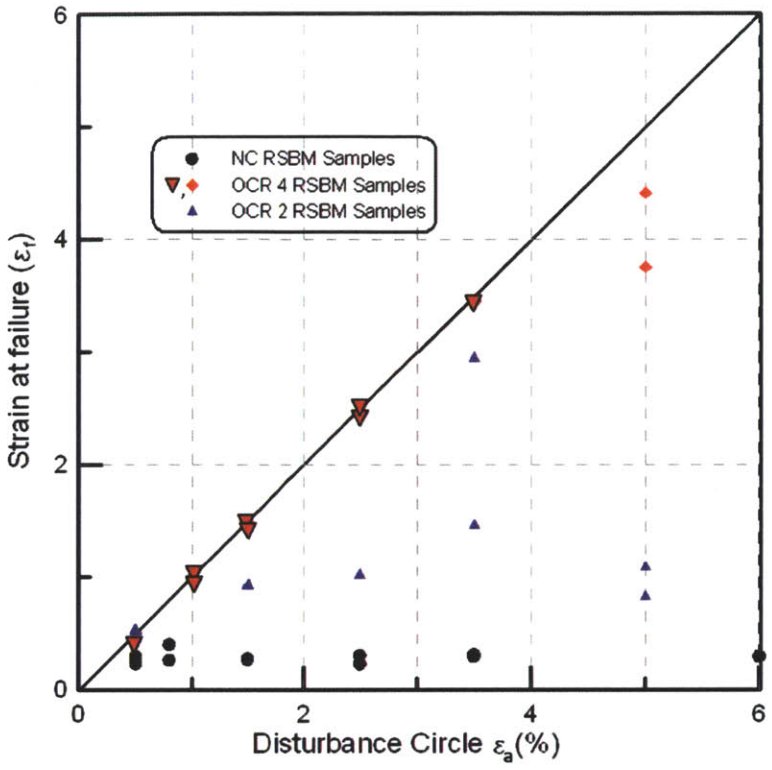

Figure 6.11: The strain at failure versus the disturbance simulation amplitude for different OCR specimens of RSFBM.

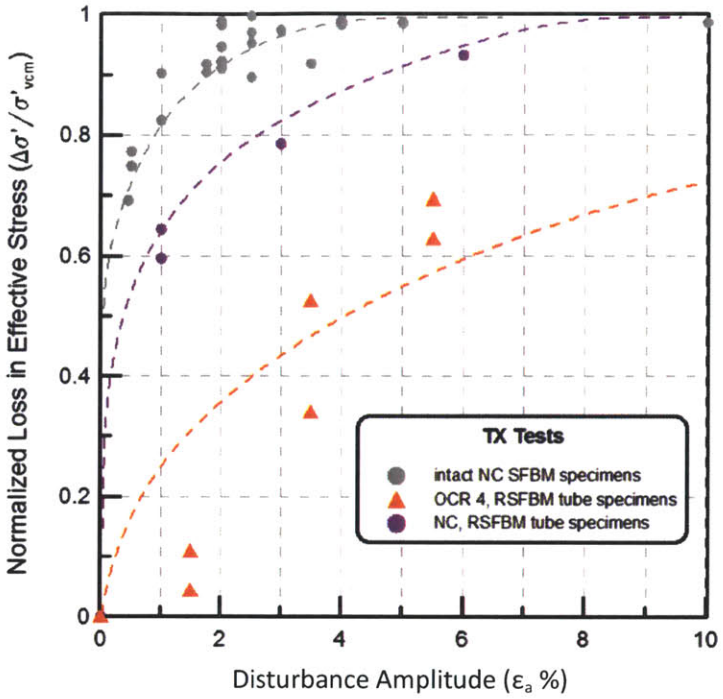

Figure 6.12: The loss of effective stress versus the disturbance simulation amplitude for tube SFBM specimens.

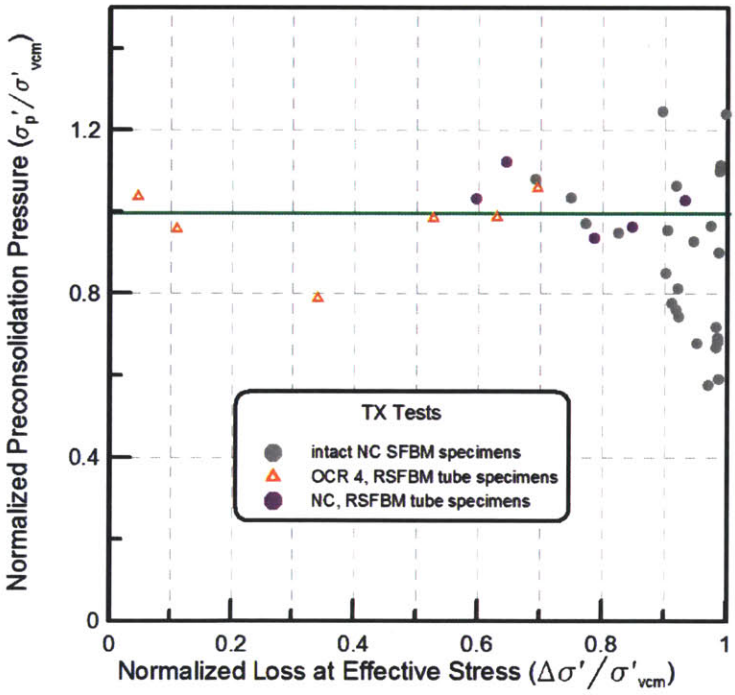

Figure 6.13: The effect of loss at effective stress on preconsolidation pressure for tube and resedimented SFBM specimens.

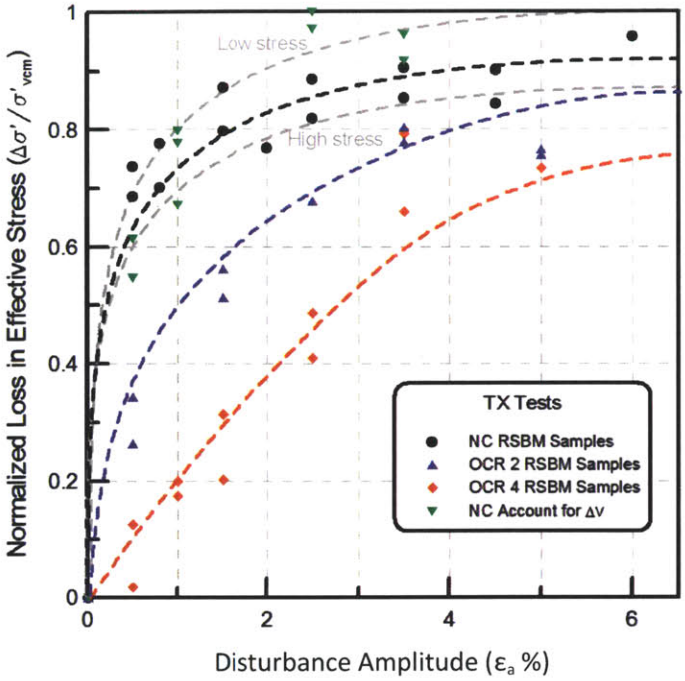

Figure 6.14: The loss at effective stress versus the disturbance simulation amplitude for resedimented SFBM specimens of different OCR and accounting for swelling.

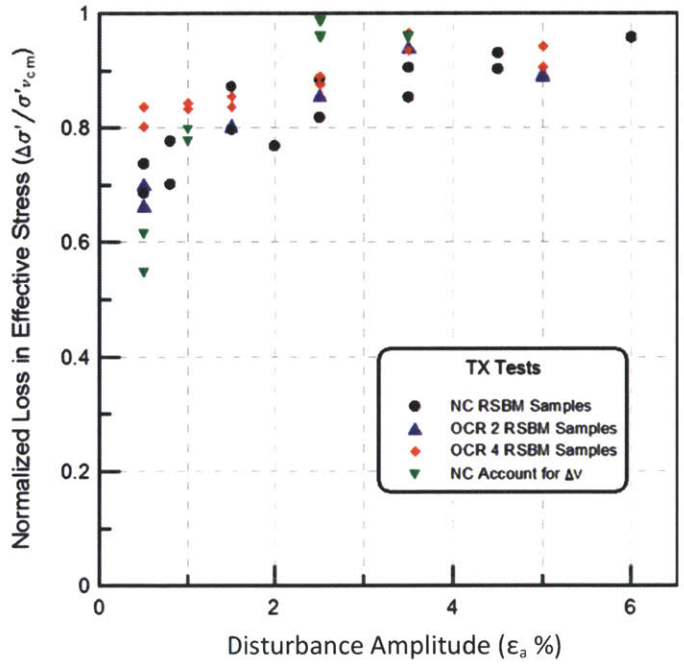

Figure 6.15: The total loss at effective stress versus the disturbance simulation amplitude for RSFBM specimens.

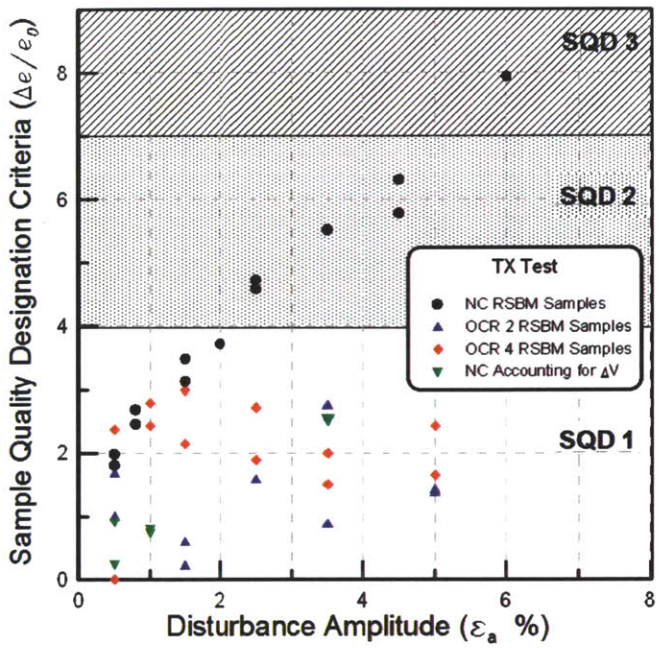

Figure 6.16: The SQD (after Lunne et al. 1997) versus the ISA disturbance simulation amplitude for RSFBM specimens of different OCR.

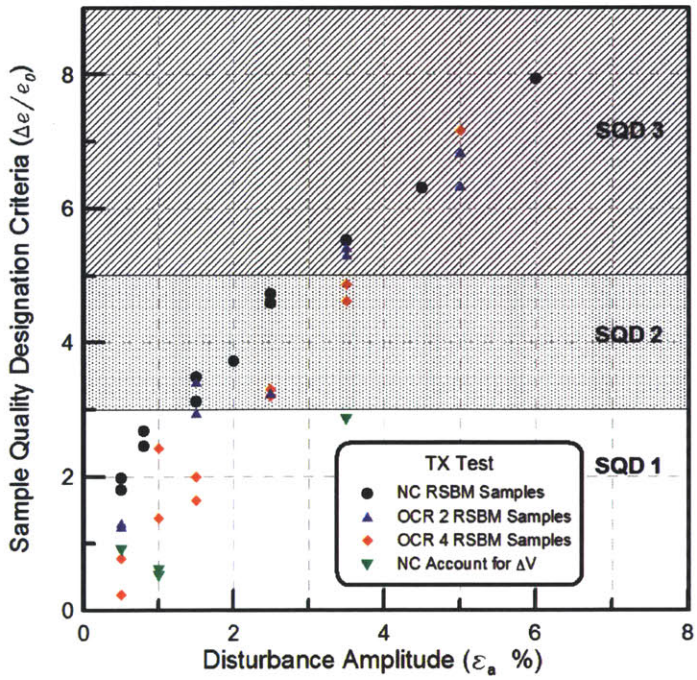

Figure 6.17: The SQD (after Lunne et al. 1997) versus the ISA disturbance simulation amplitude for RSFBM specimens of different OCR.

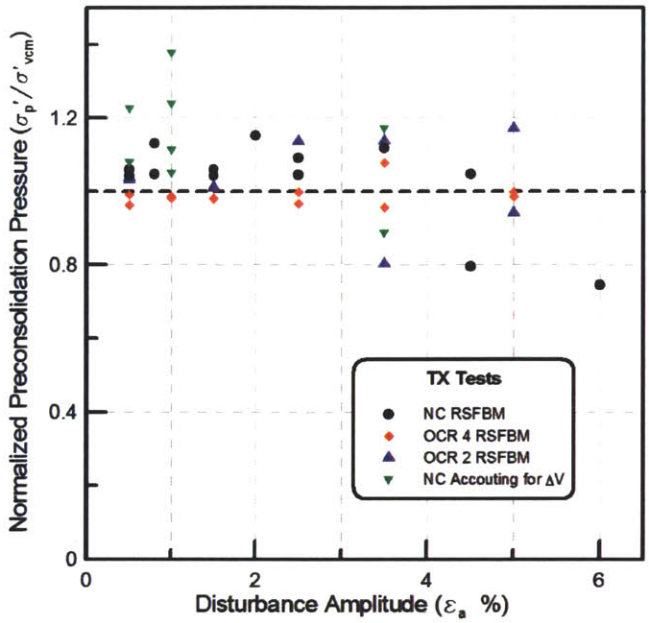

Figure 6.18: The normalized preconsolidation pressure versus the ISA disturbance simulation amplitude for RSFBM specimens of different OCR.

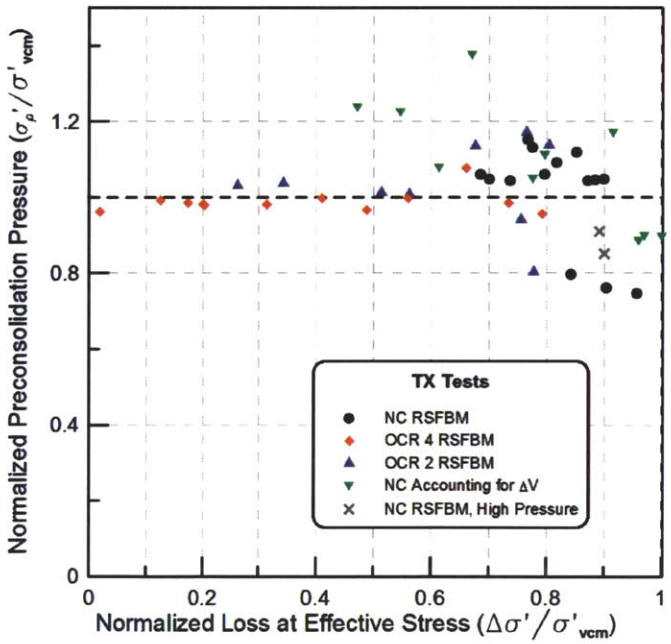

Figure 6.19: The normalized preconsolidation pressure versus the normalized loss of effective stress for RSFBM specimens of different OCR.

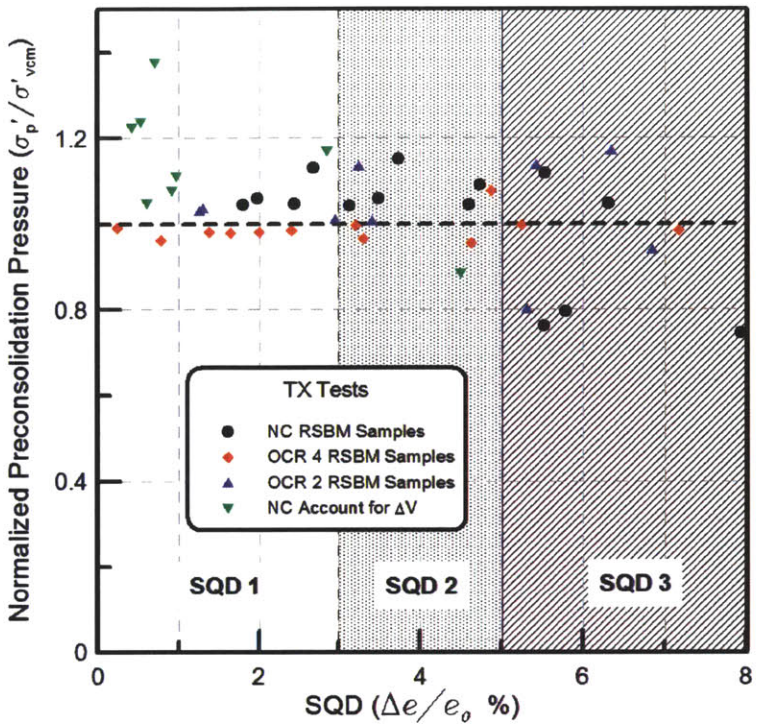

Figure 6.20: The normalized preconsolidation pressure versus the SQD (after Lunne et al. 1997) for RSFBM specimens of different OCR.

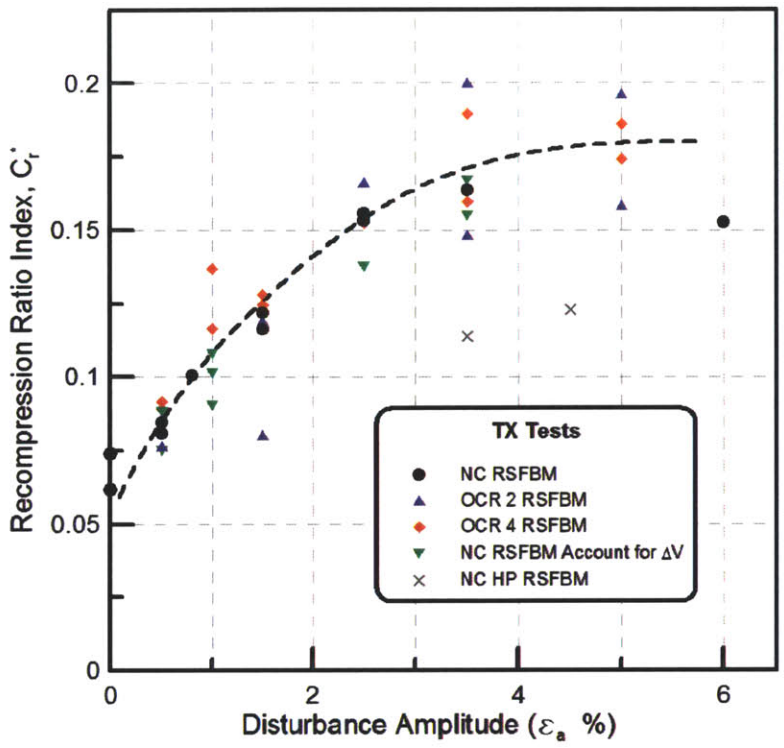

Figure 6.21: The recompression ratio index, Cr* versus the ISA disturbance simulation amplitude, ε_a %.

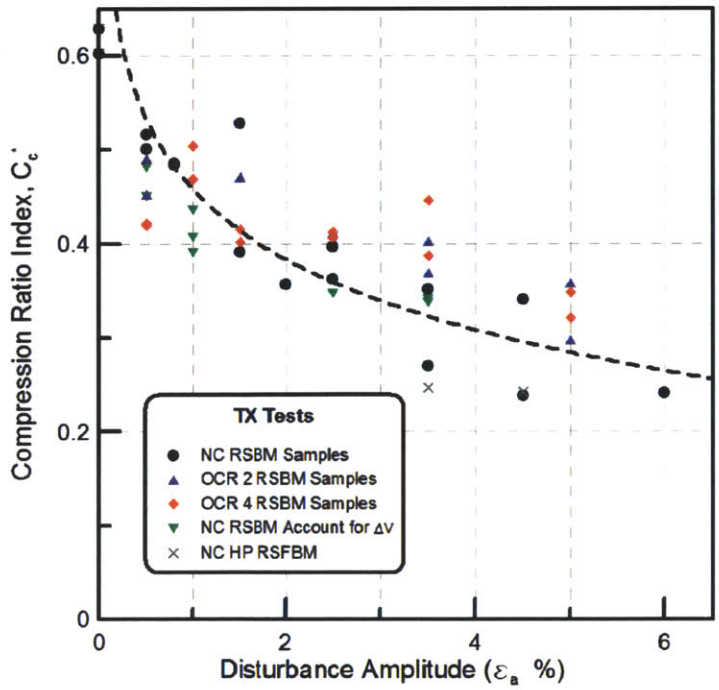

Figure 6.22: The compression ratio index, Cc* versus the ISA disturbance simulation amplitude, ε_a %.

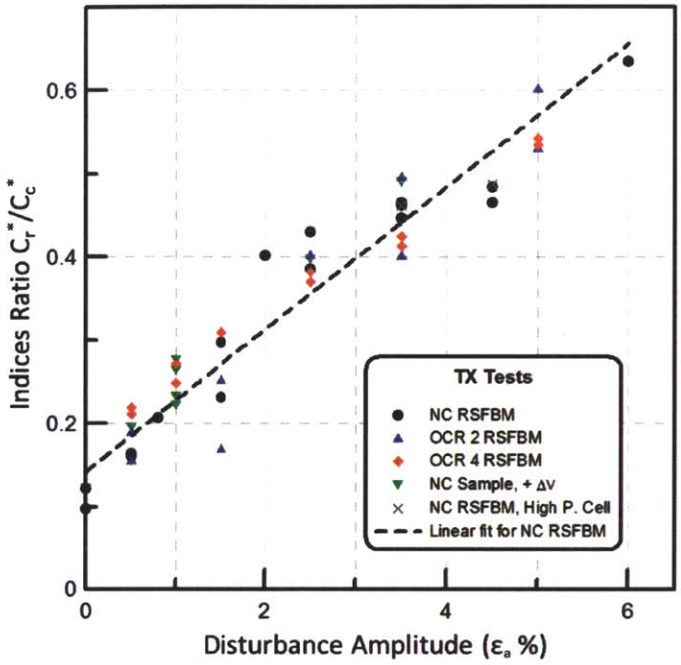

Figure 6.23: The indices ratio C_r^*/C_c^* versus the disturbance simulation amplitude.

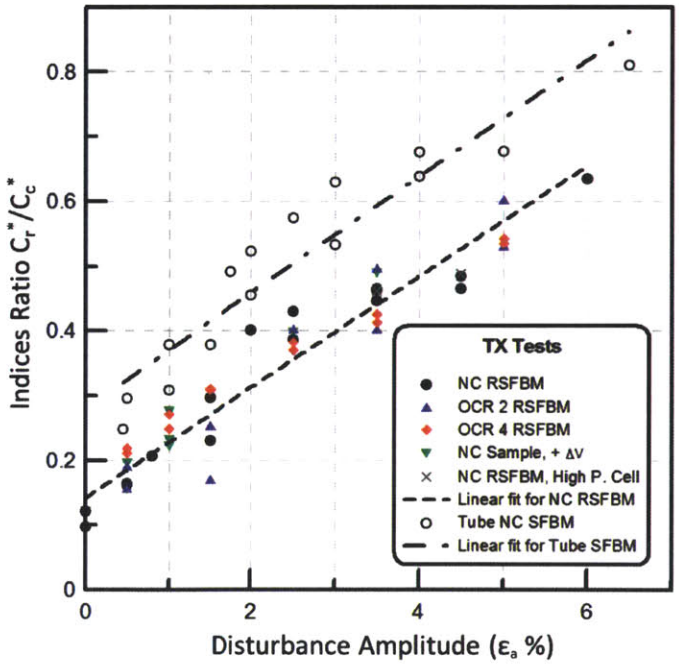

Figure 6.24: The indices ratio C_r^*/C_c^* versus the disturbance simulation amplitude for resedimented and tube SFBM specimens.

Chapter 7 CONCLUSIONS AND RECOMMENDATIONS

7.1 Overview

This research program examined the effects of disturbance on normally consolidated and overconsolidated specimens of San Francisco Bay Mud (SFBM). Disturbance was simulated using the ISA approach and SHANSEP reconsolidation technique was used to recover the intact behavior of the soil, erasing all the previous effects of disturbance. Special interest was put to identify the change in the preconsolidation pressure and the shape of the compression curve with increasing disturbance. The main phase of this testing program consists of a total of 45 triaxial tests. In the first part of the program, disturbance was simulated on intact specimens of SFBM. A total of 12 triaxial tests were performed on NC tube SFBM specimens of disturbance amplitude ranging from 0.5% to 10% axial strain.

For the second phase of this research, resedimentation was employed to better identify the effects of disturbance on the compression curves and rule out tube specimen non-uniformities. A total of 10 triaxial tests were performed on NC specimens using disturbance amplitudes from 0.5% to 6% axial strain. The effect of disturbance was also examined on OCR specimens. A total of 5 triaxial tests were performed unloading to an OCR of 2 and 10 tests were performed unloading to an OCR of 4. Finally, 4 triaxial tests were performed accounting for volumetric change after disturbance (swelling) and 3 tests were performed consolidating to higher stresses (up to 150 ksc), using the high pressure MIT triaxial apparatus. Complementary CRS and index tests were performed on intact and resedimented material and served as a guide for the consolidation behavior of the soil.

The main objectives of the research program can be summarized as the followings:

i) Examine the effects of disturbance on Preconsolidation pressure and on the shape of the compression curve for NC soft clays. Try to verify and quantitatively evaluate Santagata and Germaine's (1994) conceptual model.

ii) Expand this understanding over a wide range of stresses and OCR values.

iii) Simulate the effects of disturbance on an element sitting outside the centerline of the sampling tube (account for swelling and extensive shearing).

iv) Define a methodology to quantitatively evaluate disturbance "in the lab" for triaxial tests.

7.2 Conclusions

The conclusions of this research are divided into two categories. The conclusive observations that support previous studies, and the findings that to a great extent are unique and innovative on the topic of sample disturbance regarding its effects on preconsolidation pressure.

7.2.1 Conclusive observation that support previous studies

During the CK_0UC-E tests performed on this research program, strong dependences were verified between the normalized undrained shear strength, s_u/σ'_{vc}, and when the stress level or the lateral stress ratio, K_0, increases. Similar observations were also noted on resedimented BBC by Abdulahandi and Germaine (2009) a few years earlier. The disturbance simulation cycles (undrained shear stress-strain behavior) showed that as the consolidation stress increases from 0.5 to about 100 ksc for the high pressure apparatus, the normalized undrained strength decreases. For the resedimented SFBM the variation in normalized undrained strength, s_u/σ'_{vc}, was rather significant; from 0.42 on low vertical consolidation stresses to 0.29 for the high pressure apparatus. At the same time, the strain at peak strength increases with increasing the vertical consolidation stress; from 0.25 up to 0.5% axial strain for the low pressure apparatus and up to 1.5% axial strain for the high pressure cell. This means that when moving to higher stresses, soil behavior does not normalize as the SHANSEP approach proposes. On the contrary, undrained response from brittle becomes more ductile. Strain softening also decreases with

increasing the stress. Increasing the overconsolidation ratio appears to have similar effects. However, for OCR of 4 in most tests and for large disturbance simulation amplitudes, the imposed strain was not enough to mobilize the peak undrained shear strength and so, conclusive results could not be drawn.

Increasing the vertical consolidation stress on NC specimens had also an apparent effect on the lateral stress ratio, K_0. Although some scatter was observed even when using resedimented material, increasing the vertical consolidation stress, increases the lateral stress ratio, K_0; from 0.35 at low stresses, up to 0.57 for high pressure. This increase in the presheared lateral stress ratio, $K_{0\,NC}$ has a direct impact on the normalized undrained strength, s_u/σ'_{vc}. As the $K_{0\,NC}$ increases the normalized undrained strength, s_u/σ'_{vc}, decreases from 0.42 to 0.29. Results from the low pressure and high pressure MIT apparatuses indicate a clear linear relationship between the two, over a significantly larger range of K_0 values than that defined for RBBC (Abdulhandi and Germaine, 2009). K_0 variation observed on RSFBM is much greater than the variation observed on RBBC specimens. The correlation between K_0 and s_u/σ'_{vc} has less scatter than either of the stress level dependency trends and suggests a more fundamental relationship. This also implies that scatter observed in strength from test to test is likely due to the pre-shear stress conditions.

Another very important outcome of this research supporting data presented by Santagata and Germaine (1994) on RBBC, is the decrease in sampling effective stress, σ'_s, when the disturbance simulation amplitude, ε_a %, increases. This relationship between sampling effective stress and disturbance amplitude appears to be independent of the OCR ratio. Interpretation of triaxial tests results on RSFBM showed that for a give disturbance, ε_a %, a NC specimen and an low OCR specimen have almost identical sampling effective stress, σ'_s. Additionally, a very distinct logarithmic relationship can be defined between the loss of effective stresses and ISA disturbance amplitude. Increasing the OCR, decreases the loss of effective stress in such a way, that the total losses of effective stress (from ISA disturbance and due to unloading to a specific OCR) are equal to the loss of effective stress expected on a NC specimen under the same ISA disturbance amplitude and on the same consolidation stress level.

Another solid conclusion from this research program is that intact specimens of SFBM are more prone to disturbance than resedimented material. ISA disturbance simulation effects appeared to be more significant on intact tube specimens of SFBM; the effects of disturbance as

measured from the loss of effective stress, the change in VCL slope (destructuring), and the change on void ratio $\Delta e/e_0$ (SQD, Lunne et al. 1987), when reconsolidating the specimen to the previous maximum stress, are more apparent. This made the estimation of preconsolidation pressure especially challenging on intact specimens for medium or large disturbance amplitudes (greater than 3%). Results indicate that for intact specimens of SFBM and loss of effective stress more that 90%, the preconsolidation pressure can be significantly underestimated as well as overestimated.

7.2.2 Novel Findings

For the resedimented SFBM material, the preconsolidation pressure is constant on average over any OCR or disturbance amplitude, ε_a %. This is true for NC, OCR of 2 and OCR 4 specimens examined and for ISA disturbance amplitude of up to 5% axial strain. The reconsolidation strains increase with large disturbance amplitudes. Increasing disturbance has a direct impact on the maximum and minimum values of σ'_p calculated using the Strain Energy Method, and so, the uncertainty associated with the interpreted preconsolidation pressure increases with increasing disturbance. For high values of disturbance simulation amplitude, $\varepsilon_a >$ 5%, the error associated with the preconsolidation pressure value was as high as 10%.

It is also noted that the average normalized preconsolidation pressure, σ'_p/σ'_{vcm} slightly decreases when the OCR increases. This cannot be justified using the Santagata and Germaine (1994) conceptual model; for increasing OCR the total loss of effective stress and the sampling effective stress, σ'_s, remains the same (although from data points the normalized total losses for an OCR of 4 appear to be on the upper limit of the calculated total losses for all specimens). On the same time the change of VCL slope is less significant. So, in theory, increasing OCR should result in higher preconsolidation pressure. However, this is without accounting for the fact that during unloading to a targeted OCR, the specimen undergoes some softening (the void ratio slightly increases).

For the triaxial tests where the combined disturbance (ISA simulation and swelling) was imposed, an increase in the normalized preconsolidation pressure σ'_p/σ'_{vcm} is observed. The imposed positive volumetric change, $+\Delta V$, increases the loss of effective stress and causes a

significant destructuring in soil skeleton as depicted by a decrease in the VCL slope. However, it appears that for the RSFBM material examined in this present research, the first effect, the decrease in sampling effective stress, σ'_s, has a much more dominant effect on the recompression behavior. This causes an overall overestimation of the normalized calculated preconsolidation pressure value σ'_p/σ'_{vcm} as indicated by the Santagata and Germaine Conceptual model (1994).

Finally, one of the most important contributions of this research is the proposed indices ratio C_r^*/C_c^* criterion as a quantitative measurement of disturbance. The modified recompression and compression indices give a better understanding of the changes of the compression curve near the point of interest, the preconsolidation pressure. The ratio is a good indication of how the shape of the stress-strain curve changes with increasing disturbance. Applying the proposed criterion one can get a quantitative approach of how disturbance can lead to "more rounded compression curves". Indices ratio criterion, C_r^*/C_c^*, was applied on resedimented as well as intact material and verify the fact that disturbance effects are more detrimental on the intact, tube specimens of SFBM. The linear relationship between indices ratio, C_r^*/C_c^*, and disturbance, ε_a %, is valid over a wide range of OCR and stresses and it does not seem to be affected much from the preconsolidation pressure value calculation itself. On soils with properties similar to SFBM, the indices ratio versus disturbance is expected to be a line parallel to the curves calculated for the intact and resedimented SFBM material. However, in order to verify and generalize this new criterion, more testing, on soils with varying sensitivity and properties is needed.

7.3 Recommendations for Future Research

This research provided a conclusive series of triaxial test results incorporating the ISA and evaluating its effects on the preconsolidation pressure and the compression curve shape. A large effort was put into resedimentation to rule out sample non-uniformities and irregularities. Future recommendations for research are divided into two categories. The first aims towards a better understanding of the SFBM behavior with increasing stress and the differences between intact and resedimented soil. The second category focuses on the proposed modified indices ratio in order to quantitatively account for disturbance and its applications on other soft clays.

7.3.1 Stress dependence and soil structure

i) More CRS and Triaxial testing is needed in order to evaluate conclusively the effect of stress level and lateral stress ratio on the undrained shear strength. A series of parallel tests on low pressure and high pressure MIT apparatuses would greatly contribute towards the understanding of these two effects.

ii) For this research, the high pressure apparatus was modified in order to incorporate extension capabilities and impose the ISA disturbance simulation. However, due to time constrains only three ISA simulation tests were run. Additional tests should be carried out, over a wide range of ISA disturbance amplitudes and OCRs in order to better understand how stress level affects disturbance's effects and consolidation behavior. This will help discriminate among the actual effect of stress level and the effects of disturbance on the compressibility parameters.

iii) The effect of swelling after ISA disturbance should be further investigated. Additional evidence is needed to conclusive determine the overestimation of preconsolidation pressure when allowing for swelling.

iv) The swelling effects on intact specimens should be evaluated for comparison with these of resedimented material. A wide range of stresses and OCRs should be used to determine its effects on the preconsolidation pressure and the compression curve.

7.3.2 Indices ratio as a quantitative method to account for disturbance

i) The SFBM and especially the resedimented batch of soil used in this research appears to have structure that is less sensitive to disturbance degradation. A more structured intact material, possibly of varying sensitivity should be used in order to verify the observations on preconsolidation pressure with increasing disturbance. A better understanding on the effects of disturbance on intact versus resedimented material is needed.

ii) The indices ratio is a good quantitative method that can be applied by investigating the consolidation curves. The MIT database for BBC and other soft soils should be used in order to reevaluate sample quality. Useful tables can be introduced to quantify disturbance based on the indices ratio (C_r^*/C_c^*), and stress level for the different soils (BBC, SFBM, Maine Clay, etc).

iii) Block Sherbrooke samples can be used in order to define a lower limit for indices ratio and the compression to recompression indices. This minimum value can be used as minimum reference to evaluate disturbance.

iv) Since with indices ratio can be used to quantify disturbance, a trial to correct some engineering properties can be made. Prasad and Nagaraj (2003) proposed corrections on the compression index, yield stress and unconfined strength based on the degree of disturbance that would be of great interest to be experimentally verified.

v) Based on this research observation on SFBM and on previous observations from Santagata and Germaine (1994) on BBC, ISA disturbance seems not to be able to fully capture the effects of "in-situ" sampling disturbance as these are depicted on sampling effective stress and reconsolidation strain. More research is needed to understand the differences between the two and possibly be able to capture these differences on the shape of the compression curve with indices ratio.

APPENDIX

No#	TX TEST	CELL	Material	Characteristic	Notes
1	689	MIT 03	Intact, SFBM	ISA ±0.5%	
2	691	MIT 03	Intact, SFBM	ISA ±1%	problem with axial motor during K_0
3	693	MIT 03	Intact, SFBM	ISA ±0.5%	
4	694	MIT 03	Intact, SFBM	ISA ±1%	
5	695	MIT 03	Intact, SFBM	ISA ±2%	
6	698	MIT 03	Intact, SFBM	ISA ±3%	
7	700	MIT 03	Intact, ARUP	-	
8	701	MIT 03	Intact, SFBM	ISA ±4%	
9	702	MIT 02	Intact, SFBM	ISA ±2%	bad set up
10	703	MIT 03	Intact, SFBM	ISA ±2%	
11	707	MIT 02	Intact, ARUP	shear to failure	
12	708	MIT 03	Intact, SFBM	ISA ±2%	lost data
13	709	MIT 04	Intact, SFBM	ISA ±2%	lost data
14	711	MIT 03	Intact, SFBM	-	problem with axial motor
15	712	MIT 04	Intact, SFBM	ISA ±2, 4%	
16	714	MIT 04	Intact, SFBM	ISA ±3%	
17	715	MIT 03	Intact, SFBM	ISA ±2%	problem with axial motor
18	717	MIT 04	Intact, SFBM	ISA ±2.5%	
19	718	MIT 03	Intact, SFBM	ISA ±2%	problem with axial motor, at the beginning of K_0
20	720	MIT 04	Intact, SFBM	ISA ±1.5%	
21	721	MIT 04	Intact, SFBM	ISA ±5%	
22	723	MIT 03	Intact, SFBM	ISA ±2%	problem with axial motor, at the beginning of K_0
23	726	MIT 04	Intact, SFBM	ISA ±3, 5%	not enough reconsolidation strain
24	731	MIT 04	Intact, SFBM	ISA ±10%	
25	733	MIT 03	Intact, SFBM	-	lost data
26	747	MIT 03	Intact, SFBM	ISA ±2%	
27	766	MIT 03	Intact, SFBM	ISA ±0.25%	lost data
28	771	MIT 03	Intact, SFBM	-	C1, C3 problem
29	772	MIT 02	Intact, SFBM	ISA ±0.25%	different compression curve!
30	779	MIT 03	Intact, IODP		

Table 1: Summary Table off all Triaxial Tests performed on this research program.

31	785	MIT 03	Dum Spec	-	tx test to check cell
32	795	MIT 02	RSFBM,tube	ISA ±1%	
33	802	MIT 04	RSFBM,tube	ISA ±3%	
34	814	MIT 04	RSFBM,tube	OCR 4, ISA ±3%	
35	838	MIT 04	RSFBM,tube	OCR 4	problem during U1
36	839	MIT 04	RSFBM,tube	OCR 4, ISA ±1.5%	
37	841	MIT 04	RSFBM,tube	OCR 4, ISA ±3.5%	
38	850	MIT 03	Dum Spec	-	tx test to check cell
39	852	MIT 02	RSFBM,tube	OCR 4, ISA ±5.5%	
40	862	MIT 04	RSFBM,tube	-	problem with motor during secondary compression
41	863	MIT 03	RSFBM,tube	-	no data
42	866	MIT 04	RSFBM,tube	ISA ±4.5%	
43	867	MIT 03	RSFBM,tube	ISA ±7%	moderate problem with axial motor
44	868	MIT 02	RSFBM,tube	ISA ±2.75%	
45	878	MIT 03	RSFBM batch	ISA ±0.5%	
46	879	MIT 04	RSFBM batch	ISA ±1.5%	
47	901	MIT 04	RSFBM batch	ISA ±3.5%	
48	902	MIT 03	RSFBM batch	ISA ±2.5%	
49	911	MIT 04	RSFBM batch	ISA ±0.8%	
50	912	MIT 03	RSFBM batch	ISA ±6, 2%	
51	915	MIT 03	RSFBM batch	ISA ±1.5%	
52	916	MIT 04	RSFBM batch	OCR 4, ISA ±1.5%	
53	942	MIT 04	RSFBM batch	OCR 4, ISA ±2.5%	
54	943	MIT 03	RSFBM batch	OCR 4, ISA ±3.5%	
55	964	MIT 03	RSFBM batch	OCR 4, ISA ±1%	
56	965	MIT 04	RSFBM batch	OCR 4, ISA ±0.5%	
57	976	MIT 03	RSFBM batch	OCR 2, ISA ±1.5%	
58	977	MIT 03	RSFBM batch	ISA ±4.5%	
59	995	MIT 04	RSFBM batch	OCR 8, ISA ±0%	
60	996	MIT 03	RSFBM batch	OCR 4, ISA ±0%	missing data

Table 1: Summary Table off all Triaxial Tests performed on this research program.

61	1016	MIT 03	RSFBM batch	OCR 2, ISA ±2.5%	
62	1017	MIT 04	RSFBM batch	OCR 2, ISA ±3.5%	
63	1024	MIT 04	RSFBM batch	OCR 2, ISA ±0.5%	
64	1025	MIT 01	RSFBM batch	OCR 2, ISA ±2.5%	
65	1028	MIT 04	RSFBM batch	OCR 2, ISA ±5%	
66	1029	MIT 01	RSFBM batch	OCR 8, ISA ±1.5%	
67	1038	MIT 04	RSFBM batch	ISA ±0.5%, +ΔV	
68	1039	MIT 02	RSFBM batch	-	Load Frame failure!
69	1044	MIT 04	RSFBM batch	ISA ±1%, +ΔV	
70	1049	MIT 04	RSFBM batch	ISA ±0.5%, +ΔV	
71	1050	MIT 03	Dum Spec	-	To check cell/ new program
72	1052	MIT 04	RSFBM batch	ISA ±1%, +ΔV	
73	1054	MIT 03	Dum Spec		To check cell/ new program
74	1055	MIT 07	RSFBM batch	HP, ISA ±3%	Some control problems
75	1058	MIT 04	RSFBM batch	ISA ±3.5%, +ΔV	
76	1060	MIT 03	RSFBM batch	ISA ±2.5%, +ΔV	moderate problems
77	1071	MIT 04	RSFBM batch	-	Internal leak
78	1076	MIT 07	RSFBM batch	HP, ISA ±3.5%	
79	1087	MIT 07	RSFBM batch	HP, ISA ±4.5%	
80	1088	MIT 04	RSFBM batch	-	Internal leak
				No good	27
				Success rate (%)	66

Table 1: Summary Table off all Triaxial Tests performed on this research program.

REFERENCES

Abdulhadi N. O. (2009), "An Experimental Investigation into the Stress-Dependent Mechanical Behavior of Cohesive Soil with Application to Wellbore Instability", PhD Thesis, Dept. of Civil and Environmental Engineering, Massachusetts Institute of Technology, Cambridge, Mass.

Baligh M. M.; (1985), "The Strain Path Method", J. Geotech. Eng., 111(9), 1108-1136.

Baligh M. M.; Azzouz A. S.; Chin C. T. (1987), "Disturbance due to "Ideal" Tube Sampling", J. Geotech. Engrg., 113(7), 739-757.

Baligh M. M.; Azzouz A.; and Chin C.-T. (1987), "Disturbance Due to Ideal Tube Sampling", J. of Geotechnical Eng., ASCE, vol. 113, No. 7, pp. 739-757.

Becker D.E.; Crooks J.H.A.; Been K.; and Jeffries M.G. (1987), "Work as a Criterion for Determination in Situ and Yield Stresses in Clays", Canadian Geotechnical J., 24(4): 549-564.

Berre T.; Lunne T.; Andersen K.H.; Strandvik S.; and Sjursen M. (2007), "Potential Improvements of Design Parameters by Taking Block Samples of Soft Marine Norwegian Clays", Can. Geotch J. 44: 698-716.

Berman D. R.; Germaine J. T.; and Ladd C. C. (1993), "Characterization of the Engineering Properties of Boston Blue Clay for the MIT Campus", Research Report, prepared for the Dept. of Physical Plant, Massachusetts Institute of Technology, Cambridge, Mass.

Boone S. J. (2010), "A Critical Reappraisal of Preconsolidation Pressure Interpretations Using the Oedometer Test", Can Geotech. J. 47: 281-296.

Burland J. B. (1990), "On the Compressibility and Shear Strength of Natural Clays", Geotechnique 40(3): 329-373.

Burland J. B. (1990), "On the Compressibility and Shear Strength of Natural Clays", Geotechnique 40, No. 3, 329-378.

Butterfield R. (1979), "A Natural Compression Law for Soils", Geotechnique 29(4): 469-480.

Casagrande A. (1936), "The determination of the Preconsolidation Load and its Practical Significance", Int. Conf. on Soil Mech. And Found. Eng., 1 Cambridge, Mass. 1936. Proc. Vol. 3, pp. 60-64.

Casagrande A. (1948), "Classification and Identification of Soils", Trans. ASCE, Vol. 113, pp.901-930.

Cinicioglu O. (2007), "Unloading – Reloading Lines as a Function of Preconsolidation Pressure", Teknik Dergi, vol. 18, No. 2, pp. 4133-4143.

Chandler R. J.; Harwood A. H.; Skinner P. J. (1992), "Sample Disturbance in London Clay", Geotechnique, 42, No. 4, 577-585.

Clayton C. R. I.; Hight D. W.; and Hopper R. J. (1992), "Progressive Destructuring of Bothkennar Clay: Implications for Sampling and Reconsolidation Procedures", Geotechnique, 42, No. 2, 219-239.

Clementino R. V. (2005), " Discussion of Oedometer Test Study on the Preconsolidation Stress of Glaciomarine Clays", Can. Geotech. J. 42: 972-974.

Cullen A. J. (2010), "Engineering Properties of Resedimented Ugnu Clay from the Alaskan North Slope", SM Thesis, Dept. of Civil and Environmental Engineering, Massachusetts Institute of Technology, Cambridge, Mass.

DeGroot D. J.; Poirier S. E.; Landon M. M. (2005), "Sample Disturbance – Soft Clays", Studia Geotechnica et Mechanica, Vol. XXVII, No. 3-4.

DeGroot J. D. (2003), "Laboratory Measurement and Interpretation of Soft Clay Mechanical Behavior", Soil Behavior and Soft Ground Construction, ASCE GSP 119, eds. Germaine, Sheahan and Whitman, pp. 167-201.

Demers D.; Leroueli S. (2002), "Evaluation of Preconsolidation Pressure and the Overconsolidation Ratio from Piezocone Tests of Clay Deposits in Quebec", Can. Geotech. J. 39: 174-192.

Dias Junior M. S.; Pierce F. J. (1995), "A Simple Procedure for Estimating Preconsolidation Pressure from Soil Compression Curves", Dept. of Crop and Soil Science, Michigan State Univ., East Lansing, MI.

Gasparre A. (2005), "Advance Laboratory Characterization of London Clay", PhD Thesis, Imperial College of Science, Technology and Medicine, University of London.

Georgiannou V. N.; Hight D. W. (1994), "The Effects of Centerline Tube Sampling Strains on the Undrained Behavior of Two Stiff Overconsolidated Clays", Geotechnical Testing Journal, ASTM, 17(4), 475-482.

Germaine J.T.; and Germaine A. V. (2009), "Geotechnical Laboratory Measurements for Engineers", Wiley and Sons, Inc.

Germaine J. T.; Ladd C. C. (1988), "Triaxial Testing of Saturated Cohesive Soils: State of the Art Paper", Advance Triaxial Testing of Soil and Rock, ASTM STP 977, Philadelphia: ASTM, 421-459.

Hight D. W.; Boese R.; Butcher A. P.; Clayton C. R. I.; Smith P. R. (1992), "Disturbance of Bothkennar Clay Prior to Laboratory Testing", Geotechnique, 42, No. 2, 199-217.

Holtz R. D.; and Kovacs W. D. (1981), "An Introduction to Geotechnical Engineering", Prentice-Hall, Englewood Cliffs, New Jersey.

Hong Z.; and Onitsuka K. (1998), "A Method of Correcting Yield Stress and Compression Index of Clays for Sample Disturbance", Soils and Foundations Japan. 38(2): 211-222.

Hvorslev M. J. (1949), "Subsurface Exploration and Sampling of Soil for Civil Engineering Purposes", Vicksburg: US Waterways Experiment Station, 521p.

Jain Subodh; Nanda Atul (2008), "Constitutive Modelling of San Francisco Bay Mud", The 12th International Conference of International Association for Computer Methods and Advances in Geomechanics (IACMAG), October 2008, Goa, India.

Jambu N., (1969), "The Resistance Concept Applied to Deformation of Soils", Proc. 7th Int. Conf. on Soil Mech. And Found. Eng., Mexico city. Vol. 1, pp. 191-196.

Korchaiyapruk A. (2007), "Experimental and Numerical Study of Primary Consolidation of Soft Clay", PhD Thesis, Dept. of Civil and Environmental Engineering, Massachusetts Institute of Technology, Cambridge, Mass.

Ladd C. C. (1964), "Stress-Strain Behavior of Saturated Clay and Basic Strength Principles", Research Report R65-17, Research on Earth Physics, Dept. of Civil Eng., MIT, Cambridge, MA.

Ladd C. C. (1973), "Settlement Analysis for Cohesive Soils", Research Report R71-2, No. 272, Dept. of Civil Engineering, Massachusetts Institute of Technology, Cambridge, MA.

Ladd C. C. (1991), "Stability Evaluation During Staged Construction", J. of Geotechnical Eng., vol. 117, No. 4.

Ladd C. C.; and Foott R. (1974), "New Design Procedure for Stability of Soft Clays", ASCE, J. of Geotechnical Engineering, 117(4), 540-615.

Ladd C. C.; Foott R.; Ishihara K.; Scholosser F.; and Poulos H. G. (1977), "Stress-Deformation and Strength Characteristics, State of the Art Report", Proceedings of the 9th International Conference of Soil Mechanics and Foundation Engineering, Tokyo, 2 , 421-494.

Ladd C. C.; and Lambe (1963), "The Shear Strength of Undisturbed Clay Determined from Undrained Tests", ASTM. STP. 361: 342-370.

Ladd C.C.; and DeGroot D.J. (2003), "Recommended Practice for Soft Ground Site Characterization: Arthur Casagrande Lecture", Proc. 12th Panamercan Conf. on Soil Mechanics and Geotch. Eng., MIT, Vol. 1, 3-57.

Lambe T. W. (1951), "Soil Testing for Engineers", John Wiley and Sons, NY.

Lambe T.W.; Whitman R. V. (1967), "Soil Mechanics", Wiley, ch. 3, NY.

Landon M. M.; DeGroot D.J.; and Jabukowski J. (2004), "Comparison of Shear Wave Velocity Measured in Situ and on Block Samples of a Marine Clay", Proc. 57th Canadian Geotechnical Conference, Quebec, in press.

Landon M. M.; DeGroot D.J.; Sheahan T. C. (2007), "Nondestructive Sample Quality Assessment of a Soft Clay Using Shear Wave Velocity", J. of Geotechnical and Geoenvironmental Engineering 1090-0241(2007) 133:4 (424).

Liu M. D.; Carter J. P.; Desai C. S.; and Xu K. J. (2000), "Analysis of the Compression of Structured Soils Using the Disturbed State Concept", International Journal for Numerical and Analytical Methods in Geomechanics, 24: 723-735.

Lunne T.; Berre T.; and Strandvik S. (1997), "Sampling Disturbance Effects in Soft Low Plastic Norwegian Clay", Recent Developments in Soil and Pavement Mechanics, Almeida, Ed. Balkema, Rotterdam, 81-102.

Lunne T.; Berre T.; Andersen K.H.; Sjursen M.; and Mortensen N. (2007), "Effects of Sample Disturbance on Consolidation Behavior of Soft Marine Norwegian Clays", Norwegian Geotechnical Institute, Oslo, Norway.

Malandraki V.; Toll D. G. (1995), "The definition of yield for Bonded Material", Geotechnical and Geological Engineering, 14,67-82.

Mayne P. W.; and Kuhawy F. H. (1982), "K_0-OCR Relationship in Soil", J. of Geotechnical Engineering Division, ASCE, 108(6), 851-872.

Mersi G.; Castro A. (1987), "C_α/C_c Concept and K0 during Secondary Compression", Journal of the Geotechnical Engineering Division, ASCE, 113(3), 230-247.

Mersi G.; and Choi Y. K. (1985), "Settlement Analysis of Embankments on Soft Clay", J. of Geotechnical Engineering, ASCE, vol. 111, GT4.

Mitchell J. K.; (1993), "Fundamental of Soil Behaviors", John Wiley and Sons, NY.

Nagaraj T. S.; Miura N.; Chung S. G.; and Prasad N. (2003), "Analysis and Assesment of Sampling Disturbance of Soft Sensitive Clays", Geotechnique, 53, No. 7, 679-683.

Nagaraj T. S.; Miura N.; and Yamadera A. (1999), "Discussion on a Method for Correcting Consolidation Parameters for Sample Disturbance Using Volumetric Stain" by T. Shogaki. Soil Found., 39, No. 1, 119-122.

Neher H. P.; and Wehnert M. (2001), "An Evaluation of Soft Soil Models Based on Trial Embankments" Inc. S. Desai (Ed.), vol. 1, Tuscin, Arizona, pp. 373-378.

Noorany I.; Seed H. B. (1965), "In-Situ Strength Characteristics of Soft Clays", J. of the Soil Mechanics and Foundation Division, ASCE, 91(2): 49-80.

Oikawa H. (1987), "Compression Curve of Soft Soils", Soils and Foundations Japan. 27(3): 99-104.

Olson, R. E. (1985), "State of the Art: Consolidation Testing", Consolidation of Soils: Testing and Evaluation, ASTM Special Technical Publication 892, pp. 7-70.

Onitsuka K.; Hong Z. (1995), "A New Method of Correcting Unconfined Compressive Strength of Natural Clays for Sample Disturbance", Soil Foundation, 35, No. 2, 95-105.

Ortega O. J. (1992), "Computer Automation of the Consolidated-Undrained Direct Simple Shear Test", SM Thesis, Massachusetts Institute of Technology, Cambridge, Mass.

Preston W. B. (1965), "The Effects of Sample Disturbance on the Undrained Strength Behavior of Boston Blue Clay", SM Thesis, Massachusetts Institute of Technology, Cambridge, Mass.

Poirier S.E; DeGroot D.J.; and Sheahan T.C. (2005), "Measurement of Suction in a Marine Clay as an Indicator of Sample Disturbance", ASCE, Site Characterization and Modeling.

Prasad K. N.; Triveni S. (2007), "Sample Disturbance in Soft and Sensitive Clays: Analysis and Assessment", Marine Georesources and Geotechnology, 25: 181-197.

Roscoe K. H.; and Burland J. B. (1968), "On the Generalized Stress-Strain Behavior of Wet Clay, in Engineering Plasticity", Cambridge University Press, 535-609.

Santagata M. C. (1994), "Simulation of Sampling Disturbance in Soft Clays Using Triaxial Element Tests", MS Thesis, Dept. of Civil and Environmental Engineering, Massachusetts Institute of Technology, Cambridge, Mass.

Santagata M. C. (1998), "Factors Affecting the Initial Stiffness and Stiffness Degradation of Cohesive Soils", PhD Thesis, Dept. of Civil and Environmental Engineering, Massachusetts Institute of Technology, Cambridge, Mass.

Santagata M. C.; and Germaine J. T. (2002), "Sampling Disturbance Effects in Normally Consolidated Clays", J. of Geotechnical and Geoenvironmental Engrg. 128(12), 997-1006.

Santagata M.; Sinfield J. V.; and Germaine J. T. (2006), "Laboratory Simulation of Field Sampling: Comparison With Ideal Sampling and Field Data", ASCE Journal of Geotechnical and Geoenvironmental Engineering, 1090-0241(2006) 132:3(351).

Schemertman J. H. (1955), "The Undisturbed Consolidation Behavior of Clay", Trans. Am. Soc. Civ. Eng., 120, 1201-1227.

Senol A.; Saglamer A. (2000), "Determination of Preconsolidation Pressure with a New, Strain Energy – log Stress Method", EJGE paper, 015.

Sheahan T. C.; Germaine J. T. (1992), "Computer Automation of Conventional Triaxial Equipment", Geotech. Test. J., 15(4), 311-322.

Sheahan T. C.; Ladd C. C.; and Germaine J. T. (1996), "Rate-Dependent Undrained Shear Behavior of Saturated Clay", J. of Geotechnical Eng., ASCE, 122(2), Feb., 99-108.

Siddique A.; Clayton C. R. I.; and Hopper R. J. (1999), "The Effects of Varying Centerline Tube Sampling Disturbance on the Behavior of Reconstituted Clay", Geotechnical Testing Journal, ASTM, 22(3): 245-256.

Simons N. E. (1974), "Normally Consolidated and Lightly Over-Consolidated Cohesive Materials", Settlement of Structures, British Geotechnical Society, Halsted Press, London.

Sinfield J. V. (1994), "An Experimental Investigation of Sampling Disturbance Effects in Resedimented Boston Blue Clay", SM Thesis, Dept. of Civil and Environmental Engineering, Massachusetts Institute of Technology, Cambridge, Mass.

Skempton A. W.; and Sowa V. A. (1963) "The behavior of Saturated Clays During Sampling and Testing" Geotechnique 12(4): 269-290.

Shogaki T. (1996), "A Method for Correcting Consolidation Parameters for Sample Disturbance Using Volumetric Strain", Soil Foundation, 36, No. 3, 123-131.

Solanki C. H.; Desai M. D. (2008), "Preconsolidation Pressure from Soil Index and Plasticity Properties", The 12th International Conference of Int. Assoc. for Computer Methods and Andvances in Geomechanics (IACMAG), Goa, India.

Tan, T. S.; Lee F. H.; Chong P. T.; and Tanaka H. (2002), "Effects of Sampling Disturbance on Properties of Singapore Clay", J. Geotech. Geoenviron. Eng., 128(11), 898-906.

Tanaka H.; Oka F.; and Yashima A. (1996), "Sampling of Soft Soil in Japan", Marine Georesources and Geotechnology, 14: 283-295.

Tavenas D. R.; Leroueil L.; and Roy (1976), "The Use of Strain Energy as a Yield and Creep Criterion for Lightly Overconsolidated Clays", Geotechnique 29, No. 3, pp. 285-303.

Tavenas D. R..; and Leroueil S. (1987), "Laboratory and In Situ Stress-Strain-Time Behavior of Soft Clays: A State of the Art", Proc. Int. Symp. On Geotechnical Eng. of Soft Soils, Mexico City, vol.4, 1-46.

Taylor D. W. (1942), "Fundamentals of Soil Mechanics", John Wiley and Sons, NY.

Terzaghi K.; Peck R. B.; and Mesri G. (1996), "Soil Mechanics in Engineering Practice", John Wiley & Sons, Inc., New York.

Wang L. B.; and Frost J. D. (2004), "Dissipated Strain Energy Method for Determining Preconsolidation Pressure", Canadian Geotechnical J., 41, 760-768.

Wissa A. E. Z.; Christian J. T.; Davis E. H.; and Heiberg S. (1971), "Consolidation at Constant Rate of Strain", J. of Soil Mechanics and Foundation, ASCE, vol. 97, No. SM10, 1393-1413.